An unbiased single copy locus proteomics approach reveals new factors in replication timing control

DISSERTATION ZUR ERLANGUNG DES DOKTORGRADES

DER FAKULTÄT FÜR BIOLOGIE

DER LUDWIG-MAXIMILIANS-UNIVERSITÄT MÜNCHEN

Matthias Weiß

August 2023

Diese Dissertation wurde angefertigt

unter der Leitung von Dr. Stephan Hamperl

am Institut für Epigenetik und Stammzellen

des Helmholtz Zentrum München

ERKLÄRUNG

Ich versichere hiermit an Eides statt, dass meine Dissertation selbständig und ohne unerlaubte Hilfsmittel angefertigt worden ist.

Die vorliegende Dissertation wurde weder ganz, noch teilweise bei einer anderen Prüfungskommission vorgelegt.

Ich habe noch zu keinem früheren Zeitpunkt versucht, eine Dissertation einzureichen oder an einer Doktorprüfung teilzunehmen.

Wesentliche Teile dieser Arbeit sind in der folgenden Publikation veröffentlicht und zusammengefasst (Weiß et al., 2023):

Weiß M, Chanou A, Schauer T, Tvardovskiy A, Meiser S, König AC, Schmidt T,

Kruse E, Ummethum H, Trauner M, Werner M, Lalonde M, Hauck SM, Scialdone A,

Hamperl S.

Single-copy locus proteomics of early- and late-firing DNA replication origins

identifies a role of Ask1/DASH complex in replication timing control.

Cell Rep. 2023 Jan 25;42(2):112045.

München, den 02.08.2023 ....

Matthias Weiß

Table of Contents

1   Summary

DNA replication is a fundamental process to duplicate the genome of a cell, which is a prerequisite for an equal distribution of chromosomes to two emerging daughter cells during the following cell division. This process already starts in G1 phase of the cell cycle where specific regions on the genome called origins of replication are prepared for the upcoming DNA duplication in a process called origin licensing. Subsequently, origins will fire in the following S phase, allowing DNA replication in a bidirectional manner. Intriguingly, this firing does not occur simultaneously, but in a continuum during S phase, with some origins firing earlier and more efficiently than others. One hypothesis suggests that the chromatin structure at replication origins is responsible for these differences in origin firing. In this work, a previously established site-specific recombination and chromatin isolation approach was utilized to purify selected early-efficient and late-inefficient replication origins from the *S.cerevisiae* genome. After several improvements to the purification process, the isolated replication origins are subjected to mass spectrometry to determine both the proteomes, as well as the histone posttranslational modification state associated with the respective replication origins. The histone post-translational modification analysis revealed clear differences mainly in the acetylation state of histones surrounding the investigated replication origins. Interestingly, late-replicating and inefficient replication origins showed higher acetylation states as compared to the early-replicating and efficient origins, strengthening the idea that the local histone modification state influences origin firing. Furthermore, several known origin interactors were detected in the proteome analysis, validating the site-specific recombination approach to isolate replication origins. Apart from expected replication factors, several other previously not described candidate factors were retrieved in the mass spectrometric analysis. Validation of these factors led to the discovery of two potential novel replication regulators, namely Set3 and Ask1. Set3 was previously described as part of the Set3 histone deacetylase complex and Ask1 as part of the microtubule binding Ask1/DASH complex. Strikingly, tethering these factors to specific replication origins advances the replication timing of the targeted regions. Additionally, depleting cells of Ask1 leads to global changes in the replication timing of several chromosomal domains. This effect could also be reproduced by targeted degradation of microtubules using nocodazole, which ultimately phenocopies Ask1 loss-of-function. Ultimately, these findings not only strengthen the link between histone acetylation and replication, but also establish a novel mechanistic connection between replication timing and the chromosomal organization mediated by the Ask1/DASH complex through the microtubule cytoskeleton.

2   Zusammenfassung

Die DNA-Replikation ist ein grundlegender Prozess zur Verdopplung des Genoms einer Zelle, was eine Voraussetzung für eine gleichmäßige Verteilung der Chromosomen auf zwei entstehende Tochterzellen während der folgenden Zellteilung ist. Dieser Prozess beginnt bereits in der G1 Phase des Zellzyklus, wo bestimmte Regionen im Genom, sogenannte Replikationsursprünge, in einem Prozess namens „origin licensing" auf die bevorstehende DNA-Verdopplung vorbereitet werden. Anschließend „feuern" diese Ursprünge in der S Phase, was eine bidirektionale DNA-Replikation ermöglicht. Interessanterweise erfolgt dieses Feuern nicht gleichzeitig, sondern über die gesamte S Phase verteilt, wobei einige Ursprünge früher und effizienter feuern als andere. Eine Hypothese besagt, dass die Chromatinstruktur an den Replikationsursprüngen für diese Unterschiede im Feuern verantwortlich ist. In dieser Arbeit wurde ein zuvor etablierter Rekombinations- und Chromatinisolierungsansatz verwendet, um ausgewählte frühe effiziente und späte ineffiziente Replikationsursprünge aus dem *S.cerevisiae* Genom zu reinigen. Nach mehreren Verbesserungen des Reinigungsprozesses wurden die isolierten Replikationsursprünge mittels Massenspektrometrie untersucht, um sowohl die Proteome als auch die posttranslationalen Histonmodifikationszustände der jeweiligen Replikationsursprünge zu bestimmen. Die Histonanalyse ergab deutliche Unterschiede im Acetylierungszustand der Histone an den untersuchten Replikationsursprüngen. Interessanterweise zeigten späte, ineffiziente Replikationsursprünge im Vergleich zu frühen, effizienten Ursprüngen einen höheren Acetylierungsgrad, was die Annahme bestärkt, dass der lokale Histonmodifikationszustand das Feuern von Replikationsursprüngen beeinflusst. Zudem wurden in der Proteomanalyse auch mehrere bereits beschriebene Interaktionspartner entdeckt, was den Rekombinationsansatz zur Isolation von Replikationsursprüngen validiert. Neben diesen erwarteten Faktoren wurden durch Massenspektrometrie auch mehrere neue noch nicht beschriebene Kandidaten gefunden. Die Validierung dieser Faktoren führte zur Entdeckung zweier potenzieller neuer Regulatoren, nämlich Set3 und Ask1. Set3 wurde zuvor als Teil des Set3 Histondeacetylase-Komplexes und Ask1 als Teil des Mikrotubuli-bindenden Ask1/DASH-Komplexes beschrieben. Bemerkenswerterweise beschleunigt die Bindung dieser Faktoren an bestimmte Replikationsursprünge den Replikationszeitpunkt der Zielregionen. Des Weiteren führte die Depletion von Ask1 auch zu globalen Veränderungen im Replikationszeitpunkt mehrerer chromosomaler Domänen. Dieser Effekt konnte auch durch den gezielten Abbau von Mikrotubuli mit Nocodazole reproduziert werden, was den Funktionsverlust von Ask1 imitiert. Diese gesamten Ergebnisse stärken nicht nur den Zusammenhang zwischen Histonacetylierung und Replikation, sondern stellen auch einen neuen mechanistischen Zusammenhang zwischen dem Replikationszeitpunkt und der chromosomalen Organisation her, die durch den Ask1/DASH-Komplex durch das Mikrotubuli-Zytoskelett vermittelt wird.

3 Introduction

3.1 The regulation of DNA replication in eukaryotic genomes

DNA replication is a fundamental process of every organism to duplicate the genome and provide an identical set of chromosomes to the two emerging daughter cells. This process is initiated at specialized DNA regions named origins of replication. Depending on genome size, eukaryotic cells utilize several hundreds to thousands of replication origins to allow duplication of their large linear chromosomes in a manageable timescale. However, initiation across this large number of origins needs to be precisely coordinated in space and time to ensure accurate genome duplication during the confined S phase of the cell cycle (reviewed in Parker et al., 2017).

The initiation of DNA replication is partitioned into temporally discrete steps: During late M/G1 phase of the cell cycle, origins are first recognized by the hexameric Origin Recognition Complex (ORC). Subsequently, the helicase-loader Cdc6 together with the Cdt1 chaperone leads to the consecutive recruitment and head-to-head binding of two inactive Mcm2-7 (Mini-Chromosome Maintenance) hexamers onto the DNA (Evrin et al., 2009; Remus et al., 2009). This completes origin licensing, the assembly of the inactive pre-replicative complex (pre-RC) and marks potential origins for firing in the following S phase.

Upon entry into S phase, Cyclin Dependent Kinases (CDKs) and Dbf4-dependent kinases (DDKs) are activated. DDK is responsible for the phosphorylation of the Mcm2-7 helicase, which in turn triggers the recruitment of Sld7 in cooperation with Sld3, as well as Cdc45 (Deegan et al., 2016; Francis et al., 2009). CDK on the other hand phosphorylates Sld3 and Sld2, which mediates interaction with Dbp11 (Kamimura et al., 1998; Masumoto et al., 2002; Zegerman and Diffley, 2007). Eventually, this leads to the association of a tetrameric protein complex consisting of Sld5, Psf1, Psf2, and Psf3, which is commonly referred to as GINS complex. Recruitment of Cdc45 and the GINS proteins to the Mcm2-7 hexamer converts the inactive complex into the active CMG (Cdc45/Mcm2-7/GINS) helicase, which is now starting to melt the DNA duplex. Additionally, the phosphorylation of Sld2 and Sld3 also leads to the recruitment of DNA polymerases and other components necessary to form an active replisome (Muramatsu et al., 2010). Ultimately, all of these steps activate the origin and generate a bidirectional replication fork. This separation of licensing and activation of origins is crucial to ensure once and only once genome replication per cell cycle (**Figure 1**).
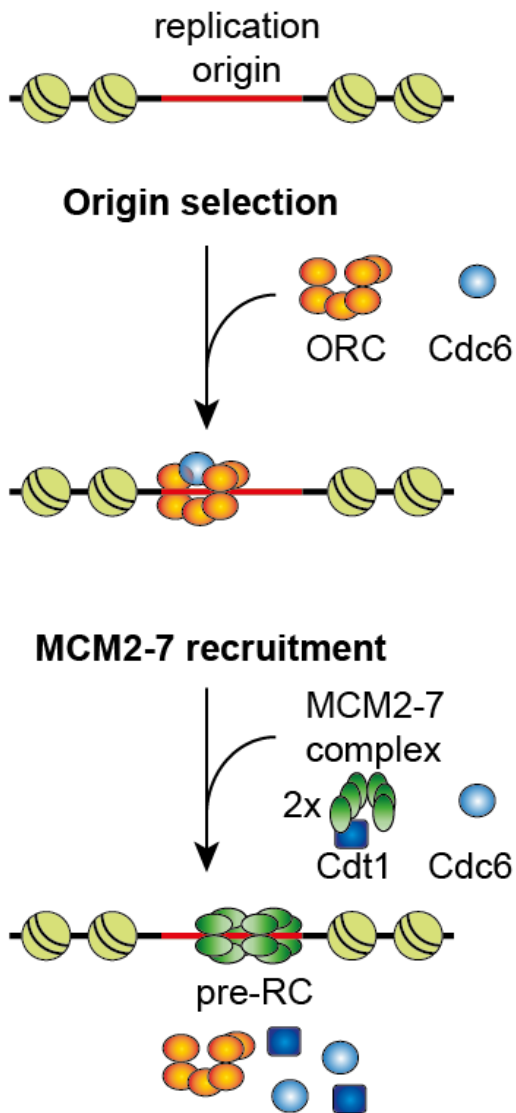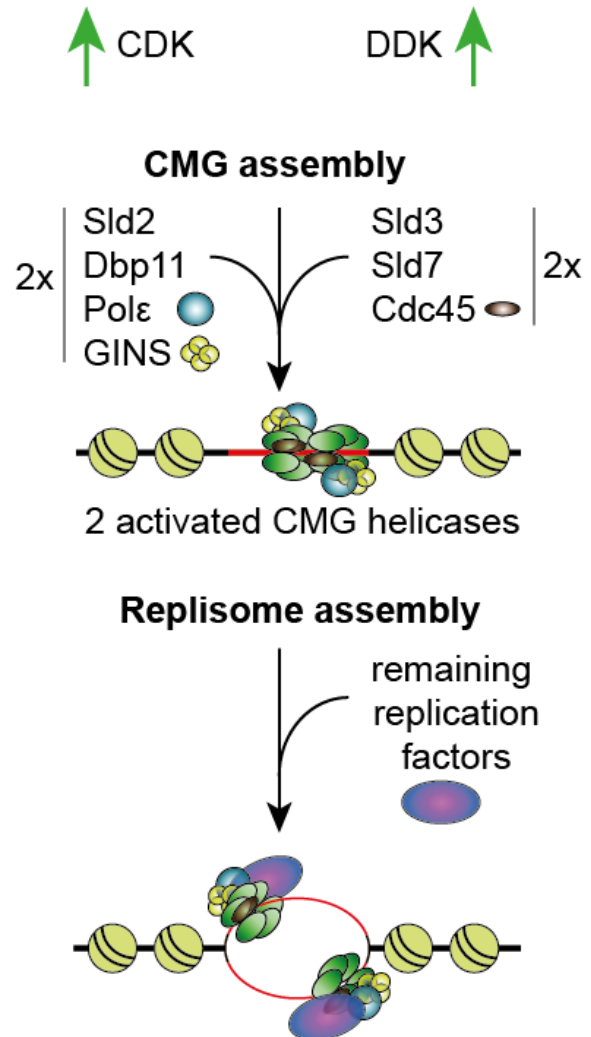
Figure 1 Replication initiation of eukaryotes during G1 and S phase The cartoon shows the different steps of eukaryotic replication initiation. During G1 phase, replication origins are licensed in multiple steps culminating in the recruitment of the MCM2-7 complex. In the subsequent S phase, the licensed origins are activated resulting in CMG and replisome assembly and bidirectional replication.

However, the activation of replication origins during S phase is not identical for all licensed origins, but differs in two important aspects. First, the replication timing depicts the timepoint of origin firing, with some origins firing reproducibly early in S phase and others firing later (Rhind and Gilbert, 2013). Importantly, the resulting replication timing program is not deterministic in the sense that every origin in every cell cycle shows identical timing of origin activation. Instead, origin firing is stochastic with no two cells replicating their genome in an identical fashion (Czajkowsky et al., 2008; Wang et al., 2021; Zhao et al., 2020).

The second feature of replication origins is the replication efficiency, which describes the probability of activation for each replication origin, since not every origin will fire in every S

4

phase. On a molecular level, this behavior can be explained by competition between origins for firing factors that are present in limiting amounts (Mantiero et al., 2011; Tanaka et al., 2011). Consistent with this notion, a recent study used a conditional system in budding yeast to simultaneously overexpress the six firing factors Sld2, Sld3, Dpb11, Dbf4, Cdc45, and Sld7 achieved a global early replication of the majority of origins in a single cell cycle (Santos et al., 2022). This adds another layer of complexity by this fact that only a subset of the licensed and thus initiation-competent origins will be activated by different cells in a stochastic manner (Czajkowsky et al., 2008; Hawkins et al., 2013; Saner et al., 2013). Nevertheless, population-based studies that average these heterogeneous replication initiation events across a large number of cells can define a reproducible temporal program of chromosome replication (Ferguson et al., 1991; Raghuraman et al., 2001). This replication timing program is highly robust and evolutionary conserved from yeast to humans, suggesting that replicating different parts of the genome at different times during S phase has an important – but yet to be fully understood - biological function. One assumption why cells limit the number of active replisomes at a given time is to better coordinate and manage the available required resources for genome replication such as the nucleotide pool and histone supply to ensure smooth S phase progression and reconstitution of the chromatin landscape (Santos et al., 2022).

3.1.1 Yeast Replication Origins show strong DNA Sequence Specificity

The first eukaryotic replication origin was identified in *S.cerevisiae* as a sequence that enables the maintenance of extrachromosomal plasmids, therefore called Autonomously Replicating Sequence (ARS) (Stinchcomb et al., 1979). Each ARS element contains at least one conserved ARS consensus sequence (ACS), which is necessary but not sufficient for origin function. In addition to this essential 11bp T-rich sequence motif, a replication origin in yeast typically spans a few hundred basepairs mostly located in intergenic regions with an average distance of 40 to 100kb (Wyrick et al., 2001). These regions show a modular structure where up to three sequence elements named A, B and C domains can be distinguished to enhance or modulate origin activity (Celniker et al., 1984; Marahrens and Stillman, 1992).

The A domain contains the ACS with the consensus sequence WTTTAYRTTTW (Broach et al., 1983). However, the ACS of individual origins is degenerate and sometimes only a 10/11- or 9/11-bp match is needed for an initiation-competent ARS. Interestingly, most origins contain multiple imperfect matches to this motif with the best match not necessarily corresponding to the site of replication initiation. The functional importance of the ACS has also been shown in mutational analyses, where even single point mutations in highly conserved ACS positions could strongly decrease or even abolish the function of the replication origin (Van Houten and Newlon, 1990). But since there are over 12,000 ACS motifs in the yeast genome, of which only 300-400 are used under normal conditions, the presence of the ACS alone does not suffice to mark an active ARS. A less conserved, 17bp long extended ACS (EACS) has later been

defined, which has improved but still not sufficient power to predict origin location in the yeast genome (Theis and Newlon, 1997). More recent bioinformatic approaches have now comprehensively identified most origins in several different yeast genomes with high accuracy (Breier et al., 2004; Dao et al., 2019; Singh et al., 2018), indicating that nucleotide sequence of the ACS is a reliable predictor of yeast origins.

The B domain, which is located 3′ to the T rich strand of the ACS has been described as a DNA unwinding element (DUE), facilitating the access of replication factors to the DNA template strands (Huang and Kowalski, 2003; Natale et al., 1993; Umek and Kowalski, 1990). The B domain can be further subdivided into B1, B2 and B3 sequence elements. The B1 element contains a conserved WTW motif 17 to 19 bp from the ACS (Chang et al., 2008) and acts together with the ACS as a bipartite DNA binding site for the ORC complex (Rao and Stillman, 1995; Rowley et al., 1995). This was later referred to as ORC-ACS (Eaton et al., 2010a; Xu et al., 2006). Recent structural studies of ORC bound to origin DNA sequence showed that specific recognition of the ACS is carried out by a conserved basic amino acid motif of Orc1 in the minor groove, and by a yeast-specific helical insertion motif of Orc4 in the major groove. Similar insertions into major and minor grooves in the B1 site induces ORC-specific bending of the DNA (Li et al., 2018; Yuan et al., 2017). Interestingly, removing this insertion helix from Orc4 disrupts the ARS sequence-specific binding, thereby changing the selectivity of the ORC complex in yeast to random accessible regions in the genome with preference for transcriptional start sites (Lee et al., 2021).

The B2 element shows the consensus sequence ANWWAAAT (Chang et al., 2011). It was shown to interact with the MCM2-7 helicase (Wilmes and Bell, 2002), whereas the B3 element, which is defined by a TnnCGTnnnnnnTGAT-motif (Beinoravičiūtė-Kellner et al., 2005), contains a binding site for the transcription factor Abf1 (ARS binding factor 1) (Diffley and Stillman, 1988). At certain origins, Abf1 binding might help to exclude nucleosomes from the ARS, thereby helping to establish a nucleosome-depleted region (NDR) (Ganapathi et al., 2011). Distinct mutations in these B elements can lead to impaired function of the origin (Lin and Kowalski, 1997; Rao et al., 1994). However, not all functionally annotated ARSs contain all three B elements and different combinations of these motifs exist, suggesting that they have auxiliary and partially redundant functions in origin specification.

The C domain is located upstream of the A element. This domain can provide binding sites for transcription factors that can enhance origin activity, like MCM1 (Chang et al., 2004), Rap1 (Sharma et al., 2001), Sum1 (Irlbacher et al., 2005), and also Abf1 (Walker et al., 1990). Again, mutations in these binding sites show an effect on origin function, but rather mild compared to mutations in the A or B domains. All sequence features are summarized in **Figure 2**.
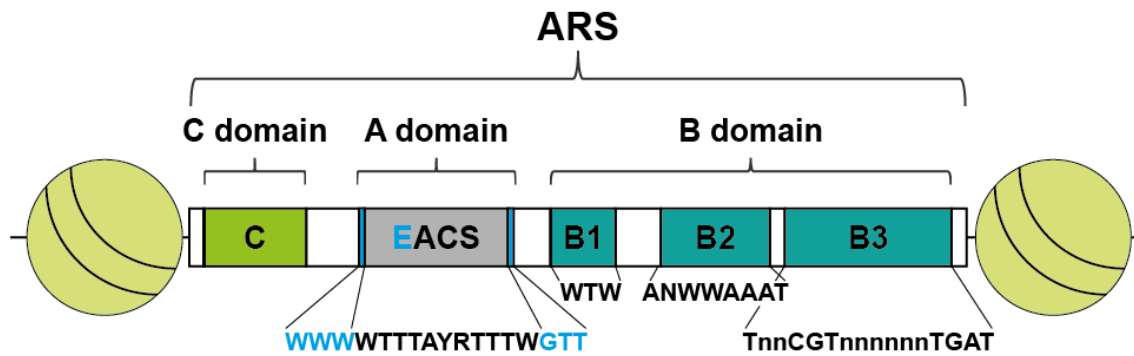
Figure 2 General structure of a replication origin in *S.cerevisiae*

Despite the knowledge that mutations in the respective DNA sequence elements are affecting replication origins, there are no studies yet that generally link their occurrence to the replication timing and efficiency features of specific replication origins. For example, it is possible that highly efficient and early firing replication origins are utilizing a different set and amount of these DNA elements, as compared to inefficient and late firing origins. Interestingly, *in vitro* experiments have shown that the ARS with its ACS and B elements are not necessarily needed for *S.cerevisiae* ORC binding and MCM loading, suggesting that there might additional chromosomal features come in play that determine the licensing and firing capabilities of replication origins in *S.cerevisiae* (Remus et al., 2009; Yeeles et al., 2015).

3.1.2 Defined positioning of origin-flanking nucleosomes

One important aspect for origin activity is the positioning of nucleosomes around replication origins. In yeast, ARS are comprised of nucleosome-depleted regions (NDRs), which are centered around the ACS. The -1 and +1 nucleosomes surrounding the NDR are well positioned (Berbenetz et al., 2010; Eaton et al., 2010b). One mechanism that likely helps creating these NDRs is the specific sequence at replication origins in yeast. Poly(dA.dT) elements, like the ones found at replication origins, were shown to destabilize the interaction of histones with DNA, resulting in preferential exclusion of nucleosomes (Anderson and Widom, 2001; Bernstein et al., 2004). Consistent with an important function of the NDR in origin function, classic experiments in yeast showed that a nucleosome encroaching an ARS sequence resulted in marked reduction of origin activation (Simpson, 1990).

In addition to this sequence property, additional protein factors binding to replication origins help to establish this distinct nucleosomal pattern. It has been shown that both ORC and Abf1 binding is crucial for positioning of nucleosomes flanking the ARS. For example, at ARS1, mutating either the ORC binding site or the Abf1 binding site results in the nucleosomes encroaching into the NDR of ARS1 from only the respective site containing the mutation. At ARS307, where no Abf1 binding site is present, mutating the ORC binding site results in the reduction of the NDR size of ARS307 from both sides (Lipford and Bell, 2001; Venditti et al., 1994). A recent study showed that ORC works in concert with the chromatin remodeling

machineries INO80, ISW1a, ISW2, and Chd1 to set up the nucleosomal landscape with these flanking arrays of regularly spaced nucleosomes at replication origins (**Figure 3**). Importantly, these chromatin remodelers act redundantly, as shown by mutational analyses where the quadruple knockout of all remodelers had a much stronger effect on nucleosomal organization as compared to single knockouts of the respective machineries which ultimately led to an abolishment of the regular nucleosome arrays. Also, impairing the nucleosome array formation by compromising the ORC – remodeler interactions led to lethal replication problems, highlighting the importance of nucleosome positioning for chromosome replication (Chacin et al., 2023).
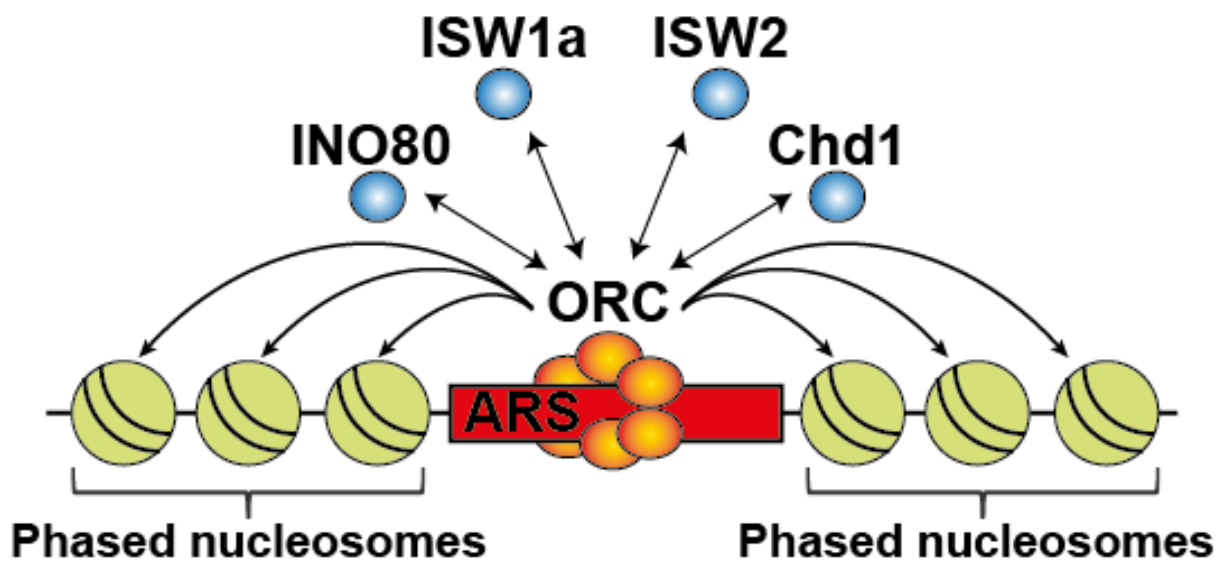
Figure 3 Nucleosome positioning around replication origins in *S.cerevisiae*

Interestingly, a recent study showed that there is an alternative sequence-independent mechanism of ORC binding and thus origin licensing. It was demonstrated in single molecule *in vitro* studies that ORC not only can bind an ACS sequence, but also has the cryptic capacity to bind nucleosomes near an NDR which also ultimately leads to origin licensing in *S.cerevisiae* (Li et al., 2022). This finding is in line with the previously mentioned fact that upon deletion of the yeast specific insertion helix of Orc4, the ORC complex will preferentially bind other genomic NDRs such as transcriptional start sites (Lee et al., 2021). Ultimately, this nucleosome directed origin licensing next to NDRs might represent a general mechanism that applies for higher eukaryotes that do not display sequence-specific ORC binding (Hoshina et al., 2013; Remus et al., 2004; Vashee et al., 2003).

In addition to the precise positioning of the adjacent nucleosomes flanking the NDR, the occupancy of nucleosomes around replication origins also plays an important role. For example, it was shown by chromatin immunoprecipitation-sequencing (ChIP-Seq) that origins that have less nucleosomes tend to be more efficient and early firing, whereas a high nucleosome occupancy leads to inefficient and late firing origins (Rodriguez et al., 2017).

Together, it is clear that the positioning and occupancy of nucleosomes at origins affect their replication properties, but the precise chromatin states that are permissive or restrictive to efficient origin activation are still under investigation.

3.1.3 Histone modifications at nucleosomes surrounding replication origins

Histones are the target substrates for a large number of posttranslational modifications, from which several have also been demonstrated to influence the replication programme. For example, it has been shown by mass spectrometry that the acetylation states of histones H3 and H4 flanking replication origins are markedly different compared to bulk histones and also show specific patterns of acetylation. These acetylation patterns are increasing over the cell cycle in S and G2/M phase, suggesting an important function in replication. Accordingly, a quintuple mutant of these investigated lysine residues resulted in prolonged S phases as well as in decreased replication efficiencies, suggesting that different acetylations could act together in regulating replication origin activation (Unnikrishnan et al., 2010a).

Consequently, targeting writers and erasers of different histone acetylations can produce changes in the replication programme. This was, for example, shown at the rDNA locus in *S.cerevisiae*, which approximately consists of 150 to 200 tandem repeats with each containing a replication origin. However, only about 20% of these replication origins will be activated during any given S phase (Brewer and Fangman, 1988). The repression of the non-active replication origins at the rDNA locus is mediated by the histone deacetylase (HDAC) Sir2. However, the activity of another HDAC, Rpd3, is able to counteract this phenomenon. Thus, these two HDACs together regulate the replication programme at the rDNA locus in *S.cerevisiae*. However, outside of the rDNA locus, Sir2 also controls the activation of certain origins. Crucially, a loss of this function results in persistent replication gaps during S phase, which ultimately leads to genome instability (Foss et al., 2017). One hypothesis proposes that, by repressing rDNA replication, important initiation factors are not sequestered by the rDNA locus, so that other replication origins can fire, which ultimately leads to a homogeneous replication of the genome (Foss et al., 2017; Pasero et al., 2002; Yoshida et al., 2014). However, other studies suggested that Sir2 acts directly on individual origins independently of its function at the rDNA locus. In this model, H4K16 deacetylation by Sir2 leads to a reduced ability of early replication origins to load MCM proteins and thus promoting the licensing of late origins. This would again contribute to an even origin activation throughout S phase (Hoggard et al., 2020, 2018).

Interestingly, Sir2 alone is acting at the rDNA locus as well as some euchromatic replication origins, whereas the silent mating type loci HML and HMR are repressed by the combination of all four proteins of the silent information regulator family (Sir1/Sir2/Sir3/Sir4) (Rine and Herskowitz, 1987) and the telomeric regions by Sir2, Sir3, and Sir4 (Aparicio et al., 1991).

Intriguingly, mutation of Sir3 caused telomeric origins to fire earlier, suggesting that this protein is also important for establishing the late replication timing at telomer-proximal origins. Consistently, transferring early replication origins to the silenced telomere region delayed their firing time significantly (Stevenson and Gottschling, 1999). Similarly, tethering Sir4 to the early firing replication origin ARS305 massively delayed the replication timing at this locus (Zappulla et al., 2002), strongly supporting a crucial role of Sir proteins in the origin regulation at specific genomic regions.

At genomic regions not affected by Sir proteins, the HDAC Rpd3 complements the regulation of replication timing of late origins. Rpd3-depleted cells show increased histone acetylation levels leading to earlier replication initiation at the affected origins (Aparicio et al., 2004; Knott et al., 2009; Yoshida et al., 2014). Accordingly, targeted histone acetylation by recruiting the SAGA complex histone acetylase Gcn5 to a late firing origin also advances the replication timing by earlier recruitment of the firing factor Cdc45 (Vogelauer et al., 2002).

Apart from acetylation events, various histone methylations are also affecting the regulation of replication origins. One example is H3K4 di-methylation, which is established by the histone methyltransferase Set1 and sets an important mark for proper origin function. This was shown by elevated loss rates in plasmid stability assays as well as by severe growth defects in several hypomorphic replication mutants (Rizzardi et al., 2012). Furthermore, H3K36 methylation by Set2 is another important mark that regulates the time of Cdc45 association with replication origins. It has been shown that H3K36me1 can be found at early-replicating origins, whereas H3K36me3 is predominantly linked to late-replicating origins. This suggests that the methylation status of this residue can determine the replication timing by advancing or delaying the association of Cdc45 to replication origins (Pryde et al., 2009). Interestingly, Set1 and Set2 are also responsible for another histone methylation mark that is only poorly characterized, namely H3K37me1. This modification can be found throughout the whole yeast genome, however, with significantly less occupancy at replication origins. Specifically, H3K37me1 is able to impair the interaction of MCM2 with chromatin. Consequently, the loss of H3K37me1 leads to replication from inefficient origins and even outside of canonical ARS sites, while at the same time decreasing replication initiation from canonical replication origins (Santos-Rosa et al., 2021).

Together, these studies illustrate that many different histone PTMs play a role in origin regulation (summarized in **Figure 4**). However, it is still not well understood how they are working together and if there are combinatorial effects at individual replication origins. Therefore, additional studies will be needed to shed more light on this complex aspect of origin regulation.

3.1.4 Other trans-acting protein factors in replication origin control

Additional to the DNA sequence and nucleosome positioning surrounding the replication origins, various other proteins are able to modulate the behaviour of replication origins. Not surprisingly, the level of loaded pre-RC complex components like the MCM2-7 double hexamer itself are crucial to replication origin activity. For example, one study using ChIP-Seq of MCM subunits in *S.cerevisiae* reported that replication origins can load different amounts of MCM2-7 helicases with early origins preferentially loading more complexes than their late counterparts (Das et al., 2015; Dukaj and Rhind, 2021). However, other studies suggested that most origins either load exactly one or no MCM2-7 double-hexamer at all (Belsky et al., 2015; Foss et al., 2021). Thus, the precise number of MCM2-7 complexes is still under intense investigation, but regardless of this gap in our knowledge, it is clear that depleting cells for MCM proteins leads to drastic changes in the replication timing of distinct replication origins (Dukaj and Rhind, 2021), suggesting that balanced cellular levels of MCM proteins is an important criteria for replication regulation.

Intrestingly, not only components of the origin licensing machinery, but also factors that are required for the MCM2-7 helicase activation in the firing process are able to influence replication initiation. As mentioned before, six factors of this process are in low abundance in the cell, namely the regulatory subunit of DDK Dbf4, as well as the activation factors Sld2, Sld3, Sld7, Dbp11, and Cdc45 (Mantiero et al., 2011; Tanaka et al., 2011). Association of these low-abundance factors is crucial for determining the order of replication initiation events, since origins have to compete for these limited factors and, generally, early replication origins will associate with these factors before late replication origins, setting them up for early activation.

A pressing question is how these limiting factors are preferentially recruited to early origins at the beginning of S phase. One mechanism involves the two forkhead box transcription factors Fkh1 and Fkh2. These factors have been shown to stimulate the early replication timing of over 100 replication origins. These fork-head-regulated origins are typically enriched for Fkh binding sites adjacent to the ACS and, consequently, disrupting this motive also leads to a deceleration in the respective replication timing. A similar result was obtained when examining the replication timing in *fkh1/2* knock-out mutants, where the early firing of over 100 replication origins was delayed (Knott et al., 2012; Ostrow et al., 2014). Additionally, overexpression of Fkh1/2 resulted in a global advancement of replication timing which demonstrates the stimulatory function in origin activation (Peace et al., 2016). On a molecular level, Fkh1/2 recruits Dbf4 as one of the limiting factors to the respective origins by a direct interaction in G1 phase, which in turn leads to the association of Cdc45 and establishes this early replication timing profile (Fang et al., 2017). Intriguingly, the activity of Fkh1 is also linked to the previously mentioned histone dacetylase Rpd3, as a recent study revealed that Rpd3 activity hinders

binding of Fkh1 and thus counteracts Dbf4 recruitment for early activation of the respective origins (He et al., 2022).

Besides these Fkh-activated replication origins, origins near centromeres typically show an early replication timing (Raghuraman et al., 2001). In a similar mechanism, the Ctf19 complex, which is a component of the kinetochore, is able to recruit Dbf4 from telophase until G1 phase. Subsequently, the Sld3 and Sld7 initiator proteins are recruited to these replication origins, which allows for the association of Cdc45 and, ultimately, the early replication in the subsequent S phase (Natsume et al., 2013).

In contrast, replication origins at "heterochromatic" telomeric and subtelomeric regions, often replicate late or are passively replicated in S phase. One protein that was demonstrated to be involved in setting up this late replication timing is the telomere-associated protein Rif1 (Rap1 interacting factor) (**Figure 4**). Deletion of Rif1 leads to an abnormal early replication of telomeric and telomere-proximal regions (Lian et al., 2011; Peace et al., 2014). Mechanistically, this late replication timing is caused by an interaction of Rif1 with the phophatase PP1/Glc7 which is able to counteract premature phosphorylation events by DDK in G1 phase (Davé et al., 2014; Hiraga et al., 2014; Mattarocci et al., 2014). The specificity towards telomeric regions is achieved by a second interaction of Rif1 with the repressor-activator protein1 (Rap1) which is a preferential telomere-binding protein. Briefly, Rap1 sequesters the limited amounts of Rif1 to telomeric regions and thus creates high concentrations of this protein at the chromosomal ends. However, recruitment of Rif1 to origins is independent of Rap1, meaning that disturbing the Rap1-Rif1 interaction or deletion of Rap1 also leads to recruitment of Rif1 to non-telomeric origins (Hafner et al., 2018). However, the mechanism how Rif1 is directly recruited to origins remains elusive. Besides the telomeric origins, also a large fraction of the replication origins at the rDNA repeats are regulated by Rif1. This helps to limit the number of active replisomes which in turn increases genome stability at this repetitive locus (Shyian et al., 2016).

3.1.5 Spatial organization of replication origins

Another important aspect that impacts the replication timing program is the spatial organization of replication origins within the nucleus. However, a distinction has to be made between the overall folding of chromosomes in the nucleus and the relative position of replication origins in reference to distinct nuclear substructures. In yeast, both centromeres and telomeres can be found at distinct and reproducible positions inside the nucleus (Taddei et al., 2004). While centromeres are positioned in proximity to the spindle pole body, telomeres are positioned at the nuclear periphery, away from the centromeres. While telomeres generally display late replication timing, it has been shown that this is not caused by the peripheral location itself. For example, after disrupting the positioning of telomeres from the nuclear periphery, replication origins still kept their late replication timing (Hiraga et al., 2006). Similarly, tethering

an early replication origin to the nuclear periphery did not change its early replication profile (Ebrahimi et al., 2010), arguing that in these cases other mechanisms are dominant and that subnuclear localization alone is not sufficient to determine replication initiation.

However, the overall genomic organization how chromosomes are folded within the nucleus has a stronger impact on the replication profile as compared to the aforementioned relative position within the nucleus. Early studies in mammalian cells have shown that during S phase, replication takes place at discrete replication foci within the nucleus (Nakamura et al., 1986). Such replication foci have later been referred to as replication factories, since several replisomes act together within these foci to duplicate the genome in a synchronous manner (Cseresnyes et al., 2009; Hozak et al., 1994; Hozák et al., 1993; Leonhardt et al., 2000). Later, the existence of such replication foci was also confirmed in budding yeast both *in vitro* (Pasero et al., 1997) and *in vivo* (Kitamura et al., 2006). Notably, this live cell imaging approach also provided strong evidence that after origin firing the two sister replisomes stay associated within these foci and that the doublestranded DNA products are extruded as loops from two replisomes. Furthermore, super-resolution microscopy also discovered that budding yeast replication factories typically consist of one up to four sister replisomes. Interestingly, the decision which replication start sites cluster together is mainly a stochastic process, meaning that the number and type of replicons which cluster together can vary from cell to cell (Saner et al., 2013). However, a preference is observed that early origins that are in close neighbourhood on the linear chromosomes show a higher frequency to cluster together (Kitamura et al., 2006).

Until now, two molecular mechanisms have been described how such a clustering of replication origins can be achieved in the nucleus (summarized in **Figure 4**). First, at centromeric regions, replicons of different chromosomes are brought in close proximity by the tethering of the kinetochores to the spindle pole body, which might help to organize these replicons into a centromeric replication factory (Natsume et al., 2013). Second, the previously mentioned Fkh1/2 transcription factors were shown to cluster individual replicons together in order to form replication factories (Knott et al., 2012). This is due to the ability of Fkh1/2 to form homodimers, with each protein being able to bind a different origin, thereby bridging them in close proximity (Ostrow et al., 2017). Another important aspect of this interaction is a relocation event within the nucleus. Precisely, upon Fkh1 and Dbf4 activation in G1 phase, Fkh-activated origins relocalize from the nuclear periphery to the nuclear interior (Zhang et al., 2019).

One potential benefit of such a clustering might be to increase the local concentration of replisome components. By bringing all these replication origins into close proximity, the efficiency of replication initiation can be increased, since the limited pool of initiation factors can be concentrated to these discrete sites and, therefore, facilitate the early firing of the clustered origins. Furthermore, this might also be particularly helpful for coping with replication

stress or fork stalling within this replication factory, since the initiation factors could be efficiently recycled to a neighbouring replication start site and otherwise dormant origins could be activated in order to finish replication of the whole genomic region within the replication factory (Natsume and Tanaka, 2010).
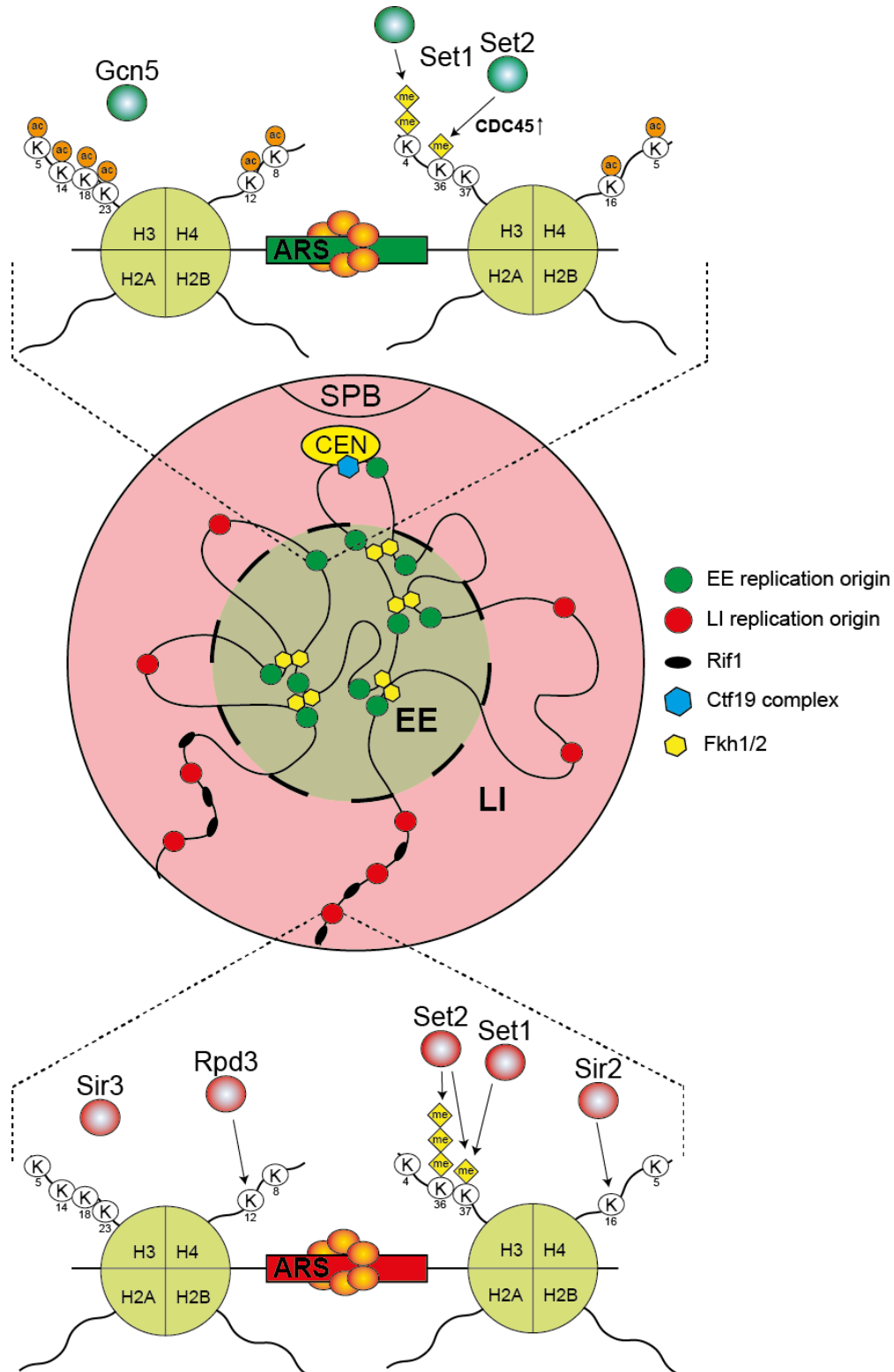
Figure 4 Spatial organization and histone PTMs of replication origins in *S.cerevisiae* The center cartoon displays the typical organization of a yeast chromosome in the nucleus with EE origins clustering in the center and LI origins preferentially located in the nuclear periphery. Top and bottom cartoons summarize known histone PTMs preferentially associated with EE or LI origins together with their corresponding writers (see main text for details).

Together, these findings demonstrate that a variety of different processes are regulating origin firing. However, because of this complex interplay, the exact mechanism of how the properties of a single, distinct origin are determined is still missing. The predominant hypothesis still proposes that the local chromatin structure and the associated proteome are a decisive factor for origin firing. In order to test this hypothesis, a holistic approach would be desirable to thoroughly study a selected replication origin in its complete chromatin context, including nucleosome positioning, histone PTMs and proteomic composition. To perform such an analysis, the replication origin would need to be isolated from the genome and subsequently purified for further unbiased analyses. Fortunately, over the last years many different methods have been developed in order to achieve such a difficult biochemical task.

3.2   Single-locus chromatin isolation

The dynamics of chromatin remains an active field of research. The chromatin structure within the whole genome is highly heterogeneous by itself, but also highly dependent on other factors like cell type or cell cycle state. Importantly, the chromatin structure at specific loci is thought to dictate functionality of the underlying genetic element such as transcription units, enhancers or replication origins. However, a detailed understanding how chromatin regulates genomic function of these diverse elements remains a much sought-after question of biology.

One major strategy to correlate chromatin states with genomic function is the use of ChIP-Seq or Cut&Run techniques to map the occurrence of specific proteins or histone PTMs (Johnson et al., 2007; Skene and Henikoff, 2017). Subsequently, this data can then be correlated with genomic processes, e.g replication initiation. However, such a strategy is not only heavily dependant on *a priori* knowledge of which factors to target, but also on the availability of specific antibodies, rendering such approaches suboptimal for examining local chromatin structures in an unbiased manner. Therefore, instead of using genome-wide strategies, purification of a specific locus of interest from the genome and then follow up with a compositional analysis of associated protein factors and histone PTMs would be desirable. Unfortunately, despite huge efforts in the field, such a locus-specific chromatin purification still remains a challenging task taking into account the following considerations.

First, the method must be able to generate soluble chromatin while at the same time minimizing the loss of any locus-interacting proteins during the purification process. Second, the method must be capable of specifically target and efficiently purify the locus of interest. This is not a trivial task, since the locus of interest might represent only a very small fraction of the large genome. Thus, the method of choice must be able to reliably discriminate between the target and the rest of the genome. Finally, the relative abundance of the purified chromatin locus compared to the rest of the genome must be sufficiently high. This is crucial, since any contaminating part of chromatin from the whole genome that is not derived from the targeted

region will contribute to a higher background and, thus, decrease the confidence of possible identified factors in follow-up analyses (Vermeulen and Déjardin, 2020).

There has been a variety of different approaches, which attempted to overcome these biochemical challenges by different experimental strategies, model organisms and cell types (reviewed in (Gauchier et al., 2020)). The next section will give an overview of some of these methods developed for chromatin purification specifically in *S.cerevisiae* as the most relevant techniques for this work.

3.2.1 Direct hybridization of capture probes to chromatinized DNA

One general strategy utilizes DNA sequence specificity in order to isolate distinct chromatin domains from the genome. In yeast this approach was introduced as "hybridization capture of chromatin-associated proteins for proteomics" or in short HyCCAP. The steps in this assay involve first crosslinking using formaldehyde in order to covalently bind proteins at the region of interest. After cell lysis, the samples are sonicated into smaller chromatin fragments followed by the hybridization capture using desthiobiotin oligonucleotides against the targeted genomic locus with streptavidin beads. After an elution step, the samples can then be used for mass spectrometric analyses in order to determine their protein composition (Johnson et al., 2007; Kennedy-Darling et al., 2014).

One advantage of this method is that there is no need for genetic engineering of the yeast strains, which makes it very fast, easy to use, and widely applicable to any targeted region in the yeast genome. However, there are also two minor disadvantages. First, the crosslinking step is absolutely required due to the heating step that denatures the DNA before hybridization of the capture probe. Thus, native chromatin for subsequent functional analysis cannot be isolated with this method. Second, due to the sonication step for chromatin solubilization, there is a large heterogeneity in the size of the targeted genomic fragments, which limits the resolution of the assay to precisely pinpoint where identified factors are bound at the target region.

3.2.2 Purification based on the binding of sequence-specific proteins

Instead of using DNA sequence as a unique property for selectively purifying a region of interest from the genome, an alternative is the use of proteins that are tightly bound to the locus of interest. However, since it is unlikely that an endogenous protein exclusively binds only one specific region,a few methods have been developed to overcome this problem. One of them utilizes the DNA binding domain of a transcription-activator-like effector (TALE) protein which can be engineered to target essentially any DNA sequence in the genome (Joung and Sander, 2013). Subsequently, the TALE protein can be immunoprecipitated in order to retrieve the associated chromatin of the targeted region. This method was used, for example, to purify telomeric chromatin in crosslinked conditions (Fujita et al., 2013), but also to purify the single

copy locus of the GAL1 gene, which was performed under native conditions (Byrum et al., 2013).

A very similar approach, instead of using a TALE protein, makes use of specifically introduced exogenous protein binding sites next to the region of interest. For this purpose, studies in yeast have mostly used a cluster of bacterial LexA binding sites, but also Lac-operator and Tet-operator binding sites have been show to be functional in yeast and should also work for chromatin isolation. After expression of the respective LexA, Lac repressor or Tet-repressor adapter protein, the heterologous protein will associate with the introduced protein binding sites, allowing for the immunoprecipitation of the adapter protein and, therefore,copurification of the target chromatin region. Using the LexA system, this chromatin affinity purification with mass spectrometry (ChAP-MS) approach could analyze the single-copy GAL1 genomic region regarding its chromatin context (Byrum et al., 2012).

One disadvantage that all of the described methods so far share is the use of sonication prior to the affinity purification. This will always yield heterogeneous fragment size distributions. To overcome this limitation, recombination sites for the site-specific R-recombinase (RS sites) from *Zygosaccharomyces rouxii* were integrated on both ends of the targeted genomic region in addition to the lexA protein binding sites. Induced expression of this R-recombinase leads to the excision of the target region in form of chromatin circles that can subsequently be purified utilizing the LexA protein. Following this RS-LexA strategy provides more flexibility in terms of the purification of well-defined regions of any size. This was shown by not only the purification and analysis of a single copy locus gene, PHO5, but also of the 9.1kb multicopy rDNA locus (Griesenbeck et al., 2003; Hamperl et al., 2014).

In this work, the RS-LexA strategy was applied to purify selected early-efficient and late-inefficient replication origins. Following up with mass spectrometry, the chromatin composition of these respective origins was analyzed in order to determine differences within these distinct classes of replication origins. One of the most exciting novel findings using this approach was that microtubule-related proteins are regulators of replication timing. Namely, we identified subunits of the microtubule-encircling Ask1/DASH complex that co-purified with specific replication origins. Using genetic and pharmacological perturbations, we established Ask1/DASH as a new *bona fide* replication timing factor that regulates more than 100 replication origins in the yeast genome. Conceptually, Ask1/DASH could provide the structural framework for sub-nuclear rearrangement of origins into early-efficiently firing replication factories and explain how this movement of individual genomic loci is physically achieved through the selected attachment of microtubules at specific origins. Thus, our unbiased proteomic approach revealed a novel connection between replication timing, chromosomal organization and the microtubule cytoskeleton.

4   Results

4.1   DNA sequence elements of yeast replication origins do not correlate with their replication timing and efficiency

To investigate replication origin characteristics that could dictate replication timing and efficiency, I focused my efforts on four selected replication origins located on yeast chromosome III. As parameters which origins to choose, the selected origins should have an intrachromosomal position with at least 40kb genomic distance to telomeric and centromere regions, so that the specialized chromatin landscape and origin regulation pathways present at these locations (see also Introduction) are not taken into account in this project. Importantly, there should also be major differences in the replication timing and efficiency properties between the selected four origins. Ultimately, ARS305 and ARS315, which are early-replicating and efficient origins (EE), as well as ARS313 and ARS316, which represent late-replicating and inefficient origins (LI) were chosen. These origins also differ in the size of their nucleosome-free region and the distribution and number of ACS, eACS, B1, B2 and B3 consensus motifs (**Figure 5**).
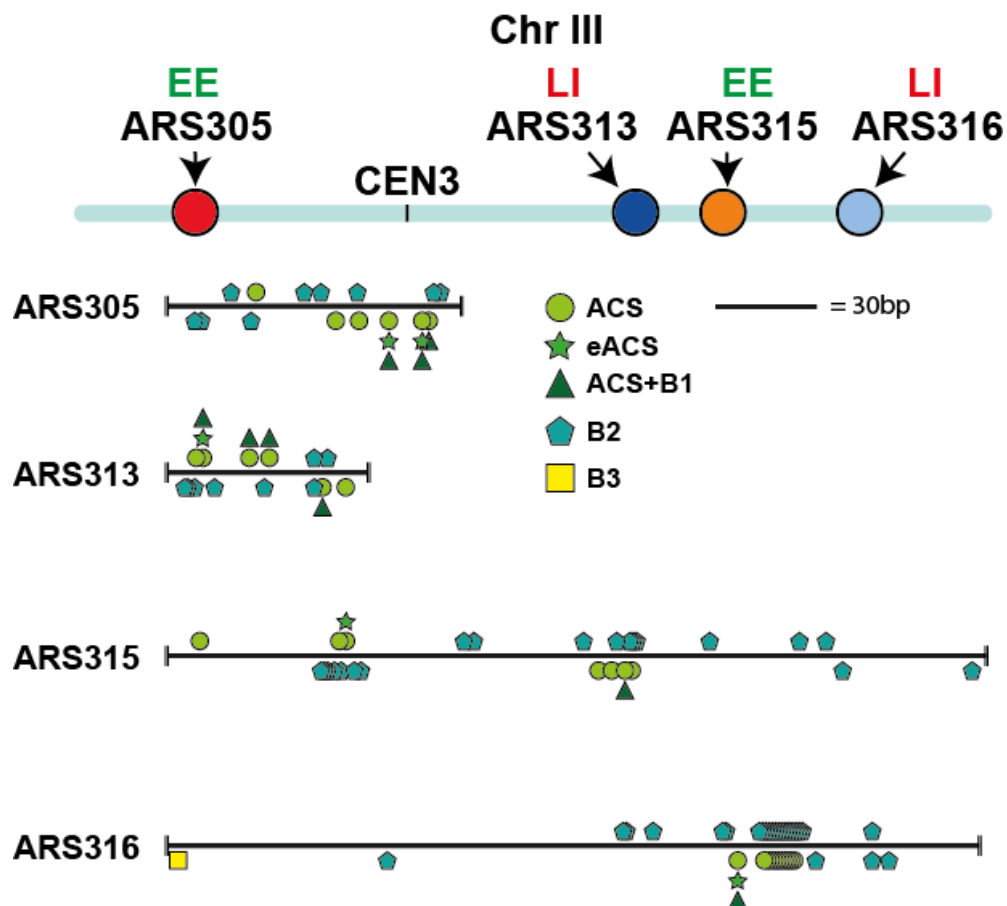
Figure 5 Chromosomal features of the Early-Efficient (EE) replication origins ARS305 and ARS315, as well as the Late-Inefficient (LI) replication origins ARS313 and ARS316 on Chromosome III of *Saccharomyces cerevisiae.* The cartoon shows the presence and location of distinct genomic sequences (ACS, eACS, B1, B2, B3) at each of the respective replication origins.

As most of the described DNA elements interact with the core licensing machinery, a primary function of these modular elements could be to efficiently guide ORC and MCM complexes during origin licensing and therefore preferentially affect *bona fide* pre-RC formation in G1 phase. Therefore, I first set out to systematically characterize the abundance of ACS, eACS, B1, B2 and B3 consensus motifs in all 352 annotated yeast origins. Each individual ARS was scanned and the occurrence of the five consensus motifs was counted, allowing for up to two mismatches for each motif instance. Additionally, the flanking 200 bp upstream and downstream of the ARS were included for the motif search of B3 elements, as Abf1 binding outside of the nucleosome-free core region was previously described at specific origins like ARS318 (Chang et al., 2008) (**Figure 6**).

Motif	Sequence	Number of mismatches allowed	Sequences found
ACS		2	2949
EACS		2	264
ACS+B1		2+0	718
B2		1	6332
B3		1	234

Figure 6 Number of DNA sequence features across all origins in the genome of *Saccharomyces cerevisiae.* 352 annotated yeast origins (Saccharomyces Genome Database (SGD)) were searched for the presence of specific DNA elements (ACS = WTTTAYRTTTW, eACS = WWWWTTTAYRTTTWGTT, ACS+B1 = WTTTAYRTTTWnnnnnnnnnnnnnnnnnnWTW, B2 = ANWWAAAT, B3 = TnnCGTnnnnnnTGAT). The table indicates the number of the respective consensus sequences found based on the number of allowed mismatches. The DNA sequence logo shows the base distribution of the consensus sequences found at the 352 annotated replication origins.

I asked as to whether the presence of these motifs might affect origin properties such as replication timing and efficiency. To this end, publicly available replication timing data for all 352 origins (Raghuraman et al., 2001) and 215 origins where replication efficiency data were available (McGuffee et al., 2013a) were correlated with the number of single DNA motifs at each origin. There were no statistically significant correlations with any of the DNA motifs that were tested (**Figure 7**).

Figure 7 DNA sequence features of yeast replication origins do not correlate with their replication timing and efficiency. **A)** The frequency of the respective DNA motifs at each origin was correlated with the known replication timing of each individual origin (Raghuraman et al., 2001). r = Spearman's Correlation Coefficient, p = p-value **B)** Similarly, the frequency of the respective DNA motifs was also correlated to available replication efficiency data (McGuffee et al., 2013b). r = Spearman's Correlation Coefficient, p = p-value

Based on this analysis, it was concluded that the timing and efficiency properties of replication origins are unlikely to be dictated by these DNA elements in isolation, strengthening the hypothesis that the local chromatin structure or other factors may be more decisive than the DNA sequence properties.

4.2 Purification of selected replication origins utilizing the RS-LexA site-specific recombination system

In order to determine the local chromatin structure at replication origins, the RS-LexA site-specific recombination approach was utilized. This allows for purification of distinct chromosomal loci in their native chromatin context as described in section 3.2.2.

4.2.1 Establishment of yeast strains competent for site specific recombination at selected replication origins

To investigate the interactome of the selected EE (ARS305 and ARS315) and LI origins (ARS313 and ARS316), a library of yeast strains, where each of the selected ARSs was tagged with RS sites and LEXA binding sites, was constructed. The RS/LEXA-RS cassettes were inserted at increasing distances from the ARS, such that the excised circular chromatin domains include the first one, two or three pairs of nucleosomes centered around the ACS (**Figure 8**).
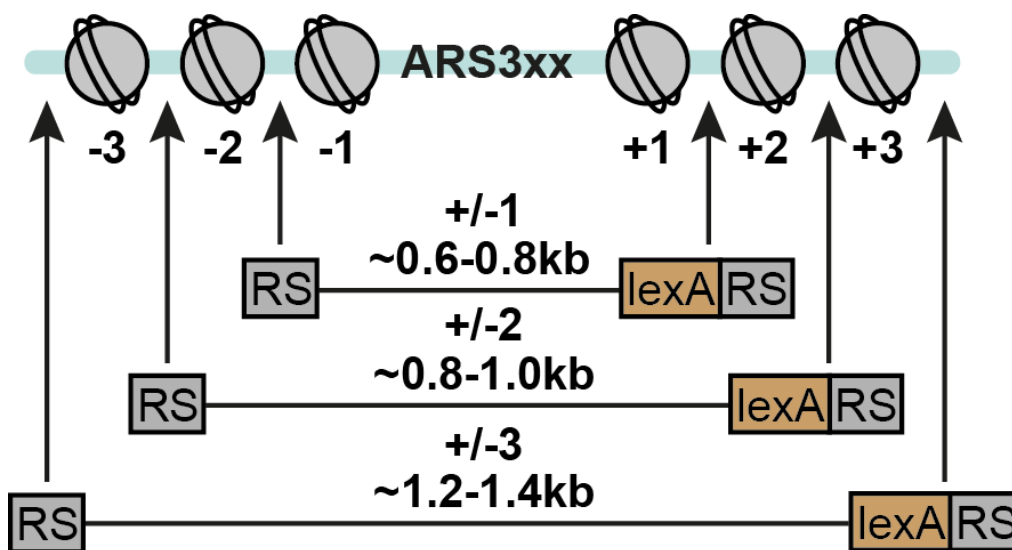
Figure 8 Schematic representation of the created strains that are competent for site specific recombination. For each origin depicted in **Figure 5**, multiple strains were created with the recombination sites integrated after either the first (+/-1), second (+/-2), or third (+/-3) pair of nucleosomes around the origin.

4.2.2 Chromatin purification of ARS305 shows low efficiency in strains expressing LexA-TAP under the control of the CYC1 promoter

To isolate the origins in the context of larger chromatin domains including the first 3 positioned nucleosomes on both sides of the origin, the biochemical purifications were focused on the ARS3xx+/-3 strains (**Figure 8**).

These ~1.2-1.4kb chromatin circles were purified via a two-step affinity purification protocol utilizing both the protein A and Calmodulin-binding protein moiety of the LexA-TAP fusion protein (**Figure 9**). As an affinity matrix, I used magnetic beads coupled to rabbit IgGs for the first purification step or magnetic beads coupled with calmodulin for the second purification step. As a negative control, the purification was performed from an isogenic strain that expresses the LexA-TAP fusion protein but lacks integrated RS and LEXA-binding sites. Importantly, the constitutive, but weak CYC1 promoter controls expression of LexA-TAP in these strains.
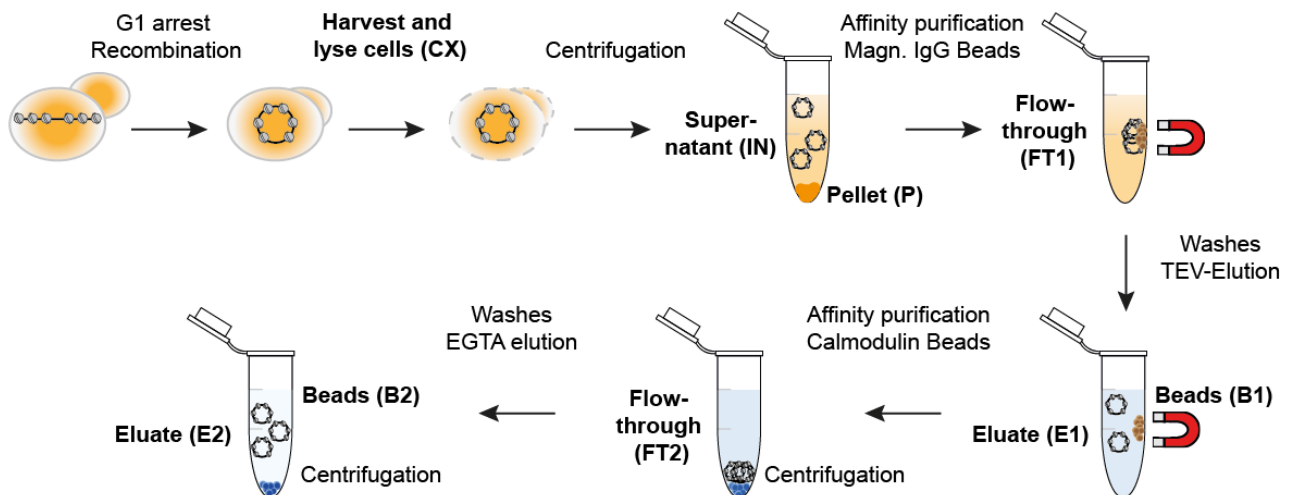
Figure 9 Experimental outline for purifying chromatin rings using the site-specific recombination system.

In an initial attempt, I attempted to purify the replication origin ARS305 using the ARS305+-3 strain. Western blot analysis using an α-PAP antibody recognizing the Prot A-component of the LexA-TAP fusion protein showed near-complete depletion of LexA-TAP in the flowthrough (**Figure 10A**). However, only 50% of the LexA-TAP molecules were cleaved during the first elution step E1 by Tobacco Etch Virus (TEV) protease, showing the expected size of the protein A moiety (15.5 kDa) that was still bound to the IgG-coupled affinity beads (B1). The other 50% of molecules were not cleaved and remained bound as full-length LexA-TAP protein in the bead fraction (81,3 kDa, B1).

The Western blot analysis was repeated with an α-CBP antibody to also monitor LexA-TAP during the second affinity purification step using Calmodulin beads. (**Figure 10B**). As expected, there was a clear depletion of the LexA-TAP fusion protein in the flowthrough 1 (FT1) from IgG

magnetic beads visible (low exposure). Additionally, the α-CBP antibody could also visualize the remaining LexA-CBP fragment after cleavage of the protein A moiety. Despite some losses during the second affinity purification step, LexA-CBP could be clearly detected in the last eluate fraction E2, suggesting successful consecutive affinity purification of this adapter protein.
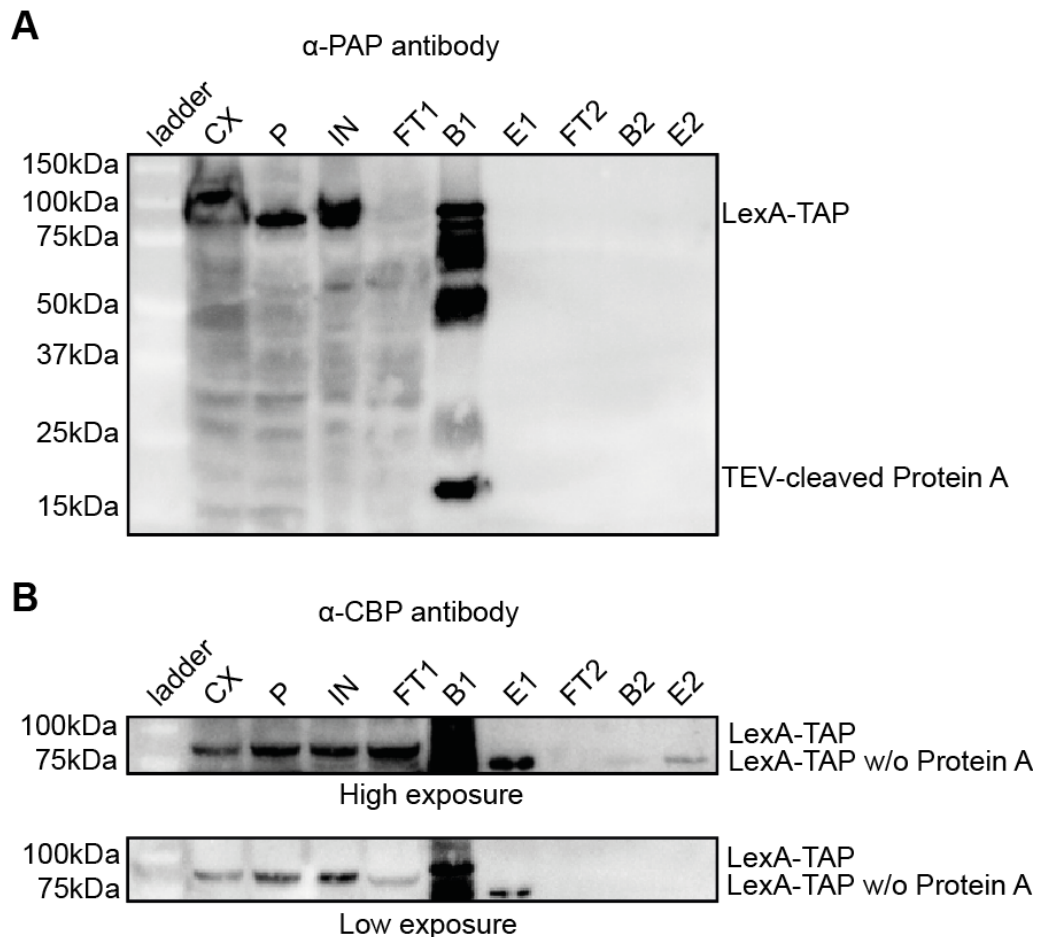
Figure 10 Western blot analysis of the initial ring purification A) The LexA affinity purification performed for yeast strain Y0037 (ARS305+/-3). Protein samples were taken for each of the fractions of the purification process shown in **Figure 5** (0.05% for Cell Extract (CX), Pellet (P), Input (IN), Flowthrough (FT1) and 2.5% for Beads (B1 and B2), Flowthrough (FT2) and Elution (E1 and E2)) and subsequently applied on a SDS polyacrylamide gel in order to follow the presence of the LexA protein during the purification by Western blotting. The applied anti-PAP antibody recognizes the Protein A moiety of the LexA-TAP protein (n = 1). **B)** The LexA affinity purification performed for yeast strain Y0034 (Control), a strain that also expresses LexA and R-Recombinase, but does not contain any recombination sites in the genome. Protein samples were taken for each of the fractions of the purification process shown in **Figure 5** (0.05% for Cell Extract (CX), Pellet (P), Input (IN), Flowthrough (FT1) and 2.5% for Beads (B1 and B2), Flowthrough (FT2) and Elution (E1 and E2)) and subsequently applied on a SDS polyacrylamide gel in order to follow the presence of the LexA protein during the purification by Western blotting. The applied anti-CBP antibody recognizes the CBP moiety of the LexA-TAP protein (n = 1).

However, the western blot analysis alone is not sufficient to verify successful chromatin purification. One possibility is that the LexA-TAP protein is successfully purified but the

interaction with desired chromatin domains is lost during the biochemical isolation. To address this concern, I isolated DNA from each of the different fractions of the purification from both control and ARS305 ring strain and performed qPCR analysis using primers against the replication origin ARS305. This analysis revealed that during the first purification step the majority of the ARS305 chromatin rings was already lost in the flowthrough.

Consequently, only about 1% of the chromatin rings were recovered in the eluate E1. However, the second purification step using calmodulin worked as expected, resulting in no additional major losses of the remaining 1% of ARS305 rings. As a control, I also tested for the unrelated genomic PDC1 locus, expecting this region not to be enriched over the course of the purification. Accordingly, this locus was quantitatively lost in the flowthrough fraction. In the control strain, recovery of ARS305 was not expected, since there were no LEXA binding sites for the LexA-TAP fusion protein present. Consequently, ARS305 behaved similar to PDC1 and was quantitatively lost in the flowthrough (**Figure 11**).
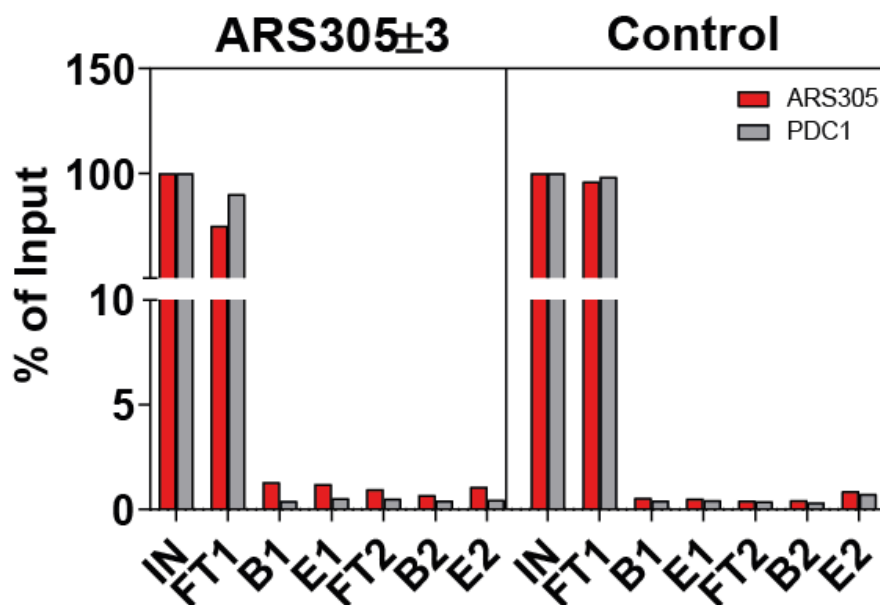
Figure 11 qPCR analysis of the different fractions of the initial ARS305 ring purification. LexA affinity purifications was performed for Y0037, a strain proficient for site-specific recombination of the targeted replication origins ARS305(+/-3), side-by-side with the purification from the control strain (Y0034). DNA samples of affinity purifications were taken (0.1% for CX, P, IN, FT and 5% for B and E). DNA was extracted and analyzed by qPCR in order to monitor the enrichment of the targeted replication origins as well as an unrelated genomic region (PDC1) during the purification process (n = 1 biological replicate).

Additionally, the enrichment of ARS305 compared to the PDC1 locus in each of the different fractions was determined. The strongest enrichment of ARS305 was observed in the bead fraction of the first purification step (> 200,000-fold), suggesting that a majority of ARS305 chromatin rings remained bound to the beads despite 50% cleavage efficiency by TEV protease. The second purification step increased the purity of ARS305 chromatin rings, leading to a 21000-fold enrichment over PDC1 in the final eluate, corresponding to a 1.75-fold

excess over any other genomic DNA in the purified material (**Figure 12A**). Therefore, about ~63% of the DNA molecules in this final sample is derived from the targeted ARS305 locus (**Figure 12B**). As expected, there was no observation of any ARS305 enrichment in the control purification (**Figure 12A**). Overall, with only a 1% recovery of the ARS305 chromatin rings and a 21000-fold enrichment over PDC1, it seemed that improvements to the efficiency of this initial purification were mandatory.
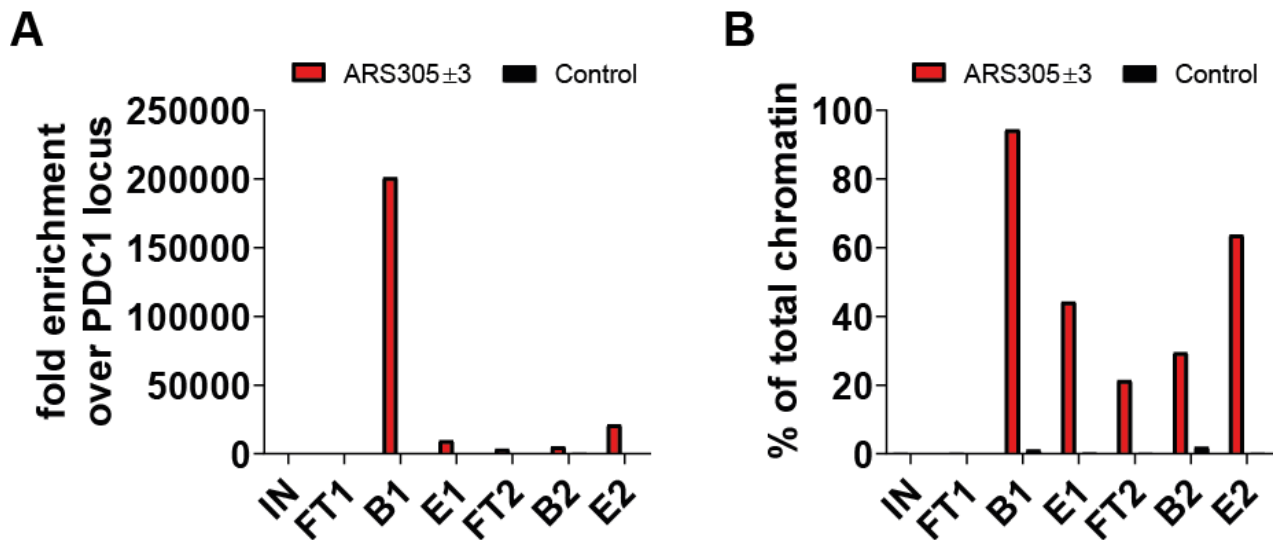
Figure 12 Enrichment of the chromatin rings during the initial purification of ARS305 A) Using the samples from **Figure 11**, the fold enrichment of the indicated fractions compared to the PDC1 locus was calculated (n = 1 biological replicate). **B)** Using the fold-enrichment values from A) and factoring in the size of the total yeast genome (~12,000kb), the proportion of total DNA present in the final eluates derived from the targeted replication origin domain (~ 1kb) was calculated (n = 1 biological replicate).

4.2.3 Basic elution increases the yield of ARS305 during the purification process as compared to an elution process using the TEV protease

One step in the purification process that did not work sufficiently was the elution using TEV protease, since 50% of the LexA-TAP protein was not cleaved and remained bound to the affinity beads. In order to increase the yield of this step, I switched to a basic elution method adding 0.5M NH_3, which should denature all proteins present including LexA-TAP and lead to the dissociation of the denatured LexA TAP bound chromatin rings from the affinity beads. The difference in the two approaches is visualized in **Figure 13**.
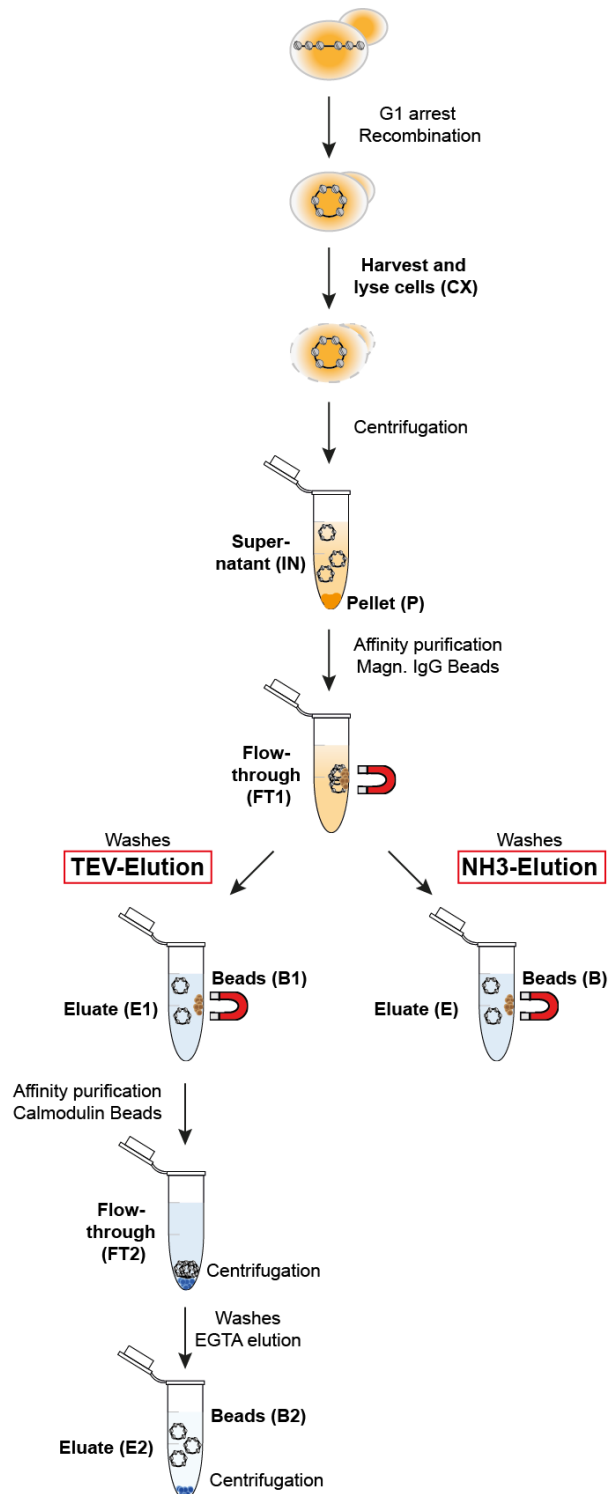
Figure 13 Experimental setup to examine the differences in purification efficiencies using either TEV-protease or NH₃ for eluting native chromatin rings Affinity purification is performed as previously described until the affinity binding of the LexA protein to the IgG beads. After binding of the chromatin domains, the beads were equally distributed to two separate elution methods either using TEV-protease or NH₃.

The purification of ARS305 chromatin was repeated. However, after the binding step of LexA-TAP to the beads, the sample was split in order to compare the efficiency of TEV elution and NH_3 elution side by side. Similar to the previous purification, DNA analysis of all fractions showed that about 3.5% of the ARS305 chromatin rings were recovered after TEV elution, which ultimately resulted in a final amount of 2% ARS305 chromatin rings after the second purification step. Importantly, eluting the LexA-TAP fusion protein with NH_3 led to a 2-3-fold improved recovery of 6% of ARS305 chromatin rings over TEV elution (**Figure 14**).
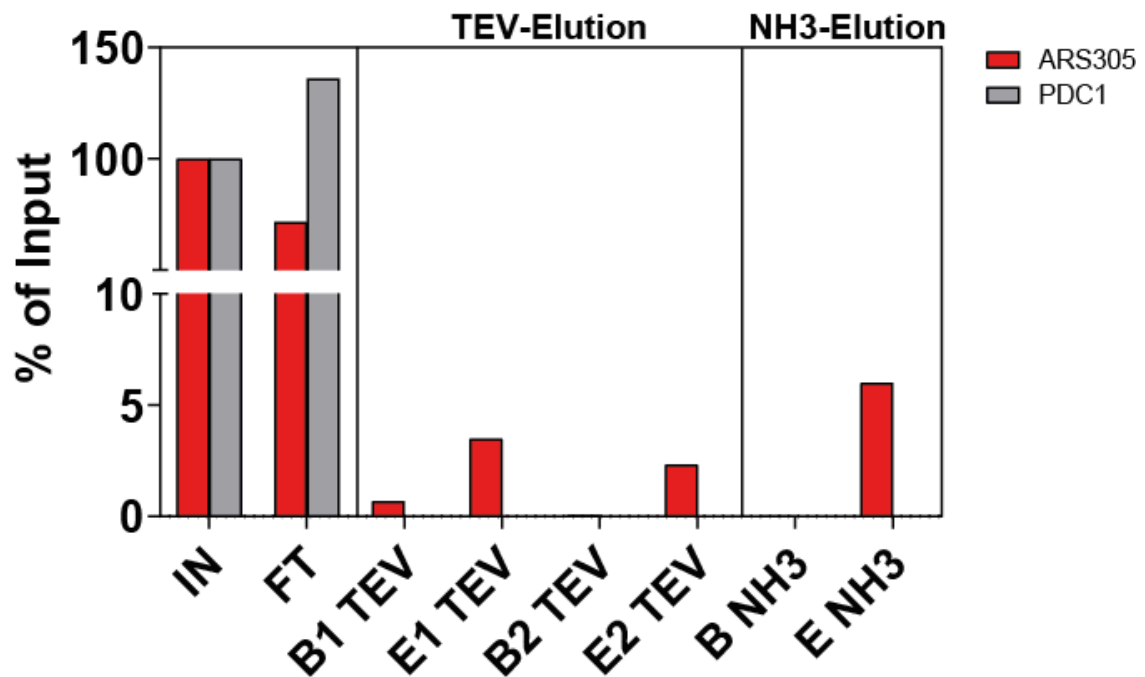
Figure 14 Comparison of the purification efficiencies using either TEV-protease or NH_3 for elution of ARS305 chromatin rings. LexA affinity purification was performed for Y0037, a strain proficient for site-specific recombination of the targeted replication origins ARS305(+/-3). After binding the chromatin rings to the IgG beads (B1), the sample was split and TEV-elution was compared side by side with NH_3-elution. DNA samples of affinity purifications were taken (0.1% for CX, P, IN, FT and 2.5% for B and E). DNA was extracted and analyzed by qPCR in order to monitor the enrichment of the targeted replication origins as well as an unrelated genomic region (PDC1) during the purification process (n = 1 biological replicate).

Strikingly, the purity of the eluates was greatly increased this time, resulting in a ~65000 and ~45000- fold enrichment of ARS305 over PDC after the first and second purification step, respectively. Importantly, elution with NH_3 resulted in a ~33000-fold enrichment of ARS305 over PDC1 and did therefore not drastically decrease the purity of the eluate. (**Figure 15A**). Thus, it can be estimated that ~73% of DNA molecules in the final sample using NH_3 elution is derived from the targeted ARS305 locus (**Figure 15B**).
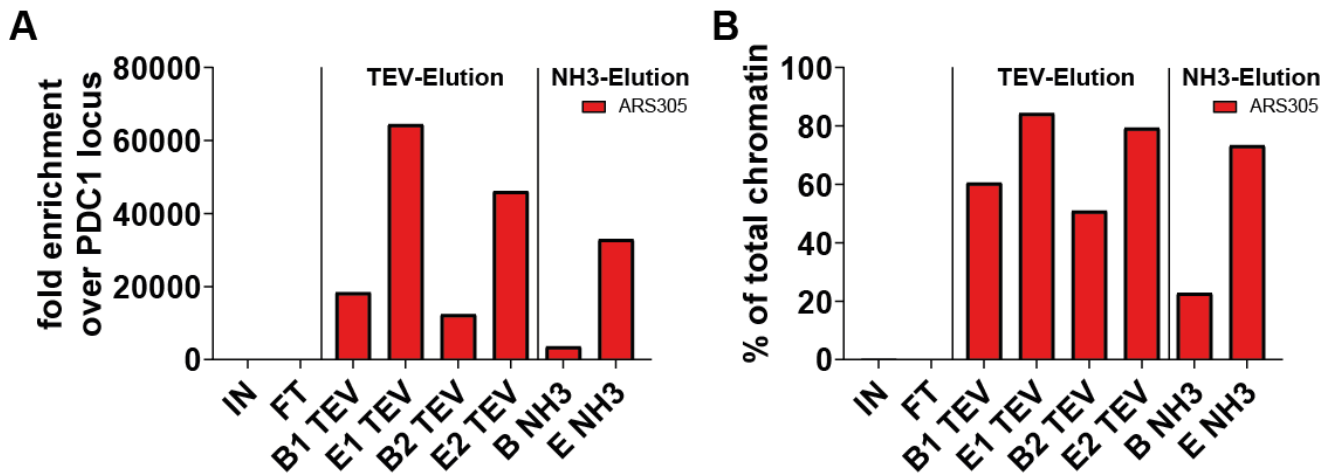
Figure 15 Comparison of the enrichment of the chromatin rings using either TEV-protease or NH₃ for elution of ARS305 chromatin rings. A) Using the eluate samples from **Figure 14**, the fold enrichment of the indicated fractions compared to the PDC1 locus was calculated (n = 1 biological replicate). **B)** Using the fold-enrichment values from A) and factoring in the size of the total yeast genome (~12,000kb), the proportion of total DNA present in the final eluates derived from the targeted replication origin domain (~ 1kb) was calculated (n = 1 biological replicate).

Altogether, this change in the elution procedure resulted in an at least two-fold increase of ARS305 recovered with no significant loss in purity, which represented a first important optimization step of the purification protocol.

4.2.4 Increasing the expression level of LexA-TAP vastly increases purification efficiency

However, despite increasing the yield two-fold, all these attempts to retrieve the target chromatin still suffered from relatively low binding efficiency to the IgG beads (compare **Figure 11** and **Figure 14**). I therefore worked out conditions to improve the yield, which was achieved by replacing the original weak promoter (CYC1) driving LexA-TAP expression by a stronger, constitutive promoter (TEF2). Western blot analysis showed that this modification increased LexA-TAP levels ~ 5 to 6-fold (**Figure 16**).
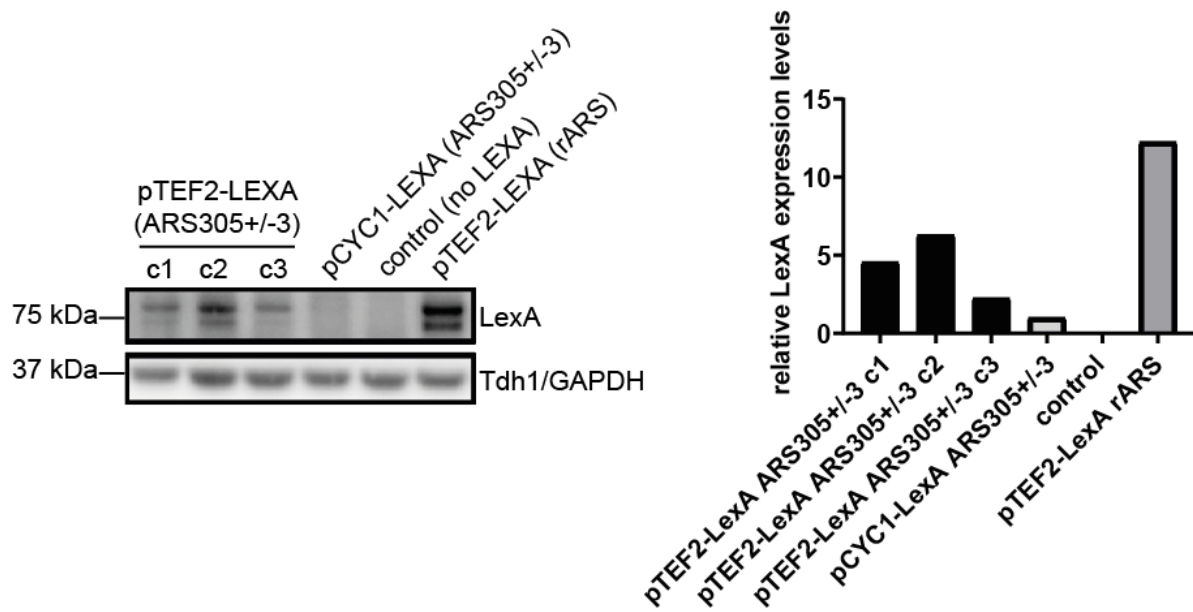
Figure 16 Western blot analysis showing promoter-mediated LexA expression levels Levels of LexA-TAP protein was examined for indicated yeast strains utilizing different constitutive promoters for LexA expression. Three independent clones of ARS305+/-3 strains (Y0065 c1, c2 and c3) as well as a strain where the ribosomal ARS (rARS) is flanked by RS sites (Y0008) utilize a TEF2 promoter for expression of LexA-TAP. Another ARS305+/-3 strain expressing LexA under control of the weak CYC1 promoter (Y0037, pCYC1-LEXA) was compared to a control strain without LexA expression (Y0034, no LEXA). Protein samples of total cell extracts were subjected to Western blot analysis using antibodies against LexA or Tdh1/GAPDH as loading control. Bar graph on the right depicts quantification of the Western blot results (n = 1).

Repeating the purification of ARS305 using both the CYC1 and TEF2 promoter strains side by side confirmed this result, as LexA-TAP levels were clearly increased in the purification samples derived from the TEF2 promoter strain. Importantly, despite the higher expression levels of LexA-TAP in this strain, LexA-TAP still binds quantitatively to the IgG affinity beads, as seen by complete depletion in the flowthrough fraction.
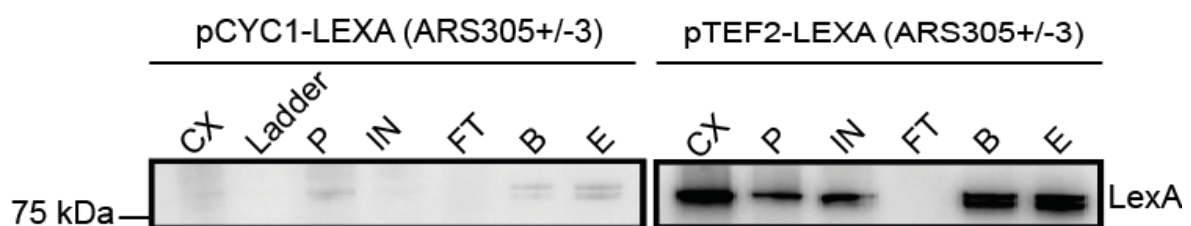
Figure 17 Western blot analysis of ARS305 chromatinring purifications using CYC1 or TEF2 promoter-mediated expression of LexA-TAP LexA affinity purification was performed for yeast strain Y0037 (ARS305+/-3) which expresses LexA-TAP under control of the CYC1 promoter as well as Y0065 (ARS305+/-3) which expresses LexA-TAP under control of the TEF2 promoter. Protein samples were taken for each of the fractions of the purification process utilizing NH_3 elution as shown in **Figure 13** (0.1% for CX, P, IN, FT and 1% for B and E) and subsequently analyzed by Western blot analysis.

Strikingly, this also markedly improved retention of the chromatin domains upon purification, giving a 3-fold higher yield of chromatin domains in the final eluate as compared to the purification with the CYC1 promoter strain. (**Figure 18A**). One concern related to the increased protein levels of LexA-TAP is that this could foster unspecific interactions with genomic chromatin resulting in higher background and reduced purification specificity. However, this was not the case, since the fold enrichment over PDC1 even increased in the TEF2 promoter strain Y65 compared to the CYC1 promoter strain Y37 (**Figure 18B and C).**
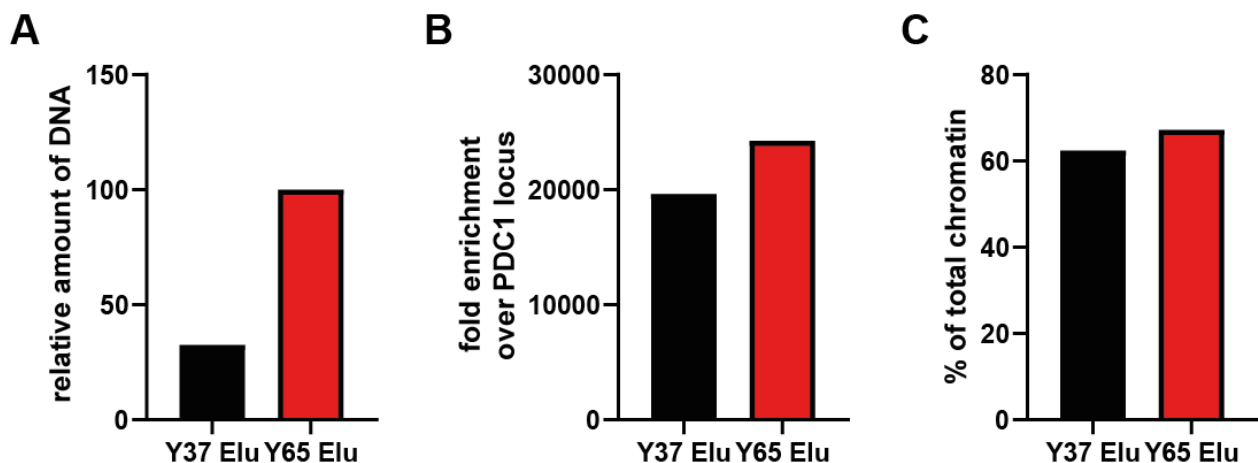
Figure 18 qPCR analysis of of ARS305 chromatin purifications using CYC1 or TEF2 promoter-mediated expression of LexA-TAP A) DNA samples from the eluates of the affinity purifications from **Figure 17** were taken (2.5%). DNA was extracted and analyzed by qPCR in order to monitor the amount of ARS305 present in the eluates (n = 1). **B)** Using the eluate samples from C), the fold enrichment of ARS305 compared to the PDC1 locus was calculated. **C)** Using the fold-enrichment values and factoring in the size of the total yeast genome (~12,000kb), the proportion of total DNA present in the final eluates derived from the targeted replication origin domain (~ 1kb) was calculated.

Altogether, switching to NH$_3$ elution combined with TEF2-mediated expression of LexA-TAP vastly improved the purification yield and efficiency.

4.2.5 The recombination process of replication origin chromatin rings is fast and efficient

Importantly, while optimizing the purification protocol, I also wanted to make sure that the generated recombination strains are suited for the analyses of chromatin structure at the respective replication origins. One important aspect is the recombination efficiency of our system, since insufficient recombination would not only lead to a decreased total amount of rings, but could also affect the purity of the samples itself. A significant amount of non-circularized ARS species in our cells would generate large randomly sheared chromatin fragments that include LEXA binding sites and could therefore display affinity to the beads and strongly affect the proteomic composition of the samples.

The recombination kinetics and efficiency under these conditions were monitored in a time-course experiment by Southern blotting of extracted genomic DNA. In all strains analyzed,

there was a near complete recombination of the targeted loci within ~60-90min after recombinase induction (**Figure 19**).
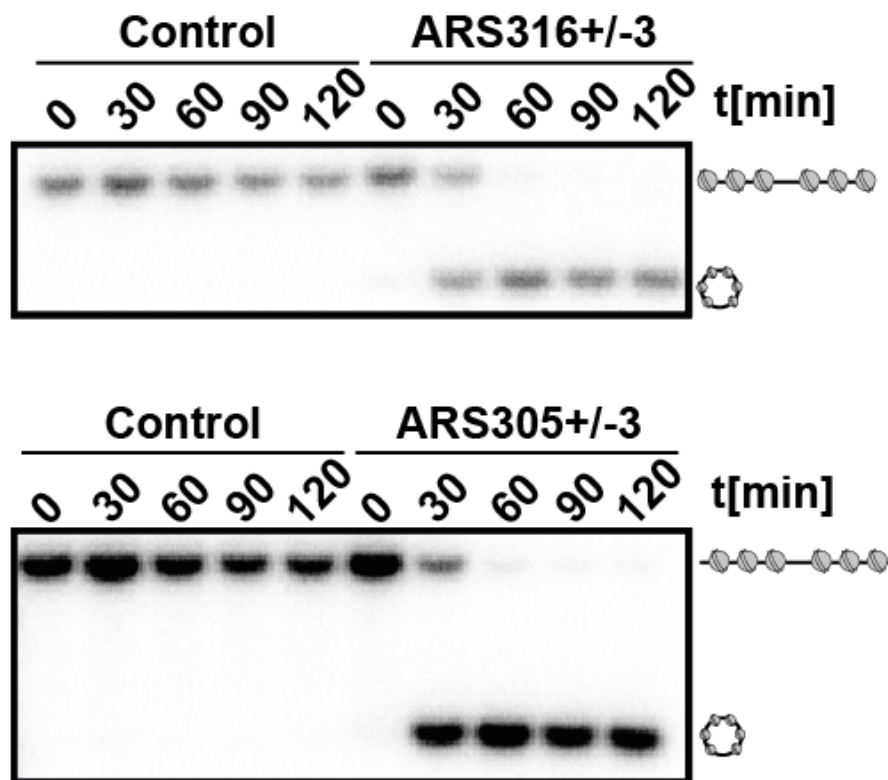
Figure 19 Characterization of the site-specific recombination kinetics using southern blot analysis Yeast strains Y0069 (ARS316+/-3) (top panel) and Y0065 (ARS305+/-3) (bottom panel) were grown in YPR medium to logarithmic phase and then arrested in G1 phase in the presence of 2% Galactose to induce recombination. Genomic DNA samples were taken at the indicated timepoints, linearized with BstBI (Y0069) or ClaI (Y0065) to allow visualization of the recombined and unrecombined genomic ARS316 and ARS305 loci by Southern blot analysis (n = 1).

The kinetics of circularization were independent of the size of the excised domain, suggesting that topological constraints were not rate-limiting even in the smallest domain encompassing only the +/-1 nucleosomes and a circular size of ~0.5kb as illustrated for the ARS316 yeast strain library (**Figure 20**).
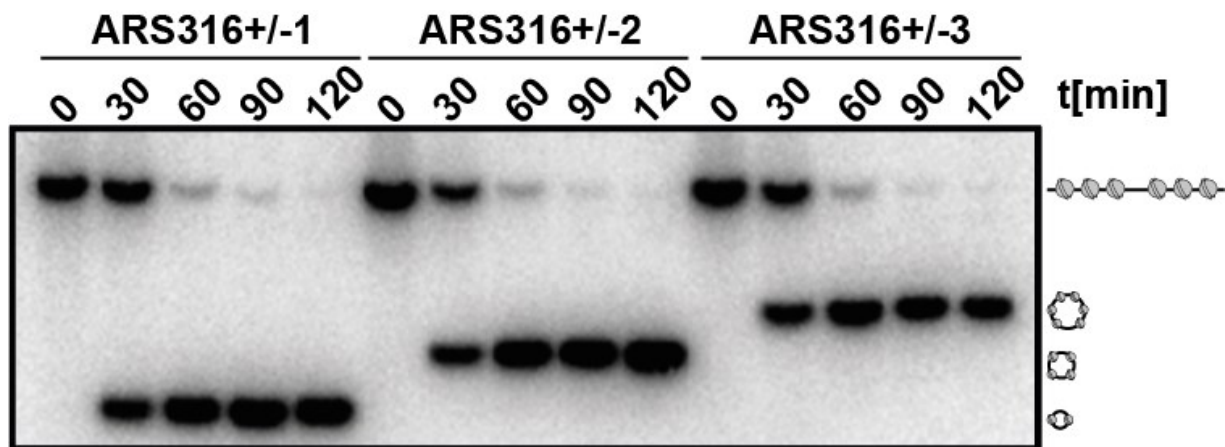
Figure 20 Dependency of the locus size on the recombination kinetics Yeast strains Y0038 (ARS316+/-1), Y0039 (ARS316+/-2), and Y0040 (ARS316+/-3) were grown in YPR medium to logarithmic phase and then 2% Galactose was added to induce recombination. Genomic DNA samples were taken at the indicated timepoints, linearized with BstBI to allow visualization of the recombined and unrecombined genomic ARS316 locus by Southern blot analysis (n = 1).

4.2.6 Alpha-factor treatment arrests the recombination strains efficiently in G1 phase

Besides the efficiency of the recombination, the stage of the cell cycle is another important aspect to be considered. It is critical to define the ARS chromatin structure present in G1 phase, as this represents the *bona fide* substrate for replication initiation in the subsequent S phase (Dimitrova and Gilbert, 1999). For this reason, the purification process of the chromatin rings always takes place in G1 arrested cells. However, I also wanted to verify efficient G1 arrest of the strains, since an incomplete arrest would again lead to different species of chromatin rings from different cell cycle stages that could change the proteomic composition of the isolated chromatin rings. Therefore, yeast strains competent for recombination of individual origin domains were arrested in G1 phase using alpha-factor, while also simultaneously inducing R-recombinase expression by addition of galactose. Successful G1 arrest was verified by FACS analysis for all replication origin strains analyzed (**Figure 21A-B**).
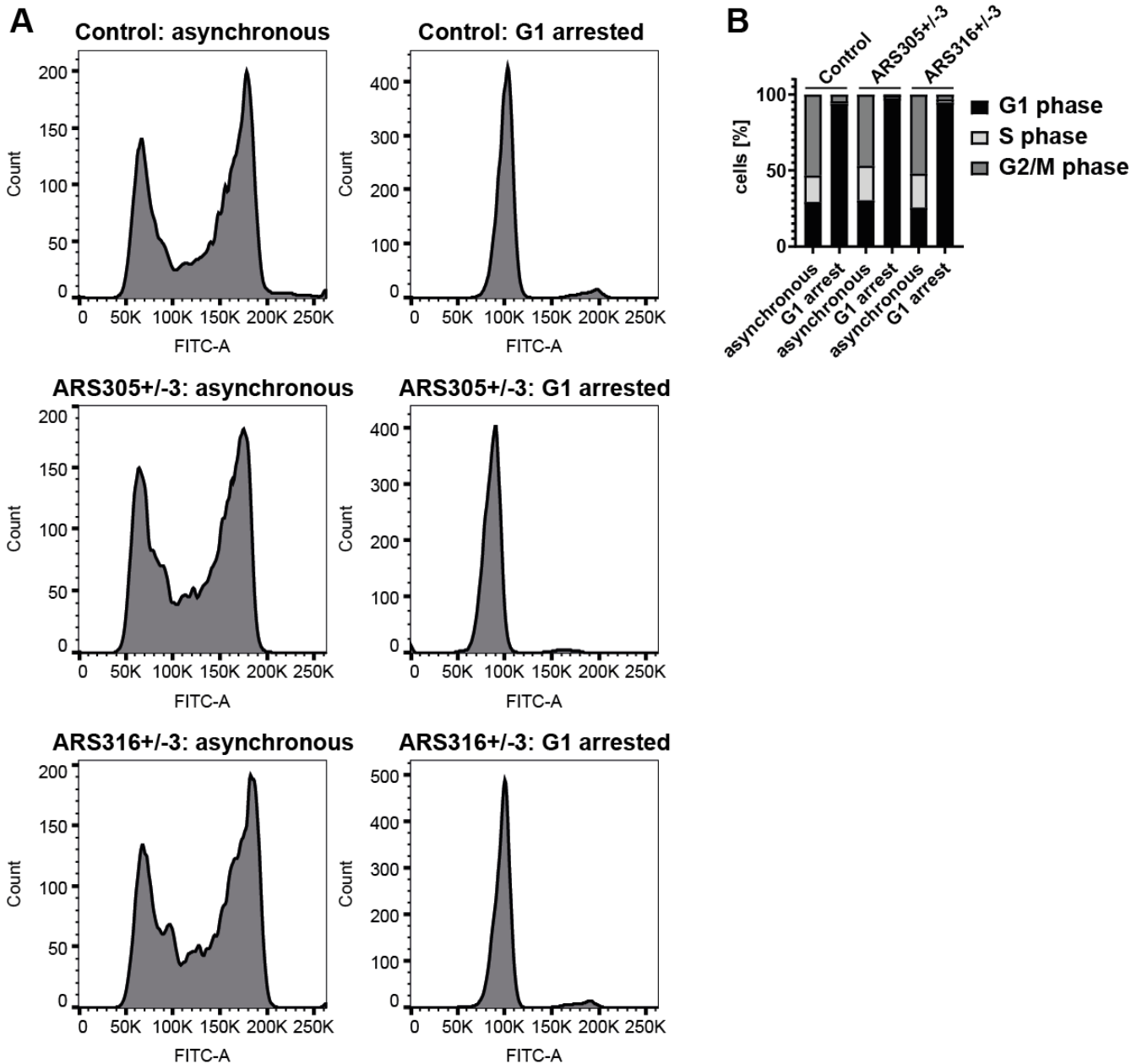
Figure 21 alpha-factor treatment arrests purification strains quantitatively in G1 phase. A) Yeast strains competent for site-specific recombination Y0065 (ARS305+/-3) and Y0069 (ARS316+/-3) as well as control strain Y0066 without RS-LEXA sites were grown to logarithmic phase. Subsequently, alpha-factor (50ng/ml) was added to the cultures. Samples for FACS analysis were taken from the asynchronous cultures as well as after 2h of alpha-factor treatment. **B)** Distribution of G1, S, and G2 phases in each of the profiles from A (n = 1 biological replicate).

4.2.7 Site specific recombination does not induce a DNA damage response that is measurable by western blotting

I also verified that the excision, which involves transient DNA breaks, did not elicit a measurable DNA damage response by monitoring global levels of γH2A phosphorylation (Kuo and Yang, 2008). The ARS305 recombination cells showed no detectable increase in γH2A levels over the time course of 2h (**Figure 22**). Thus, it can be concluded that transient excision

of the chromatin circles and re-ligation of the genomic ends does not lead to a major DNA damage response.
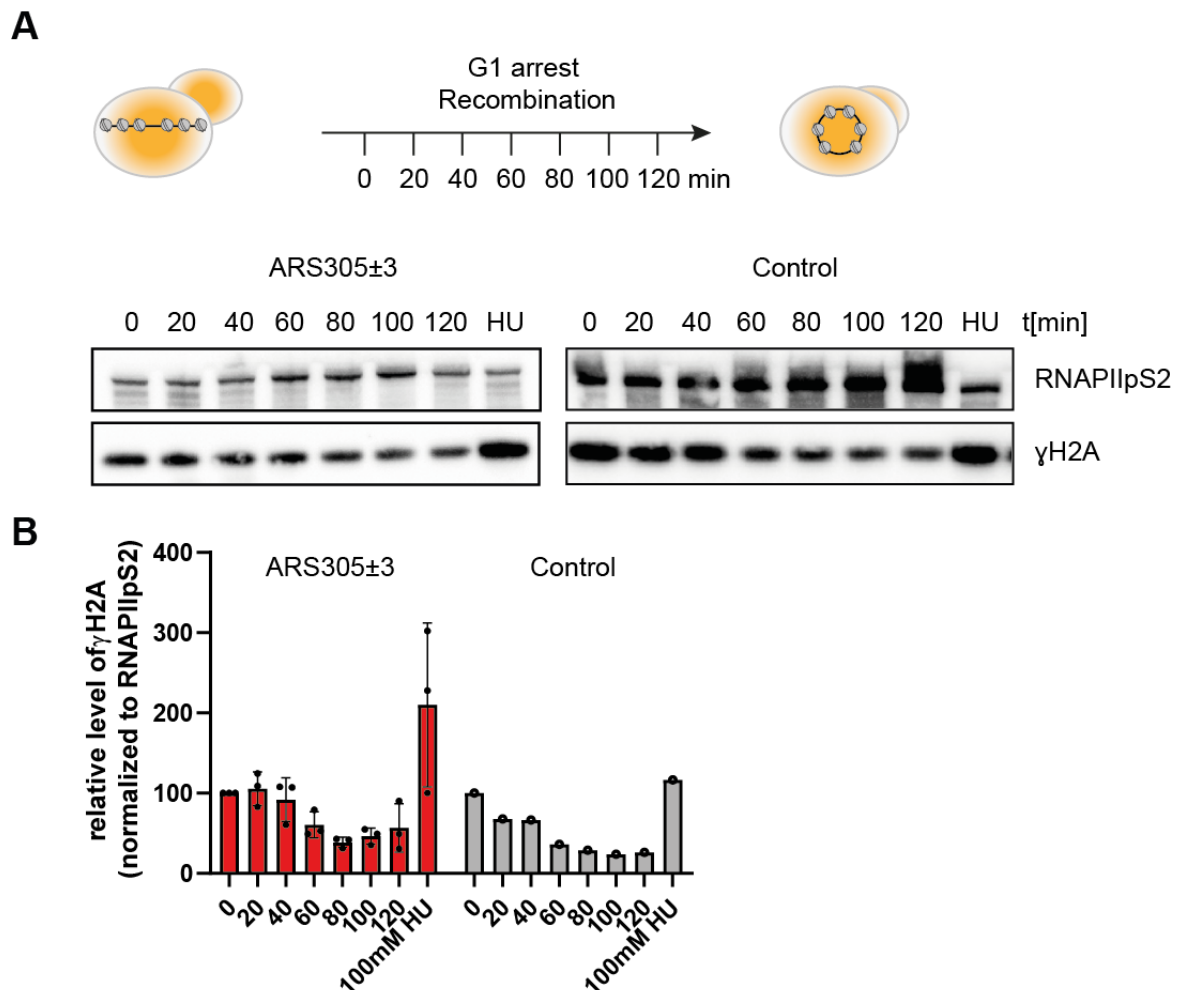
Figure 22 Site-specific recombination does not induce detectable levels of DNA damage A) Experimental outline for γH2A detection upon recombination induction. Yeast cells Y0037 (ARS305+/-3) and parental Control strain Y0034 without RS- and LEXA-binding sites were grown in YPR medium to logarithmic phase and then arrested with alpha-factor in G1 phase in the presence of 2% Galactose to induce recombination. During these two hours, protein samples were taken every 20min which were subsequently subjected to Western blot analysis. As a positive control, cells were treated with 100mM hydroxyurea (HU) for 1h. Western blot analysis using antibodies against H2ApS129 (γH2A) and RNAPII as a loading control. **B)** The bar plot shows the mean γH2A levels with standard deviation from n = 3 biological replicates for Y0037 and n = 1 biological replicate for Y0034.

4.2.8 The introduced genetic modifications do not change the replication profile of the investigated replication origins

Importantly, I verified that the necessary genetic manipulations did not interfere with origin function by comparing the replication timing of the origins in recombination strains with an isogenic control strain, using DNA copy number analysis by quantitative real-time PCR (qPCR). Cells were arrested in G1 phase with alpha-factor and synchronously released into S phase. A copy number analysis of the early-replicating ARS305 versus the late-replicating ARS316, or a late-replicating region on 9 chromosome IV (Chr4, (Batrakou et al., 2018)),

showed that both ARS305 and ARS316 loci replicated with highly similar relative kinetics in the wildtype and modified strains (**Figure 23**). The copy number of the EE region ARS305 increased from 0 to 24min after release, reflecting the earlier replication status compared to the LI origin ARS316 or a late-replicating region on Chr4. After this timepoint, replication is also initiated from the LI region and copy number ratios decrease until S phase is completed ~ 48min after release into S phase. When comparing the copy numbers of both late-replicating regions ARS316 and Chr4, the ratio only increased slightly after 32min, suggesting only a slightly increased replication at ARS316 as compared to the late-replicating Chr4 region.
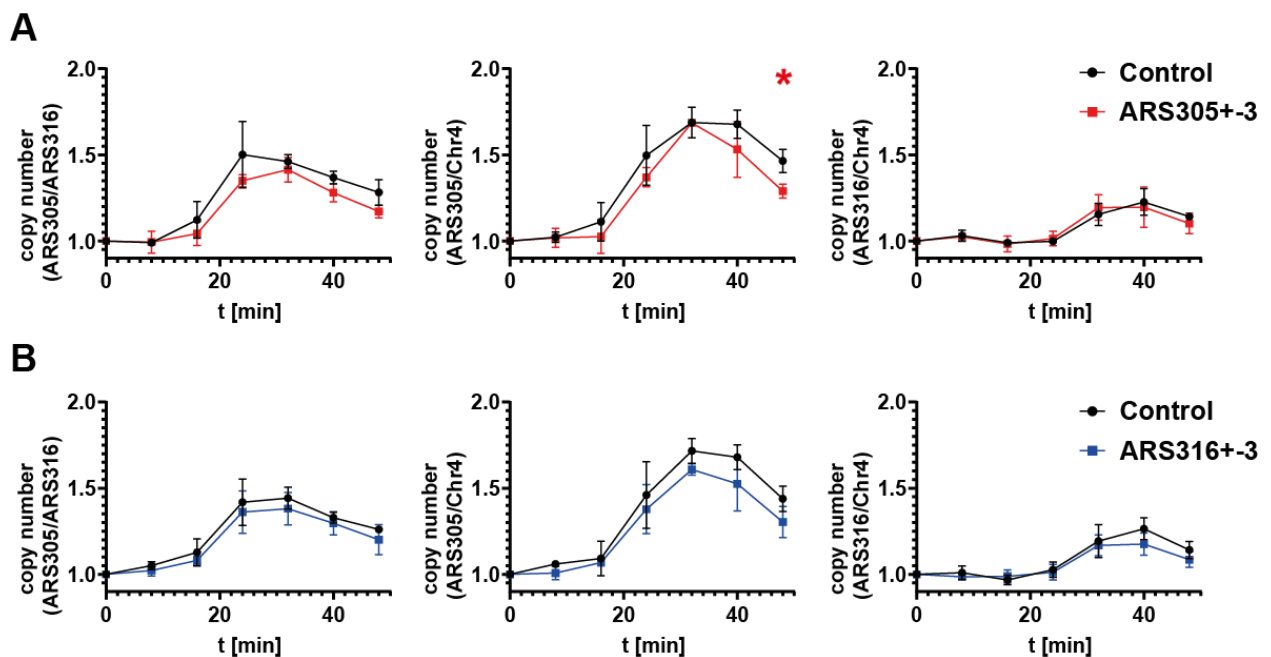
Figure 23 Integration of RS- and LexA-binding sites does not affect the replication profile of the modified origins. (A-B) Analysis of the replication timing of ARS305 and ARS316 for the strains where RS-sites and LexA binding sites were integrated next to ARS305+/-3 (Y0065) (A) or ARS316+/-3 (Y0069) (B) in comparison to a parental control strain (Y0066) that does not have RS- and LexA- binding sites integrated in its genome. Samples for genomic DNA extraction were taken at the indicated timepoints for copy number analysis by qPCR to determine the relative replication timing of depicted loci. The plots show the average copy number ratios of early (ARS305) to late-replicating regions (ARS316, Chr 4) with standard deviation from n = 3 biological replicates (* indicates statistical significance $p < 0.05$, unpaired t-test).

4.3 Mass spectrometric analysis of selected EE and LI replication origins

After the improvement of the purification system as well as the careful characterization and validation of the newly established strains, I continued to purify the selected replication origins ARS305 (EE), ARS315 (EE), ARS313 (LI), and ARS316 (LI) in order to analyze the protein composition of these origins using mass spectrometry.

4.3.1 Purifying chromatin rings for mass spectrometry works very efficiently

In these purifications, I targeted the replication origins with a surrounding area spanning the first three nucleosomes both up- and downstream of the origins (+/-3). Similar as before, a negative control purification was done side by side using a strain that does not have any integrated RS and LEXA binding sites. Western blot analysis of LexA-TAP in the different fractions showed near-complete depletion of LexA-TAP in the flowthrough and recovery in the final elution in all strains as expected (**Figure 24**).
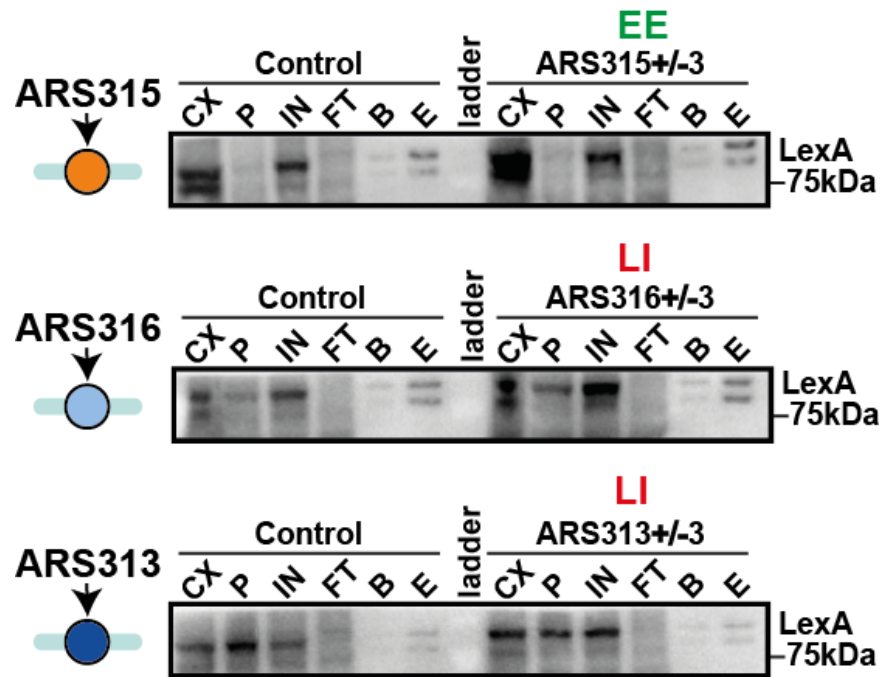
Figure 24 Western blot analysis of the chromatin ring purifications prior to mass spectrometry
The LexA affinity purification was performed for yeast strains Y0091(ARS315+/-3), Y0094 (ARS313+/-3), Y0069 (ARS316+/-3), and Y0066 (Control), a strain that also expresses LexA and R-Recombinase but does not contain RS and LEXA sites in the genome. Protein samples were taken for each of the fractions of the purification process shown in (C) (0.1% for Cell Extract (CX), Pellet (P), Input (IN), Flowthrough (FT) and 1% for Beads (B) and Elution (E)) and subsequently applied on a SDS polyacrylamide gel in order to follow the presence of the LexA protein during the purification by Western blotting (n = 1).

Similar to before, the enrichment of origin DNA in these fractions was also quantified by qPCR, where between ~20-100% recovery of the specific domains in the four recombination strains, but no enrichment in the control strain, was observed. The unrelated single copy gene locus PDC1 was similarly lost in both origin and control purifications, indicating an expected specific enrichment of our targeted loci (**Figure 25**).
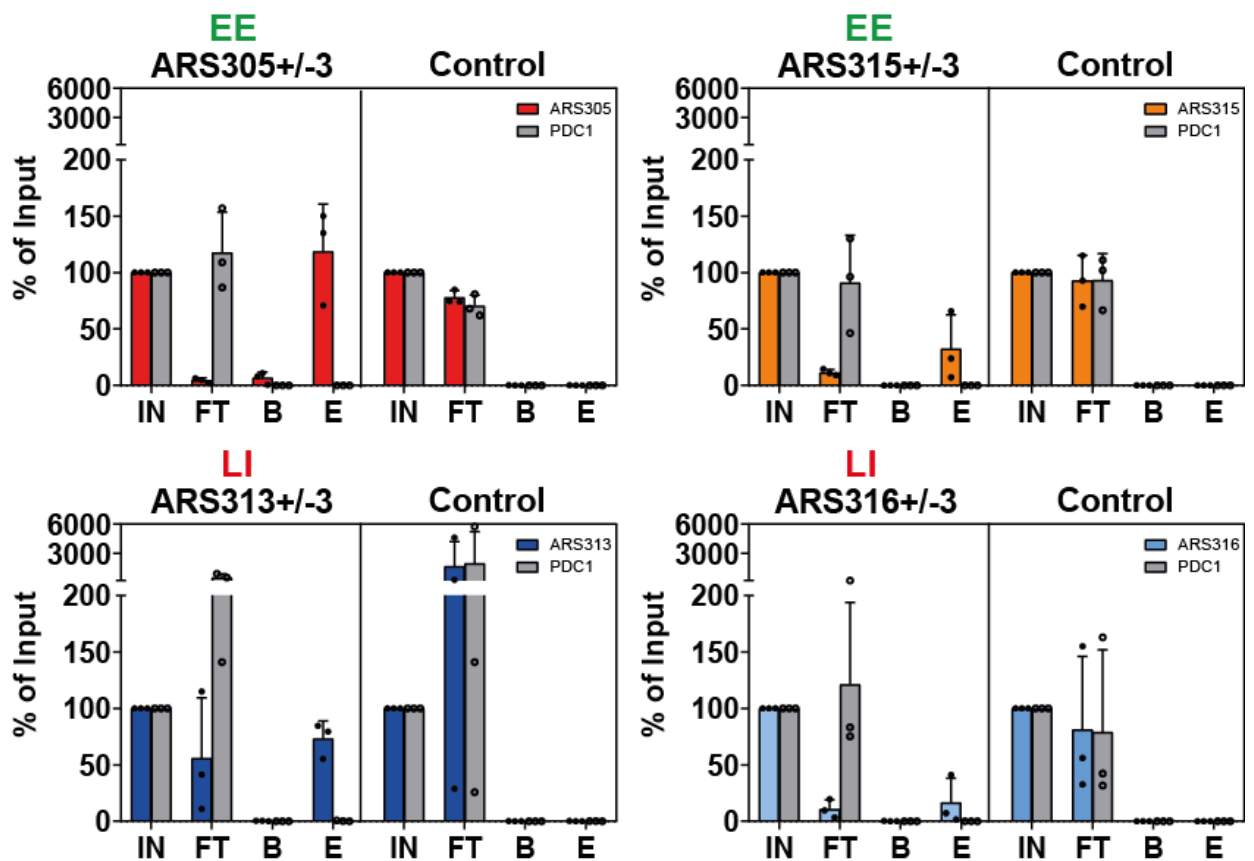
Figure 25 qPCR analysis of the different fractions of the chromatin ring purification prior to mass spectrometry LexA affinity purifications were performed for all the strains proficient for site-specific recombination of the targeted replication origins (Y0065 (ARS305+/-3), Y0091(ARS315+/-3), Y0094 (ARS313+/-3), Y0069 (ARS316+/-3)) side-by-side with the purification from the control strain (Y0066). DNA samples from 3 biological replicates of affinity purifications were taken (0.1% for CX, P, IN, FT and 2.5% for B and E). DNA was extracted and analyzed by qPCR to monitor the enrichment of the targeted replication origins as well as an unrelated genomic region (PDC1) during the purification process (n = 3 biological replicates).

Indeed, the final eluates showed at least a 40,000 – 170,000-fold excess over the PDC1 locus (**Figure 26A**), corresponding to a 15- to 20-fold excess over any other genomic DNA in the purified material. Therefore, roughly ~60-90% of all DNA molecules in these samples were derived from our targeted loci (**Figure 26B**).
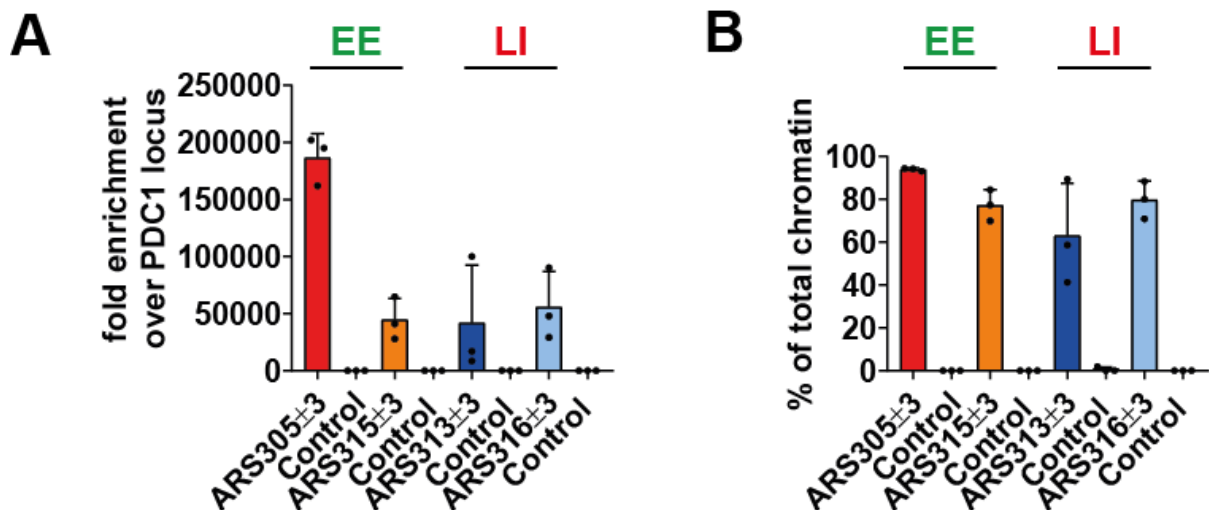
Figure 26 Enrichment of the chromatin rings during the purification prior to mass spectrometry
A) Using the eluate samples from **Figure 25**, the fold enrichment of the indicated origins compared to the PDC1 locus was calculated (n = 3 biological replicates). **B)** Using the fold-enrichment values from A) and factoring in the size of the total yeast genome (~12,000kb), the proportion of total DNA present in the final eluates derived from the targeted replication origin domain (~ 1kb) was calculated (n = 3 biological replicates).

4.3.2 Mass spectrometry reveals the proteomes of the investigated replication origins

Having established the specificity and high yield of the single-locus chromatin isolation, I next determined protein composition at individual origins using quantitative label-free liquid chromatography tandem mass spectrometry (LC-MS/MS). To this end, the proteomes derived from each EE and LI +/-3 origin purification were compared to a control purification from a strain that lacks the ability to excise and purify specific origin chromatin. For each origin, similar proteome coverages were achieved, with ~1500 to ~3000 proteins identified with more than two unique peptides from three biological replicates. To reduce potential background contaminants, I only considered protein factors that were on average at least 1.4-fold enriched over the negative control pulldowns. This arbitrary threshold resulted in 94, 29, 635, and 25 putative ARS-interacting proteins with ARS305, ARS315, ARS313 and ARS316, respectively, which were considered for subsequent systematic analysis (**Figure 27**).
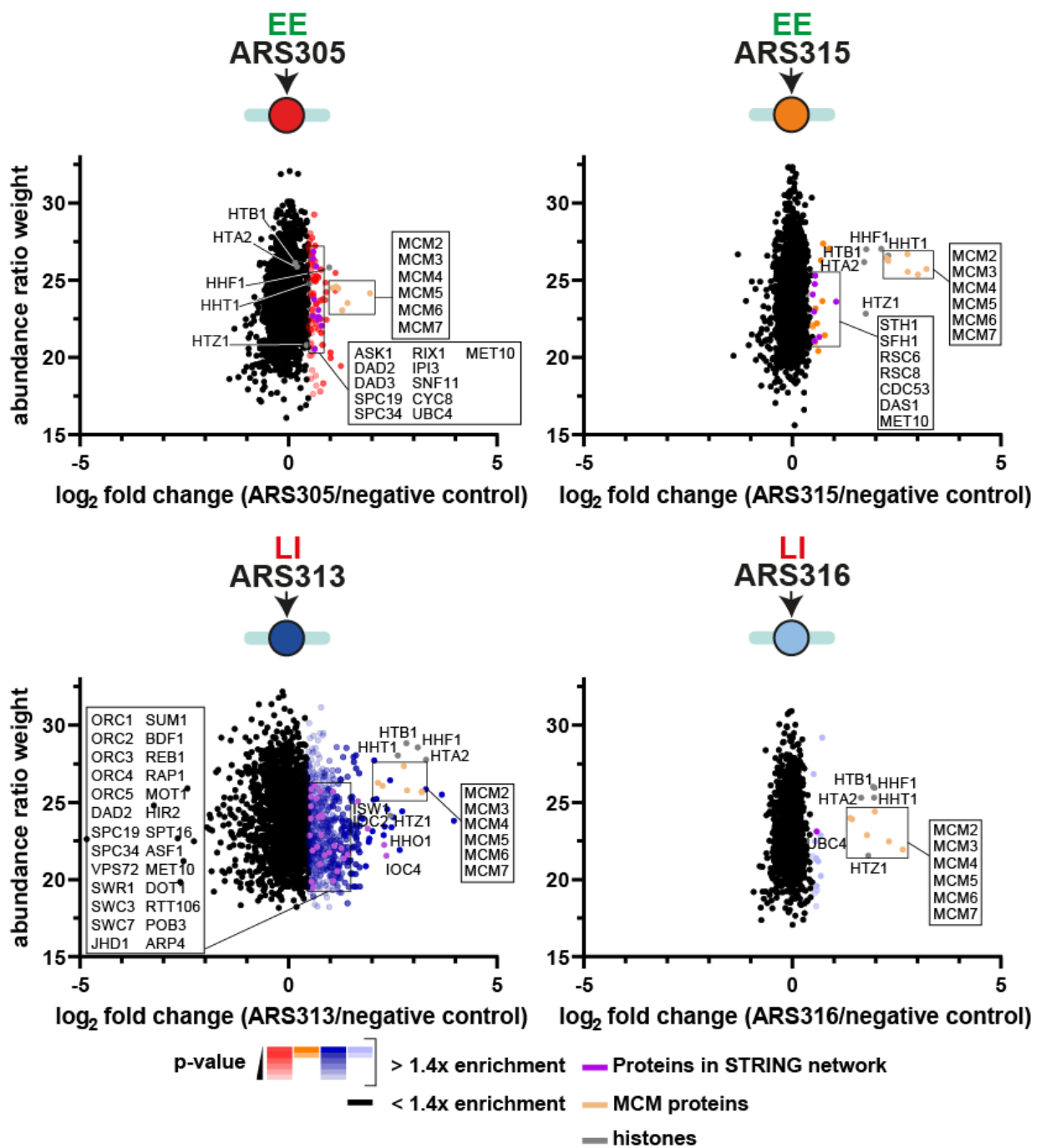
Figure 27 Scatter plots showing the protein enrichment at each investigated replication origin. Scatter plots of abundance ratio weights vs. the average log2-fold enrichment of proteins at each replication origin purification (n = 3 biological replicates). Proteins of the MCM2-7 complex are shown in light orange, histones in grey and selected protein factors are displayed in purple with their gene names. All proteins that were statistically enriched at least 1.4-fold over the control purification are colored according to the origin and decreasing p-value as indicated in the legend.

4.3.2.1 MCM2-7 complex and histones represent the most abundant proteins identified at replication origins using mass spectrometry

Nucleosomes and loaded MCM2-7 double-hexamer complexes are expected to represent the

most abundant and stably associating protein factors at all licensed replication origins

(Fernández-Cid et al., 2013). In agreement, histones and all subunits of the MCM2-7 complex were highly enriched in all origin purifications (**Figure 27**). Interestingly, the histone variant H2AZ was specifically enriched at 3 origins, except for ARS305, whereas generally lower abundance of histones was detected in comparison to the other 3 origins. The presence of H2AZ in the purifications is consistent with genome-wide analyses showing an enrichment of H2AZ, which promotes ORC1 binding at early replication origins (Cayrou et al., 2015; Long et al., 2020). In contrast, the yeast homologue of the linker histone H1, HHO1, was only detected at ARS313, indicating the presence of a more protected, nucleosomal chromatin structure at this LI origin. In support of this notion, the highest abundance of canonical histones was observed at ARS313 compared to all other origin purifications. Notably, the two EE origins ARS305 and ARS315 showed 1.84-fold or 1.69-fold higher relative enrichment of MCM molecules over histones whereas the two LI origins showed lower (0.87-fold for ARS313) or equal (1.08-fold for ARS316) levels of MCM and histone molecules in this analysis (**Figure 28**).
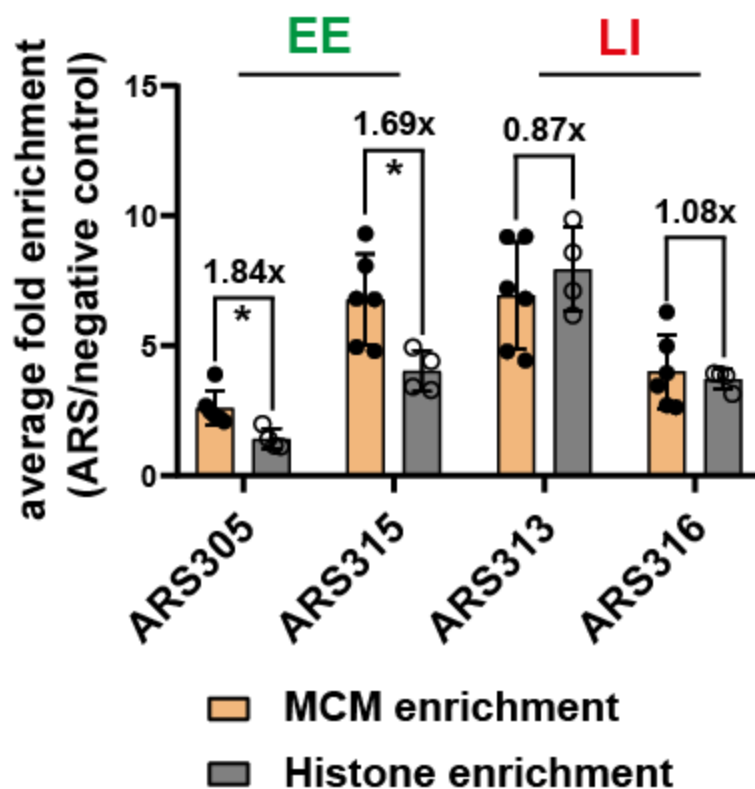
Figure 28 Mass spectrometry reveals a high enrichment of histones and MCM2-7 proteins at the investigated replication origins Bar plots representing the average enrichment of the four canonical histones (H2A, H2B, H3, H4) and the six MCM2-7 subunits (MCM2, MCM3, MCM4, MCM5, MCM6, MCM7) over the control purification for each replication origin. The bars indicate mean and standard deviations from each subunit of the complexes from 3 biological replicates (* indicates statistical significance $p < 0.05$, unpaired t-test).

This difference in MCM stoichiometry is consistent with previous reports showing that early origins can load multiple MCM double-hexamers (Das et al., 2015; Dukaj and Rhind, 2021).

To confirm this result by an independent method, ChIP was performed against an HA-tagged allele of MCM2 and canonical histone H3 at the 4 origins. Importantly, this ChIP analysis was done in the endogenous chromosomal context without inducing recombination or biochemical purifications. Consistent with the proteomic datasets of the isolated chromatin circles, the two EE origins showed a higher level of HA-MCM2 compared to the two LI origins (**Figure 29A)**, whereas histone H3 was particularly enriched at the LI origin ARS313 (**Figure 29B**).
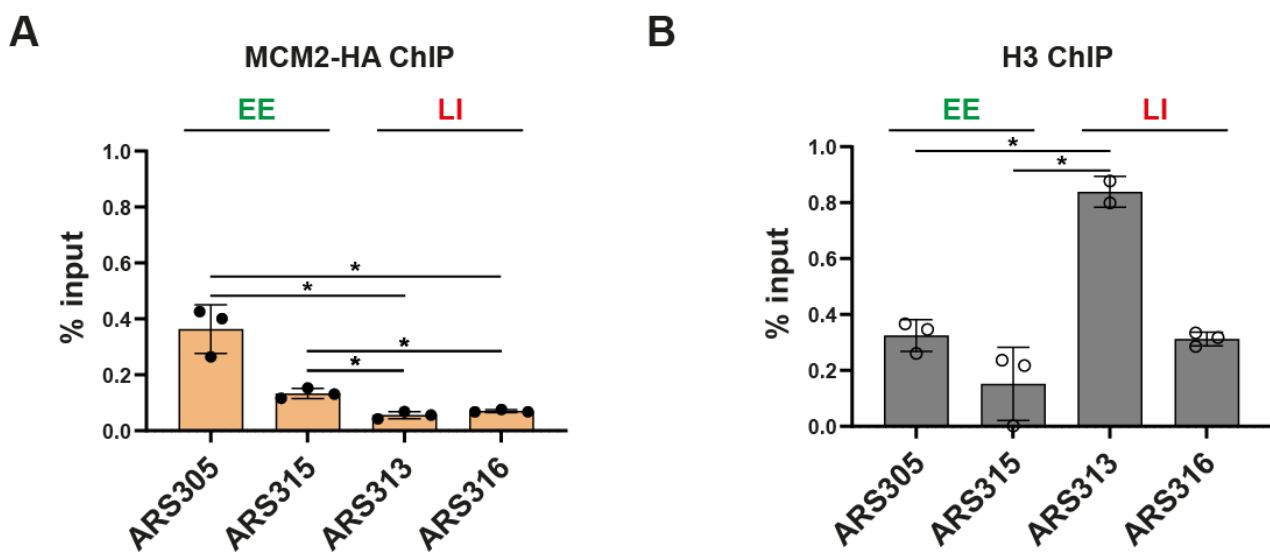
Figure 29 ChIP-qPCR analysis confirms the difference in MCM2-7 to histone ratios at EE and LI origins in their endogenous chromosomal context. A) ChIP-qPCR analysis in yeast strain Y0124 expressing MCM2 as an HA-tagged allele at the indicated EE origins ARS305/ARS315 and LI origins ARS313/ARS316. An HA-antibody was used to immunoprecipitate MCM2-HA at the indicated genomic regions. The bars indicate mean and standard deviations from 3 biological replicates (* indicates statistical significance $p < 0.05$, unpaired t-test). **B)** ChIP-qPCR analysis in yeast strain Y0001 at the indicated EE origins ARS305/ARS315 and LI origins ARS313/ARS316. A pan-H3 antibody was used to immunoprecipitate H3 at the indicated genomic regions. The bars indicate mean and standard deviations from 3 biological replicates (* indicates statistical significance $p < 0.05$, unpaired t-test).

I conclude that the two investigated EE origins show a higher MCM to histone ratio compared to the LI origins and this chromatin feature is preserved during recombination and purification of the origin domains.

4.3.2.2 The proteomes at each replication origin show a limited overlap

Next, I intersected the proteomes of the two EE and LI origins to identify common hits that could potentially promote EE versus LI firing of replication origins. Surprisingly, limited overlap between the factors enriched at both EE origins ARS305 and ARS315 (9/114 proteins) as well as factors shared between the two LI origins ARS313 and ARS316 (13/647 proteins) were observed (**Figure 30**).
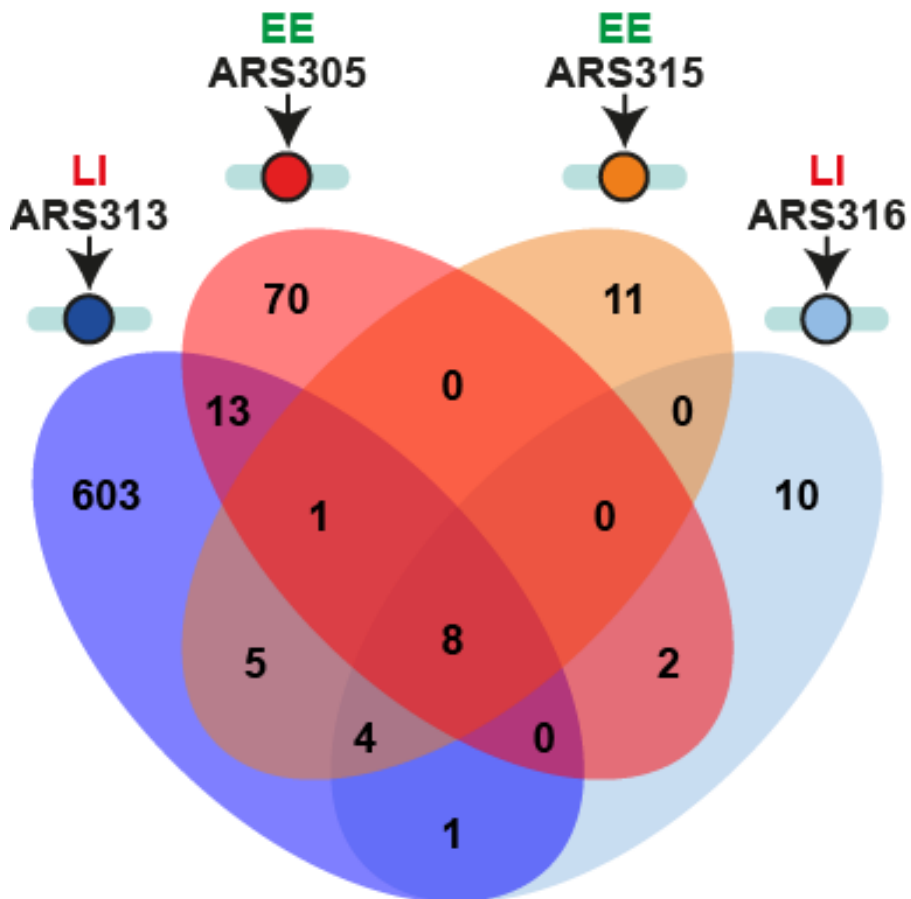
Figure 30 Venn diagram showing the overlap of proteins detected in the four replication origin purifications Only proteins that were at least 1.4-fold enriched over the negative control are included.

However, examining this dataset in more detail, various protein factors as well as protein complexes identified with several subunits on the same replication origin were identified. In order to visualize these potentially interesting proteins as well as their interactions, a STRING protein-protein interaction network analysis was performed (**Figure 31**).
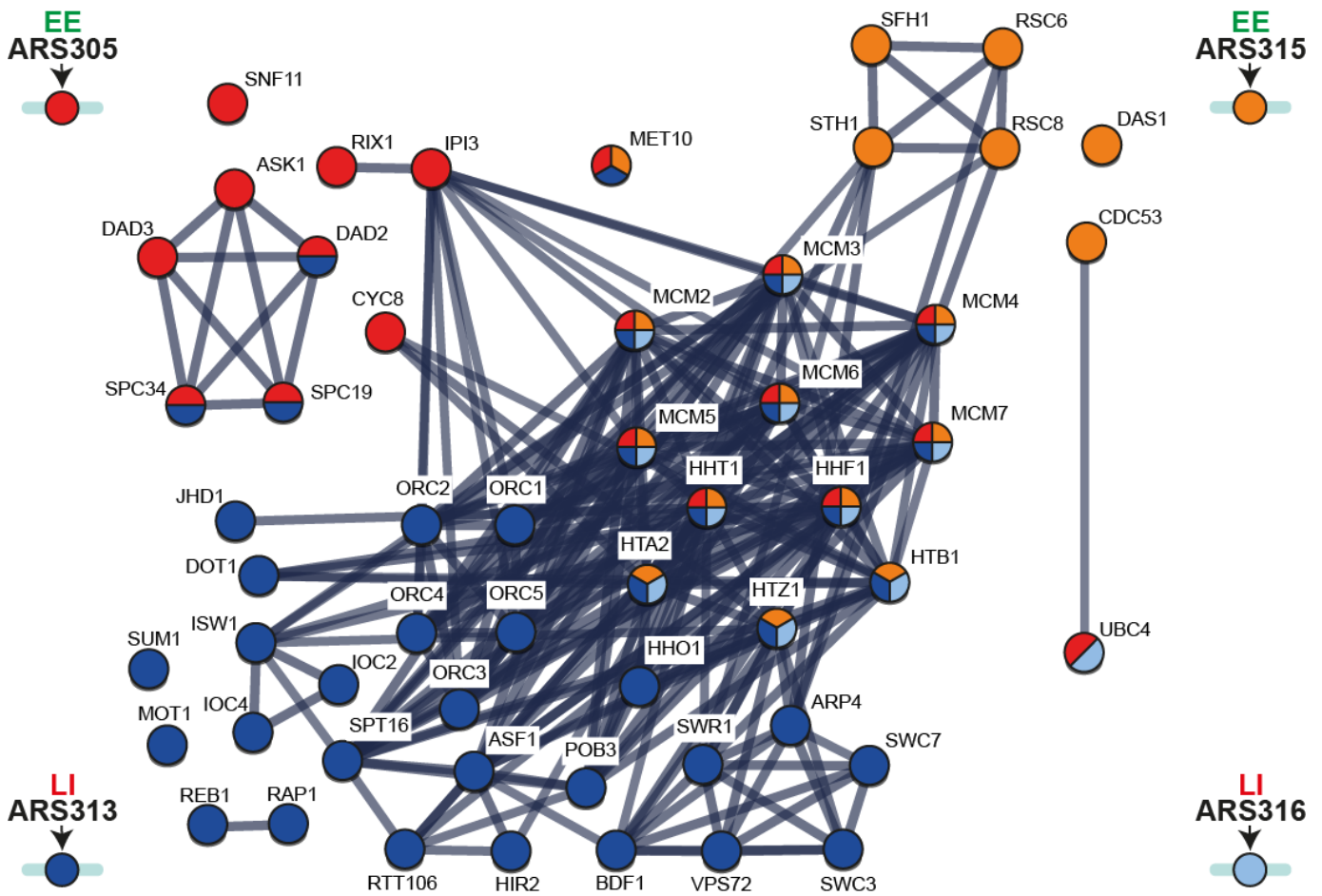
Figure 31 String network analysis of selected proteins revealed by mass spectrometry Only selected proteins that were at least 1.4-fold enriched over the negative control were included in this analysis. Individual proteins are shown as nodes, and edges indicate interactions retrieved from the STRING database (interaction score > 0.9). Significantly enriched proteins are colored according to the origin at which they were identified.

Specific factors found at ARS305 (EE) included two subunits of the RIX complex (Rix1 and Ipi3), previously described to facilitate pre-RC formation and maintenance during DNA replication licensing (Huo et al., 2012). Interestingly, ARS305 also interacted with 5 subunits of the DASH complex (Ask1, Dad2, Dad3, Spc19 and Spc34), a large essential complex that associates with microtubules and connects the outer kinetochore to the spindle for proper chromosome segregation (Jenni and Harrison, 2018; Miranda et al., 2007; Westermann et al., 2005).

Besides canonical histones and MCMs, the other EE origin ARS315 showed few other specific interactions. Two factors specifically enriched at ARS315 were Cdc53 together with the F-box protein Das1, strengthening a potential role of SCF (Skp, Cullin, F-box containing complex) complexes at EE replication origins. Strikingly, I also found four subunits of the RSC chromatin remodeling complex (Rsc6, Rsc8, Sth1 and Sfh1) at this particular origin. Among the few common interactors between the EE origins ARS305 and ARS315 was the alpha-subunit of the sulfite reductase Met10, which was identified in high- throughput screens as a negative

genetic interactor with several RIX, MCM and ORC complex subunits (Costanzo et al., 2016). However, this factor was also identified at the LI origin ARS313 and thus in 3 out of 4 origin purifications, which could point towards a more general role of this factor at replication origin chromatin independent of their timing or efficiency (**Figure 31)**.

Similar to ARS315, only few specific interactions were identified at the LI origin ARS316 including the E2 enzyme Ubc4. Besides that, canonical histones and MCM proteins appeared to be the major structural chromatin components of this LI origin. This was in strong contrast to the second LI origin ARS313, where the largest number of protein interactions was identified. Interestingly, three subunits of the ISW1b complex (Isw1, Ioc2, Ioc4) were also present at ARS313. Isw1b is required to establish regular arrays of phased nucleosomes at genic regions (Eriksson and Clark, 2021). I also identified nucleosome assembly factors and histone chaperones such as Asf1, Rtt106, Hir2 as well as both subunits of the FACT (facilitates chromatin transcription) complex (Spt16, Pob3) with high confidence. However, it was shown that only the chromatin remodelers INO80, ISW1a, ISW2, and Chd1 are needed to create regularly spaced nucleosomes at more than 80% of the replication origins in yeast (Chacin et al., 2023). Interestingly, ISW1b was not investigated in this study raising the possibility that this complex might be needed to create arrays of phased nucleosomes at a subset of replication origins, including ARS313. Additionally, the H3K36 demethylase Jhd1 was identified, as well as Dot1, the writer of H3K79 methylation. I also found six subunits of the SWR1 chromatin remodeling complex (Arp4, Bdf1, Vps72, Swr1, Swc3 and Swc7) that is important for the exchange of H2AZ:H2B dimers as well as many transcription factors such as Rap1, Reb1, Sum1 and Mot1. Intriguingly, ARS313 also interacted with 3 subunits of the DASH complex (Dad2, Spc19 and Spc34). As this complex was also identified at ARS305 and thus appeared in 2 out of 4 origin purifications, I decided to further investigate and characterize a functional role of this complex in the context of replication origin chromatin.

It is important to note that 5 out of 6 ORC subunits could be detected in the ARS313 dataset, but not in the purification of the other origin domains (**Figure 27**). This could be caused by the stringent washing steps of our native purification procedure at a salt concentration of 200mM KCl, that may result in the loss of more transient interactors as described for the yeast ORC complex (Donovan et al., 1997).

4.3.3 Repetition of the mass spectrometry analysis of chromatin rings purified in a low salt condition

Besides ORC subunits, other expected interactors such as Fkh1/2 transcription factors at ARS305 were not detected (see also Discussion). For this reason, to increase our ability to potentially purify transient, low-affinity interactors, I repeated all origin purifications under more physiological salt concentration of 150mM KCl instead of the previously used 200mM KCl

3.3.3.1 The purifications in low salt conditions show similar chromatin ring enrichments

Since this decreased stringency could affect the purification efficiency, I first determined the recovery, as well as the enrichment of the desired chromatin rings under these new conditions. The remaining setup of the experiment was identical to the previous experiments, meaning that I always purified the origins spanning three nucleosomes up- and downstream (+/-3) and compare to a negative control not harboring any recombination sites (**Figure 32**).
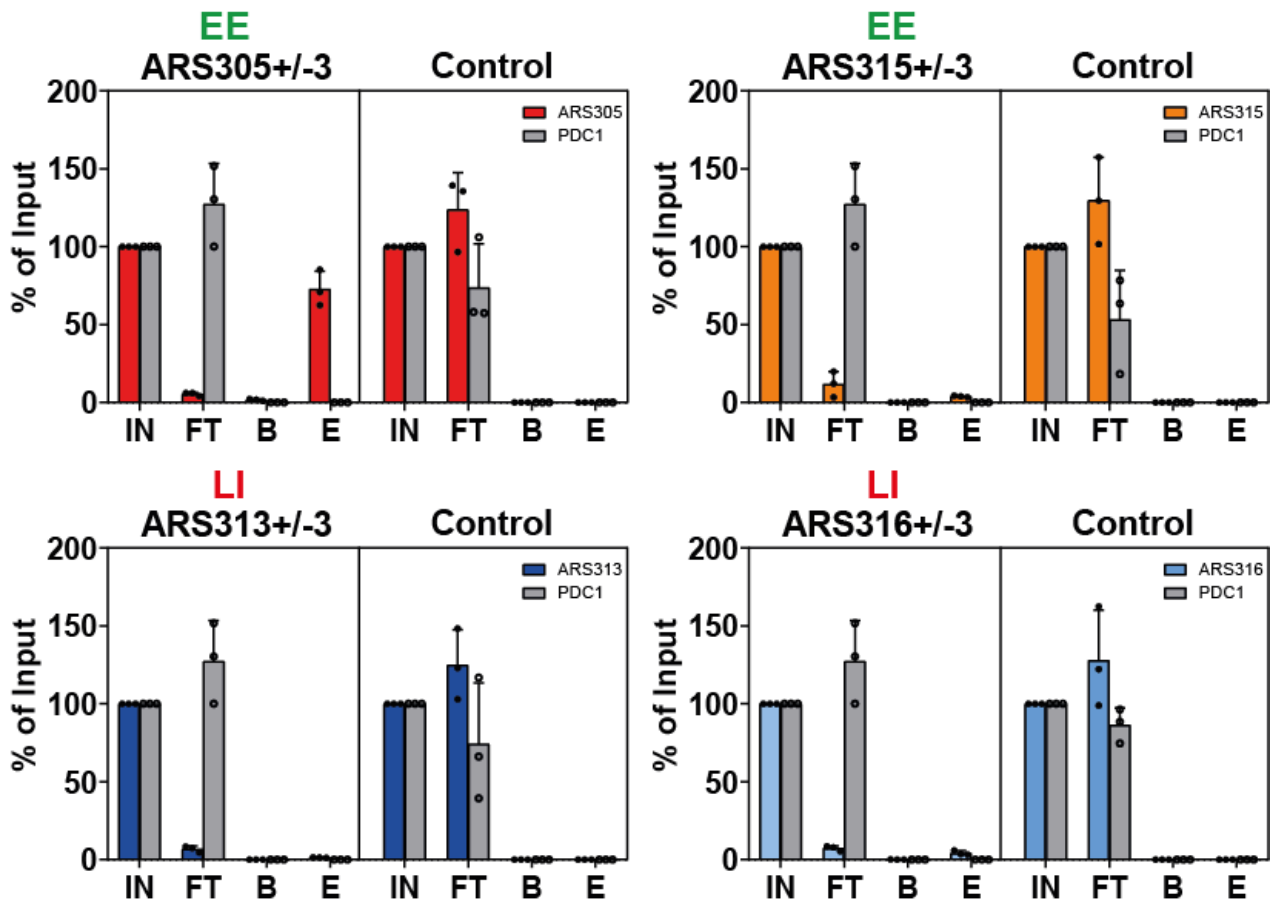
Figure 32 qPCR analysis of the different fractions of the chromatin ring purification performed in low salt conditions LexA affinity purifications were performed under low-salt conditions (150mM KCl) for all the strains proficient for site-specific recombination of the targeted replication origins (Y0065 (ARS305+/-3), Y0091(ARS315+/-3), Y0094 (ARS313+/-3), Y0069 (ARS316+/-3)), as well as one purification from the control strain (Y0066). DNA samples from 3 biological replicates of affinity purifications were taken (0.1% for CX, P, IN, FT and 2.5% for B and E). DNA was extracted and analyzed by qPCR to monitor the enrichment of the targeted replication origins as well as an unrelated genomic region (PDC1) during the purification process (n = 3 biological replicates).

The recovery of chromatin rings during the ARS305 purification showed similar efficiency as in the 200mM condition, with ~73% chromatin rings recovered in the final eluate. From this analysis, the other three origin purifications showed much less recovery (**Figure 32**). This negative result, however, is very likely a technical problem of the qPCR reactions as chromatin rings were efficiently depleted from the flowthrough similar to the ARS305 purification and the

enrichment of the chromatin rings over genomic background was comparable in all 4 purifications (**Figure 33**).
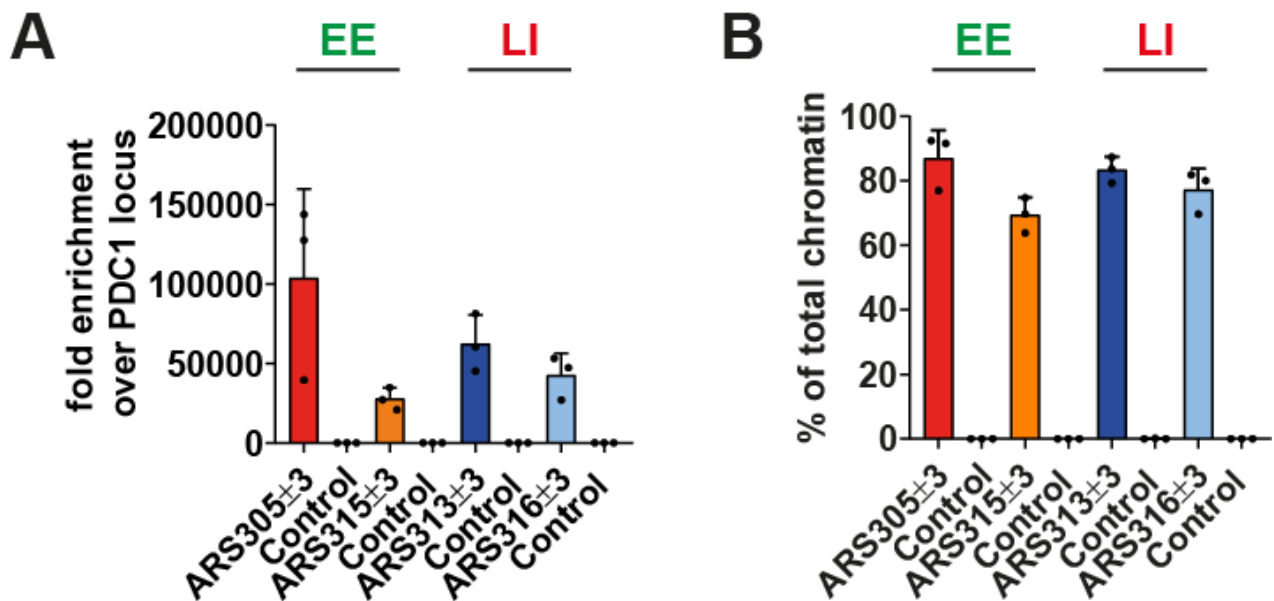
Figure 33 Enrichment of the chromatin rings during the low salt purification A) Using the eluate samples from **Figure 28**, the fold enrichment of the indicated origins compared to the PDC1 locus was calculated (n = 3 biological replicates). **B)** Using the fold-enrichment values from A) and factoring in the size of the total yeast genome (~12,000kb), the proportion of total DNA present in the final eluates derived from the targeted replication origin domain (~ 1kb) was calculated (n = 3 biological replicates).

In addition, similar enrichment levels of origin DNA as compared to the purifications with 200mM KCl (**Figure 33 and Figure 26**) was obtained, suggesting that the less stringent conditions did not have a major impact on the specificity of the purifications on the DNA level. I therefore proceeded with mass spectrometry to compare the proteomes of these "low-salt samples".

3.3.3.2   Mass spectrometry reveals the proteomes of replication origins that were purified in low salt conditions

The procedure was identical to the previous experiment. The proteomes derived from each EE and LI +/-3 origin purification were compared to a control purification. However, the proteome coverage was higher than in the "high-salt condition". For each origin, about ~3000 proteins with at least two unique peptides and from three biological replicates were identified.

Applying the same threshold as before and only considering proteins that are at least 1.4-fold enriched over the negative control, resulted in 44, 151, 916, and 17 putative ARS-interacting proteins with ARS305, ARS315, ARS313, and ARS316, respectively (**Figure 34**).
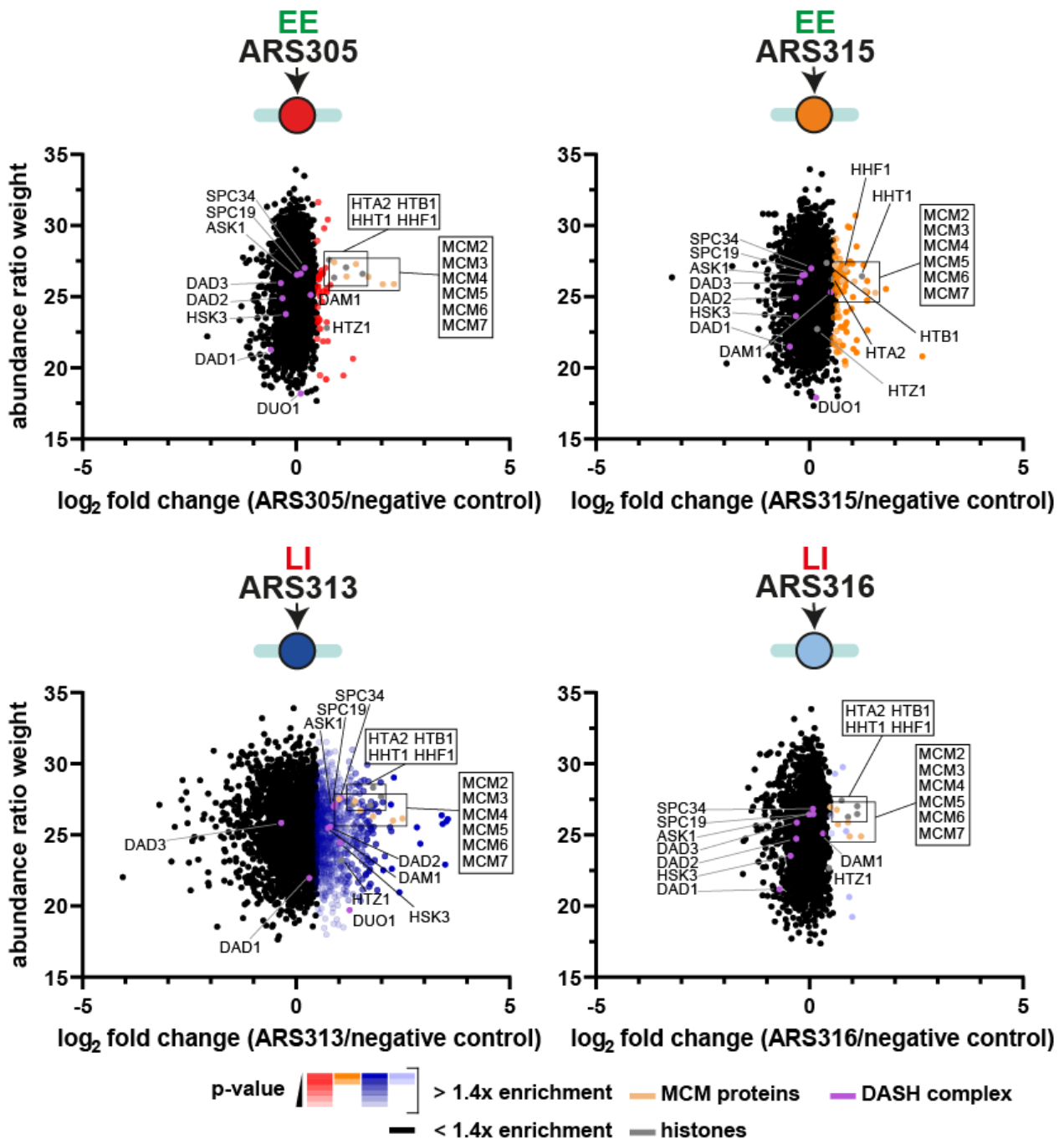
Figure 34 Scatter plots showing the protein enrichment at each investigated replication origin when using a low salt purification approach Scatter plots of abundance ratio weights vs. the average log2-fold enrichment of proteins at each of the respective replication origin purification performed in low salt conditions (n = 3 biological replicates). Proteins of the MCM2-7 complex are shown in light orange, histones in grey and DASH complex subunits in purple. All proteins that were statistically enriched at least 1.4-fold over the control purification are colored according to the origin and decreasing p-value as indicated in the legend below.

3.3.3.3 Low salt purifications do not change the enrichment of the MCM2-7 complex and histones

When examining histones as well as the subunits of the MCM2-7 complex in the less stringent purification conditions, the results show that I could not only reproduce the strong enrichment of histones and MCM2-7 complexes (**Figure 35**), but I could similarly obtain a higher relative enrichment of MCM molecules over histones at the two EE origins ARS305 (1.45-fold) and ARS315 (1.21-fold) over the two LI origins ARS313 (1.07-fold) and ARS316 (0.90-fold) (**Figure 35**), confirming that the change in KCl concentration did not affect the stoichiometry of these strongly interacting proteins.
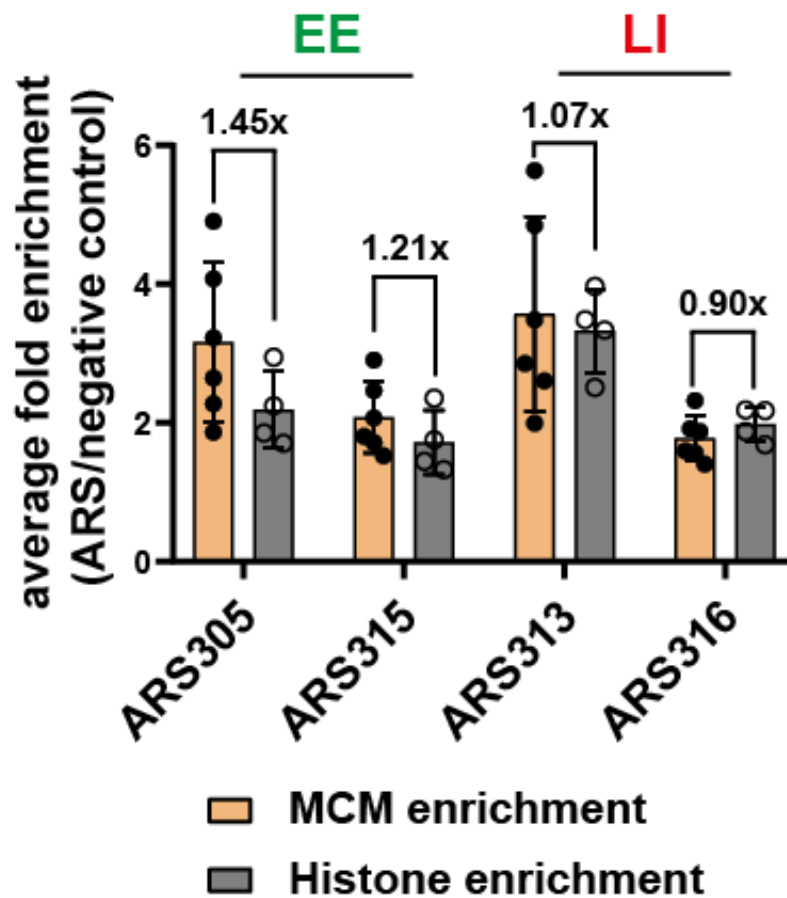
Figure 35 Mass spectrometry reveals a high enrichment of histones and MCM2-7 proteins at the investigated replication origins even in low salt purification conditions Bar plots representing the average enrichment of the four canonical histones (H2A, H2B, H3, H4) and the six MCM2-7 subunits (MCM2, MCM3, MCM4, MCM5, MCM6, MCM7) over the control purification for each replication origin. The purifications were performed in low salt conditions. The bars indicate mean and standard deviations from each subunit of the complexes from 3 biological replicates (* indicates statistical significance $p < 0.05$, unpaired t-test).

3.3.3.4 The low-salt conditions slightly changed the identified proteomes at the respective replication origins

Interestingly, lowering the salt concentration to 150mM KCl did not drastically improve the number of overlapping proteins at EE origins (27 out of 168 proteins) nor LI origins (13 out of 920 proteins) **(Figure 36).**
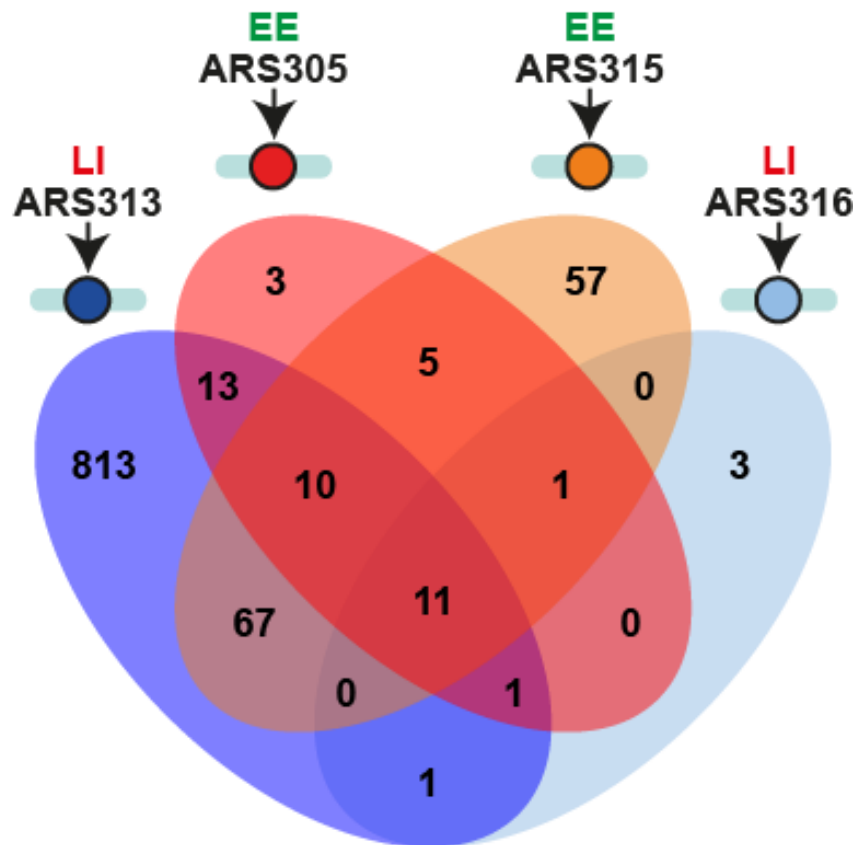
Figure 36 Venn diagram showing the overlap of proteins detected in the four replication origin purifications at low-salt conditions (150mM KCl) Only proteins at least 1.4-fold enriched over the negative control are included.

Furthermore, consistent with the results obtained under high-salt conditions, only 3 out of 6 ORC complex subunits were detected at ARS313, but not at the other 3 origins.

Other proteins that were detected in both the high- and low-salt conditions for each origin consisted mostly of the MCM2-7 proteins, as well as canonical histones. For ARS313, however, some additional proteins overlapped in both conditions, namely the transcription factor Rap1, the nucleosome assembly factors Hir2 and Asf1, Arp4 and Bdf1 as parts of the SWR1 chromatin remodeling complex, the H3K36 histone demethylase Jhd1, as well as three components of the DASH complex Dad2, Spc19, and Spc34. The fact, that these proteins are reproducibly detected in both salt conditions for ARS313 could suggest that these factors or complexes are strong interactors with ARS313 and therefore potentially play a role in replication timing control at this origin.

It is also important to note that ARS313 origin purifications gave yield to almost 10-fold more specific proteins than the other 3 origins, which was a reproducible result under both low-salt and high-salt conditions (**Figure 27, 30, 34, and 36**). This indicated a larger biological complexity of interacting proteins at this origin, although I cannot rule out other purification-related sources of this imbalance (see Discussion). Together, these results suggest that the four isolated proteomes are highly distinct from each other, with each chromatin domain showing a distinct set of protein interactors with varying complexity that could play a role in defining the replication features of the individual origin.

However, since the high-salt condition represents the most stringent condition, I considered the proteins enriched in these experiments as more likely to be interactors of the respective replication origins.

4.3.5 Histone PTM analysis shows differences in various histone marks among the investigated replication origins

The enrichment of canonical histones in the origin purification over the control samples prompted me to monitor the specific histone PTM landscape associated with EE and LI origins. To this end, high-resolution mass spectrometry of gel-purified histones from the individual origin purifications was employed (Maile et al., 2015). To benchmark the enrichment of histone PTMs on origin chromatin with the general level of histone modifications in the entire genome, I also purified bulk histones from the isogenic control strain under asynchronous as well as G1-arrested yeast cultures (**Figure 37**). Additionally, the same affinity purification protocol was applied to the control strain lacking the ability to excise and purify specific origin chromatin, so that any histone molecules and associated PTM levels present in this sample must be derived from background binding of genomic chromatin or free histones.
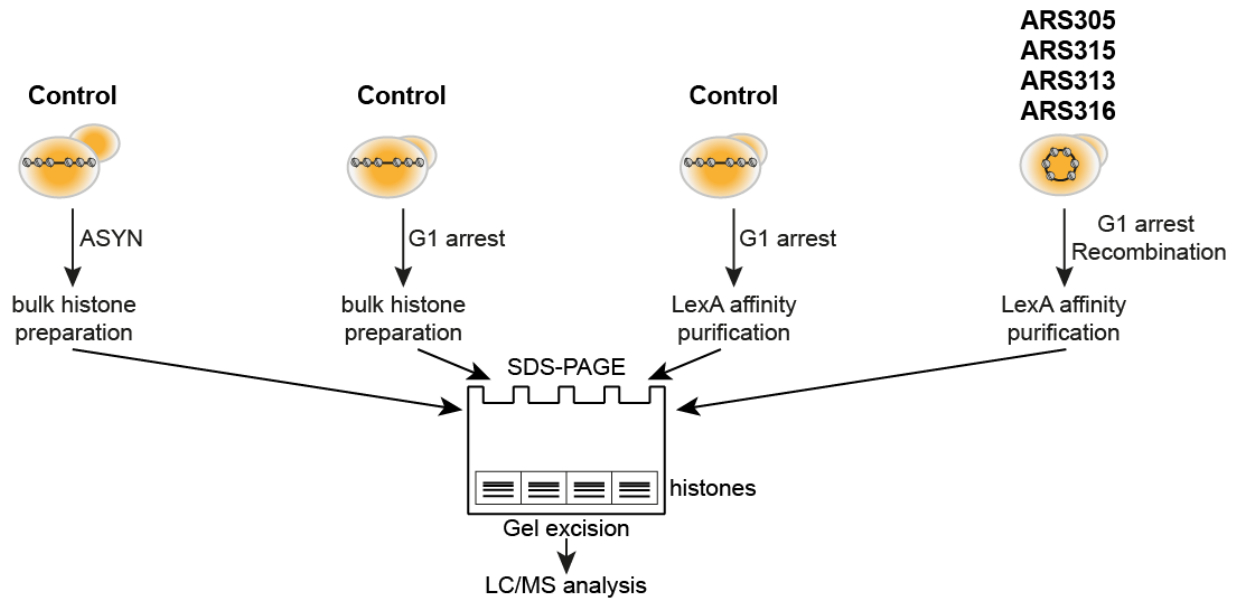
Figure 37 Schematic experimental outline for the histone PTM analysis. Mass spectrometric analysis of histone modifications of bulk histones isolated from asynchronous and G1-arrested cultures as well as histones extracted from the respective origin purifications. After purification, histone samples were gel-purified by SDS-PAGE and excised from the gel for histone PTM analysis.

Overall, this analysis detected and quantified multiple histone methylations and acetylations on histones H3 and H4 with high confidence in all samples. Generally, the H3 K4, K36 and K79 methylation levels in the origin purifications reflected the genome-wide levels in the control and the G1-arrested bulk samples (**Figure 38**). ARS313 histones were exceptional as they showed a reduced level of H3K4me3 and a corresponding increase in H3K4me0 and H3K4me1 (**Figure 38, H3K4 methylation**) as well as a decrease of H3K36me3/increase in H3K36me2 in comparison to all other origin purifications (**Figure 38, H3K36 methylation**). As these trimethylation marks have a prominent role in active transcription, this suggested that ARS313 histones are in a less open, transcriptionally inactive state than the other origins, consistent with the strong enrichment of total histones in the previous proteomic dataset (**Figures 27, 28, 34, and 35**). Intriguingly as mentioned before, I also identified the H3K36 demethylase Jhd1 enriched on ARS313 chromatin (**Figure 27**), which is consistent with the reduction of H3K36 methylation levels at this origin. In contrast, ARS313 histones showed an enrichment for H3K79me3 (**Figure 38, H3K79 methylation**), a mark linked to active transcription as well as DNA damage repair (Nguyen and Zhang, 2011). In agreement, Dot1 (the writer of H3K79 methylation) was also specifically co-purified with ARS313 origin chromatin **(Figure 27)**.
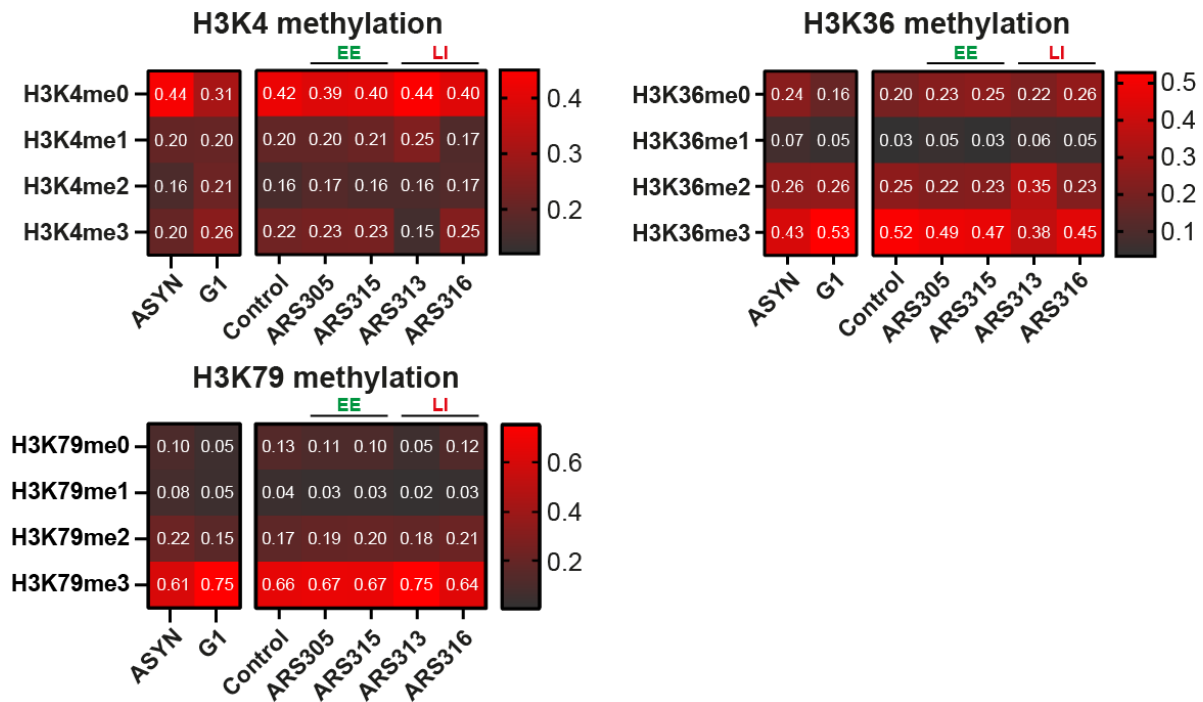
Figure 38 Heatmaps depicting the methylation states present at the investigated replication origins The heatmaps show H3K4, H3K36, and H3K79 for asynchronous and G1-arrested bulk histones as well as the replication origin and control purifications. Average values indicate the fraction of the respective modification over the total amount of this peptide (n = 3 biological replicates for bulk samples, n = 2 biological replicates for origin purification samples).

Next, the changes in acetylation of lysine residues in the N-terminal tail of histone H3 were examined. I found no major difference in the acetylation state of the H3K9/K14 peptide between the origin and the control versus bulk purifications (**Figure 39, H3K9/K14 acetylation**).

However, all origin samples showed a slight enrichment of di-acetylated H3K18/K23ac (9-13%) over the control (7%) and the bulk histone samples (4%) (**Figure 39, H3K18/K23 acetylation**), suggesting that hyperacetylated H3K18/K23 is enriched at origin chromatin independently of their timing and/or efficiency features.

H3K56 acetylation was not detectable for the G1 arrested cells in the bulk purification. In the asynchronous population, however, there is an enrichment of H3K56 acetylation (20%), which is in agreement with previous studies, which show that this mark is predominantly present in S phase (Masumoto et al., 2005; Recht et al., 2006) and, therefore, can explain the increased amounts of acetylated histones in this condition. Surprisingly, the pattern in the control purification is vastly different, as 50% of H3K56 residues are acetylated. This is likely due to unspecific binding of preferentially acetylated free histones to the affinity matrix. The two EE origins ARS305 and ARS315 behave very similar, showing ~40% acetylated histones. Interestingly, the two LI origins differ from each other, with ARS313 only showing ~30% acetylation levels and ARS316 nearly 50%. However, a similarly high acetylation level is also observed in the control purification, making a definitive conclusion of H3K56 acetylation levels

on the different origin chromatin rings difficult and will require further future investigation (**Figure 39, H3K56 acetylation**).

Finally, I determined the acetylation patterns on the histone H4 N-terminal peptide that comprises 4 neighbouring lysine residues (H4K5/K8/K12/K16) (**Figure 39, H4 acetylation**). On bulk histones, the acetylation levels do not vary greatly between the asynchronous and G1-arrested chromatin. Most of the acetylated H4 (~46%) on bulk histones were mono-acetylated, which is in good agreement with a previous study showing that a large proportion of the mono-acetylated H4 (~50%) in bulk chromatin can be attributed to K16 acetylation, a modification maintained by Sas2 throughout the cell cycle (Unnikrishnan et al., 2010a).
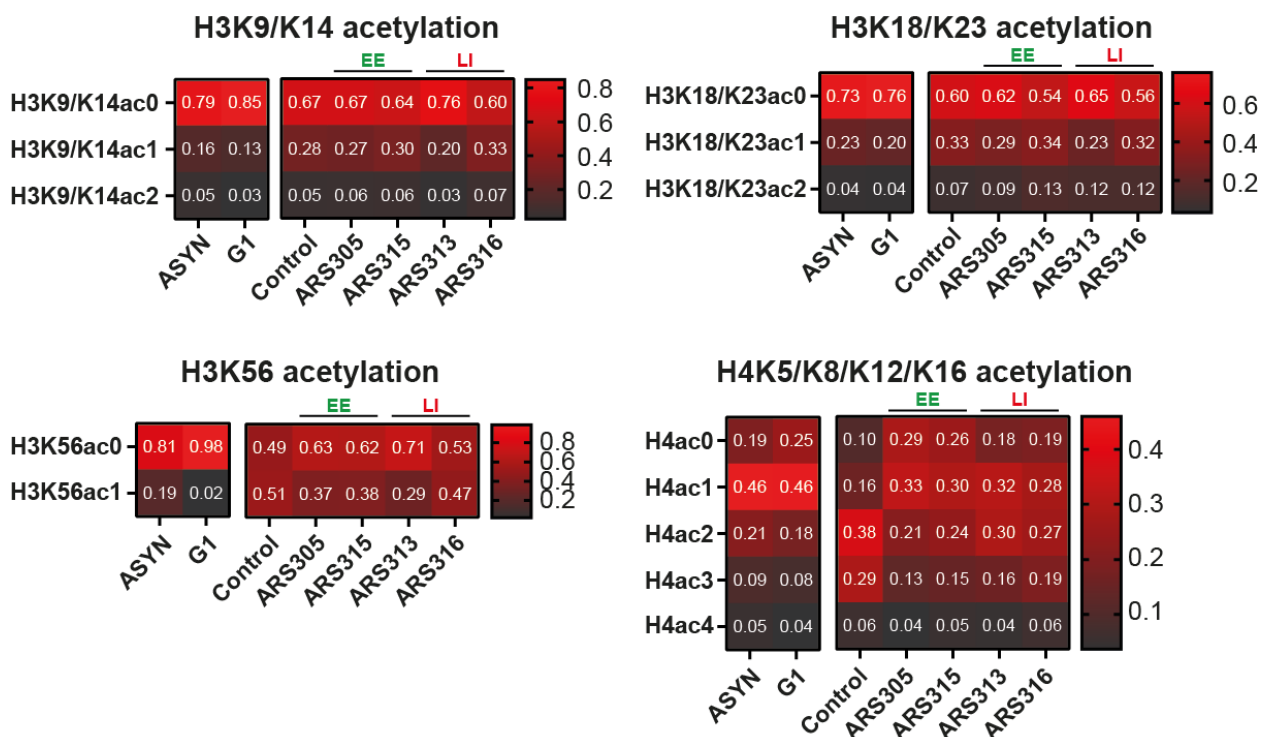
Figure 39 Heatmaps depicting the acetylation states present at the investigated replication origins. The heatmaps show the acetylation states of H3K19/K14, H3K18/K23, H3K56, and H4K5/K8/K12/K16 for asynchronous and arrested bulk histones as well as the replication origin and control purifications. Average values indicate the fraction of the respective modification over the total amount of this peptide (n = 3 biological replicates for bulk samples, n = 2 biological replicates for origin purification samples).

In the purification samples, however, the pattern of H4 acetylation was strikingly different from bulk. The level of H4 acetylation was generally low at the EE origins ARS305 and ARS315 with H4ac0 and H4ac1 being the predominant modification states. The two LI origins ARS313 and ARS316 shifted towards higher acetylation levels containing preferentially mono- and di-acetylated H4 peptides. Importantly, the proportion of hyperacetylated H4 histones again increased further in the control purification, likely reflected by unspecific binding of free histones to the affinity matrix. This means that the large decrease in H4 acetylation on EE origins is primarily due to the modification status of the origin-chromatin associated H4

histones. It was previously shown that the ARS1 EE origin shows a sharp wave of histone H4 deacetylation from G2/M into G1 (Unnikrishnan et al., 2010b), which is fully consistent with these results. My data reveal that LI origins show higher levels of histone H4 acetylation, which could contribute to their lower affinity towards replication initiation factors in the subsequent S phase.

Together, this initial characterization of histone PTMs of the EE and LI replication origin domains gave promising, but preliminary results and will need to be validated by an independent method such as histone PTM-specific ChIP experiments.

4.4 Hit validation by tethering of distinct proteins to determine a potential influence on replication timing

After examining both the proteome as well as the histone-PTM state at each of the respective origins, I next wanted to validate some of the candidate factors identified in the proteomic dataset for a potential role in replication timing control.

4.4.1 Sir4 is used as a proof of concept to efficiently decrease replication timing at ARS305

The general strategy for validating hits was to utilize the library of yeast strains with integrated LexA binding sites next to EE or LI replication origins. To determine, if selected proteins can affect origin firing, I expressed the respective protein as a LexA-fusion protein in the strains where the LEXA binding sites are ~200bp away from a specific origin (ARS3XX+/-1 strains). In order to determine if this system works, the histone deacetylase Sir4 was used as a positive control, as a previous study had shown with a similar experimental setup to decrease origin firing at ARS305, when tethered to this origin (Zappulla et al., 2002). Therefore, I expressed Sir4 as a LexA-fusion protein in the ARS305+/-1 recombination strain, which should similarly decrease ARS305 origin firing (**Figure 40**).
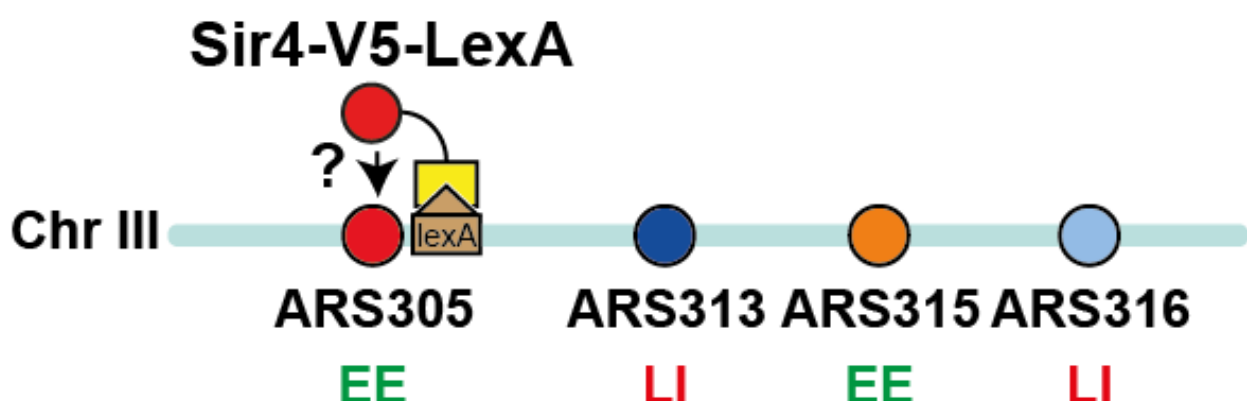
Figure 40 Experimental outline for assessing the effect of Sir4 tethering at the EE replication origin ARS305 Yeast strain Y0051 expresses Sir4 as a LexA-V5 fusion protein. This allows artificial recruitment of the fusion proteins to ARS305 in the yeast strain containing a cluster of 3x LEXA binding sites in close proximity to ARS305.

To measure replication timing of ARS305, the previously introduced copy number analysis assay by qPCR was used (**Figure 23**). Cells were arrested in G1 phase with alpha-factor and synchronously released into S phase in the presence of 200mM hydroxyurea (HU). The HU treatment leads to nucleotide depletion, which allows initiation of EE origins but then leads to checkpoint activation that restricts replication elongation to a region of 5kb around EE origins (Poli et al., 2016).

Besides the strain in which Sir4 is targeted to ARS305 (ARS305+/-1 Sir4-LexA), we used three additional control strains. The first strain does not express any LexA fusion protein (ARS305+/-1), which allows us to assess the effect of Sir4 tethering. The second strain expresses LexA-TAP, which is targeted to ARS305 (ARS305+/-1 LexA-TAP) in order to determine whether the targeting of an unrelated protein with similar molecular weight as Sir4-LexA to ARS305 affects replication of the origin. In the last control, Sir4 was targeted to ARS316 origin (ARS316+/-1 Sir4-LexA) in order to test if the tethering of Sir4 is affecting the replication origin locally or if this has a widespread genomic effect on other origins of the same chromosome.

The copy number analysis of the early-replicating ARS305 versus the late-replicating region on chromosome IV showed that none of the three control strains affected the EE replication of ARS305 origin. (**Figure 41, black and grey bars**). However, targeting Sir4 to ARS305 did not increase the copy number of ARS305 (**Figure 41, red bar**), suggesting that tethering Sir4 to this origin strongly delayed its firing time, since it does not fire prior to replication checkpoint activation.
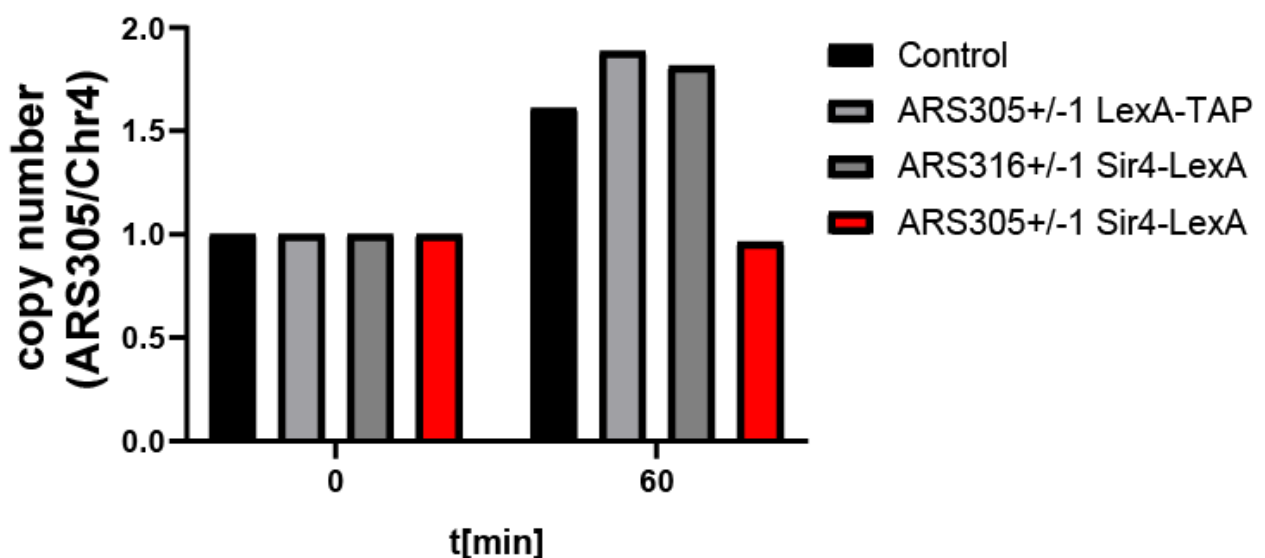
Figure 41 Targeting of Sir4 to ARS305 decreases the replication timing at this replication origin
Analysis of the replication timing for the strain Y0051 which targets Sir4-LexA to ARS305+/-1. Three other strains were used as controls. Y0016 has RS-sites and LexA binding sites integrated next to ARS305+/-1 but does not express any LexA protein. Y0035 targets LexA-TAP to ARS305+/-1 and Y0070 targets Sir4-LexA to ARS316+/-1. Cells were released into S phase in the presence of 200mM HU.

Samples for genomic DNA extraction were taken at the indicated timepoints for copy number analysis by qPCR to determine the relative replication timing of depicted loci. The plots show the average copy number ratios of early (ARS305) to a late-replicating region (Chr 4) (n = 1 biological replicate).

To summarize, this experiment showed that the integrated LEXA binding sites allows me to influence replication of individual origins by tethering candidate LexA fusion proteins to replication origins *in vivo.*

4.4.2 LexA was utilized to guide twelve proteins identified at the EE replication origin ARS305 to the LI replication origin ARS316

For validation of potential candidate factors affecting replication timing, I focused on proteins that were enriched under high-salt conditions as the most stringent condition tested. Additionally, we focused on proteins that were detected at the EE replication origin ARS305, since this was the first complete dataset that was obtained during this thesis project.

For hit validation, proteins from the EE replication origin ARS305 mass spectrometry dataset were expressed as LexA-fusion proteins in the ARS316+-1 (LI) strains (**Figure 42**). Additionally, I also included a V5-tag for complementary ChIP analysis to confirm binding of the fusion protein at the integrated LEXA binding sites. If these selected proteins play a role in EE replication timing control of ARS305, this should allow more efficient or advanced origin firing at the LI origin ARS316.
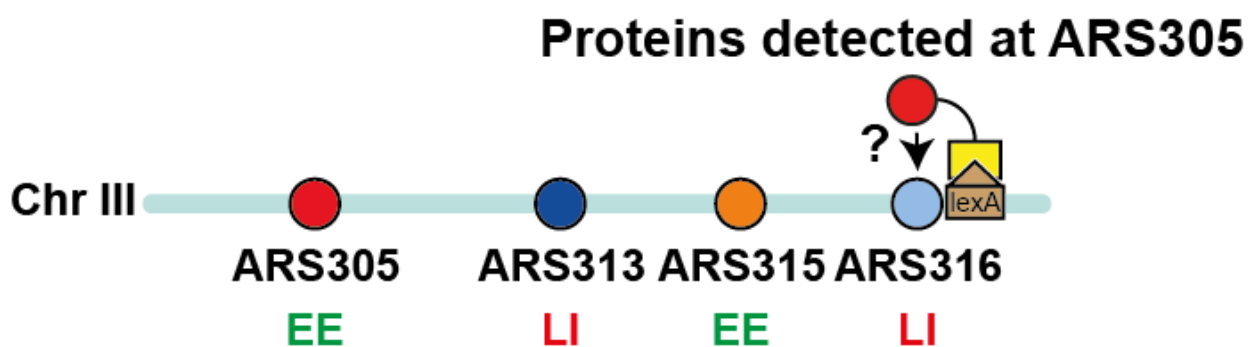
Figure 42 Experimental outline for assessing the effect of tethering proteins detected at the EE replication origin ARS305 to the LI replication origin ARS316. Selected proteins are expressed as LexA-V5 fusion proteins. This allows artificial recruitment of the fusion proteins to ARS316 in the yeast strain containing a cluster of 3x LEXA binding sites in close proximity to ARS316.

The proteins that were targeted to ARS316 by this approach included the previously introduced Ask1, Ipi3, and Cyc8 proteins (**Figure 27 and 31**). Besides that, we chose 9 other proteins of particular interest. Among these proteins were a subunit of the Set3 histone deacetylase complex Set3, a subunit of the SWI/SNF chromatin remodeling complex Snf6, a subunit of the cohesion complex Smc3, a subunit of the SAGA histone acetyltransferase complex Sgf11, a subunit of the cytosolic iron-sulfur protein assembly (CIA) machinery Met18, the transcription factor Swi6, as well as the two open reading frames YCR087C-A and YDL144C. As a positive

control, we also included a strain expressing the Gcn5 histone acetyltransferase as LexA-V5 fusion protein, as the tethering of this protein has been previously shown to advance the replication of a single late origin (Vogelauer et al., 2002).

For the experiment, the cells were arrested in G1 phase with alpha-factor and synchronously released to S phase to monitor the replication timing of ARS316 by qPCR copy number analysis. In this analysis, the copy number of the LI region ARS316 was also compared to a late-replicating region on chromosome IV (Chr4). In a preliminary screen, the experiments were performed as one biological replicate for each protein, always including the Gcn5 positive control as well as a wildtype control (ARS316+/-1) containing the LEXA binding sites but no protein is targeted to ARS316 (**Figure 43 A-C**).
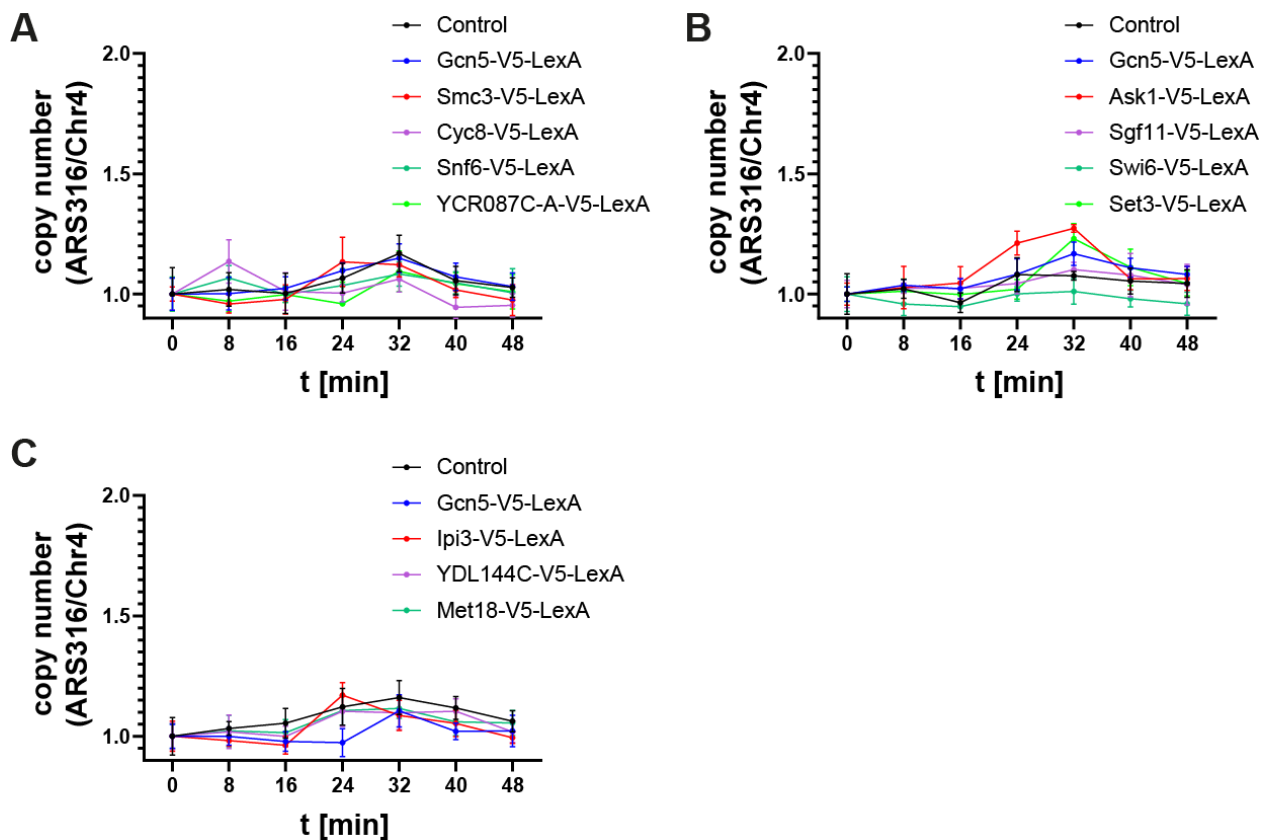
Figure 43 Effect of the tethering of EE factors to the LI replication origin ARS316 (A-C) Analysis of the replication timing of ARS316 for strains where different proteins were targeted to ARS316+/-1 utilizing the LexA tethering approach. RS-sites and LexA binding sites were integrated next to ARS316+/-1. In total, twelve different factors were targeted to ARS316 (Y0071-Y0082). As a control, Y0019 was used. This strain has RS-sites and LexA binding sites integrated next to ARS316+/-1 but does not express any LexA protein. Samples for genomic DNA extraction were taken at the indicated timepoints for copy number analysis by qPCR to determine the relative replication timing of depicted loci. The plots show the average copy number ratios of the targeted ARS316 locus to late-replicating region (Chr 4) with standard deviation from n = 3 technical replicates.

The results showed that most of the investigated proteins did not change the copy number ratio as compared to the ARS316+/-1 control, meaning that replication was not affected by tethering these proteins at ARS316. However, two proteins, Ask1 and Set3, were able to increase the copy number ratio, especially between the 24min and 32min timepoints (**Figure 43B, green and red lines**).

The Ask1/DASH protein complex is a microtubule- and kinetochore-associated complex required for proper chromosome segregation and bipolar attachment of sister chromatids on the mitotic spindle (Jenni and Harrison, 2018; Miranda et al., 2007; Westermann et al., 2005) and has thus not previously been reported in the context of replication origin chromatin.

The second candidate Set3 is part of a seven-subunit large histone deacetylase complex, Set3C. Set3 contains both a PHD and a SET domain. While The PHD finger can bind H3K4me2 with high affinity, the function of the SET domain is still unknown. Recruitment of this complex to nucleosomes by Set3 leads to deacetylation events caused by the two catalytic subunits Hos2 and Hst1 which causes transcriptional regulation at various genomic loci (Kim and Buratowski, 2009; Pijnappel et al., 2001; Wang et al., 2002).

Since this initial screening suggested Ask1 and Set3 as promising candidates affecting replication timing, I repeated this experiment in two more biological replicates in order to confirm these results. Similarly, I investigated both the copy number ratios of the origins ARS305 to ARS316 (**Figure 44, top panel**), as well as ARS316 to a late-replicating region (Chr 4) (**Figure 44, bottom panel)**. Gcn5 recruitment caused a modest decrease of the copy number ratio between ARS305 and ARS316 over the time course compared to the untagged control strain, suggesting that ARS316 replication was slightly more efficient upon Gcn5 recruitment (**Figure 44, top panel**). However, both Set3-V5-LexA and especially Ask1-V5-LexA showed a much stronger decrease in the copy number ratio of ARS305 to ARS316 at all timepoints, suggesting that replication timing of ARS316 was substantially advanced in these strains (**Figure 44, top panel**). I obtained similar results when comparing the copy number ratio of ARS316 with another late-replicating region of Chromosome IV, where Ask1 recruitment - but not the recruitment of Gcn5 or Set3 - showed a significant increase of ARS316 replication (**Figure 44, bottom panel**). Therefore, I conclude that recruitment of Ask1 to the LI origin ARS316 has the strongest effect on replication timing out of this pool of investigated proteins.
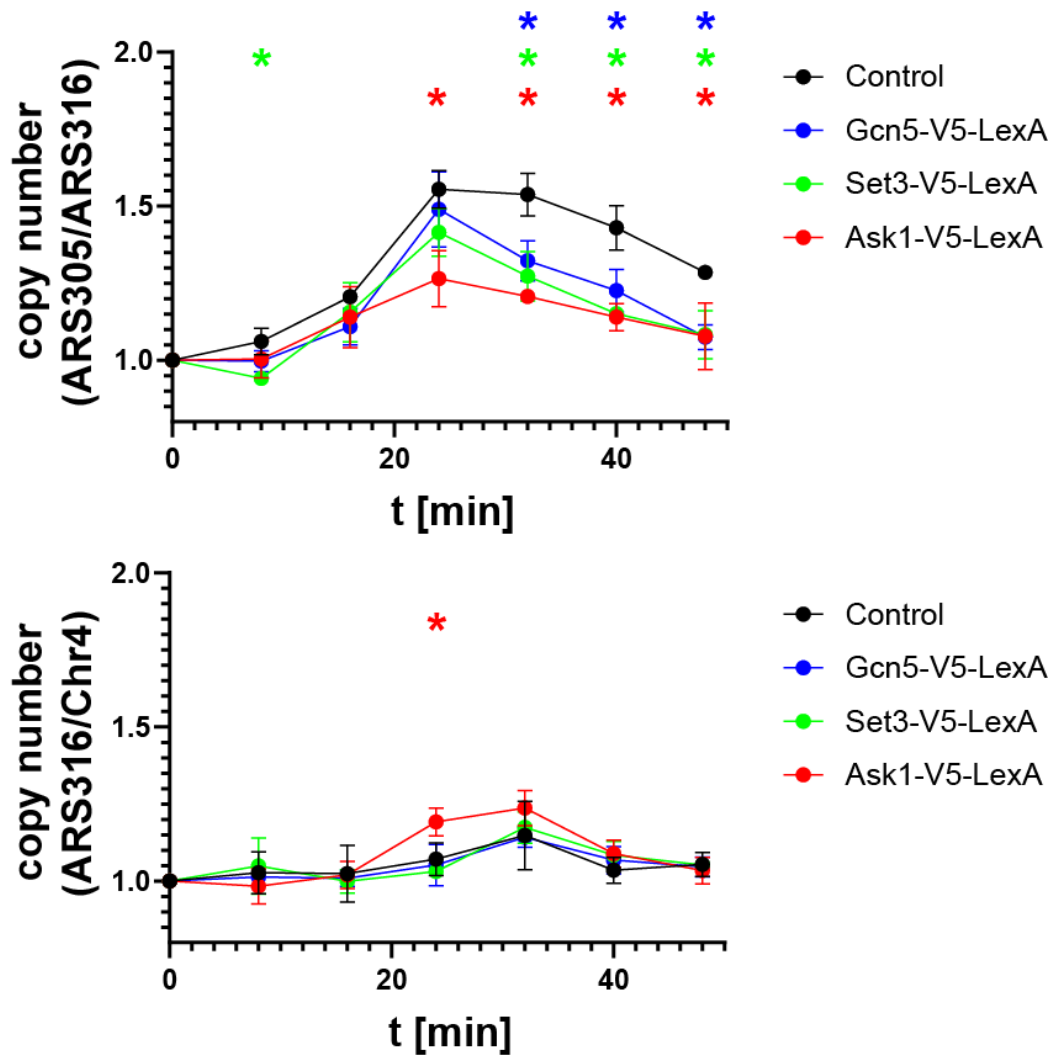
Figure 44 Confirming the effect of the tethering of Ask1 and Set3 to the LI replication origin ARS316 Analysis of the replication timing by copy number analysis in the yeast strains Y0071 expressing Ask1-V5-LexA, Y0076 expressing Set3-V5-LexA, Y0079 expressing Gcn5-V5-LexA and Y0019 as an untagged control strain. Samples for genomic DNA extraction were taken at the indicated timepoints for copy number analysis by qPCR to determine the relative replication timing of depicted loci. The plots show the average copy number ratios of the origins ARS305 to ARS316 (top panel), as well as ARS316 to a late-replicating region (Chr 4) (bottom panel) with standard deviation from n = 3 biological replicates (* indicates statistical significance $p < 0.05$, unpaired t-test).

Importantly, recruitment of LexA-TAP as a control LexA-fusion protein gave an identical replication timing profiles compared to the control cells (**Figure 45**), strongly suggesting that the Ask1 moiety is responsible for this specific effect on replication timing.
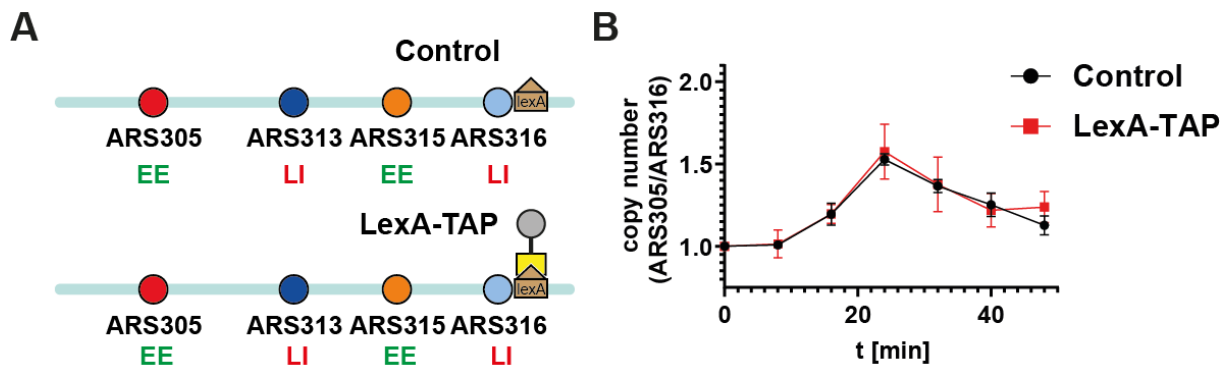
Figure 45 Effect of the tethering of LexA-TAP to the LI replication origin ARS316 A) Experimental outline for assessing the effect of tethering LexA-TAP at the LI replication origin ARS316. Yeast strains Y0019 (Control) and Y0067 (LexA-TAP) contain a cluster of 3x LEXA binding sites in close proximity to ARS316. Y0067 but not Y0019 expresses a LexA-TAP fusion protein that can bind to the 3xLEXA sites. **B)** Analysis of the replication timing by copy number analysis. Samples for genomic DNA extraction were taken at the indicated timepoints for copy number analysis by qPCR to determine the relative replication timing of depicted loci. The plots show the average copy number ratios of the origins ARS305 and ARS316 with standard deviation from n = 1 biological replicates.

Similarly, to make sure that this effect on replication stems from the tethering of Ask1 to ARS316, I also performed ChIP analysis in order to confirm the recruitment of Ask1-V5-LexA to its target site. ChIP-qPCR with an anti-V5 antibody revealed an enrichment of Ask1-V5-LexA in the vicinity of the LEXA binding site at ARS316 in comparison to an untagged control strain (**Figure 46**), indicating successful recruitment of Ask1 to ARS316.
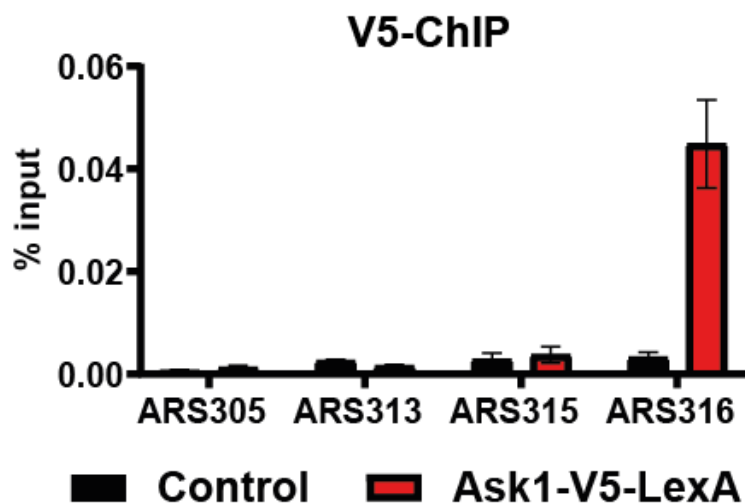
Figure 46 ChIP-qPCR analysis to confirm recruitment of Ask1-V5-LexA to ARS316 ChIP-qPCR analysis using a V5-antibody to immunoprecipitate Ask1-V5-LexA at the indicated genomic regions in the yeast strain expressing Ask1-V5-LexA (Y0071) and untagged Control strain (Y0001). The bars indicate mean and standard deviations from 3 biological replicates.

4.4.3 DNA copy number sequencing confirms the effect of Ask1 on the LI replication origin ARS316

To confirm these results of the Ask1 recruitment and to extend the analysis to the entire chromosome III, I next monitored DNA replication in the same strains by DNA copy number sequencing (Fang et al., 2017; Müller et al., 2019). Briefly, cells were arrested in G1 phase with alpha-factor and released synchronously into S phase for 24min to allow both initiation and elongation of DNA replication. Additionally, cells were also released in the presence of 200 mM hydroxyurea (HU) for 60min to only allow initiation of EE origins. In biological triplicates, cells were collected in G1, 24min, and 60 min + HU treatment conditions after release into S phase, genomic DNA was extracted and analyzed by qPCR or DNA sequencing (**Figure 47**).
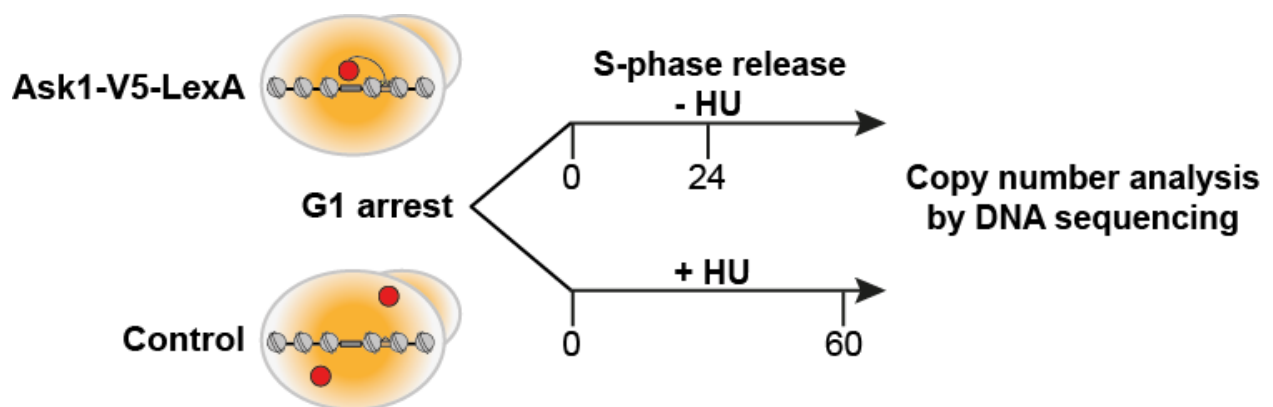
Figure 47 Experimental outline for the DNA copy number sequencing analysis Analysis of the replication timing by copy number DNA sequencing in the yeast strains Y0071 expressing Ask1-V5-LexA and Y0019 as an untagged Control strain. Cells were released into S phase for 24min in the absence or 60min in the presence of 200mM HU as indicated.

The qPCR analysis reproduced a significant increase of DNA copy number at Ask1-V5-LexA-targeted ARS316 24min after release compared to control cells without Ask1-V5-LexA-fusion protein expression, whereas the 60min +HU condition showed a similar but less pronounced tendency (**Figure 48**).
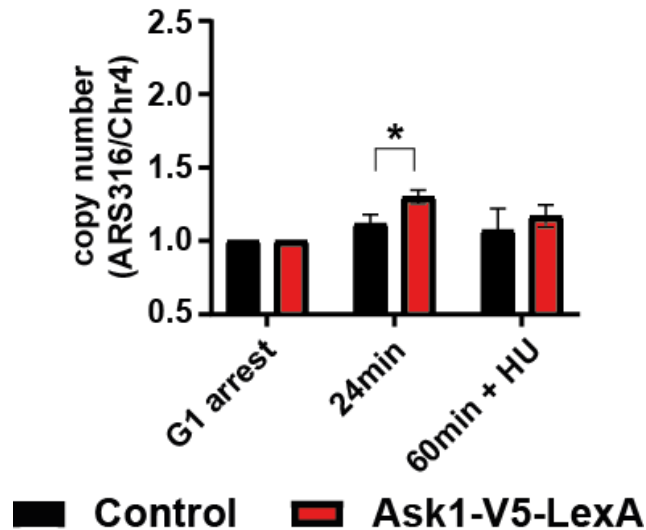
Figure 48 qPCR analysis to determine the effect of Ask1 on the LI replication origin ARS316 Genomic DNA samples from G1 arrest, 24min release and 60min release + HU were analyzed by qPCR for copy number analysis to determine the relative replication timing of depicted loci in yeast strains Y0071, expressing Ask1-V5-LexA, and Y0019 as an untagged control strain. The plots show the average copy number ratios of the origin ARS316 to a late-replicating region (Chr 4) with standard deviation from n = 3 biological replicates (* indicates statistical significance $p < 0.05$, unpaired t-test).

To generate replication profiles, the log2 ratio of uniquely mapped reads in 24min and 60min + HU-arrested cells to G1 samples was calculated with a bin size of 500bp. Unreplicated regions of the genome presented the same copy number as in the G1-sample and therefore show a lower ratio. In contrast, origin firing results in an increased relative copy number around active origins in both 24min release and 60min + HU conditions (**Figure 49A-B**). In Ask1-V5-LexA cells, we observed a marked increase in the activity of ARS316 relative to control cells (**Figure 49A-B, black arrow**), which is consistent with the results obtained by qPCR (**Figures 48**). Interestingly, additional two regions on the right arm of chromosome III significantly advanced replication timing (**Figure 49A, green asterisk**), whereas 3 intervening late-replicating regions close to the targeted ARS316 showed decreasing copy number ratios (**Figure 49A, red asterisks**). Under 60min + HU conditions, Ask1 recruitment to ARS316 also showed a small but significant increase in DNA copy number of the target origin (**Figure 49B, black arrow**), suggesting that a population of cells shifted replication timing of this origin into early S phase. Similar to the 24min samples, neighboring EE origins including ARS315 advanced replication (**Figure 49B, green asterisk**), whereas multiple late-replicating regions scattered along chromosome III were further delayed (**Figure 49B, red asterisk**). Together, these data show that Ask1 tethering to the LI origin ARS316 is sufficient to advance replication

of this origin as well as neighboring EE regions at the cost of less efficient replication of intervening late-inefficient regions. These data are consistent with a model that Ask1/DASH recruitment at specific chromosomal sites can rearrange or cluster larger chromosomal regions in such a way that the difference of replication timing between EE and LI regions become more pronounced.
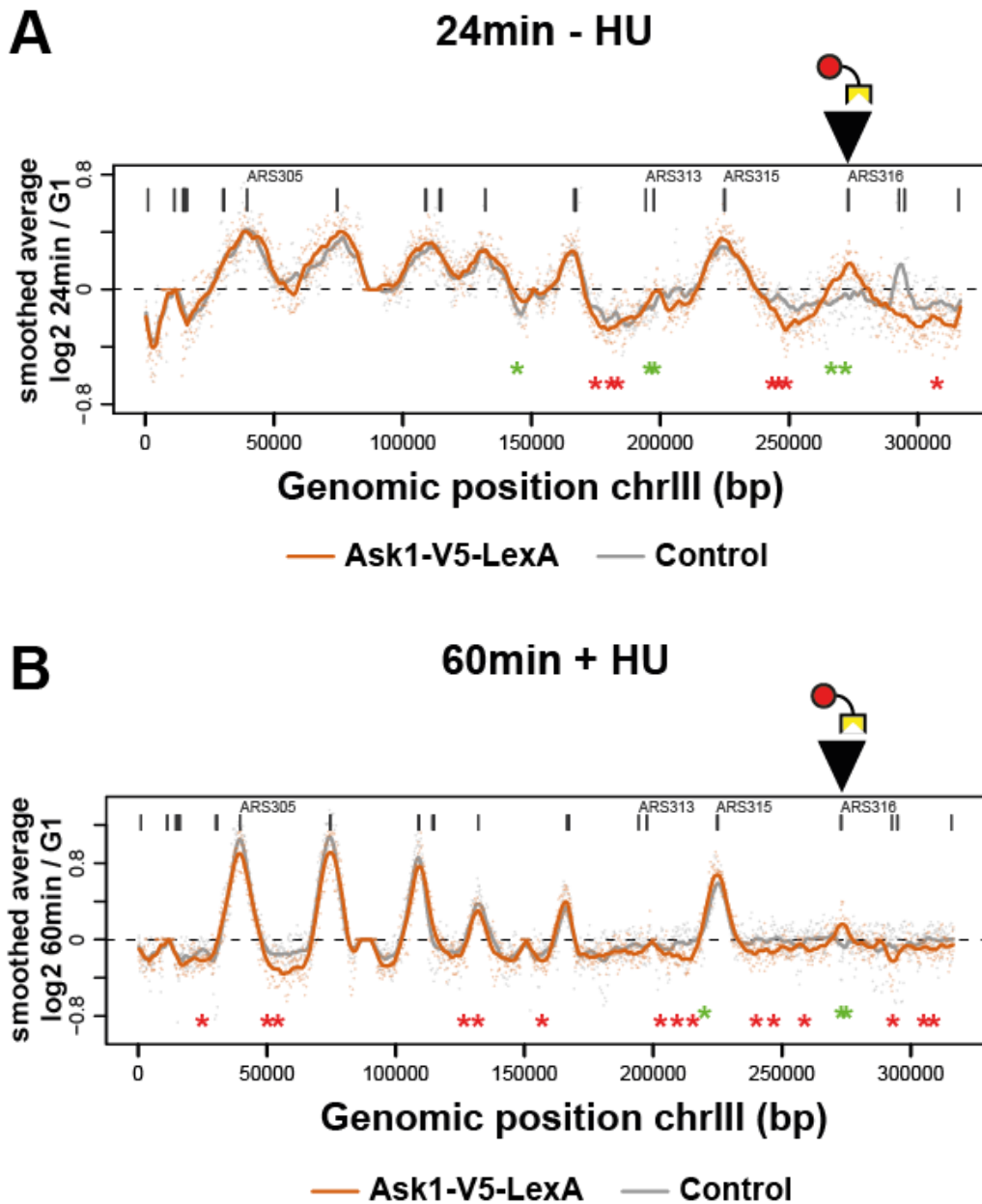
Figure 49 DNA copy number sequencing to determine the effect of Ask1 on the LI replication origin ARS316 A) Replication profiles of chromosome III at 24 minutes after release into S phase in the strain expressing Ask1-V5-LexA tethered to ARS316 (Y0071) (black triangle) compared to an isogenic Control strain containing LEXA binding sites at ARS316 but not expressing a LexA fusion protein (Y0019). Regions that significantly increased or decreased replication timing were obtained using Welch two sample t-test (unequal variances) in each genomic bin with a p-value cutoff of 0.05 and a mean difference of at least 0.1 and indicated with green or red asterisks, respectively. **B)** Replication profiles of chromosome III at 60min release into S phase and 200mM HU treatment in the same strains as in G). Regions that significantly increased or decreased replication timing were obtained using Welch two sample t-test (unequal variances) in each genomic bin with a p-value cutoff of 0.05 and a mean difference of at least 0.1 and indicated with green or red asterisks, respectively.

4.4.4 DNA copy number sequencing reveals further origins affected by Ask1 tethering experiments

DASH complex subunits were detected in the mass spectrometry datasets of the two origins ARS305 and ARS313. Thus, I asked if and how artificial tethering of Ask1 at these two distinct locations in addition to the endogenous binding of the complex can affect the replication profile of chromosome III. To this end, I took advantage of our LEXA strains and recruited Ask1-V5-LexA to ARS313 (**Figure 50A**) or ARS305 (**Figure 50B**) replication origins, then performed DNA copy number analysis by qPCR and DNA sequencing at 24min after release and 60min + HU treatment.
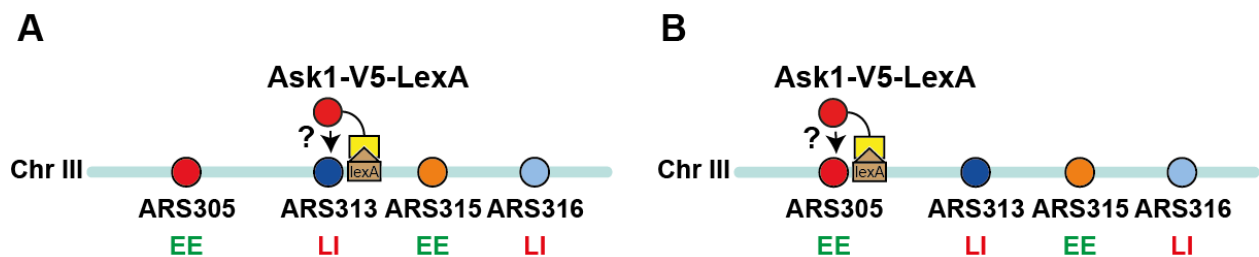
Figure 50 Effect of the tethering of Ask1-V5-LexA to the origins ARS313 and ARS305 A) Experimental outline for assessing the effect of Ask1 tethering at the LI replication origin ARS313. Yeast strain Y0139 expresses Ask1 as LexA-V5 fusion protein. This allows artificial recruitment of Ask1/DASH to the ARS313 origin in the yeast strain background that contains a cluster of 3x LEXA binding sites in close proximity to ARS313. **B)** Experimental outline for assessing the effect of Ask1 tethering at the EE replication origin ARS305. Yeast strain Y0138 expresses Ask1 as LexA-V5 fusion protein. This allows artificial recruitment of Ask1/DASH to the ARS305 origin in the yeast strain background that contains a cluster of 3x LEXA binding sites in close proximity to ARS305.

ChIP-qPCR with a V5 antibody confirmed similar enrichment of Ask1-V5-LexA in the vicinity of the LEXA binding sites of ARS313 (**Figure 51A**) and ARS305 (**Figure 51B**), indicating successful recruitment of Ask1 in both experiments.
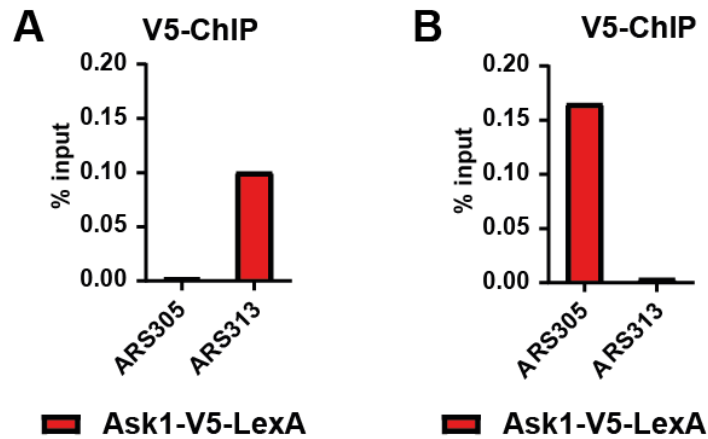
Figure 48 ChIP-qPCR analysis to confirm recruitment of Ask1-V5-LexA to ARS313 and ARS305
A) ChIP-qPCR analysis using a V5-antibody to immunoprecipitate Ask1-V5-LexA at the indicated genomic regions in the yeast strain tethering Ask1-V5-LexA to ARS313 (Y0139) (n=1). **B)** ChIP-qPCR analysis using a V5-antibody to immunoprecipitate Ask1-V5-LexA at the indicated genomic regions in the yeast strain tethering Ask1-V5-LexA to ARS305 (Y0138) (n=1).

Intriguingly, Ask1 recruitment to ARS313 advanced replication of ARS313 LI origin as shown by qPCR (**Figure 52**). Both after 24min, as well as 60min in the HU condition, there was a significant increase in replication at the LI replication origin ARS313.
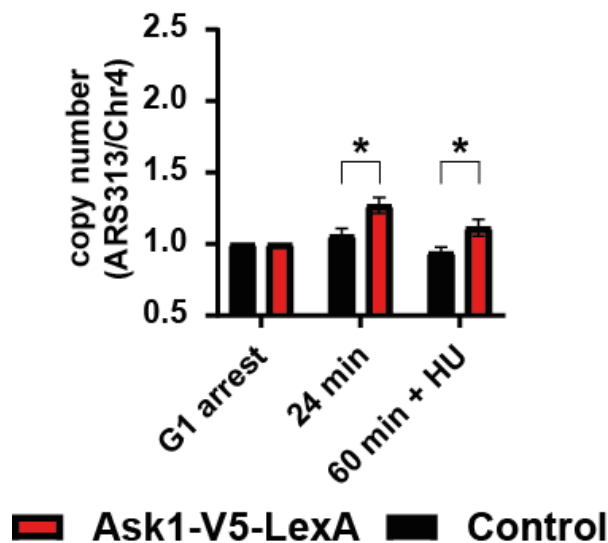
Figure 52 qPCR analysis to determine the effect of Ask1 on the LI replication origin ARS313
Analysis of the replication timing by copy number analysis in the yeast strains Y0139 expressing Ask1-V5-LexA and Y0045 as an untagged Control strain. Genomic DNA samples from G1 arrest, 24min release and 60min release + HU were analyzed by qPCR for copy number analysis to determine the relative replication timing of depicted loci. The plots show the average copy number ratios of the origin ARS313 to a late-replicating region (Chr 4) with standard deviation from n = 3 biological replicates (* indicates statistical significance $p < 0.05$, unpaired t-test).

Additionally, DNA replication was measured by DNA copy number sequencing in these samples, which confirmed the results of the qPCR analysis. The resulting replication profiles revealed that the neighboring active replication origins ARS307, ARS308 and ARS309 showed increased activity (**Figure 53A, green asterisks**), whereas the intervening region of ARS315

and ARS316 showed a decrease in DNA copy number similar to the effect observed after Ask1 tethering to ARS316 (**Figure 53A, red asterisk**). Thus, Ask1 recruitment to ARS313 positively affected a cluster of EE origins in the close neighbourhood of the targeted origin. Surprisingly, an increase in the replication of ARS313 in the HU condition after 60min was detected (**Figure 53B, green asterisks**). This indicates that there is a population of cells where the tethering of Ask1 made ARS313 an early firing origin that could even fire before replication checkpoint activation.
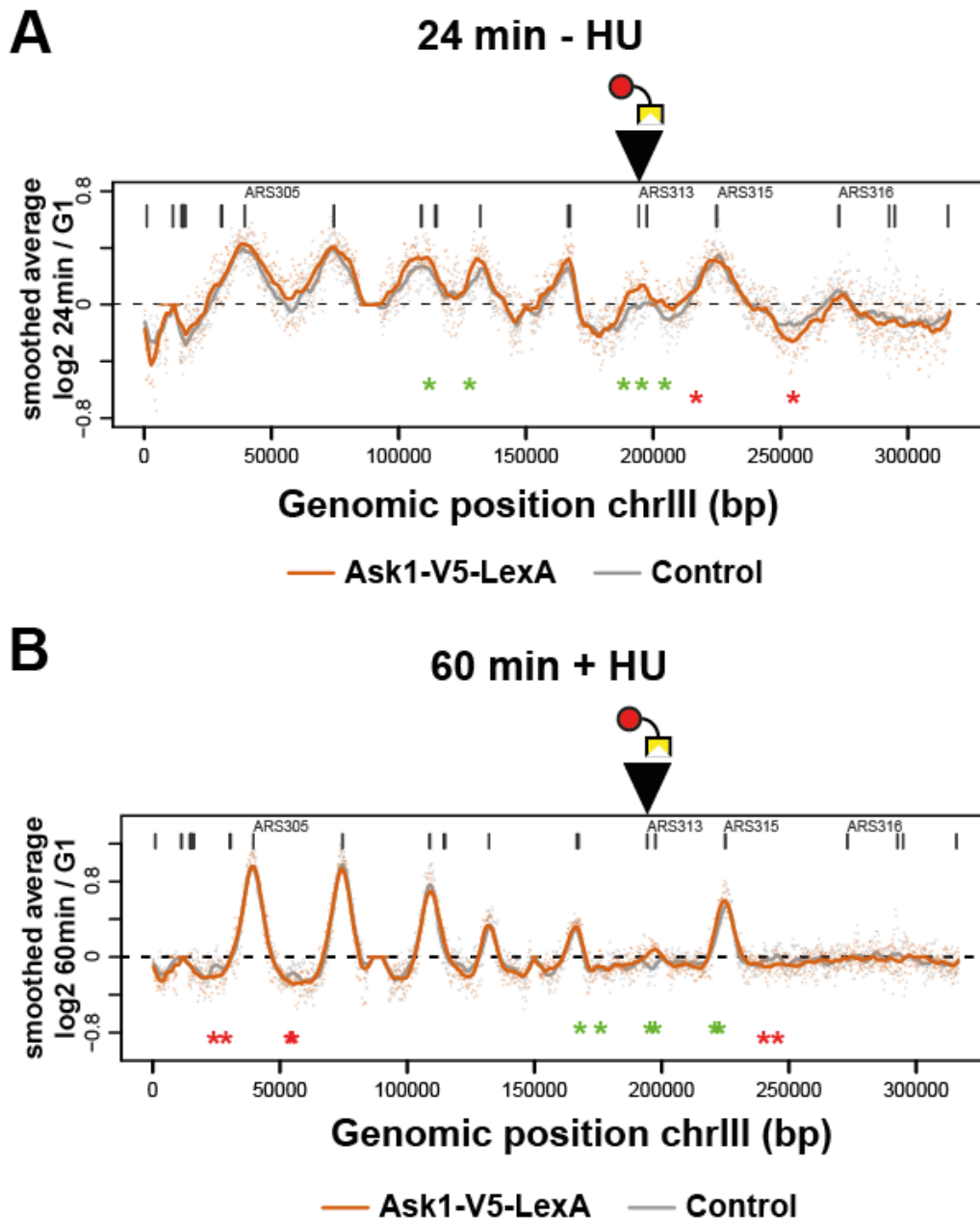
Figure 53 DNA copy number sequencing to determine the effect of Ask1 on the LI replication origin ARS313 A) Replication profiles of chromosome III at 24 minutes after release into S phase in the strain expressing Ask1-V5-LexA tethered to ARS313 (Y0139) (black triangle) compared to an isogenic Control strain containing LEXA binding sites at ARS313 but not expressing a LexA fusion protein (Y0045). Regions that significantly increased or decreased replication timing were obtained using Welch two sample t-test (unequal variances) in each genomic bin with a p-value cutoff of 0.05 and a mean

difference of at least 0.1 and are indicated with green or red asterisks, respectively. **B)** Replication profiles of chromosome III at 60min release into S phase and 200mM HU treatment in the same strains as in D). Regions that significantly increased or decreased replication timing were obtained using Welch two sample t-test (unequal variances) in each genomic bin with a p-value cutoff of 0.05 and a mean difference of at least 0.1 and indicated with green or red asterisks, respectively.

When examining the effects of tethering Ask1 to the EE replication origin ARS305 by qPCR, there were no significant changes detectable compared to the control strain (**Figure 54**).
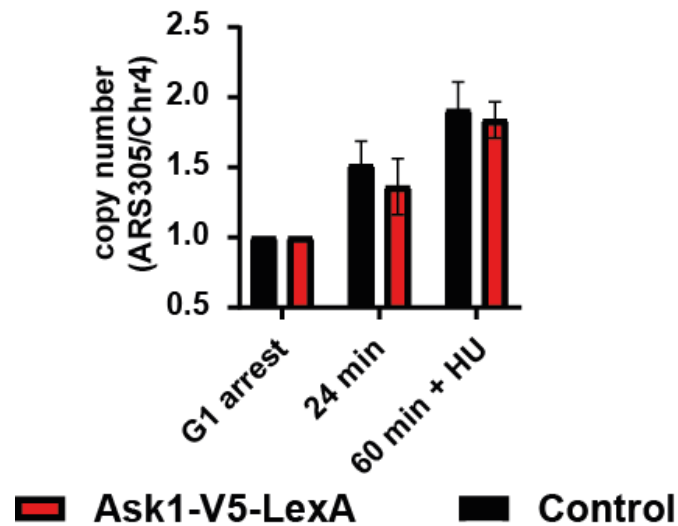
Figure 54 qPCR analysis to determine the effect of Ask1 on the EE replication origin ARS305
Analysis of the replication timing by copy number analysis in the yeast strains Y0138 expressing Ask1-V5-LexA and Y0016 as an untagged Control strain. Genomic DNA samples from G1 arrest, 24min release and 60min release + HU were analyzed by qPCR for copy number analysis to determine the relative replication timing of depicted loci. The plots show the average copy number ratios of the origin ARS305 to a late-replicating region (Chr 4) with standard deviation from n = 3 biological replicates (* indicates statistical significance p < 0.05, unpaired t-test).

However, when conducting the copy number sequencing experiment, I strikingly obtained similar results by tethering Ask1 to ARS305 on the other arm of the chromosome. First, DNA sequencing analysis showed a small increase in origin activity at ARS305 at the 24min timepoint, despite the fact that ARS305 is already early-efficient under wildtype conditions (**Figure 55A**). Second, the same cluster of origins in the center of the chromosome (ARS307, ARS308 and ARS309) advanced replication to a similar extent as after recruitment to ARS313 (**Figure 55A, green asterisks**). Under 60min + HU conditions, Ask1 recruitment to ARS305 did not show dramatic changes in the firing of EE origins except for a region around ARS308, but further dropped the DNA copy number of several late-replicating inter-origin regions (**Figure 55B, red asterisks**).
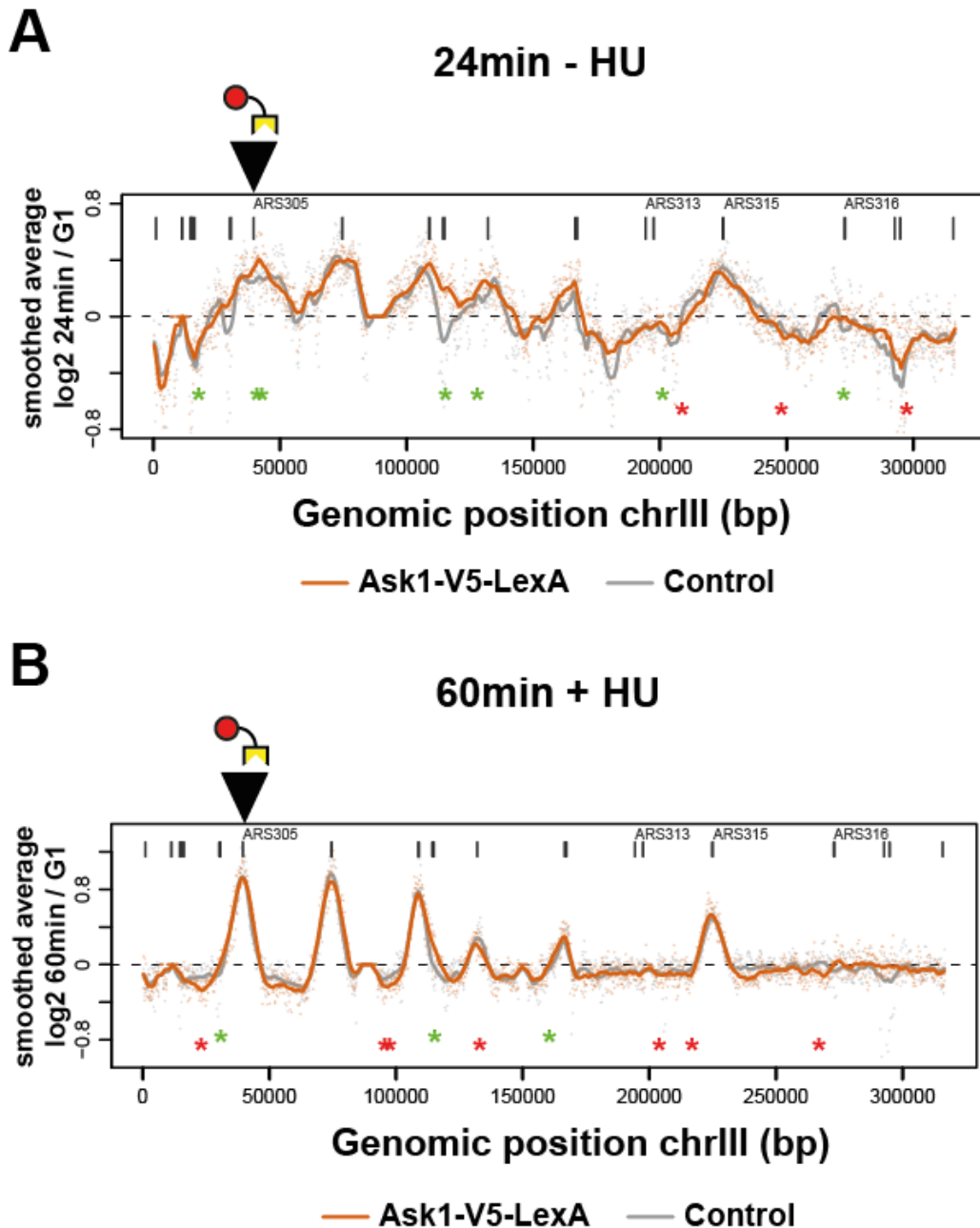
Figure 55 DNA copy number sequencing to determine the effect of Ask1 on the EE replication origin ARS305 A) Replication profiles of chromosome III at 24 minutes after release into S phase in the strain expressing Ask1-V5-LexA tethered to ARS305 (Y0138) (black triangle) compared to an isogenic Control strain containing LEXA binding sites at ARS305 but not expressing a LexA fusion protein (Y0016). Regions that significantly increased or decreased replication timing were obtained using Welch two sample t-test (unequal variances) in each genomic bin with a p-value cutoff of 0.05 and a mean difference of at least 0.1 and indicated with green or red asterisks, respectively. **B)** Replication profiles of chromosome III at 60min release into S phase and 200mM HU treatment in the same strains as in I). Regions that significantly increased or decreased replication timing were obtained using Welch two sample t-test (unequal variances) in each genomic bin with a p-value cutoff of 0.05 and a mean difference of at least 0.1 and indicated with green or red asterisks, respectively.

In general, the replication profiles in all the tethering and control strains showed very high correlations among the biological replicates (**Figure 56A**) except for a region on the right arm of chromosome III downstream of ARS318 that showed significant variability among the individual replicates (**Figure 56B, black triangle**).
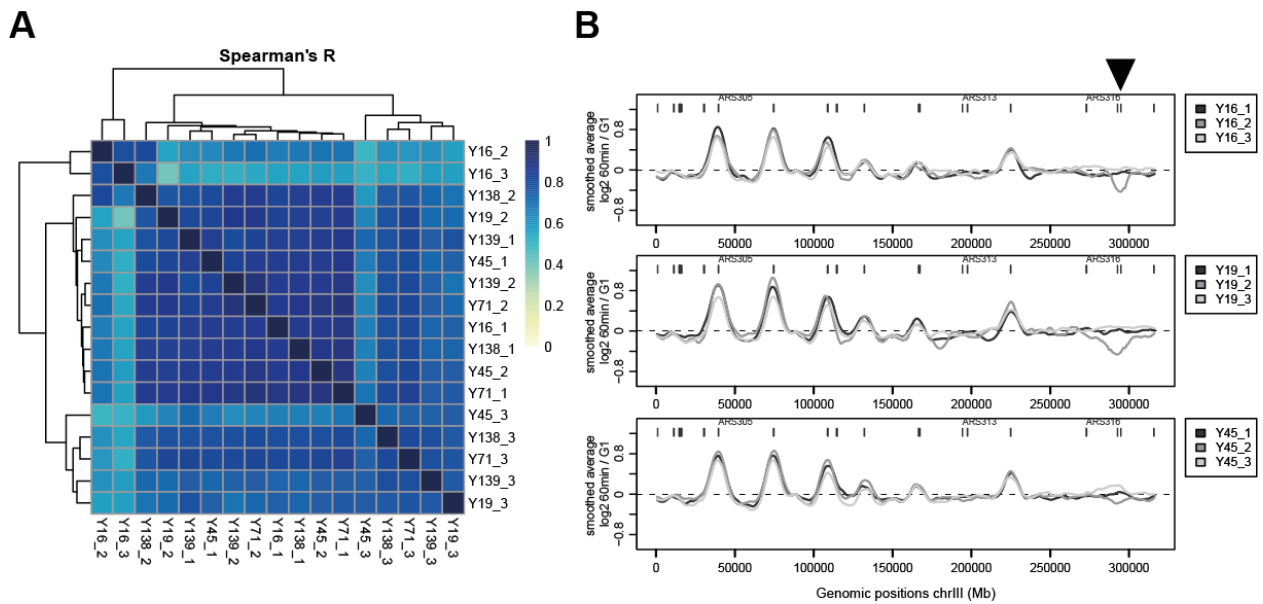
Figure 56 Correlation analysis between the replication profiles determined by copy number sequencing A) Spearman correlation matrix of the replication timing profiles of all biological replicates of the Control (Y16, Y19 and Y45) and tethering strains (Y71, Y138, Y139) at the 24min release timepoint. **B)** Replication profiles of chromosome III at 60min +HU after release into S phase of the individual biological replicates of the control strains Y16, Y19 and Y45). The black arrow indicates a region with high variability among biological replicates.

Importantly, all significant changes reported above were highly reproducible and significant across the 3 biological replicates, thereby avoiding such rare regions with large intrinsic noise in the replication timing profiles. Together, these results suggested a model where Ask1/DASH complex could provide individual chromosomal attachment points that support efficient origin clustering in G1 phase cells and therefore explain the observed long-range effects of individual neighboring chromosomal domains while leaving others unaffected.

4.5 Loss-of-function experiments to further characterize the potential novel replication factors Ask1 and Set3

Apart from the strategy above to tether the proteins of interest to specific replication origins, I also examined the effect of a global loss of Set3 and Ask1 proteins on replication timing control.

4.5.1 Knocking out Set3 has a minor impact on replication timing

When tethering Set3 to the LI replication origin ARS316, it produced a weaker effect as compared to Ask1 (**Figure 44**). Nevertheless, it was a significant increase in replication which prompted me to test the effect of a loss of this protein to the replication landscape. Since SET3 is not an essential gene, I created Set3 knockout strains. For the experiment, cells were arrested in G1 phase with alpha-factor and synchronously released to S phase to monitor the replication timing of the four investigated replication origins ARS305, ARS313, ARS315, and ARS316 by qPCR copy number analysis. In this analysis, the copy number of the origins was always compared to the LI region on chromosome IV (Chr4). The two EE replication origins

ARS305 and ARS315 showed very similar replication profiles compared to the wildtype control upon loss of Set3 (**Figure 57 A-B**). However, the two LI replication origins ARS313 and ARS316 displayed an increase in replication, especially towards the later timepoints at 40min (**Figure 57 C-D**). It has to be noted, however, that this experiment was only performed once, so more biological replicates would be needed to confirm these results. If these findings are reproducible, it would be intriguing to study the effect of this histone deacetylase in more detail, especially considering the fact that we also detected different acetylation levels at EE and LI origins in our mass spectrometry experiments (**Figure 39**). However, I focused on further investigating Ask1 that affected replication timing with higher effect size.
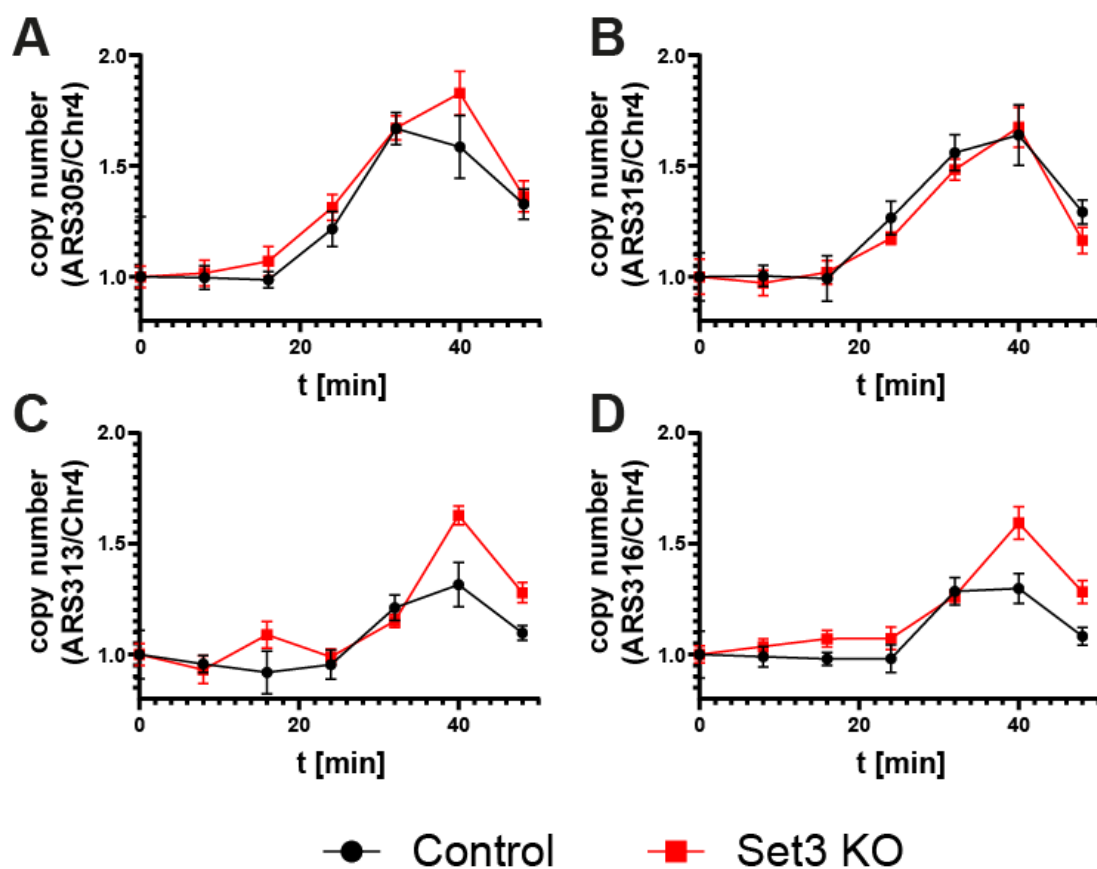
Figure 57 qPCR analysis to determine the effect of a Set3 KO on replication timing A-D) Analysis of the replication timing of the EE origins ARS305 (**A**) and ARS315 (**B**), as well as the LI replication ARS313 (**C**) and ARS316 (**D**) for the Set3 KO strain (Y117) in comparison to a parental control strain (Y0001). Samples for genomic DNA extraction were taken at the indicated timepoints for copy number analysis by qPCR to determine the relative replication timing of depicted loci. The plots show the copy number ratios of the respective origins to a late-replicating region (Chr 4) with standard deviation from 3 technical replicates (n = 1 biological replicate).

4.5.2 Temperature sensitive Ask1 mutants show increased sensitivity to HU

Since ASK1 is an essential gene, studying the effect of a global loss of Ask1 was more difficult to achieve. For this reason, I first took advantage of three temperature sensitive Ask1 mutants that have previously been described in other studies (Li et al., 2002). Using these mutants, I determined whether these strains are sensitive to replication stress by HU treatment, which would imply a possible role in DNA replication. The three temperature sensitive mutants *ask1-1*, *ask1-2*, and *ask1-3* were grown together with the corresponding wildtype strain on YPD with or without 10mM HU at either room temperature or 30°C. Indeed, the two mutants *ask1-2*, and *ask1-3* showed a growth defect in the HU condition at the restrictive temperature (**Figure 58, right panels**). The *ask1-1* mutant, however, did not show this behavior, suggesting that this mutation may be a separation of function that does not affect DNA replication/HU sensitivity. This data gave further confidence that Ask1 could play a role in DNA replication timing, but eventually a cleaner loss of function system would be desirable to study this loss-of-function effect in more detail.
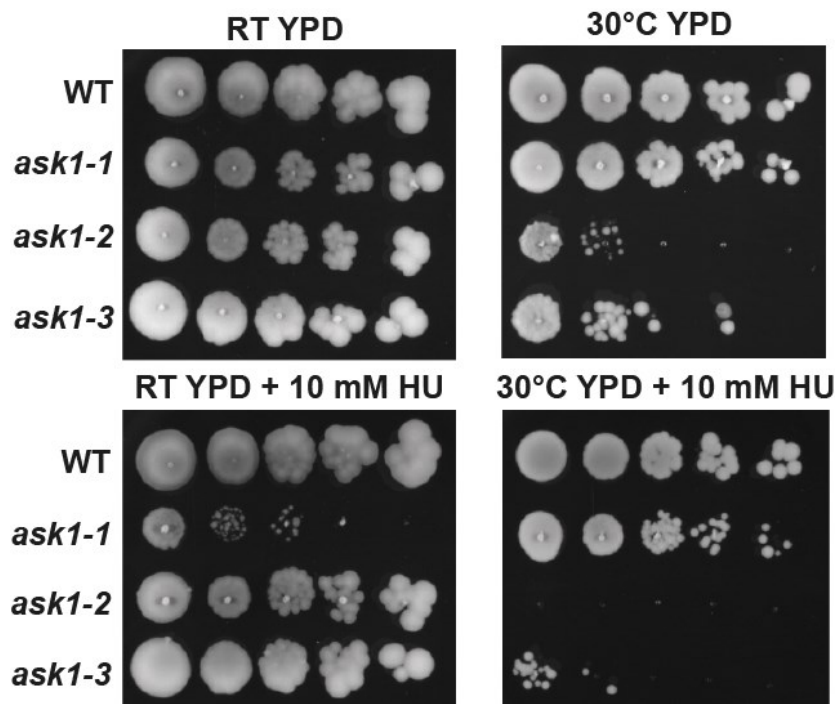
Figure 58 *Ask1-2* and *Ask1-3* temperature-sensitive mutants are sensitive to HU-induced replication stress Spot tests of the three temperature-sensitive Ask1 mutants ask1-1 (Y0099), ask1-2 (Y0100), and ask1-3 (Y0101) together with the corresponding wildtype strain (Y0098). Growth inhibition was monitored on YPD plates of serial dilutions of the strains with or without 10mM HU and incubation for 3 days at the indicated temperatures (RT = room temperature).

4.5.3 An auxin-inducible degron (AID) system to study loss-of-functions

Therefore, to further test the functional relevance of Ask1/DASH on the DNA replication program, I took advantage of an auxin-inducible degron (AID) system to conditionally degrade AID-tagged Ask1 protein (Morawska and Ulrich, 2013). After 20-40min of auxin treatment, Ask1 protein levels were undetectable in the Ask1-inducible degradation strain (Ask1-3xAID*-9xMYC) (**Figure 59**), which provided me with a tool to conditionally control the degradation and study the loss of function of this protein.
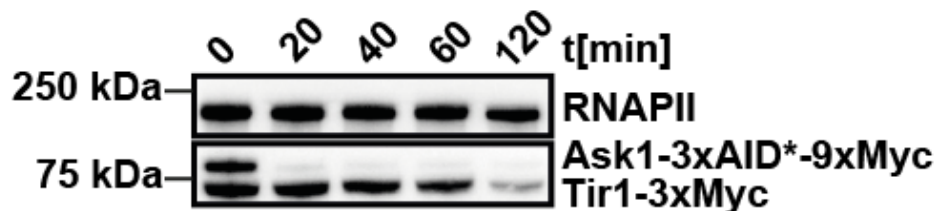
Figure 59 Western blot analysis to verify the efficiency of the AID system Yeast strain Y0123 expressing Ask1 fused to a 3xAID*-9xMyc tag was arrested in G1 phase by alpha-factor and then cultured in the presence and absence of 1mM auxin for the indicated timepoints. Western blot analysis shows the rapid degradation of Ask1 after 20-40min of auxin incubation. 3xMyc-tagged Tir1 and RNAPII were used as loading controls (n=1)

4.5.4 Ask1 depletion influences DNA replication on a global level

To examine a putative role of Ask1 in DNA replication, this strain was arrested in G1 phase using alpha-factor, followed by Ask1 degradation for 30min and subsequent release into S phase (**Figure 60**).
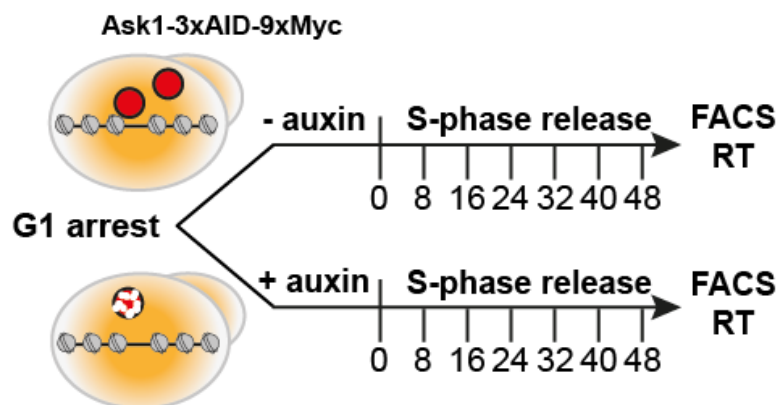
Figure 60 Schematic outline of the G1 arrest and release experiment in presence or absence of Ask1 Y0123 was grown to logarithmic phase and arrested in G1 phase by alpha-factor treatment. Cells were then cultured for 30min in the presence or absence of 1mM auxin before release into S phase by addition of 125 U Pronase. Samples were then taken at the indicated timepoints for FACS and replication timing (RT) analysis.

Ask1 degradation in this experiment was also confirmed by Western blot analysis (**Figure 61**).
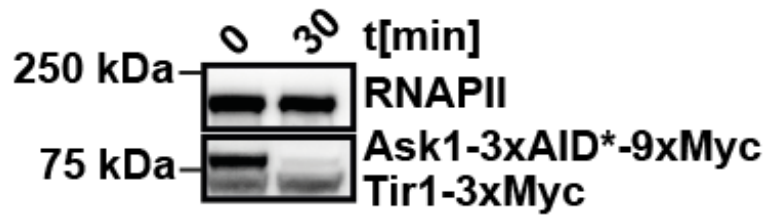
Figure 61 Western blot analysis to verify Ask1 depletion in the G1 arrest and release experiment
Western blot analysis shows the rapid degradation of Ask1 after 30min of auxin incubation during a G1
arrest. 3xMyc-tagged Tir1 and RNAPII were used as loading controls.

3.5.4.1 Cell cycle progression does not change upon Ask1 depletion

In time course experiments, I then monitored S phase progression using flow cytometry. Taking
samples every 8min after S phase release, control cells were compared to the Ask1 depletion
condition. No major differences in S phase progression kinetics between the control and Ask1-
depleted cells were detectable (**Figure 62**), suggesting that Ask1 does not affect or perturb the
DNA replication program on a global scale.
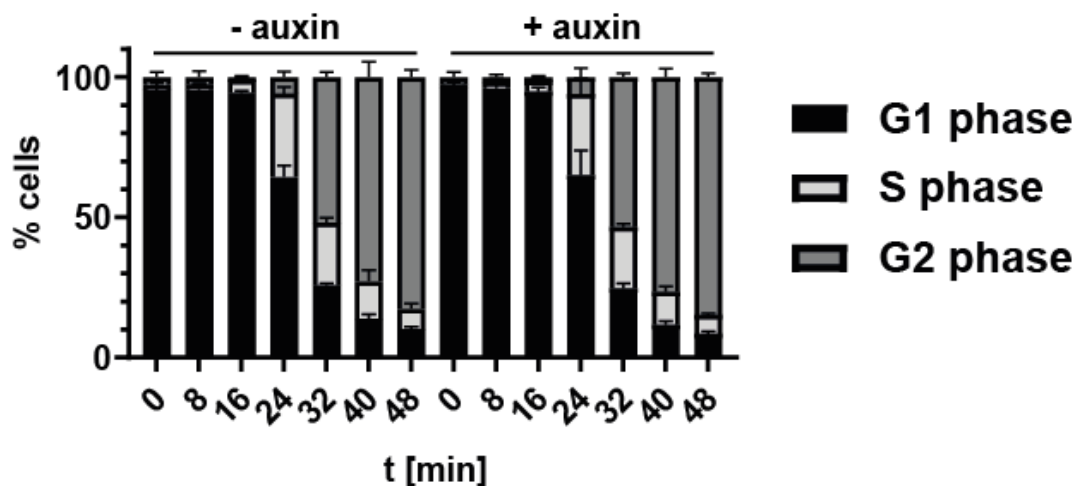
Figure 62 FACS analysis to determine the effect of Ask1 degradation on cell cycle progression.
S phase progression analysis by flow cytometry. Total DNA content was measured by SYTOX green-
staining after release into S phase. Bar graphs depict the percentage of G1, S and G2/M phase cells at
the indicated timepoints (n=3 biological replicates).

3.5.4.2 Replication timing analysis reveals an influence of Ask1 degradation on ARS313

However, the excess of eukaryotic origins may compensate the acute loss of Ask1 to complete
DNA synthesis and there could nevertheless be changes in replication timing at selected
specific origins under the control of Ask1. Therefore, I wanted to determine the effect of Ask1
degradation on the replication profile of specific EE or LI origins of chromosome III. To this
end, qPCR copy number analysis was used as above, to determine copy number ratios of EE
and LI origins (**Figure 63**). Ask1-depleted cells (+ auxin) showed no significant change in the
replication timing of the EE origin ARS305 or ARS315 in comparison to the LI origin ARS316
(**Figure 63, top panels**). Importantly, however, the LI origin ARS313 changed significantly

compared to the EE origins ARS305 and ARS315 between wildtype and Ask1-depleted cells (**Figure 63, bottom panels**). For both origins, Ask1-depleted cells showed lower copy number ratios, suggesting that replication of ARS313 was more efficient in the absence of Ask1 leading to earlier completion of replication after ~40min at this origin.
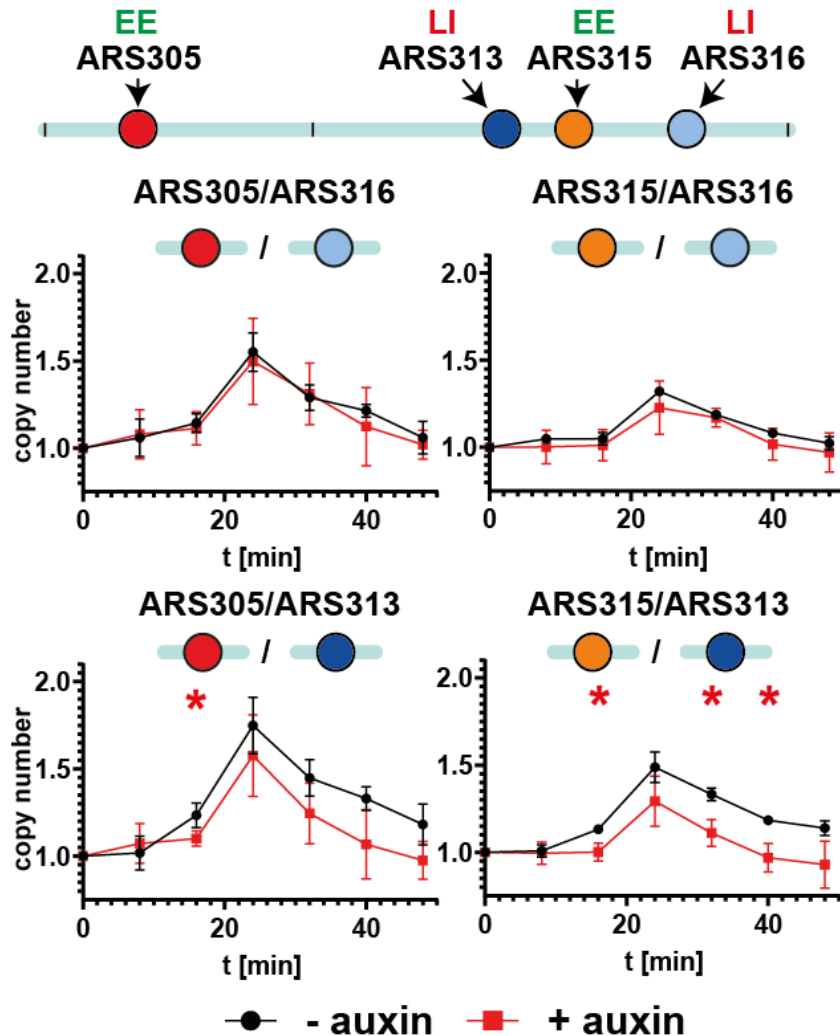
Figure 63 qPCR analysis to determine the effect of Ask1 degradation on replication timing Samples for genomic DNA extraction were taken at the indicated timepoints for copy number analysis by qPCR to determine the relative replication timing of depicted loci. The plots show the average copy number ratios of early (ASR305 and ARS315) to late origins (ARS313 and ARS316) with standard deviation from n=3 biological replicates (*indicates statistical significance $p < 0.05$, unpaired t-test)

Similar results were obtained when comparing the replication timing of the respective 4 origins to an independent late-replicating region on chromosome IV, where only the copy number ratio of ARS313 revealed significantly more efficient replication of this origin (**Figure 64**). Thus, it

can be concluded that endogenous Ask1 has a functional role in replication timing of the LI origin ARS313.
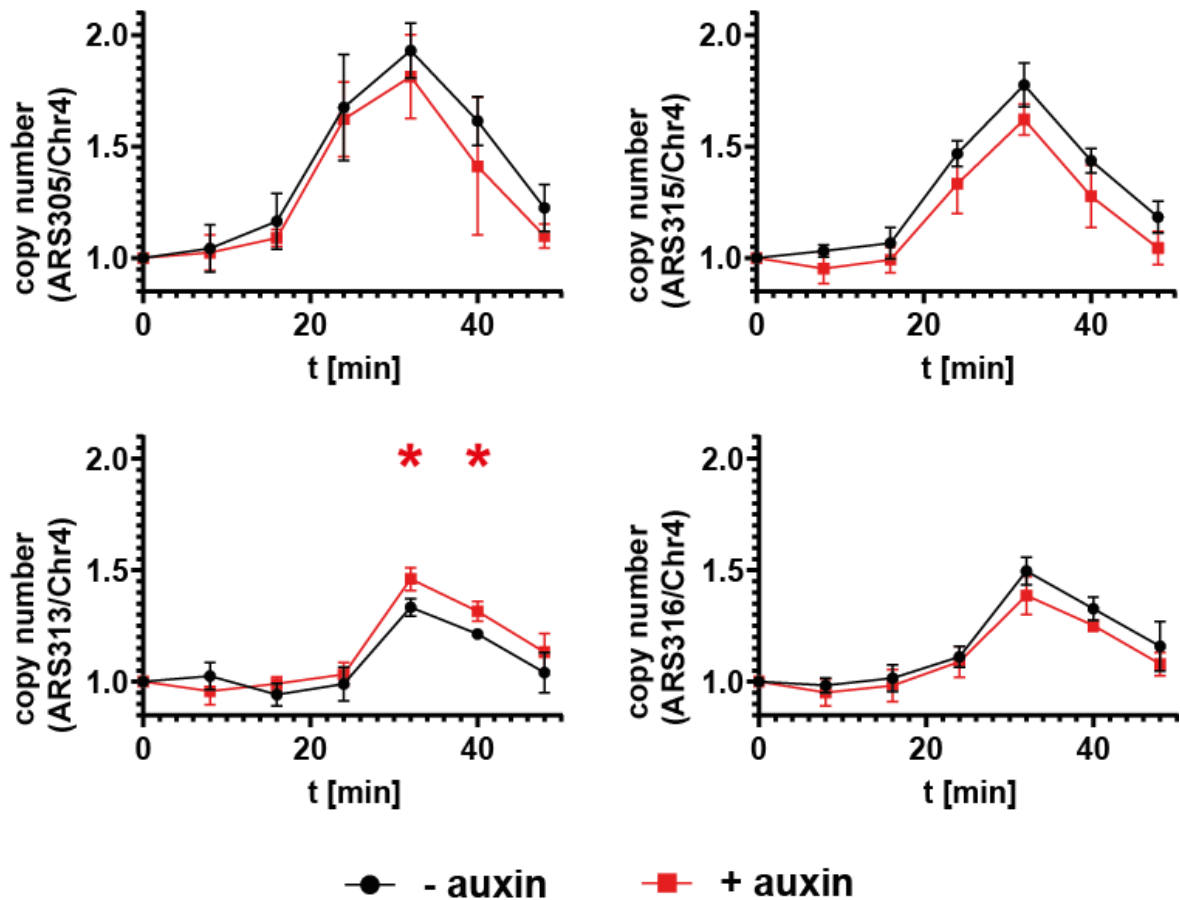
Figure 64 Additional qPCR analysis to determine the effect of Ask1 degradation on replication timing Samples for genomic DNA extraction were taken at the indicated timepoints for copy number analysis by qPCR to determine the relative replication timing of depicted loci. The plots show the average copy number ratios of early (ARS305 and ARS315) and late origins (ARS313 and ARS316) in comparison to a late-replicating region on Chr. 4 with standard deviation from n=3 biological replicates (*indicates statistical significance $p < 0.05$, unpaired t-test)

3.5.4.3 DNA copy number sequencing reveals global replication changes upon Ask1 degradation

To confirm these results and extend the analysis to the entire yeast genome, I next monitored DNA replication in Ask1 wildtype (- auxin) and Ask1-depleted cells (+ auxin) by DNA copy number sequencing (**Figure 65**).
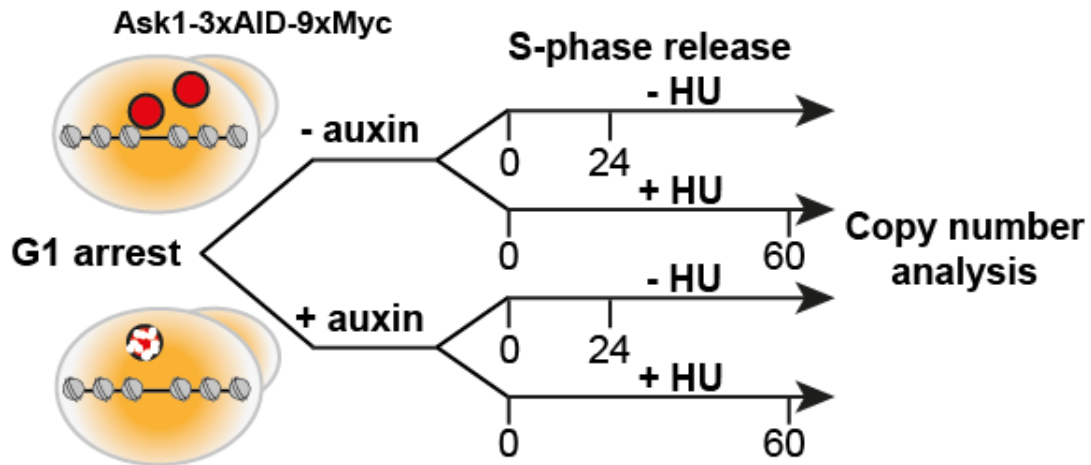
Figure 65 Schematic outline of the G1 arrest and release experiment to determine the effect of Ask1 degradation using copy number analysis. Y0123 was grown to logarithmic phase and arrested in G1 phase by alpha-factor treatment. Cells were then cultured for 30min in the presence or absence of 1mM auxin. The two cultures were then released into S phase by addition of 125U Pronase and harvested 24min after release or 60min after release in the presence of 200mM HU

After release into S phase for 24min, three major changes in the replication profile of chromosome III were observed. As expected, a region of ~ 15kb around ARS313 advanced replication (**Figure 66A, green asterisk**), further confirming our initial qPCR results (**Figure 63 and 64**). Interestingly, one additional region on chromosome III shifted to earlier replication in vicinity to ARS309. At the same time, several regions showed delayed replication in Ask1-depleted cells, including the left end of the chromosome upstream of ARS305 as well as a region around the ARS308 origin. In fact, this origin overlaps with the CEN3 centromeric region of chromosome III, where Ask1/DASH complex is expected to bind as part of the kinetochore (**Figure 66A, red asterisks**). In cells released for 60min + HU treatment, the general pattern of EE origin firing was preserved with only very few regions showing small but significant changes towards earlier replication (**Figure 66B, green asterisks**). Importantly, ARS313 and CEN3 were not significantly affected in this condition, suggesting that the Ask1-dependent change of replication at these sites is not occurring at the initiation stage of early replication origins, but rather at a later elongation stage during S phase progression (**Figure 66B**). This data suggested that chromosome III normally contains three major positions where Ask1/DASH exerts a functional role in replication timing including ARS313, ARS309 and the centromeric ARS308.
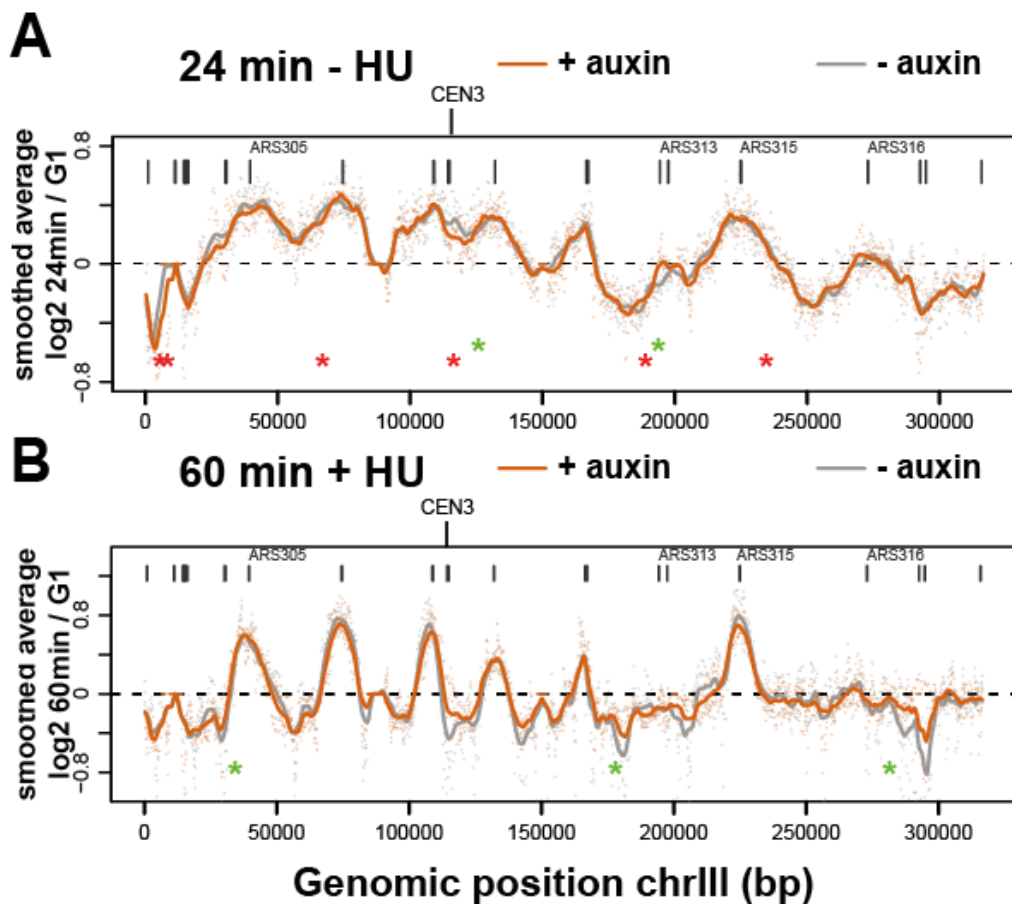
Figure 66 DNA copy number sequencing to determine the effect of Ask1 degradation. A) Replication profiles of chromosome III at 24min after release into S phase with and without degrading Ask1 by addition of auxin in the strain Y0123. Regions that significantly increased or decreased replication timing were obtained using Welch two sample t-test (unequal variances) in each genomic bin with a p-value cutoff of 0.05 and a mean difference of at least 0.1 and indicated with green or red asterisks, respectively. **B)** Replication profiles of chromosome III at 60min release into S phase in the presence of 200mM HU with and without degrading Ask1 by addition of auxin in the strain Y0123. Regions that significantly increased or decreased replication timing were obtained using Welch two sample t-test (unequal variances) in each genomic bin with a p-value cutoff of 0.05 and a mean difference of at least 0.1 and indicated with green or red asterisks, respectively.

Importantly, similar results were obtained for the other chromosomes, where overall 236 regions were detected that showed advanced replication in the Ask1-depleted cells (Ask1-repressed) (**Figure 67, Appendix 1-4)**, whereas 224 regions showed delayed replication compared to the Ask1 wildtype cells (Ask1-activated) (**Figure 67, Appendix 1-4)**. Among these regions, the centromeres of chromosome V, VII and VIII (CEN5, CEN7 and CEN8) showed a similar delay of replication as CEN3, whereas three other chromosomes advanced centromeric replication (CEN2, CEN11 and CEN15) in Ask1-depleted cells. In general, regions with delayed replication (Ask1-activated) tend to be located in inter-origin locations as only 29 of the 224 regions overlapped within 5kb of annotated replication origins (13%). In contrast, regions that advanced replication were more frequently associated with replication origins (80/236, 34%) (**Figure 67**).
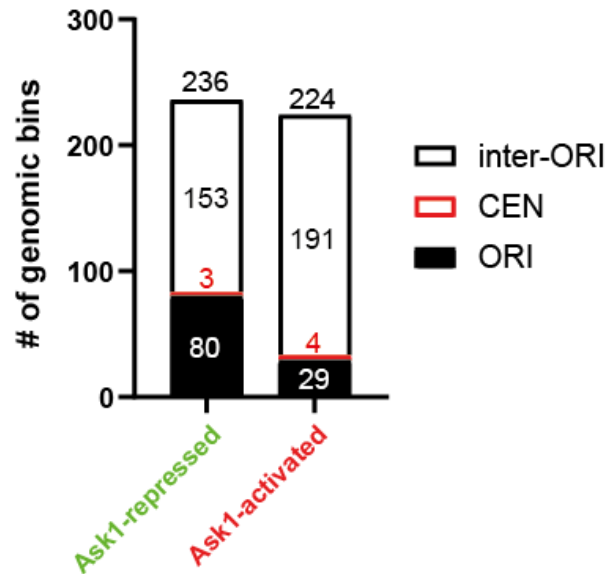
Figure 67 Bar graph of the number of genomic bins that changed replication timing. The graphs show regions in proximity to centromeres (CEN), origins (ORI) or inter-origin locations, which advanced (Ask1-repressed) or delayed replication timing (Ask1-activated).

Consistent with the initial FACS analysis (**Figure 62**), these data support the notion that endogenous Ask1/DASH recruitment at origins does not act as a global regulator of replication timing, but rather regulates the replication of specific chromosomal regions including a subset of replication origins, centromeric as well as non-origin regions. The fact that the changes were often scattered throughout the individual chromosomes in both positive and negative directions suggested that the function of Ask1/DASH in replication timing may not be locally restricted to individual origins but rather involve concerted changes of larger chromosomal regions in the nucleus.

4.5.5 Ask1 regulation of replication origins shows similarities to the forkhead transcription factors Fkh1/2

Previous studies showed that efficient origin clustering in the nuclear center is important for early replication timing, whereas late-replicating regions are preferentially located at the nuclear periphery (Duan et al., 2010; Knott et al., 2012). As mentioned in the introduction, it was shown that the forkhead transcription factors Fkh1 and Fkh2 are required for this clustering of early origins, thereby recruiting the key initiation factor Cdc45 in G1 phase (Fang et al., 2017; Knott et al., 2012; Lõoke et al., 2013; Ostrow et al., 2014). When comparing Fkh-regulated origins with Ask1-regulated origins, I found that out of the 80 Ask1-repressed origins, only 17 overlapped with Fkh-repressed origins and 13 overlapped with Fkh-activated origins. Similarly, out of the 29 Ask1-activated origins, only 13 overlapped with Fkh-activated origins and 2 overlapped with Fkh-repressed origins (**Figure 68**).
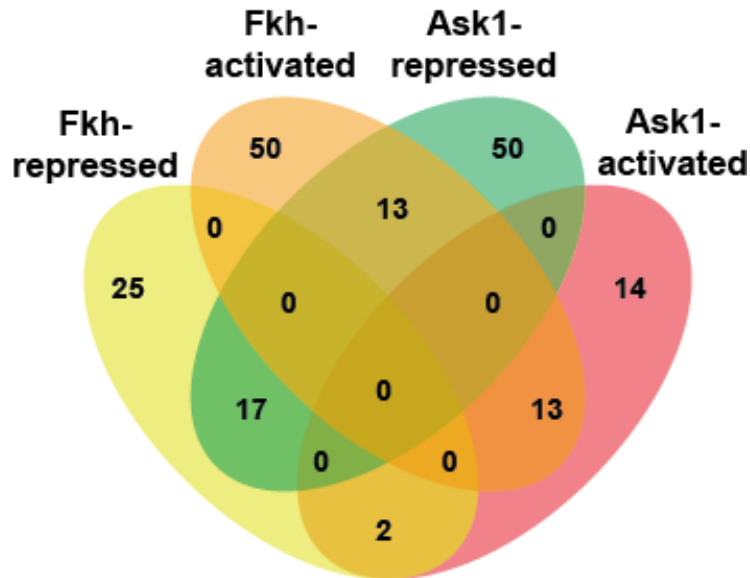
Figure 68 Venn-Diagram of Ask1-activated, Ask1-repressed, Fkh-activated and Fkh-repressed origin classes.

This suggested that most of the Ask1-regulated origins are located at distinct genomic positions from Fkh-regulated origins. Intriguingly, however, Ask1-dependent origins showed a similar behavior in replication timing and replication efficiency as Fkh-dependent origins, namely that activated origins show earlier replication timing and higher replication efficiency than repressed origins (**Figure 69A-B**).
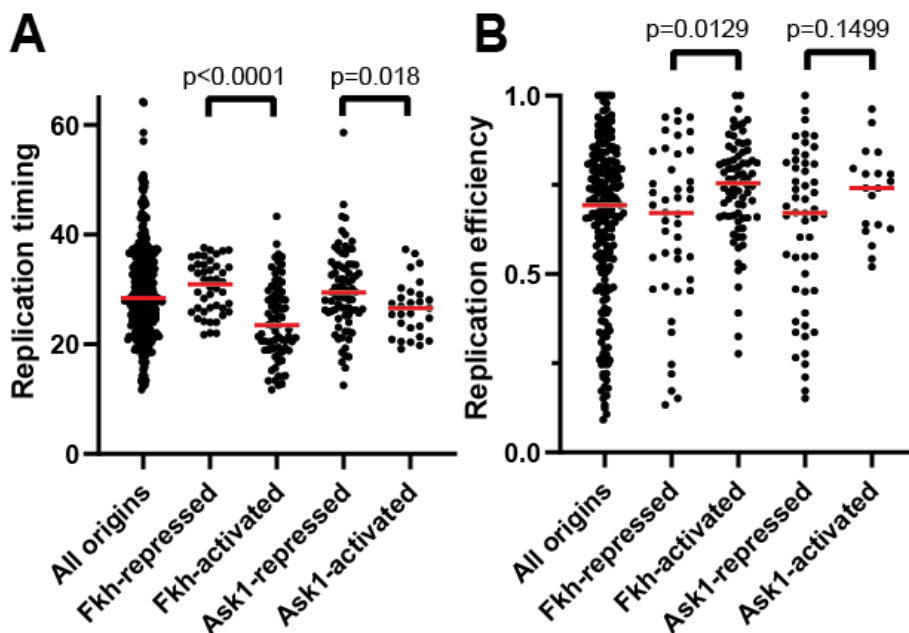
Figure 69 Replication timing and efficiency at the Ask1 and Fkh regulated replication origins A) Replication timing distribution taken from Raghuraman et al., 2001 of all origins, Fkh1-activated, Fkh-repressed, Ask1-activated and Ask1-repressed origin classes (p-value denotes results from unpaired t-test). **B)** Replication efficiency distribution taken from McGuffee et al., 2013 of all origins, Fkh1-activated, Fkh-repressed, Ask1-activated and Ask1-repressed origin classes (p-value denotes results from unpaired t-test).

This indicates that Ask1 and Fkh recruitment to origins have a similar functional impact on the origin properties and strongly suggests a mechanistic link of Ask1 with efficient origin clustering in G1 phase as previously reported for Fkh-regulated origins.

4.5.6 Nocodazole dependent microtubule degradation phenocopies the effect of Ask1 degradation

As the canonical function of the Ask1/DASH complex is to form a microtubule-encircling ring to allow efficient attachment of microtubules to yeast kinetochores (Jenni and Harrison, 2018; Miranda et al., 2007; Westermann et al., 2005), I hypothesized that Ask1/DASH binding to selected non-centromeric regions may serve as specific attachment points to connect the ends of microtubules with chromatin and therefore provide a structural framework for this intranuclear organization of chromosomes. To test this hypothesis, I treated alpha-factor arrested G1 phase cells with nocodazole for 2h to inhibit microtubule dynamics during G1 phase. Next, cells were washed to remove the nocodazole and released into S phase to determine replication timing of Ask1-dependent origins on chromosome III (**Figure 70**).
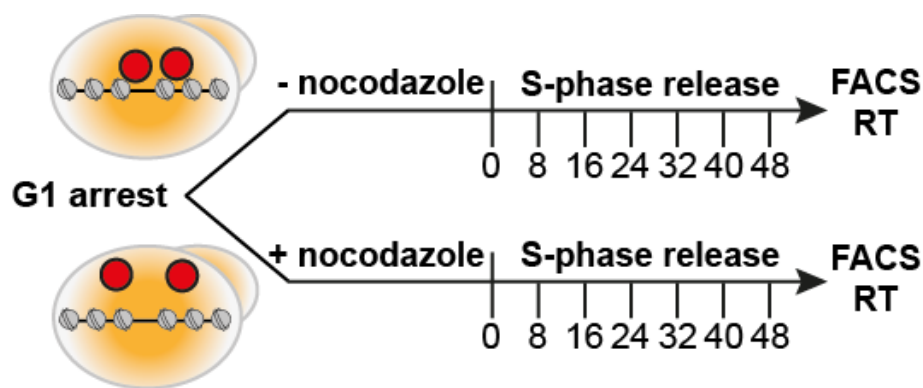
Figure 70 Schematic outline of the G1 arrest and release experiment to determine the effect of microtubule degradation on replication Y0001 was grown to logarithmic phase and arrested in G1 phase by alpha-factor treatment. Cells were then cultured for 2h in the presence or absence of 15µg/ml nocodazole before release into S phase by addition of 125 U Pronase. Samples were then taken at the indicated timepoints for FACS and replication timing (RT) analysis.

Addition of nocodazole to an asynchronously growing yeast culture arrested the cells efficiently in G2 phase (**Figure 71**), supporting the notion that the chosen time and concentration of nocodazole was sufficient to block microtubule dynamics in the cells.
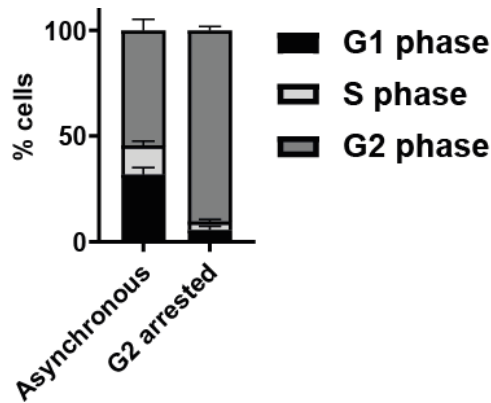
Figure 71 FACS analysis confirms the efficacy of nocodazole as shown by a strong G2 arrest.
FACS analysis of an asynchronous yeast culture (Y0001) with or without treatment with 15µg/ml
nocodazole for 2h. Bar graphs depict the percentage of G1, S and G2 phase cells at the indicated
timepoints (n=3 biological replicates).

In time course experiments, S phase progression was then measured using flow cytometry.

Similar to the results obtained after auxin-mediated Ask1 degradation (**Figure 62**), I could not

detect a major difference in S phase progression kinetics between the control and nocodazole

treated cells (**Figure 72**), suggesting that inhibition of microtubule dynamics does not affect or

perturb the DNA replication program on a global scale.
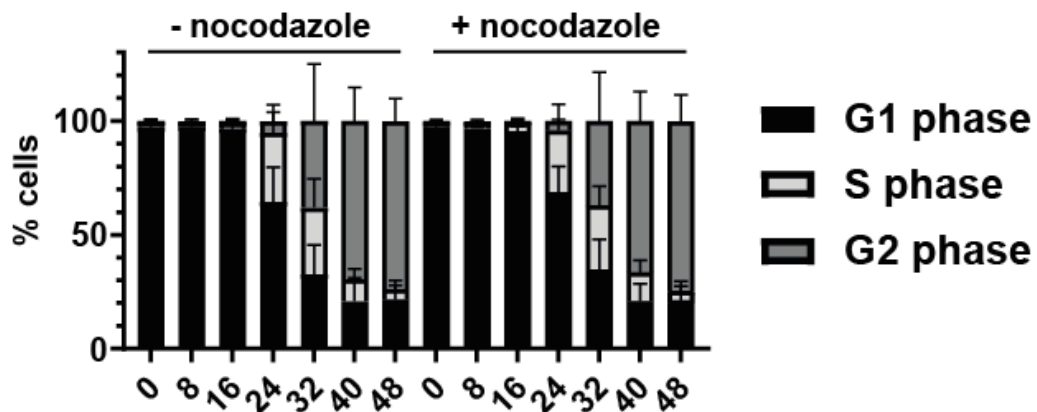
Figure 72 FACS analysis to determine the effect of nocodazole on cell cycle progression FACS
analysis of an asynchronous yeast culture (Y0001) with or without treatment with 15µg/ml nocodazole
for 2h. Bar graphs depict the percentage of G1, S and G2 phase cells at the indicated timepoints (n=3
biological replicates).

If the mechanistic role of Ask1/DASH is to allow microtubule binding and facilitate origin

clustering/chromosome organization, my results would predict that nocodazole-induced

changes in replication timing would phenocopy the results obtained from the replication timing

analysis in Ask1-depleted cells. Therefore, the replication profile of the selected EE or LI

origins on chromosome III was determined by qPCR in the absence or presence of

nocodazole (**Figure 73**).
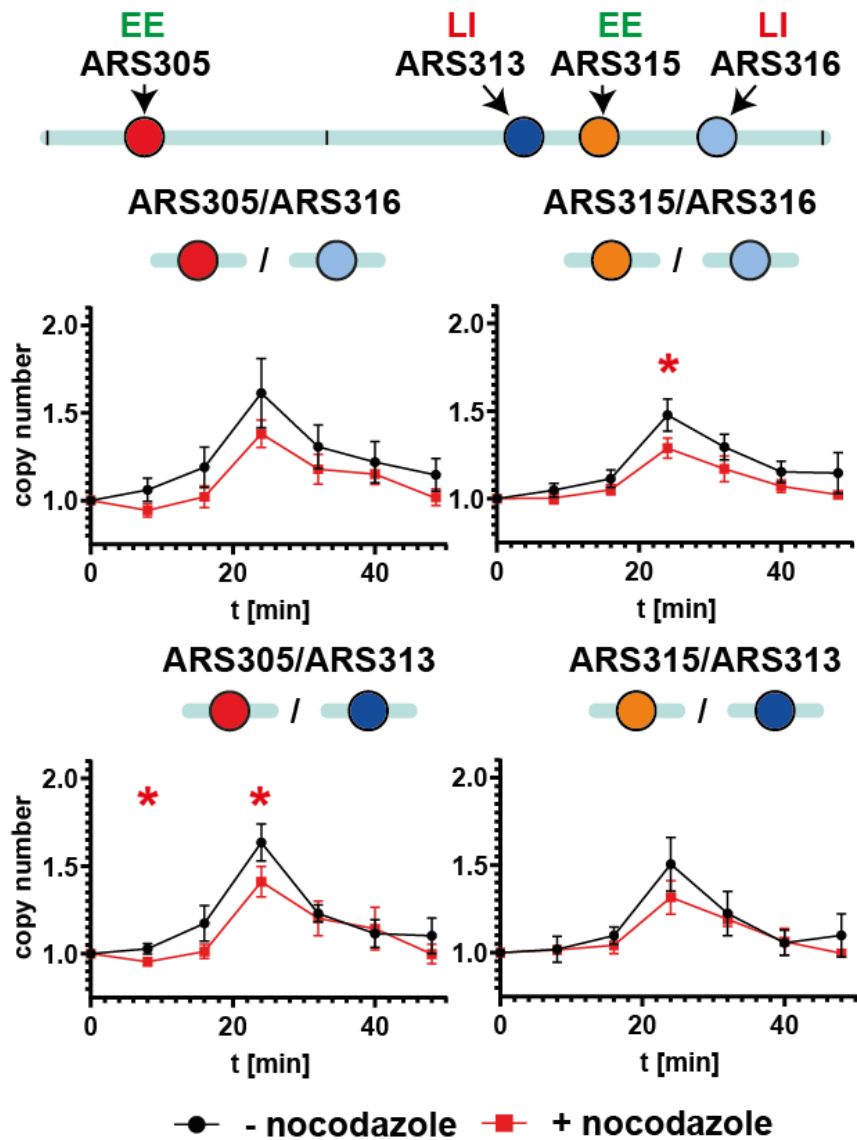
Figure 73 qPCR analysis to determine the effect of nocodazole on replication timing. Samples for genomic DNA extraction were taken at the indicated timepoints for copy number analysis by qPCR to determine the relative replication timing of depicted loci. The plots show the average copy number ratios of early (ARS305 and ARS315) to late origins (ARS313 and ARS316) with standard deviation from n=3 biological replicates (*indicates statistical significance $p < 0.05$, unpaired t-test).

In general, nocodazole-treated cells showed slightly lower copy number ratios when comparing both EE origins ARS305 and ARS315 with the LI origins ARS313 or ARS316. Importantly, however, the EE origin ARS305 showed most significant changes in replication timing in comparison to the LI origin ARS313, consistent with the replication profile changes of these two regions that were most prominently shifted in opposite direction in Ask1-depleted cells (**Figure 63 and 66**). Thus, it can be concluded that Ask1/DASH has a functional role at selected chromosomal origins and this role is dependent on functional microtubules. Therefore, my data show a previously not established connection of the replication timing program and intact microtubule dynamics.

5　Discussion

The goal of this study was to analyze the chromatin composition of two early-efficient and two late-inefficienct replication origins from chromosome III of *S.cerevisiae*.To this end, I wanted to test if and how the local chromatin environment differs between these two distinct classes of replication origins and, therefore, test the hypothesis whether the local chromatin landscape is a major determinant of replication timing control of individual origins of replication.

5.1　The RS-LEXA recombination approach is a promising system for locus-specific chromatin isolation

The identification of the proteome and the histone PTM landscape of a specific target genomic region in an unbiased manner remains a major challenge in chromatin research (Gauchier et al., 2020; Vermeulen and Déjardin, 2020). Utilizing the RS-LEXA system was beneficial for this ambitious goal for several reasons. First, the enrichment of a specific locus compared to genomic background was shown to be superior with this approach. Other methods suffer from very low enrichment factors compared to other genomic loci, for example both ChAP-MS and TAL-ChAP-MS enrich the GAL1 gene only approximately 5 to 6-fold as compared to an unrelated genomic region (Byrum et al., 2013, 2012). Similarly, the HyCCAPP approach was able to enrich the GAL1-10 promoter only about 100-fold (Kennedy-Darling et al., 2014). In contrast, the RS-LexA method could enrich the single-copy PHO5 gene locus with an enrichment factor of ~146000 (Hamperl et al., 2014). This enrichment factor is a crucial parameter for locus-specific chromatin isolation methods, since only a small chromatin fragment typically in the range of a few kb needs to be purified against a large genomic background in the megabase range. Strikingly, when factoring in the relative low abundance of target loci, only ~1% of the total chromatin in the 100-fold HyCCAPP enrichment would be derived from the target region, whereas in the 146000-fold RS-LexA purification, this number increases to near purity of ~92%. Such low recovery rates of 1% or less would consequently lead to a high background of unspecific proteins, which would make it difficult to identify maybe less frequent interactors of the target region. Therefore, in this regard the RS-LEXA approach for single-locus purifications has proved to be superior to comparable methods in yeast.

Another advantage is that the isolated genomic region is defined in size and sequence by the position of the inserted RS sites in the yeast genome, increasing the homogeneity of the chromatin preparations compared to methods that rely on random shearing by sonication. At the same time, the precise location of the RS sites is alterable, allowing for a high degree of flexibility in the size of the chromatin domains and in the choice of genetic elements included or excluded from the recombination region.

Furthermore, the purification scheme was developed under native conditions without chemical crosslinkers like formaldehyde. Intriguingly, a comparison between the proteomes co-purifying with formaldehyde-crosslinked and native rDNA chromatin showed an almost complete overlap between the factors enriched with the two methods (see discussion section in (Hamperl et al., 2014) for details), suggesting that many *in vivo* protein-DNA interactions are preserved on the isolated material. Therefore, purified native chromatin could provide a highly defined template for *in vitro* experiments likely reflecting the *in vivo* situation with regard to nucleosome positioning and histone modifications. This can be an advantage over the use of artificial, *in vitro* reconstituted nucleosomal arrays. For example, the isolated origin chromatin can serve as a template for *in vitro* replication assays and the efficiencies and kinetics of replication initiation from the native *ex vivo* assembled EE and LI origins can be compared to *in vitro* reconstituted chromatin templates (Kurat et al., 2017). Furthermore, the EE and LI origins could be purified from mutants of transcription factors such as Fkh1/2 and chromatin modifying enzymes to detect how the absence of these factors affects overall origin chromatin composition.

Finally, the purity and yield of the chromatin domains also makes it ideal for single-molecule analysis of specific chromatin states, such as the precise nucleosome configuration and their observed frequencies in EE and LI replication origins, which can inform about the presence and probability of alternative chromatin states in a population of cells. ChIP and most other chromatin analysis methods instead average over large numbers of molecules of the same genomic region, therefore neutralizing the structural variation between molecules indicative of dynamic behaviour.

In summary, this methodology opens an exciting avenue in chromatin research, as it is now possible to follow the collective compositional and structural chromatin changes of a specific genomic region that undergoes a certain chromosomal transaction such as DNA replication initiation.

5.2   Single-locus proteomics analysis of EE and LI origins

Utilizing the RS-LexA approach allowed me to comprehensively identify the proteomic landscape around selected EE and LI replication origins (**Figure 27 and 34**). Importantly, these purified domains were previously located in their native chromosomal context, whereas other approaches to purify replication origin chromatin reported so far were restricted to the single-copy EE ARS1 origin cloned on a plasmid (Unnikrishnan et al., 2010a), which might not fully reflect the chromatin context on an endogenous chromosome. However, one disadvantage of this approach, is the need of genetic engineering in order to insert RS and LEXA sites at the respective replication origins. The possibility cannot be excluded that the binding of LexA-TAP to the origin-proximal LEXA binding sites or the process of circularization

during recombination may trigger eviction or shifts of individual nucleosomes or dissociation of other chromatin factors from the domains. However, the DNA replication timing of the origins in the genetically-modified strains were identical to a wildtype strain and exactly as expected for EE and LI origins (**Figure 23**). Furthermore, quantitative ChIP analysis against canonical histone H3 and MCM2 levels at the endogenous chromosomal origins confirmed the results from the proteomic analysis that the isolated EE chromatin circles showed a higher MCM to histone ratio compared to the two LI origins (**Figure 29**). Thus, it can be assumed that the critical chromatin features that define the different replication timing profiles of these origins were not affected by the necessary genetic manipulations.

Nevertheless, maintaining the diversity and stoichiometry of the locus-bound factors during its biochemical isolation is a major challenge. Purifying the domains under native conditions without assistance from chemical crosslinkers to stabilize more loosely bound chromatin interactions is a clear limitation that may explain why some expected interaction partners were not retrieved in the analysis. For example, Fkh1/Fkh2 was not detected at ARS305, a well-established forkhead-activated origin (Knott et al., 2012; Reinapae et al., 2017) , and I could also not recover ORC subunits in 3 out of the 4 origin purifications. Therefore, I do not recover a "complete" list of all origin-bound proteins as some of the more transient, unstable interactors might get lost that are more sensitive to high salt and detergent concentrations persisting throughout the biochemical isolation. This is consistent with the observed strong enrichment of histones and MCM2-7 complexes and may also explain the surprising result that very limited overlap of factors between the two selected EE and LI origins was observed (**Figure 30 and 36**). Initial attempts to purify the domains after formaldehyde crosslinking were not successful, but future work using optimized crosslinking conditions or crosslinking reagents might help to capture more transient, but biologically important proteins with this system. This would facilitate the detection of proteins that are usually weak and transiently binding to the investigated genomic regions. Considering this work, this might have led to the detection of further expected origin interactors like the ORC complex at all origins or Fkh1/2.

5.3 EE origin-associated histones show reduced H4 acetylation in G1 phase

The strong enrichment of histones in our origin purifications allowed me to investigate the patterns of histone PTMs flanking EE and LI replication origins in comparison to bulk histones (**Figure 38 and 39**). Although these initial experiments gave promising results in regard to the observed patterns of H3 and H4 acetylation, this approach suffered from certain limitations, so that conclusions have to be taken with some caution.

For example, it is important to note that histone molecules were also recovered from a control purification of a strain that lacks the ability to excise and purify specific origin chromatin, suggesting that the solid-phase support, affinity reagent or epitope tag can interact

unspecifically to a certain degree with genomic chromatin or destabilized free histones. The second possibility is favored for two reasons. First, a strong discrepancy between the fold enrichment of histones (**Figure 27 and 28, ~2-8-fold**) versus the fold enrichment of the target versus genomic loci (**Figure 26A, ~40.000 - 170.000-fold**) between control and origin purifications was observed, supporting that genomic chromatin is strongly depleted in these samples. Secondly, histones present in the control purification showed hyperacetylation of N-terminal H4 tails as well as H3K56 (**Figure 39**), two modifications that are expected to destabilize nucleosomes by reducing DNA-histone contacts (Gershon and Kupiec, 2021). However, there are potential solutions to this limitation by adjusting the purification protocol. During the project, since elution with TEV-protease only released 50% of the chromatin rings (**Figure 10A**), the elution step was changed to a basic NH_3 elution (**Figure 13)**. However, other non-specific proteins that are potentially bound to the affinity matrix are also denatured and eluted, which could be the case for hyperacetylated histones. One way to solve this problem would be to optimize the TEV elution efficiency, which occurs under native conditions and should therefore increase specificity and purity of the eluted chromatin rings for histone PTM analysis.

Nevertheless, despite this contaminating pool of free histones, unique patterns of methylation and acetylation for individual origins was identified, in particular at the H4 N-terminus. While H4 acetylation remained relatively constant on bulk histones, the levels of multiple acetylations of H4 were sharply decreased on EE origins compared to the LI origins. These data are fully consistent with an earlier study determining the acetylation levels of the EE origin ARS1 on the TALO8 plasmid that showed a sharp wave of deacetylation in G1 phase and subsequent acetylation in S phase (Unnikrishnan et al., 2010a). Our comparison of EE and LI origins indicates that the hypoacetylated state in G1 may represent a distinct and specific feature of EE origins.

How exactly histone acetylation affects early- or late-firing of replication origins has been a long-standing question. Tethering the histone acetyltransferase Gcn5 near a late origin partially advances its initiation time (**Figure 43 and 44, and Vogelauer, Rubbi, Lucas, Bonita J. Brewer, *et al.*, 2002**). Moreover, the histone deacetylase Rpd3 delays initiation at a large number of origins (Aparicio et al., 2004; Knott et al., 2009; Vogelauer et al., 2002). However, another H4K5-specific histone deacetylase, the Hst1-Sum1-Rfm1 complex, was shown to promote initiation at a number of origins (Irlbacher et al., 2005; Weber et al., 2008). My results could provide a simple solution in which the extent of H4 deacetylation of origin chromatin in G1 phase may enforce temporally controlled loading of general replication initiation factors. Consistent with this hypothesis, synthetic hyperacetylated histones were shown to significantly delay the chromatin binding of the pre-initiation complex factor Cdc45 (Kajino et al., 2020). In addition, the low levels of histone acetylation at EE origins could serve as a better substrate

and improve recognition by histone acetyltransferases such as Gcn5. In this model, the resulting sharper wave of histone acetylation at the onset of S phase would destabilize the chromatin and allow efficient DNA unwinding and therefore, timely replication initiation.

5.4 Single-locus proteomics identifies two potential new *bona fide* replication timing factors

5.4.1 Set3 as a component of a deacetylase complex

One factor that was identified in this study to potentially play a role in replication timing control was Set3, which is part of the heteroheptameric Set3 deacetylase complex. This complex itself has previously not been described to play a functional role in replication. However, one catalytic component of this complex, the histone deacetylase Hst1, has, in fact, been suggested to promote replication as part of another complex consisting of the Hst1, Sum1 and Rfm1 subunits (Weber et al., 2008). Taking this into consideration, since sharing this catalytic subunit, the Set3 complex might be able to regulate replication in a similar fashion. Unfortunately, it has to be stressed that some of the experiments regarding Set3 have only been performed once, meaning that further validation in form of more biological replicates has to be done in order to draw reliable conclusions. Nevertheless, these preliminary experiments seem to indicate that this factor could play a role at the EE replication origin ARS305 since it was found in this respective proteomic dataset associated with ARS305. Consistent with that, tethering this factor to the LI origin ARS316 increased replication at this origin, albeit not as strong as when tethering Ask1 (**Figure 43B and 44**). These findings argue for a scenario where Set3 is able to promote early and efficient replication at origins. Intriguingly, the fact that the Set3 complex has a histone deacetylase activity is also in line with the histone PTM analysis. Here, I also saw an overall decreased acetylation status of histones at EE origins as compared to LI origins (**Figure 39**). Therefore, it is possible that Set3C is helping to set up this hypoacetylated status at some EE replication origins, like ARS305, and therefore regulating replication through this specific mechanism, as also discussed in the previous part. But as mentioned, apart from replicating these experiments, more research has to be done in this regard to further support this idea. Another way to more reliably validate these findings would be to perform ChIP-qPCR and ChIP-Seq experiments to confirm origin association of Set3. This would also help to examine the genome-wide binding pattern of Set3 and clarify to what extent this protein interacts with more replication origins or if just very few selected origins are regulated by this complex.

5.4.2 DASH complex subunit Ask1 as a microtubule-binding complex

One interesting finding was that a significant number of DASH complex subunits including Ask1 co-purified with the ARS305 and ARS313 replication origins. Degrading Ask1 protein in G1 phase had no measurable impact on global S phase progression (**Figure 62**), suggesting that Ask1 does not affect or perturb the DNA replication program on a global scale. However,

replication timing measurement of individual origins along chromosome III revealed a functional role of Ask1 in the replication timing of ARS313 and other replication origins tested on chromosome III (**Figure 66**). Importantly, induced tethering of an Ask1-LexA fusion protein to different origin-proximal positions along chromosome III advanced replication timing of the targeted chromosomal domain (**Figure 49, 53, and 55**). Together, these data are consistent with a potential role of this factor in replication timing control.

How might the heterodecameric DASH/Ask1 complex mechanistically advance or delay replication timing of specific replication origins. In mitosis, this complex assembles into a microtubule-encircling ring that helps to attach microtubules to the outer kinetochore and therefore establish bi-orientation of the mitotic spindle. Interestingly, it was shown that tethering Ask1 onto a plasmid DNA is also able to create a full artificial kinetochore on its own (Lacefield et al., 2009). Therefore, the tethering of Ask1 at replication origins might also create kinetochores at these regions. This could also explain the local advancement in replication timing in the tethering experiments, since another part of the kinetochore, the Ctf19 complex, was shown to trigger early replication at kinetochore-located replication origins (Natsume et al., 2013). However, this mechanism would not be able to explain the long-range changes in the replication profile in both the tethering as well as the degradation experiments (**Figure 49, 53, 55, and 66**).

Alternatively, the DASH complex-mediated attachment of microtubules at DNA replication origins in G1 phase may serve a similar function as in mitosis to establish correct sub-nuclear positioning of specific origins. Indeed, it was shown that the Fkh1 and Fkh2 transcription factors are required for the clustering of early origins and the emergence of such replication factories (Knott et al., 2012). Thus, in addition to centromere and telomere anchoring at the nuclear membrane, the selected attachment of microtubules via the DASH complex could provide the structural framework for this sub-nuclear rearrangement of specific replication origins in G1 phase and explain how this movement of individual genomic loci is physically achieved (**Figure 74**).
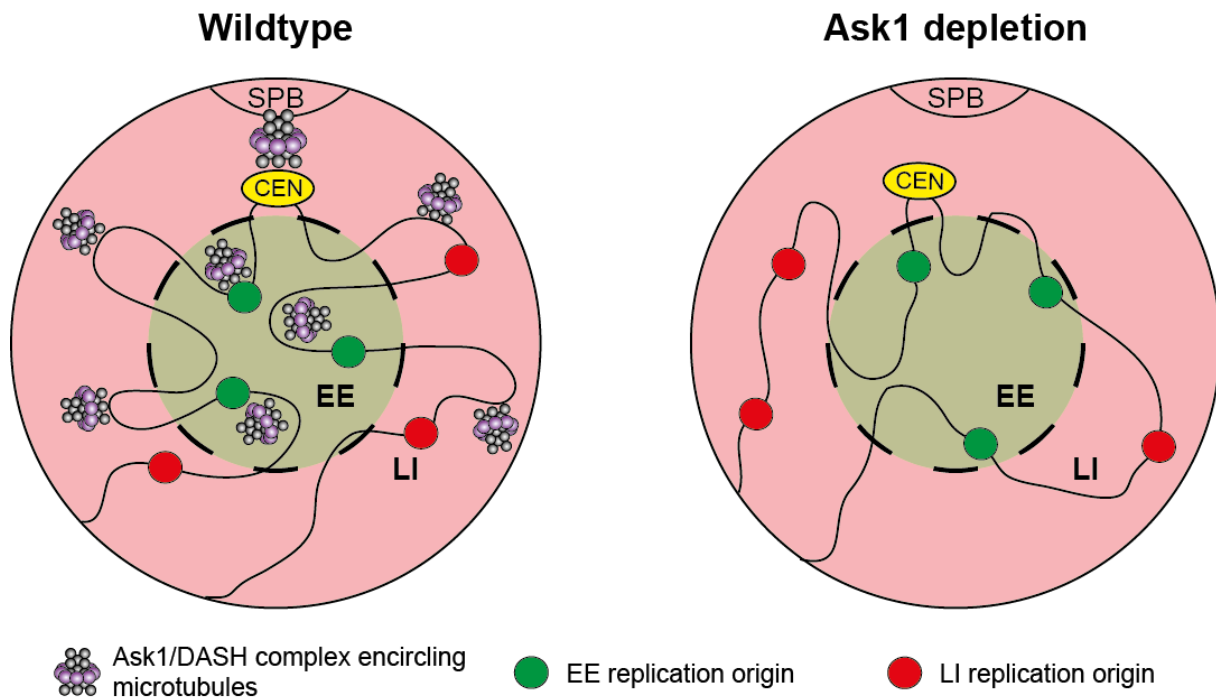
Figure 74 Model of a potential Ask1/DASH complex mediated mechanism to regulate replication origins through nuclear clustering

A function of Ask1/DASH in the targeted 3D organization of specific origins would also explain how replication of broader genomic regions are affected as observed in our tethering and degradation experiments. The mechanistic details how the local chromatin structure of origins impacts the selective recruitment of Ask1/DASH at specific origins and how Fkh1 and Fkh2 might interplay and regulate this directionality to specific origins requires further investigations.

Unfortunately, initial ChIP-qPCR experiments to verify the direct interaction of endogenous Ask1 protein with ARS313 and ARS305 origins suffered from low IP efficiencies, which is likely caused by the fact that Ask1/DASH has no direct DNA-binding interface for efficient crosslinking with the DNA. Thus, the genome-wide binding profiles of Ask1/DASH to determine how widespread the association of Ask1 is to other replication origins, remains to be further investigated.

5.5 Outlook and Perspectives

Conceptually, this work has established a highly efficient site-specific recombination system to purify selected chromosomal domains from yeast that allows researchers to carry out an unbiased compositional, structural and functional analysis of virtually any genomic locus in its native chromatin context in *S.cerevisiae*. With this powerful tool in hand, it would be interesting to analyze the dynamic changes of replication origin chromatin in different cell cycle stages and upon genetic and environmental perturbations, for example in mutant strains lacking chromatin modifying and remodeling enzymes, such as INO80, ISW1a/b, and SAGA, previously implicated in efficient DNA replication (Azmi et al., 2017; Cutler et al., 2018; Kurat

et al., 2017) or during heat shock or growth arrest. In the long term, defining the precise changes of chromatin composition under these multiple conditions could contribute towards the ultimate goal to define the molecular basis of DNA replication origin firing plasticity.

Furthermore, another desirable goal would be to enhance the efficiency of this assay. Purification efficiencies with ~40.000-170.000-fold enrichment over unrelated genomic loci (**Figure 26**) is vastly sufficient for studies in yeast due to the small genome size. However, large genome sizes make it difficult to apply this approach in higher eukaryotes at the moment, since high genomic background wouldn't allow for similar signal to noise ratios of examined loci. However, improving the general conditions of the assay, as well as utilizing both parts of the TAP tag of the LexA protein in order to perform tandem-affinity purification instead of the single-step NH_3 elution might increase the efficiency greatly. This could possibly make this purification system not only limited to yeast, but also applicable in other organisms and, therefore, provide a much sought after versatile tool for chromatin research in general.

Generally, the origin purification system presented in this work and the resulting proteomic analysis of selected EE and LI origins provides an ideal framework to understand the basis for differential origin regulation and its connection to chromosomal domain organization. Considering, that origin clustering in replication factories is conserved in human cells (Cseresnyes et al., 2009; Hozak et al., 1994; Hozák et al., 1993; Leonhardt et al., 2000), this mechanism is likely to also play an important role in human cells. However, due to the lack of a spindle pole body and thus microtubules, human cells might employ other mechanisms for setting up such a clustering within the nucleus. For example, actin as another integral part of the cytoskeleton could potentially fulfill a similar role in human cells as microtubules in *S.cerevisiae*. Intriguingly, actin was shown to have various different functions within the nucleus (reviewed in (Kelpsch and Tootle, 2018). Strikingly, it was shown that actin is, in fact, also important for replication and also increases its nuclear localization upon replication stress (Johnson et al., 2013; Parisis et al., 2017). Therefore, it might be interesting to determine the exact mechanism of how actin is able to regulate replication and if it is similar to the findings of this project. But regardless of the precise target, it will be interesting to explore approaches to manipulate such a clustering of replication origins in human cells, opening new pharmacological targets to locally revert replication timing changes frequently occurring in cancer cells for example (Dietzen et al., 2022; Du et al., 2019).

6 Material and methods

6.1 Material

6.1.1 Chemicals

Chemicals	Source	Identifier
1 kb plus DNA ladder	NEB	Cat# N3200L
3-(N-morpholino)propanesulfonic acid (MOPS)	Millipore	Cat# 475922-100GM
4-(2-hydroxyethyl)-1-piperazineethanesulfonic acid (HEPES)	Sigma-Aldrich	Cat# H3375-1KG
5-Fluoroorotic acid (5-FOA)	Thermo Fisher Scientific	Cat# R0811
$[\alpha-32P]dATP$	Hartmann Analytik	Cat# SRP-203
A-D-Raffinose	SERVA	Cat# 34140.03
Acetic acid	SERVA	Cat# 45638.01
Acetone	Carl Roth	Cat# 5025.1
Acetonitrile	Chemsolute	Cat# 2690.1
Agarose	Serva	Cat# 11406.03
Ammonia (NH_3)	Kraft	Cat# 20069.5010
Ammonium acetate (NH_4OAc)	Sigma-Aldrich	Cat# A7262-5KG
Ammonium sulfate	Santa Cruz	Cat# Sc-29085
Ampicillin	Fisher BioReagents	Cat# BP1760-5
Auxin	MP Biomedicals	Cat# 102037
Bacto agar	BD	Cat# 214010
Bacto peptone	BD	Cat# 211677
Bacto Tryptone	BD	Cat# 211699
β-Mercaptoethanol	Sigma-Aldrich	Cat# P7626-5G
Bromphenol blue	Alfa Aesar	Cat# A18469
Boric acid	Carl Roth	Cat# 6943.1
Calcium chloride ($CaCl_2$)	Sigma-Aldrich	Cat# C5080-500G
D-(+)-Galactose	Sigma Aldrich	Cat# G0625-5KG
D-(+)-Glucose	Sigma-Aldrich	Cat# G8270-10KG
Dimethylsulfoxide (DMSO)	SERVA	Cat# 20385.01
Dipotassium phosphate (K_2HPO_4)	PanReac AppliChem	Cat# A1041,0500
Disodium phosphate (Na_2HPO_4)	Sigma Aldrich	Cat# 1.06580.0500
Dithiothreitol (DTT)	Thermo Fisher Scientific	Cat# R0861
Doxycycline (DOC)	Sigma Aldrich	Cat# D3447-500MG
Ethanol	Merck	Cat# 1.00983.1000
Ethylenediaminetetraacetic acid (EDTA)	Sigma-Aldrich	Cat# ED-100G
Ethyleneglycol-bis(β-aminoethyl)-N,N,N',N'-tetraacetic acid (EGTA)	Santa Cruz	Cat# Sc-3593A
Formaldehyde	Thermo Fisher Scientific	Cat# 28908
Glycerol	Fisher BioReagents	Cat# BP229-1

Glycine	Carl Roth	Cat# 0079.4
Glycogen	Thermo Fisher Scientific	Cat# AM9510
Hydrochloric acid (HCl)	PanReac AppliChem	Cat# 182109.1211
Hydroxylamine	Merck	Cat# 8.14441.0100
Hydroxyurea (HU)	Biomol	Cat# H9120.10
Hygromycine B	Carl Roth	Cat# CP12.2
Iodoacetamide (IAA)	Sigma-Aldrich	Cat# I1149-5G
Isopropanol	Acros Organics	Cat# 327270010
Lithium acetate dihydrate (LiAc)	Santa Cruz	Cat# Sc-257671
Lithium Chloride (LiCl)	Carl Roth	Cat# 3739.1
Magnesium acetate tetrahydrate (MgAc)	Kraft	Cat# 15247.26
Magnesium chloride (MgCl$_2$)	Sigma-Aldrich	Cat# M8266-100G
Magnesium Sulfate (MgSO$_4$)	Carl Roth	Cat# 0261.2
Manganese dichloride (MnCl$_2$)	Sigma-Aldrich	Cat# 63535-50G-F
Methanol	Merck	Cat# 1.06009.2500
Milk powder	Carl Roth	Cat# T145.2
Monopotassium phosphate (KH$_2$PO$_4$)	Sigma-Aldrich	Cat# P5655-500G
Monosodium phosphate (NaH$_2$PO$_4$)	Sigma-Aldrich	Cat# 71496-1KG
Nocodazole	Merck	Cat# 487928
NuPAGE LDS sample buffer	Invitrogen	Cat# NP0007
NuPAGE MES SDS running buffer	Invitrogen	Cat# NP0002
PEG 4000	Carl Roth	Cat# 0156.3
Phenol:Chloroform:Isoamyl Alcohol	Invitrogen	Cat# 15593-031
Phenyl isocyanate (PIC)	Sigma Aldrich	Cat# 185353-100G
Potassium acetate (KAc)	Merck	Cat# 529543-250GM
Precision Plus Protein All Blue Standards	Bio-Rad	Cat#1610373
Propionic anhydride	Sigma Aldrich	Cat# 240311-50G
Protease and Phosphatase Inhibitor Cocktail 100x	Thermo Fisher Scientific	Cat# 78446
Salmon Sperm DNA	Invitrogen	Cat#15632-011
Sirtinol	TargetMol	Cat# T6671
Sodium azide	Santa Cruz	Cat# sc-208393
Sodium citrate	Sigma Aldrich	Cat# 71402-1KG
Sodium chloride (NaCl)	Merck	Cat# 1064040500
Sodium dodecyl sulfate (SDS)	Alfa Aesar	Cat# A11183
Sodium hydroxide (NaOH)	Sigma-Aldrich	Cat# S5881-1KG
Sodium phosphate	Sigma-Aldrich	Cat# 71496-1KG
Sorbitol	Calbiochem	Cat# 56755-1KG
Spermidine	MP Biomedicals	Cat# 100472
Spermine	MP Biomedicals	Cat# 100474
Sytox Green	Thermo Fisher Scientific	Cat# S7020

Tergitol (NP-40) solution 70%	Sigma-Aldrich	Cat# NP40S-100ML
Trichostatin A	Sigma-Aldrich	Cat# T8552
Triethylamine	Sigma-Aldrich	Cat# 90340-1L
Triethylammonium bicarbonate (TEAB)	Sigma-Aldrich	Cat# T7408-100ML
Trifluoroacetic acid (TFA)	VWR	Cat# 85049.001
Tris (hydroxymethyl) aminomethane hydrochloride (Tris-HCl)	Merck	Cat# 1.08382.2500
Triton X-100	Sigma-Aldrich	Cat# X100-100ML
Tween20	Kraft	Cat# 18014332
Uracil	Sigma-Aldrich	Cat# U0750-25G
Urea	Sigma-Aldrich	Cat# U5378-100G
Yeast extract	BD	Cat# 212750
Yeast nitrogen Base without amino acids	Sigma-Aldrich	Cat# Y0626-1KG
Yeast synthetic Drop-out medium Supplements without leucine	Sigma-Aldrich	Cat# Y1376-20G
Yeast synthetic Drop-out medium Supplements without uracil	Sigma-Aldrich	Cat# Y1501-20G

6.1.2 Buffers and media

Unless stated otherwise, all solutions have been prepared with purified, ultrapure H_2O. pH values were measured at room temperature. Unless stated otherwise, percentages were calculated as mass per volume (m/w) and pH was adjusted with HCl or NaOH.

Media and Buffer	Ingredients	Concentration
2x SCD-Leucine medium	Yeast Nitrogen Base without aminio acids Yeast Synthetic Drop-out Medium Supplements without Leucine Glucose (Agar for plates) Autoclaved afterwards	1.36g/l 3.84g/l 20g/l 20g/l
2x SCD medium + 5-FOA	2x SCD-Uracil medium Uracil 5-FOA (add dissolved 5-FOA after autoclaving)	 0.02mg/ml 0.1%
2x SCD-Uracil medium	Yeast Nitrogen Base without aminio acids Yeast Synthetic Drop-out Medium Supplements without Uracil Glucose (Agar for plates) Autoclaved afterwards	1.36g/l 3.84g/l 20g/l 20g/l
4x Laemmli buffer	Tris base SDS Glycerol β-Mercaptoethanol Bromphenol blue	250mM 280mM 40% (v/v) 20% (v/) 4mg/ml
10x TBE buffer	Tris base	1M

	Boric acid	1M
	EDTA	20mM
20x SSC buffer	NaCl	3M
	Sodium citrate	0.3M
	pH7	
AC buffer	NH$_4$Ac	100mM
	MgCl$_2$	0.1mM
	pH 7.4 titrated with NH$_3$	
Buffer 1	Tris-HCl pH7.5	50mM
	Sorbitol	1M
	MgCl$_2$	5mM
Buffer A	Tris-HCl pH7.4	15mM
	KCl	80mM
	EDTA	2mM
	EGTA	2mM
	Spermidine	0.5M
	Spermine	0.2M
	Trichostatin A	0.5µM
	Sirtinol	25µM
	Protease and Phosphatase Inhibitor Cocktail	1x
Buffer B	Formic acid	0.1% (v/v)
	Acetonitrile	98% (v/v)
CEB buffer	Tris-HCl pH8	20mM
	KCl	200mM
	EDTA	1mM
	EGTA	10mM
	Triton X-100	0.5% (v/v)
	Tween-20	0.1% (v/v)
	DTT	1mM
CWB buffer	Tris-HCl pH8	20mM
	KCl	300mM
	MgAc	5mM
	Triton X-100	0.5% (v/v)
	Tween-20	0.1% (v/v)
	CaCl$_2$	2mM
	DTT	1mM
Denaturing solution	NaOH	0.5M
	NaCl	1.5M
Depurination solution	HCl	0.2M
Destaining buffer	Triethylammonium bicarbonate	100mM
	Acetonitrile	50%
Hybridization buffer	Sodium Phosphate buffer pH7.2	0.5M
	SDS	7%
IRN buffer	Tris-HCl pH8	50mM
	NaCl	0.5mM
	EDTA	20mM
LB medium	Tryptone	10g/l
	Yeast extract	5g/l
	NaCl	5g/l
	1M NaOH	1ml/l
	(Agar for plates)	20g/l
	Autoclaved afterwards	
LB medium with Ampicillin (Amp)	LB medium	
	Ampicillin	50µg/ml

Lysis buffer	HEPES pH7.5	50mM
	NaCl	140mM
	EDTA	5mM
	EGTA	5mM
	Triton X-100	1% (v/v)
	DOC	0.1%
MB150 buffer	Tris-HCl pH8	20mM
	KCl	150mM
	MgAc	5mM
	Triton X-100	0.5% (v/v)
	Tween-20	0.1% (v/v)
	DTT	1mM
MB200 buffer	Tris-HCl pH8	20mM
	KCl	200mM
	MgAc	5mM
	Triton X-100	0.5% (v/v)
	Tween-20	0.1% (v/v)
	DTT	1mM
PBS	NaCl	8g/l
	KCl	0.2g/l
	Na_2HPO_4	1.42g/l
	KH_2PO_4	0.24g/l
Potassium phosphate buffer 1M pH7	KH_2PO_4 1M	385ml/l
	K_2HPO_4 1M	615ml/l
RINB buffer	Tris-HCl pH8	50mM
	EDTA	100mM
	β-Mercaptoethanol	0.1% (v/v)
SDS sample buffer	NuPAGE LDS sample buffer	1x
	β-Mercaptoethanol	5%
SOB medium	Tryptone	20g/l
	Yeast extract	5g/l
	NaCl	10mM
	KCl	2.5mM
	Autoclaved afterwards	
	$MgCl_2$	10mM
	$MgSO_4$	10mM
Sodium phosphate buffer 1M pH7.2	NaH_2PO_4 1M	280ml/l
	Na_2HPO_4 1M	720ml/l
Sodium phosphate buffer 0.1M pH7.4	NaH_2PO_4 1M	77.4ml/l
	Na_2HPO_4 1M	22.6ml/l
Southern transfer buffer	Ammonium acetate	1M
TE buffer	Tris-HCl pH7.5	10mM
	EDTA	1mM
TfbI buffer	KAc	30mM
	$MnCl_2$	50mM
	KCl	100mM
	Glycerol	15%
	pH5.8 with acetic acid	
	filtered through a 0.22µm filter	
TfbII buffer	MOPS	10mM
	$CaCl_2$	75mM
	KCl	10mM
	Glycerol	15%
	pH7	
	filtered through a 0.22µm filter	

UA buffer	Tris-HCl pH 8.5	100mM
	Urea	8M
Wash1	SSC buffer	0.3x
	SDS	0.1%
Wash2	SSC buffer	0.1x
	SDS	0.1%
Wash3	SSC buffer	0.1x
	SDS	1.5%
Washing buffer 1	HEPES pH7.5	50mM
	NaCl	500mM
	EDTA	2mM
	Triton X-100	1% (v/v)
	DOC	0.1%
Washing buffer 2	Tris-HCl	10mM
	LiCl	250mM
	EDTA	2mM
	Nonidet P-40	0.5% (v/v)
	DOC	0.5%
Western transfer buffer	Tris base	25mM
	Glycine	192mM
	Methanol	20% (v/v)
Yeast Transformation solution	PEG4000	50%
	LiAc	100mM
	Salmon sperm DNA	277µg/ml
	DNA fragment of choice	
	H_2O ad 360µl	
YP medium	Yeast extract	10g/l
	Peptone	20g/l
	(Agar for plates)	20g/l
	Autoclaved afterwards	
YPD medium	YP medium	
	Glucose	20g/l
YPD with Hygromycine B	YP medium	
	Hygromycine B	200mg/l
	(add Hygromycine B after autoclaving)	
YPR medium	YP medium	
	Raffinose	20g/l

6.1.3 Kits

Kits	Manufacturer	Identifier
GeneJet PCR Purification Kit	Thermo Fisher Scientific	Cat# K0702
GeneJet Plasmid Miniprep Kit	Thermo Fisher Scientific	Cat# K0503
Gibson Assembly® Master Mix	NEB	Cat# E2611L
iTaq Universal SYBR Green Supermix	Bio-Rad	Cat# 1725124
NEBNext Multiplex Oligos for Illumina (Dual Index Primer Set 1)	NEB	Cat# E7600S
NEBNext ultra II DNA library prep kit	NEB	Cat# E7645L
RadPrime DNA labeling system	Invitrogen	Cat# 18428-011

| SuperSignal West Pico Plus | Thermo Fisher Scientific | Cat#34580 |
| Qubit 1x dsDNA HS Assay Kit | Invitrogen | Cat# 33230 |

6.1.4 Nucleic acids

6.1.4.1 Oligonucleotides

Name	Sequence 5' - 3'	Description
0016	GATAAGCTTTTTTGGGTCCTTTGTTTTCG	Cloning of K094
0017	GATGAATTCATTTGGAGGGAGGAGAAGGA	Cloning of K094
0020	TCAGAATTCTCCTCCAGTGGGATTGCTAC	Cloning of K095
0021	TCACTGCAGGCCTAGCGGGCTATTACCTT	Cloning of K095
0040	TTTTGGGTCCTTTGTTTTCGTTGTTTCAGTCTGGATAAATTT TAAGTTAC TCGATCCGATGATAAGCTGTC	Cloning of Y0010
0041	ATTTGGAGGGAGGAGAAGGATAACAGCGACGAAACACCG GACAGATTCCCTGCCACCTGACGTCTAAGAA	Cloning of Y0010
0042	CTTATTTTTTTCAAGCGATACAAAGTAAACAGTTAC	Cloning of K111
0043	GAGACCTCATCAAAGTGC	Cloning of K111
0044	GTTTACTTTGTATCGCTTGAAAAAAATAAGTCGACCCGAGA TCATATC	Cloning of K111
0045	TCTTAGTTGGTAGCACTTTGATGAGGTCTCCCACGATTTGA TGAAAGAATAAC	Cloning of K111
0046	GAAAGTAGTTATTACGGCGTCGG	Cloning of K112
0047	GGCTCTAGGGTAGTTGCG	Cloning of K112
0048	GCGACGCCCGACGCCGTAATAACTACTTTCTCGACCCGAG ATCATATC	Cloning of K112
0049	CAATGAGAGAAACGCAACTACCCTAGAGCCCCACGATTTG ATGAAAGAATAAC	Cloning of K112
0050	GTGTGCTAAGTGTCCTGTTTC	Cloning of K113
0051	AATATTGTCTTTGGACGTTTG	Cloning of K113
0052	GAACGTTCCGAAACAGGACACTTAGCACACTCGACCCGAG ATCATATC	Cloning of K113
0053	TGGTTTGGGCAAACGTCCAAAGACAATATTCCACGATTTGA TGAAAGAATAAC	Cloning of K113
0066	GTTCCTTCTGTCTGTTGTAAATAG	Cloning of K114
0067	CGGCATCAAAAGGTACCG	Cloning of K114
0068	TCAAGAAAGATGCGGTACCTTTTGATGCCGTCGACCCGAG ATCATATC	Cloning of K114
0069	TGCATCCTATTTACAACAGACAGAAGGAACCCACGATTTG ATGAAAGAATAAC	Cloning of K114
0070	ATATTTAATGTGCTAGTGACAATC	Cloning of K115
0071	GGTCAAAGAAGATTCTTTCATTCCTTTAAG	Cloning of K115
0072	CTTAAAGGAATGAAAGAATCTTCTTTGACCTCGACCCGAG ATCATATC	Cloning of K115
0073	CACTAGGATTGTCACTAGCACATTAAATATCCACGATTTGA TGAAAGAATAAC	Cloning of K115

0074	GAAAAGGGCATGTAATATTG	Cloning of K116
0075	CTTGGGGAAGAAGTAACAATGAC	Cloning of K116
0076	GAAATCAGTCATTGTTACTTCTTCCCCAAGTCGACCCGAGATCATATC	Cloning of K116
0077	CAAATTAACGCAATATTACATGCCCTTTTCCCACGATTTGATGAAAGAATAAC	Cloning of K116
0080	TCCTCCAGTGGGATTGCTACTTCTTTTGTTGCTGCTGCATCCTCAACTTG TCGATCCGATGATAAGCTGTC	Cloning of Y0011
0081	GCCTAGCGGGCTATTACCTTGTAAATACCACACTATCAATCCTTAAATGT TGCCACCTGACGTCTAAGAA	Cloning of Y0011
0117	AAATCGTGGTCGACCGGCATGCAAGCTCCCTCGAGCATTTC AGAGCCTTC	Cloning of K101
0118	AACCAGTGGTTATATGTACAGTAGTACGTTATCTAGCAAAAAGTCTACAAACAAATTC	Cloning of K101
0119	AAATCGTGGTCGACCGGCATGCAAGCTCCCTCGAGGACAGACCACTTATG	Cloning of K102
0120	AACCAGTGGTTATATGTACAGTAGTACGTTATCTCTCCGCCTGAATAAG	Cloning of K102
0121	AAATCGTGGTCGACCGGCATGCAAGCTCCCTCGAGAAATACAGAATAGGAAAG	Cloning of K103
0122	AACCAGTGGTTATATGTACAGTAGTACGTTATCGTAGCGGTGTTTATC	Cloning of K103
0123	AAATCGTGGTCGACCGGCATGCAAGCTCCCTCGAGGCATAGCATATTC	Cloning of K104
0124	AACCAGTGGTTATATGTACAGTAGTACGTTATCTGACGTGTTTTTCGTG	Cloning of K104
0125	AAATCGTGGTCGACCGGCATGCAAGCTCCCTCGAGTTCGATAAACCATG	Cloning of K105
0126	AACCAGTGGTTATATGTACAGTAGTACGTTATCATATATTTATATTGGTCCTTATTTTTATG	Cloning of K105
0127	AAATCGTGGTCGACCGGCATGCAAGCTCCCTCGAGGTTGTC ATCATAATC	Cloning of K106
0128	AACCAGTGGTTATATGTACAGTAGTACGTTATCACCGTATCATGGTATAC	Cloning of K106
0137	TTTTCGCTGCTTGTCCTTTT	qPCR detection of the K71 plasmid spike-in for the affinity purifications (Affinity purification)
0138	CATTTTCGTCCTCCCAACAT	qPCR detection of the K71 plasmid spike-in for the affinity purifications (Affinity purification)
0182	TCAGCGGCCGCCCTGCAGGTGCAAGCGGATCTAAGGATG	Cloning of K121
0183	TCAGCGGCCGCCCTGCAGGACTTTTACATTATCTCGAAA	Cloning of K121
0223	GGCTTTTCGATCAGACTTGGCATGTGACTAATCAAGTATGGCATGCTGGT TTTTGGGTCCTTTGTTTTCG	Cloning of Y0016 - Y0018
0224	TAGTAAATAACGGAGACTGGCGAACCGAATGGGCACCTGCCTCTGACTGC ATTTGGAGGGAGGAGAAGGA	Cloning of Y0016 - Y0018

0251	TAACTTCAGCACCAAAGCCAACAACTACGACCTATGTCGA GCAACGACTTTCCTCCAGTGGGATTGCTAC	Cloning of Y0019 - Y0021
0252	TTCTTGGCAGTCACATATATGGAAGGTGAATTTAGAGTAGT TTCCTTATAGCCTAGCGGGCTATTACCTT	Cloning of Y0019 - Y0021
0270	TCAGCTAGCTTAATTAAAAGACAACAGATTTATTGTA	Cloning of K139
0271	TCAGGCGCGCCCCCGAGGATTATAATTGTTC	Cloning of K139
0272	TCAGGCGCGCCTTTCGTCTCGCGCGTTTCGG	Cloning of K139
0273	TCAGCTAGCAGTAGTTGGAATATCATAAT	Cloning of K139
0274	TCAGCTAGCGAGAATTTGTATTTTCAGGG	Cloning of K139
0275	TCATTAATTAACCCCGTTCCACAACACAACA	Cloning of K139
0301	CATGATCAGATGGGGCTTGA	qPCR detection of the PDC1 locus (Affinity purification)
0302	ACCGGTGGTAGCGACTCTGT	qPCR detection of the PDC1 locus (Affinity purification)
0338	AGAAAGTGCTTTTGGATCGTCCGGTGAAATTGCAGTAATAC CGATAGTCC TCGATCCGATGATAAGCTGTC	Cloning of Y0042
0340	GCCGAATAAACTTAAAATTGAAACAAAACGCACCATTACT CTCACTATTTTCGATCCGATGATAAGCTGTC	Cloning of Y0043
0370	CATTTCAGAGCCTTCTTTGGAGCTC	Creating a probe for southern blot detection of ARS305
0371	ACATACATATGATTTTTATCTTGTG	Creating a probe for southern blot detection of ARS305
0437	AAATTCTGCCCTTGATTCGT	Creating a probe for southern blot detection of ARS316
0438	TTTGTTTATCTCATCACTAAT	Creating a probe for southern blot detection of ARS316
0457	ATACTAATTGAAGAGAAAGCTGGTGGCCAAAATAGGATAT TGATTGTAGA TGCCACCTGACGTCTAAGAA	Cloning of Y0042
0458	GAGCTTTTCTTTCCTCTCTCTTTTTTTTTTCTTGTTACATATT CCTATAT TGCCACCTGACGTCTAAGAA	Cloning of Y0043
0463	TTTCATGTACTGTCCGGTGT	qPCR detection of ARS305 (Affinity purification, Replication timing, ChIP)
0466	TTTTTAGCCCCCGTGTAAGTT	qPCR detection of ARS305 (Affinity purification, Replication timing, ChIP)
0493	GTGTTCGCCGCCAACTCCGCAGGTCTTTCGCAATTTATACC TTGGGTCAC TCGTACGCTGCAGGTCGAC	PCR on K155 to create the Mcm2-MNase-HA strains
0494	CAGAGAATTTTTTATCTTCATATCCAGATATTCGTAGGAATA ACAAAGTT ATCGATGAATTCGAGCTCG	PCR on K155 to create the Mcm2-

		MNase-HA strains
0552	TCAAAGAAAAGGTGCTGCTGA	qPCR detection of ARS313 (Affinity purification, Replication timing, ChIP)
0553	TCTTCCGTCTTAAAAGGTAGCAC	qPCR detection of ARS313 (Affinity purification, Replication timing, ChIP)
0627	TCAAAGCTTGGCGCTGGATGAAAAGGAAA	Cloning of K219
0628	TCAGAATTCTGGTATTTGATGGGTTGCTCA	Cloning of K219
0631	TGTAGCTTTCGACATCTTTTTATCATTCTACAAAAGACCAG	Cloning of K224
0632	GCTTCCACCTCCGCCATACGGTTTTATCTCCTTATTCAC	Cloning of K224
0633	GAGATAAAACCGTATGGCGGAGGTGGAAGCGGTGGCGG	Cloning of K224
0634	CGTTAACGCTTTCATGCCACCTCCGCCGCTGCCACCGC	Cloning of K224
0635	AGCGGCGGAGGTGGCATGAAAGCGTTAACGGCCAGGCAAC	Cloning of K224
0636	CTTATCATCGGATCGTCACAGCCAGTCGCCGTTGCGAA	Cloning of K224
0637	GGCGACTGGCTGTGACGATCCGATGATAAGCTGTCAAAC	Cloning of K224
0638	TAGAATGATAAAAAGACTCTTCCTTTTTCAATATTATTGAAGC	Cloning of K224
0639	GGCGCTGGATGAAAAGGAAA	Cloning of Y0051
0640	TGGTATTTGATGGGTTGCTC	Cloning of Y0051
0769	TACGCCAACTTAAGACCATG	Cloning of K238
0770	TCTCTTTTCCATGGTCATGA	Cloning of K238
0834	ACGGCGTAATGGATCAGAAATA	qPCR detection of a late-replicating region on ChrIV (Replication timing)
0835	CTGGCTCACCAGAATCTTCAT	qPCR detection of a late-replicating region on ChrIV (Replication timing)
0837	CGGCATTATCGTACACAACCT	qPCR detection of ARS316 (Affinity purification, Replication timing, ChIP)
0838	GTTCTTCGTTGCCTACATTTTCT	qPCR detection of ARS316 (Affinity purification, Replication timing, ChIP)
0858	TCCATGTCCATGTCCATGTCATCATGGGCCGTGACAAGCGTCGCCGCGCAGCCGAATAAACTTAAAATTGA	Cloning of Y0088 - Y0089
0859	CCTCGACGGCCTCCAGTTCTTCGACCAACTGTTCGTGATCGTCATCCATTGAGCTTTTCTTTCCTCTCTCT	Cloning of Y0088 - Y0089
0906	CGAAAGAAGTACCAAAGCCTGGGACCATCATTCATTTTTCT	Cloning of Y0071

	ACGAATAGAGGCGGAGGTGGAAGCGGTGG	
0907	CCTGCGTTCTGATATTCATCACTAGTAAAAATTGTATGTAC TTATTTATTACTCTTCCTTTTTCAATATT	Cloning of Y0071
0908	CAAGAGAAAATGTAGTAAGGCAAGTGGAAGAAGATGAAAAC TACGACGACGGCGGAGGTGGAAGCGGTGG	Cloning of Y0072
0909	ATTTCTCGTTGATTATAAATTAGTAGATTAATTTTTTGAATGC AAACTTTACTCTTCCTTTTTCAATATT	Cloning of Y0072
0910	TCTTCAATAATAAAGTAAAAGAAATACCTGAATATTCTCAC CTTATTGATGGCGGAGGTGGAAGCGGTGG	Cloning of Y0079
0911	ATTTATTTCTTCTTCGAAAGGAATAGTAGCGGAAAAGCTTC TTCTACGCAACTCTTCCTTTTTCAATATT	Cloning of Y0079
0912	ACATGCACGAAAAGCTGTACGAGGAACACCAACAGATGCTT GACAAGCAAGGCGGAGGTGGAAGCGGTGG	Cloning of Y0077
0913	TATTTTAATAACATTCCTATTTTATTGTACAAAATGCGCGACT ATTCCGTACTCTTCCTTTTTCAATATT	Cloning of Y0077
0914	GCGTTGACACAAGACAGGTTTATTATGAATTAGGCCAAATC CCGTTCGAGGGCGGAGGTGGAAGCGGTGG	Cloning of Y0078
0915	TAAGATTTTCACGTGCTCATCAATGTGAACAAATTATTAAAT ACAAGCGTACTCTTCCTTTTTCAATATT	Cloning of Y0078
0918	ATTCGAAAAGAAATTAAGCTTTGCGGATTACAGAAAAAAAC TACTGAAAGGCGGAGGTGGAAGCGGTGG	Cloning of Y0076
0919	CTTTTGAATATACTTAAGTTTATATAGGTGTAAGAAGGAAAT GTCCATGTACTCTTCCTTTTTCAATATT	Cloning of Y0076
0920	ACAGACTAGCAGCTCATTTACAGAGATGTTTGAGTAGGGGT GCTAGACGTGGCGGAGGTGGAAGCGGTGG	Cloning of Y0075
0921	GCTAAAATCTGTCTGTGCCTTTTCAATTACCCATAAACCACC ACCTAGTGACTCTTCCTTTTTCAATATT	Cloning of Y0075
0922	GAGAAGAAGCAATCGGATTCATTAGAGGTAGCAATAAATTC GCTGAAGTCGGCGGAGGTGGAAGCGGTGG	Cloning of Y0082
0923	TTATGTAAGCAAAACTGATATTTTTATATACAAATCGTTTCAA ATATCTCACTCTTCCTTTTTCAATATT	Cloning of Y0082
0924	TCAACACCAATTTCGACGATGAATTTGGAGATCTTGATGCT GTATTTTTTGGCGGAGGTGGAAGCGGTGG	Cloning of Y0080
0925	AATATGTAAAAGGAAAGTATATATTTCCAAGAAGTAGCCGCC CATGGCTAACTCTTCCTTTTTCAATATT	Cloning of Y0080
0926	AAGACATTGACACTGACGAAATGCAAGATTTTTTAAAAAAGC ATGCTTCAGGCGGAGGTGGAAGCGGTGG	Cloning of Y0073
0927	AATAACTTCAAATAAAGTCATAAAAGTTAATGCAATGAAATC ACATGCCCACTCTTCCTTTTTCAATATT	Cloning of Y0073
0928	TGAAAAGTCTGGTTGTGGATTCTGAGGGGCAAATCAGGTAT GCAAAGGAAGGCGGAGGTGGAAGCGGTGG	Cloning of Y0081
0929	ACCGAGTAAGCTGCTACATAATGTCTATATATCTACACATAA AATTCCGAACTCTTCCTTTTTCAATATT	Cloning of Y0081
0930	GGAAAGGCCTATTGAAGTTCGACGAAAAAACTGCCACTCTT GTGGACGAGGGCGGAGGTGGAAGCGGTGG	Cloning of Y0074
0931	TTACAATATACTAGATGAAGGCTCGTCAACGAGGCAAGCAA TGGTTGGAAACTCTTCCTTTTTCAATATT	Cloning of Y0074
0970	CTTCGCGCGTCAACTTTCTA	qPCR detection of ARS315 (Affinity purification,

0971	ATCGAAGTTTTAAGCGGCAAA	qPCR detection of ARS315 (Affinity purification, Replication timing, ChIP)
0998	GTATATACAACAGTTTTAGATCGTACTTCACAAAATACGAGA ACTGAATCCGATCCGATGATAAGCTGTC	Cloning of Y0117
1069	CCCTTTCGTCTTTGCGAAACCTAGTTCATTG	Cloning of K289
1070	AAACGCGCGATGCAAGTTATCGACCATG	Cloning of K289
1071	ATAACTTGCATCGCGCGTTTCGGTGATG	Cloning of K289
1072	GTTCCGATTTAGTGCTTTACGGCACCTC	Cloning of K289
1073	GTAAAGCACTAAATCGGAACCCTAAAGG	Cloning of K289
1074	GTTTTCTTCCATTTCATTGGAACCATCTC	Cloning of K289
1075	CCAATGAAATGGAAGAAAACCATGGTGACTTG	Cloning of K289
1076	GTTTCGCAAAGACGAAAGGGCCTCGTGATAC	Cloning of K289
1093	CGAAAGAAGTACCAAAGCCTGGGACCATCATTCATTTTTCT ACGAATAGACGTACGCTGCAGGTCGAC	Cloning of Y0123
1094	CCTGCGTTCTGATATTCATCACTAGTAAAAATTGTATGTAC TTATTTATTATCGATGAATTCGAGCTCG	Cloning of Y0123

6.1.4.2 Plamids

Name	Source	Description	Cloning strategy
K001 (K322)	(Gietz and Sugino, 1988)	E. coli/yeast shuttle vector for expression of proteins with URA3 marker and 2μ origin of replication	-
K004 (pM49.2)	(Griesenbeck et al., 2004a)	Plasmid pM49.2 is a derivative of pABX22, and has been modified by addition of a LexA-binding cluster juxtaposed to an RS element.	-
K005 (K2049)	(Hamperl et al., 2014)	Yeast expression vector for constitutive expression of LexA-TAP under control of TEF2 promoter and inducible expression of R Recombinase under control of GAL1-10 promoter; LEU2 selection marker framed with RS sites	-
K009 (K2054)	(Hamperl et al., 2014)	E. coli/yeast shuttle vector used for genomic integration	-

		of CYC1 LexATAP GAL1-10 RecR expression cassette by recombination in URA3 locus	
K018		pBlueSkript SK (+)	-
K071 (pSH36)	(Hamperl et al., 2017)	Plasmid used as a spike in in the chromatin ring purifications in order to assess the efficiency of DNA extraction of different fractions	-
K094 (pMW2)		Plasmid containing wildtype ARS305 locus in pBlueScript backbone	HindIII/PstI cut amplicon (primer 0016/0017) from yeast gDNA into K18
K095 (pMW3)		Plasmid containing wildtype ARS316 locus in pBlueScript backbone	EcoRI/PstI cut amplicon (primer 0020/0021) from yeast gDNA into K18
K101 (pMW7)		Vector with ARS305 +/-1 nucleosome sequence next to lexA/RS sites	Gibson assembly of two fragments (primer 0117/0118 with K94 as template + HpaI/XhoI cut backbone from K0004)
K102 (pMW8)		Vector with ARS305 +/-2 nucleosome sequence next to lexA/RS sites	Gibson assembly of two fragments (primer 0119/0120 with K94 as template + HpaI/XhoI cut backbone from K0004)
K103 (pMW9)		Vector with ARS305 +/-3 nucleosome sequence next to lexA/RS sites	Gibson assembly of two fragments (primer 0121/0122 with K94 as template + HpaI/XhoI cut backbone from K0004)
K104 (pMW10)		Vector with ARS316 +/-1 nucleosome sequence next to lexA/RS sites	Gibson assembly of two fragments (primer 0123/0124 with K95 as template + HpaI/XhoI cut backbone from K0004)
K105 (pMW11)		Vector with ARS316 +/-2 nucleosome	Gibson assembly of two fragments (primer 0125/0126

		sequence next to lexA/RS sites	with K95 as template + HpaI/XhoI cut backbone from K0004)
K106 (pMW12)		Vector with ARS316 +/-3 nucleosome sequence next to lexA/RS sites	Gibson assembly of two fragments (primer 0127/0128 with K95 as template + HpaI/XhoI cut backbone from K0004)
K111 (pMW16)		Vector for yeast transformation in order to modify ARS305 locus and insert RS sites next to NS+/-1	Gibson assembly of two fragments (primer 0042/0043 with K94 as template + primer 0044/0045 with K101 as template)
K112 (pMW17)		Vector for yeast transformation in order to modify ARS305 locus and insert RS sites next to NS+/-2	Gibson assembly of two fragments (primer 0046/0047 with K94 as template + primer 0048/0049 with K102 as template)
K113 (pMW18)		Vector for yeast transformation in order to modifiy ARS305 locus and insert RS sites next to NS+/-3	Gibson assembly of t wo fragments (primer 0050/0051 with K94 as template + primer 0052/0053 with K103 as template)
K114 (pMW19)		Vector for yeast transformation in order to modifiy ARS316 locus and insert RS sites next to NS+/-1	Gibson assembly of two fragments (primer 0066/0067 with K95 as template + primer 0068/0069 with K104 as template)
K115 (pMW20)		Vector for yeast transformation in order to modifiy ARS316 locus and insert RS sites next to NS+/-2	Gibson assembly of two fragments (primer 0070/0071 with K95 as template + primer 0072/0073 with K105 as template)
K116 (pMW21)		Vector for yeast transformation in order to modifiy ARS316 locus and insert RS sites next to NS+/-3	Gibson assembly of two fragments (primer 0074/0075 with K95 as template + primer 0076/0077 with K106 as template)
K121 (pMW22)		Backbone for yeast transformation vectors	NotI cut amplicon (primer 0182/0183)

		with 500bp homologue region to yeast chr1 with a BbsI site in the middle; add insert with Gibson assembly	from yeast gDNA into K18
K139 (pMW23)		E. coli/yeast shuttle vector used for genomic integration of pCYC1 LexA-TAP GAL1-10 RecR expression cassette by recombination in 500bp homology region from K121 of yeast chromosome I, LEU2 selection marker framed with RS sites (two mutations in the lexA gene that stop binding to lexA binding site: V11A, N171D)	AscI/NheI cut amplicon (primer 0270/0271 template K121) inserted with AscI/NheI cut amplicon (primer 0272/0273 template K009). Resulting plasmid was cut with NheI/PacI and inserted with NheI/PacI cut amplicon (primer 0274/0275 template K009).
K155	Prof. Dr. Joachim Griesenbeck	Vector containing the sequence of Mnase fused to HA epitope together with uracil marker	
K167 (pMW24)		E. coli/yeast shuttle vector used for genomic integration of pCYC1 LexA-TAP GAL1-10 RecR expression cassette by recombination in 500bp homology region from K121 of yeast chromosome I, LEU2 selection marker framed with RS sites	Insert from K009 (NsiI/BlpI) cloned into K139
K168 (pAC01)	Anna Chanou, unpublished	Vector for yeast transformation in order to modifiy ARS313 locus and insert RS sites next to NS+/-1	-
K169 (pAC02)	Anna Chanou, unpublished	Vector for yeast transformation in order to modifiy ARS313 locus and insert RS sites next to NS+/-2	-
K170 (pAC03)	Anna Chanou, unpublished	Vector for yeast transformation in order to modifiy	-

		ARS313 locus and insert RS sites next to NS+/-3	
K196 (pBluescript_GS14a-V5- GS14)	Henning Ummethum, unpublished	Plasmid used to amplify a glycine-serine linker sequence	-
K219 (pMW25)		E. coli/yeast shuttle vector with homology arms for integration at the yeast Sir4 locus	HindIII/EcoRI cut amplicon (primer 0627/0628) from yeast gDNA into K18
K224 (pMW26)		E. coli/yeast shuttle vector with homology arms for integration at the yeast Sir4 locus for expressing Sir4- GlySer-V5-GlySer-lexA fusion protein	Gibson assembly of four fragments (primer 0631/0632 with K219 as template + primer 0633/0634 with K196 as template + primer 0635/0636 with K167 as template + primer 0637/0638 with K001 as template)
K238 (pTS1)		E.coli/yeast shuttle vector used for genomic integration of pTEF2 LexA-TAP GAL1-10 RecR expression cassette by recombination in 500bp homology region from K121 of yeast chromosome I, LEU2 selection marker framed with RS sites	NcoI/AflII cut amplicon (primer 0769/0770 template K005) into K167
K273 (pAC05)	Anna Chanou, unpublished	Vector for yeast transformation in order to modifiy ARS313 locus and insert RS sites next to NS+/-2	-
K278 (pMP10)	(Reusswig et al., 2022)	Plasmid containing pGPD-TIR1-3myc (in pRS305 (LEU2), codon-optimized) for yeast transformation	-
K282 (pKR586)	(Reusswig et al., 2022)	Plasmid containing 3x aid*– 9x myc (in pFA6a- hphNT1) for yeast transformation	-
K289 (pMW28)		pGPD-TIR1-3myc (in pRS305 (LEU2),	Gibson assembly of four fragments (primer 1069/1070 with gDNA as

		codon- optimized) Derived from K278, with an added homology region to transform into yeast ChrI (NdeI RS site for trafo)	template + primer 1071/1072 with K278 as template + primer 1073/1074 with K278 as template + primer 1075/1076 with K278 as template)
K293 (pAC06)	Anna Chanou, unpublished	Vector for yeast transformation in order to modifiy ARS315 locus and insert RS sites next to NS+/-2	-

6.1.5 Enzymes and polypeptides

All restriction enzymes were bought from NEB at the highest quality. All enzymes were used with the provided buffers.

Enzymes and polypeptides	Source	Identifier
Antarctic Phosphatase	NEB	Cat# M0289S
Bovine Serum Albumin (BSA)	Roche	Cat# 10735078001
Lysyl Endopeptidase (Lys-C)	Wako Chemicals	Cat# 121-05063
Pronase	Sigma-Aldrich	Cat# 53702
Proteinase K	Serva	Cat# 33756
Phusion High-Fidelity DNA Polymerase	Thermo Fisher Scientific	Cat# F-530S
Rabbit IgGs	Sigma-Aldrich	Cat# I5006
RNAse A	Thermo Fisher Scientific	Cat# EN0531
T4 DNA Ligase	NEB	Cat# M0202L
TEV Protease	NEB	Cat# P8112S
Trypsin	Promega	Cat# V528A
Yeast Mating Factor Alpha	Biomol	Cat# Y2016.5
Zymolyase	Biomol	Cat# Z1005

6.1.6 Antibodies

Antibody	Western blot dilution	Source	Identifier
HRP-conjugated goat anti-mouse	1:10000	Invitrogen	Cat# G21040 // RRID:AB_2536527
HRP-conjugated goat anti-rabbit	1:10000	Invitrogen	Cat# G21234 // RRID:AB_2536530
Mouse Monoclonal anti-c-MYC clone 9E10	1:400	Sigma-Aldrich	Cat# 11667149001 // RRID:AB_390912
Mouse Monoclonal anti-GAPDH	1:1000	Novus Biologicals	Cat# NB600-502 // RRID:AB_10077682
Mouse Monoclonal anti-V5	Used for ChIP only	Thermo Fisher Scientific	Cat# R96025 // RRID:AB_159313
Rabbit monoclonal anti-H2A (phospho S129)	1:2000	Abcam	Cat# ab181447 //

Rabbit Monoclonal anti-RNA polymerase II CTD repeat YSPTSPS (phospho S2)	1:500	Abcam	Cat# ab193468 // RRID:AB_2905557
Rabbit Peroxidase Anti-Peroxidase Soluble Complex antibody	1:1000	Sigma-Aldrich	Cat# P1291 // RRID:AB_1079562
Rabbit polyclonal anti-CBP	1:100	Sigma-Aldrich	Cat# 07-482 // RRID:AB_310653
Rabbit polyclonal anti-H3	Used for ChIP only	Abcam	Cat# ab1791 // RRID:AB_302613
Rat monoclonal anti-HA (3F10)	Used for ChIP only	Sigma-Aldrich	Cat# 11867423001 // RRID:AB_390918

6.1.7 Organisms

6.1.7.1 Bacteria

For all cloning experiments, chemical competent DH5alpha host bacteria by NEB were used.

6.1.7.2 Yeast strains

Name	Genotype	Description	Cloning strategy
Y0001 (Y01408)	MATa; ura3Δ0; leu2Δ0; his3Δ1; met15Δ0; bar1::kanMX4	Wildtype strain	EUROSCARF
Y0008	MATa; ade2-1; ura3-1; trp1-1; leu2-3,112; his3-11; can1-100	RS sites and lexA binding sites flanking the ribosomal ARS. Expression cassette for R Recombinase and lexA (TEF2 promoter)	(Hamperl et al., 2014)
Y0010 (yMW2)	MATa; ura3Δ0; leu2Δ0; his3Δ1; met15Δ0; bar1::kanMX4; ARS305::URA3	ARS305 exchanged for URA3	Transformation of amplicon derived from K001 (primer 0040/0041) into Y0001. Selection on Ura
Y0011 (yMW3)	MATa; ura3Δ0; leu2Δ0; his3Δ1; met15Δ0; bar1::kanMX4; ARS316::URA3	ARS316 exchanged for URA3	Transformation of amplicon derived from K001 (primer 0080/0081) into Y0001. Selection on Ura
Y0016 (yMW4)	MATa; ura3Δ0; leu2Δ0; his3Δ1; met15Δ0; bar1::kanMX4; RS_LEXA_NS-1_ARS305_NS+1_RS	RS sites and lexA binding sites at ARS305 after +/-1 nucleosomes	Transformation of amplicon derived from K111 (primer 0223/0224) into Y0010. Selection on FOA
Y0017 (yMW5)	MATa; ura3Δ0; leu2Δ0; his3Δ1; met15Δ0; bar1::kanMX4; RS_LEXA_NS-2_ARS305_NS+2_RS	RS sites and lexA binding sites at ARS305 after +/-2 nucleosomes	Transformation of amplicon derived from K112 (primer 0223/0224) into Y0010. Selection on

			FOA
Y0018 (yMW6)	MATa; ura3Δ0; leu2Δ0; his3Δ1; met15Δ0; bar1::kanMX4; RS_LEXA_NS-3_ARS305_NS+3_RS	RS sites and lexA binding sites at ARS305 after +/-3 nucleosomes	Transformation of amplicon derived from K113 (primer 0223/0224) into Y0010. Selection on FOA
Y0019 (yMW7)	MATa; ura3Δ0; leu2Δ0; his3Δ1; met15Δ0; bar1::kanMX4; RS_LEXA_NS-1_ARS316_NS+1_RS	RS sites and lexA binding sites at ARS316 after +/-1 nucleosomes	Transformation of amplicon derived from K114 (primer 0251/0252) into Y0011. Selection on FOA
Y0020 (yMW8)	MATa; ura3Δ0; leu2Δ0; his3Δ1; met15Δ0; bar1::kanMX4; RS_LEXA_NS-2_ARS316_NS+2_RS	RS sites and lexA binding sites at ARS316 after +/-2 nucleosomes	Transformation of amplicon derived from K115 (primer 0251/0252) into Y0011. Selection on FOA
Y0021 (yMW9)	MATa; ura3Δ0; leu2Δ0; his3Δ1; met15Δ0; bar1::kanMX4; RS_LEXA_NS-3_ARS316_NS+3_RS	RS sites and lexA binding sites at ARS316 after +/-3 nucleosomes	Transformation of amplicon derived from K116 (primer 0251/0252) into Y0011. Selection on FOA
Y0034 (yMW17)	MATa; ura3Δ0; leu2Δ0; his3Δ1; met15Δ0; bar1::kanMX4; Chr I 212kb::LEU2 pCYC1-LEXA-TAP pGAL1-10 RecR	WT strain with expression cassette for R Recombinase and lexA (CYC1 promoter)	Transformation of SbfI digested plasmid K167 into Y0001. Selection on Leu
Y0035 (yMW18)	MATa; ura3Δ0; leu2Δ0; his3Δ1; met15Δ0; bar1::kanMX4; RS_LEXA_NS-1_ARS305_NS+1_RS; Chr I 212kb::LEU2 pCYC1-LEXA-TAP pGAL1-10 RecR	RS sites and lexA binding sites at ARS305 after +/-1 nucleosomes. Expression cassette for R Recombinase and lexA (CYC1 promoter)	Transformation of SbfI digested plasmid K167 into Y0016. Selection on Leu
Y0036 (yMW19)	MATa; ura3Δ0; leu2Δ0; his3Δ1; met15Δ0; bar1::kanMX4; RS_LEXA_NS-2_ARS305_NS+2_RS; Chr I212kb::LEU2 pCYC1-LEXA-TAP pGAL1-10 RecR	RS sites and lexA binding sites at ARS305 after +/-2 nucleosomes. Expression cassette for R Recombinase and lexA (CYC1 promoter)	Transformation of SbfI digested plasmid K167 into Y0017. Selection on Leu
Y0037 (yMW20)	MATa; ura3Δ0; leu2Δ0; his3Δ1; met15Δ0; bar1::kanMX4; RS_LEXA_NS-3_ARS305_NS+3_RS; Chr I 212kb::LEU2 pCYC1-LEXA-TAP pGAL1-10 RecR	RS sites and lexA binding sites at ARS305 after +/-3 nucleosomes. Expression cassette for R Recombinase and lexA (CYC1 promoter)	Transformation of SbfI digested plasmid K167 into Y0018. Selection on Leu
Y0038 (yMW21)	MATa; ura3Δ0; leu2Δ0; his3Δ1; met15Δ0;	RS sites and lexA Binding sites at	Transformation of SbfI digested

	bar1::kanMX4; RS_LEXA_NS-1_ARS316_NS+1_RS; Chr I 212kb::LEU2 pCYC1-LEXA-TAP pGAL1-10 RecR	ARS316 after +/-1 nucleosomes. Expression cassette for R Recombinase and lexA (CYC1 promoter)	plasmid K167 into Y0019. Selection on Leu
Y0039 (yMW22)	MATa; ura3Δ0; leu2Δ0; his3Δ1; met15Δ0; bar1::kanMX4; RS_LEXA_NS-2_ARS316_NS+2_RS; Chr I 212kb::LEU2 pCYC1-LEXA-TAP pGAL1-10 RecR	RS sites and lexA Binding sites at ARS316 after +/-2 nucleosomes. Expression cassette for R Recombinase and lexA (CYC1 promoter)	Transformation of SbfI digested plasmid K167 into Y0020. Selection on Leu
Y0040 (yMW23)	MATa; ura3Δ0; leu2Δ0; his3Δ1; met15Δ0; bar1::kanMX4; RS_LEXA_NS-3_ARS316_NS+3_RS; Chr I 212kb::LEU2 pCYC1-LEXA-TAP pGAL1-10 RecR	RS sites and lexA Binding sites at ARS316 after +/-3 nucleosomes. Expression cassette for R Recombinase and lexA (CYC1 promoter)	Transformation of SbfI digested plasmid K167 into Y0021. Selection on Leu
Y0042 (yAC02)	MATa; ura3Δ0; leu2Δ0; his3Δ1; met15Δ0; bar1::kanMX4; ARS313::URA3	ARS313 exchanged for URA3	Transformation of amplicon derived from K001 (primer 0338/0457) into Y0001. Selection on Ura
Y0043 (yAC03)	MATa; ura3Δ0; leu2Δ0; his3Δ1; met15Δ0; bar1::kanMX4; ARS315::URA3	ARS315 exchanged for URA3	Transformation of amplicon derived from K001 (primer 0340/0458) into Y0001. Selection on Ura
Y0044 (yAC04)	MATa; ura3Δ0; leu2Δ0; his3Δ1; met15Δ0; bar1::kanMX4; RS_LEXA_NS-3_ARS313_NS+3_RS	RS sites and lexA binding sites at ARS313 after +/-3 nucleosomes	Transformation of EcoRI/HindIII digested plasmid K170 into Y0042. Selection on FOA
Y0045 (yAC05)	MATa; ura3Δ0; leu2Δ0; his3Δ1; met15Δ0; bar1::kanMX4; RS_LEXA_NS-1_ARS313_NS+1_RS	RS sites and lexA binding sites at ARS313 after +/-1 nucleosomes	Transformation of EcoRI/HindIII digested plasmid K168 into Y0042. Selection on FOA
Y0046 (yAC06)	MATa; ura3Δ0; leu2Δ0; his3Δ1; met15Δ0; bar1::kanMX4; RS_LEXA_NS-2_ARS313_NS+2_RS	RS sites and lexA binding sites at ARS313 after +/-2 nucleosomes	Transformation of EcoRI/HindIII digested plasmid K169 into Y0042. Selection on FOA
Y0051 (yMW24)	MATa; ura3Δ0; leu2Δ0; his3Δ1; met15Δ0; bar1::kanMX4; RS_LEXA_NS-1_ARS305_NS+1_RS; Sir4-GlySer-lexA; Ura3	Sir4-lexA fusion protein targeted to ARS305+/-1	Transformation of amplicon derived from K224 (primer 0639/0640) into Y0016. Selection on Ura

Y0063 (yTS1)	MATa; ura3Δ0; leu2Δ0; his3Δ1; met15Δ0; bar1::kanMX4; RS_LEXA_NS-1_ARS305_NS+1_RS; Chr I 212kb::LEU2 pTEF2-LEXA-TAP pGAL1-10 RecR	RS sites and lexA binding sites at ARS305 after +/-1 nucleosomes. Expression cassette for R Recombinase and lexA (TEF2 promoter)	Transformation of SbfI digested plasmid K238 into Y0016. Selection on Leu
Y0064 (yTS2)	MATa; ura3Δ0; leu2Δ0; his3Δ1; met15Δ0; bar1::kanMX4; RS_LEXA_NS-2_ARS305_NS+2_RS; Chr I 212kb::LEU2 pTEF2-LEXA-TAP pGAL1-10 RecR	RS sites and lexA binding sites at ARS305 after +/-2 nucleosomes. Expression cassette for R Recombinase and lexA (TEF2 promoter)	Transformation of SbfI digested plasmid K238 into Y0017. Selection on Leu
Y0065 (yTS3)	MATa; ura3Δ0; leu2Δ0; his3Δ1; met15Δ0; bar1::kanMX4; RS_LEXA_NS-3_ARS305_NS+3_RS; Chr I 212kb::LEU2 pTEF2-LEXA-TAP pGAL1-10 RecR	RS sites and lexA binding sites at ARS305 after +/-3 nucleosomes. Expression cassette for R Recombinase and lexA (TEF2 promoter)	Transformation of SbfI digested plasmid K238 into Y0018. Selection on Leu
Y0066 (yTS4)	MATa; ura3Δ0; leu2Δ0; his3Δ1; met15Δ0; bar1::kanMX4; Chr I 212kb::LEU2 pTEF2-LEXA-TAP pGAL1-10 RecR	WT strain with expression cassette for R Recombinase and lexA (TEF2 promoter)	Transformation of SbfI digested plasmid K238 into Y0001. Selection on Leu
Y0067 (yMW36)	MATa; ura3Δ0; leu2Δ0; his3Δ1; met15Δ0; bar1::kanMX4; RS_LEXA_NS-1_ARS316_NS+1_RS; Chr I 212kb::LEU2 pTEF2-LEXA-TAP pGAL1-10 RecR	RS sites and lexA binding sites at ARS316 after +/-1 nucleosomes. Expression cassette for R Recombinase and lexA (TEF2 promoter)	Transformation of SbfI digested plasmid K238 into Y0019. Selection on Leu
Y0068 (yMW37)	MATa; ura3Δ0; leu2Δ0; his3Δ1; met15Δ0; bar1::kanMX4; RS_LEXA_NS-2_ARS316_NS+2_RS; Chr I 212kb::LEU2 pTEF2-LEXA-TAP pGAL1-10 RecR	RS sites and lexA binding sites at ARS316 after +/-2 nucleosomes. Expression cassette for R Recombinase and lexA (TEF2 promoter)	Transformation of SbfI digested plasmid K238 into Y0020. Selection on Leu
Y0069 (yMW38)	MATa; ura3Δ0; leu2Δ0; his3Δ1; met15Δ0; bar1::kanMX4; RS_LEXA_NS-3_ARS316_NS+3_RS; Chr I 212kb::LEU2 pTEF2-LEXA-TAP pGAL1-10 RecR	RS sites and lexA binding sites at ARS316 after +/-3 nucleosomes. Expression cassette for R Recombinase and lexA (TEF2 promoter)	Transformation of SbfI digested plasmid K238 into Y0021. Selection on Leu
Y0071 (yMW40)	MATa; ura3Δ0; leu2Δ0; his3Δ1; met15Δ0; bar1::kanMX4; RS_LEXA_NS-	Ask1-lexA fusion protein targeted to ARS316	Transformation of amplicon derived from K224 (primer 0906/0907) into

	1_ARS316_NS+1_RS; Ask1-GlySer-V5-GlySer-lexA; Ura3		Y0019. Selection on Ura
Y0072 (yMW41)	MATa; ura3Δ0; leu2Δ0; his3Δ1; met15Δ0; bar1::kanMX4; RS_LEXA_NS-1_ARS316_NS+1_RS; Cyc8-GlySer-V5-GlySer-lexA; Ura3	Cyc8-lexA fusion protein targeted to ARS316	Transformation of amplicon derived from K224 (primer 0908/0908) into Y0019. Selection on Ura
Y0073 (yMW42)	MATa; ura3Δ0; leu2Δ0; his3Δ1; met15Δ0; bar1::kanMX4; RS_LEXA_NS-1_ARS316_NS+1_RS; Swi6-GlySer-V5-GlySer-lexA; Ura3	Swi6-lexA fusion protein targeted to ARS316	Transformation of amplicon derived from K224 (primer 0926/0927) into Y0019. Selection on Ura
Y0074 (yMW43)	MATa; ura3Δ0; leu2Δ0; his3Δ1; met15Δ0; bar1::kanMX4; RS_LEXA_NS-1_ARS316_NS+1_RS; Ydl144C-GlySer-V5-GlySer-lexA; Ura3	Ydl144C-lexA fusion protein targeted to ARS316	Transformation of amplicon derived from K224 (primer 0930/0931) into Y0019. Selection on Ura
Y0075 (yMW44)	MATa; ura3Δ0; leu2Δ0; his3Δ1; met15Δ0; bar1::kanMX4; RS_LEXA_NS-1_ARS316_NS+1_RS; Sgf11-GlySer-V5-GlySer-lexA; Ura3	Sgf11-lexA fusion protein targeted to ARS316	Transformation of amplicon derived from K224 (primer 0920/0921) into Y0019. Selection on Ura
Y0076 (yMW45)	MATa; ura3Δ0; leu2Δ0; his3Δ1; met15Δ0; bar1::kanMX4; RS_LEXA_NS-1_ARS316_NS+1_RS; Set3-GlySer-V5-GlySer-lexA; Ura3	Set3-lexA fusion protein targeted to ARS316	Transformation of amplicon derived from K224 (primer 0918/0919) into Y0019. Selection on Ura
Y0077 (yMW46)	MATa; ura3Δ0; leu2Δ0; his3Δ1; met15Δ0; bar1::kanMX4; RS_LEXA_NS-1_ARS316_NS+1_RS; Ipi3-GlySer-V5-GlySer-lexA; Ura3	Ipi3-lexA fusion protein targeted to ARS316	Transformation of amplicon derived from K224 (primer 0912/0913) into Y0019. Selection on Ura
Y0078 (yMW47)	MATa; ura3Δ0; leu2Δ0; his3Δ1; met15Δ0; bar1::kanMX4; RS_LEXA_NS-1_ARS316_NS+1_RS; Met18-GlySer-V5-GlySer-lexA; Ura3	Met18-lexA fusion protein targeted to ARS316	Transformation of amplicon derived from K224 (primer 0914/0915) into Y0019. Selection on Ura
Y0079 (yMW48)	MATa; ura3Δ0; leu2Δ0; his3Δ1; met15Δ0; bar1::kanMX4;	Gcn5-lexA fusion protein targeted to ARS316	Transformation of amplicon derived from K224 (primer

	RS_LEXA_NS-1_ARS316_NS+1_RS; Gcn5-GlySer-V5-GlySer-lexA; Ura3		0910/0911) into Y0019. Selection on Ura
Y0080 (yMW49)	MATa; ura3Δ0; leu2Δ0; his3Δ1; met15Δ0; bar1::kanMX4; RS_LEXA_NS-1_ARS316_NS+1_RS; Snf6-GlySer-V5-GlySer-lexA; Ura3	Snf6-lexA fusion protein targeted to ARS316	Transformation of amplicon derived from K224 (primer 0924/0925) into Y0019. Selection on Ura
Y0081 (yMW50)	MATa; ura3Δ0; leu2Δ0; his3Δ1; met15Δ0; bar1::kanMX4; RS_LEXA_NS-1_ARS316_NS+1_RS; Ycr087C-GlySer-V5-GlySer-lexA; Ura3	Ycr087C-lexA fusion protein targeted to ARS316	Transformation of amplicon derived from K224 (primer 0928/0929) into Y0019. Selection on Ura
Y0082 (yMW51)	MATa; ura3Δ0; leu2Δ0; his3Δ1; met15Δ0; bar1::kanMX4; RS_LEXA_NS-1_ARS316_NS+1_RS; Smc3-GlySer-V5-GlySer-lexA; Ura3	Smc3-lexA fusion protein targeted to ARS316	Transformation of amplicon derived from K224 (primer 0922/0923) into Y0019. Selection on Ura
Y0088 (yAC13)	MATa; ura3Δ0; leu2Δ0; his3Δ1; met15Δ0; bar1::kanMX4; RS_LEXA_NS-2_ARS315_NS+2_RS	RS sites and lexA binding sites at ARS315 after +/-2 nucleosomes	Transformation of amplicon derived from K293 (primer 0858/0859) into Y0043. Selection on FOA
Y0089 (yAC14)	MATa; ura3Δ0; leu2Δ0; his3Δ1; met15Δ0; bar1::kanMX4; RS_LEXA_NS-3_ARS315_NS+3_RS	RS sites and lexA binding sites at ARS315 after +/-3 nucleosomes	Transformation of amplicon derived from K273 (primer 0858/0859) into Y0043. Selection on FOA
Y0090 (yAC15)	MATa; ura3Δ0; leu2Δ0; his3Δ1; met15Δ0; bar1::kanMX4; RS_LEXA_NS-2_ARS315_NS+2_RS; Chr I 212kb::LEU2 pTEF2-LEXA-TAP pGAL1-10 RecR	RS sites and lexA binding sites at ARS315 after +/-2 nucleosomes. Expression cassette for R Recombinase and lexA (TEF2 promoter)	Transformation of SbfI digested plasmid K238 into Y0088. Selection on Leu
Y0091 (yAC16)	MATa; ura3Δ0; leu2Δ0; his3Δ1; met15Δ0; bar1::kanMX4; RS_LEXA_NS-3_ARS315_NS+3_RS; Chr I 212kb::LEU2 pTEF2-LEXA-TAP pGAL1-10 RecR	RS sites and lexA binding sites at ARS315 after +/-3 nucleosomes. Expression cassette for R Recombinase and lexA (TEF2 promoter)	Transformation of SbfI digested plasmid K238 into Y0089. Selection on Leu
Y0092 (yAC17)	MATa; ura3Δ0; leu2Δ0; his3Δ1; met15Δ0; bar1::kanMX4;	RS sites and lexA binding sites at	Transformation of SbfI digested

	RS_LEXA_NS-1_ARS313_NS+1_RS; Chr I 212kb::LEU2 pTEF2-LEXA-TAP pGAL1-10 RecR	ARS313 after +/-1 nucleosomes. Expression cassette for R Recombinase and lexA (TEF2 promoter)	plasmid K238into Y0045. Selection on Leu
Y0093 (yAC18)	MATa; ura3Δ0; leu2Δ0; his3Δ1; met15Δ0; bar1::kanMX4; RS_LEXA_NS-2_ARS313_NS+2_RS; Chr I 212kb::LEU2 pTEF2-LEXA-TAP pGAL1-10 RecR	RS sites and lexA binding sites at ARS313 after +/-2 nucleosomes. Expression cassette for R Recombinase and lexA (TEF2 promoter)	Transformation of SbfI digested plasmid K238 into Y0046. Selection on Leu
Y0094 (yAC19)	MATa; ura3Δ0; leu2Δ0; his3Δ1; met15Δ0; bar1::kanMX4; RS_LEXA_NS-3_ARS313_NS+3_RS; Chr I 212kb::LEU2 pTEF2-LEXA-TAP pGAL1-10 RecR	RS s ites and lexA binding sites at ARS313 after +/-3 nucleosomes. Expression cassette for R Recombinase and lexA (TEF2 promoter)	Transformation of SbfI digested plasmid K238 into Y0044. Selection on Leu
Y0098	MATa trp-l-l ura3-1 his3-11, 3 leu2-3, 112 ade2-l can1-100	Wildtype strain	(Li et al., 2002)
Y0099	As Y0098 except LEU2, ask1-1	*ask1-1* temperature sensitive mutant	(Li et al., 2002)
Y0100	As Y0098 except ask1-3	*ask1-2* temperature sensitive mutant	(Li et al., 2002)
Y0101	As Y0098 except ask1-2	*ask1-3* temperature sensitive mutant	(Li et al., 2002)
Y0117 (yMW57)	MATa; ura3Δ0; leu2Δ0; his3Δ1; met15Δ0; bar1::kanMX4; set3::ura3	Set3 knockout strain	Transformation of amplicon derived from K224 (primer 0998/0919) into Y0001. Selection on Ura
Y0122 (yMW62)	MATa; ura3Δ0; leu2Δ0; his3Δ1; met15Δ0; bar1::kanMX4; pGPD- TIR1-3myc; leu2	WT strain with expression cassette for OsTir1	Transformation of NdeI digested plasmid K289 into Y0001. Selection on Leu
Y0123 (yMW63)	MATa; ura3Δ0; leu2Δ0; his3Δ1; met15Δ0; bar1::kanMX4; pGPD- TIR1-3myc; leu2; Ask1-3x aid* – 9x myc	Ask1 fused to 3x aid* – 9x myc. Expression cassette for OsTir1	Transformation of amplicon derived from K282 (primer 1093/1094) into Y122. Selection on Hygromycine B
Y0124 (yAC34)	MATa; ura3Δ0; leu2Δ0; his3Δ1; met15Δ0; bar1::kanMX4; RS_LEXA_NS-3_ARS305_NS+3_RS; Chr I 212kb::LEU2 pTEF2-LEXA-TAP pGAL1-10 RecR; MNAse-HA; URA3	Endogenous Mcm2 protein is fused to Mnase-HA- Uracil marker	Transformation of amplicon derived from K155 (primer 493/494) into Y065. Selection on Ura

Y0125 (yAC35)	MATa; ura3Δ0; leu2Δ0; his3Δ1; met15Δ0; bar1::kanMX4;RS_LEXA_NS-3_ARS313_NS+3_RS; Chr I 212kb::LEU2 pTEF2-LEXA-TAP pGAL1-10 RecR; MNAse-HA; URA3	Endogenous Mcm2 protein is fused to Mnase-HA- Uracil marker	Transformation of amplicon derived from K155 (primer 493/494) into Y094. Selection on Ura
Y0138 (yMW65)	MATa; ura3Δ0; leu2Δ0; his3Δ1; met15Δ0; bar1::kanMX4; RS_LEXA_NS-1_ARS305_NS+1_RS; Ask1-GlySer-V5-GlySer-lexA; Ura3	Ask1-lexA fusion protein targeted to ARS305	Transformation of amplicon derived from K224 (primer 0906/0907) into Y0016. Selection on Ura
Y0139 (yMW66)	MATa; ura3Δ0; leu2Δ0; his3Δ1; met15Δ0; bar1::kanMX4; RS_LEXA_NS-1_ARS305_NS+1_RS; Ask1-GlySer-V5-GlySer-lexA; Ura3	Ask1-lexA fusion protein targeted to ARS313	Transformation of amplicon derived from K224 (primer 0906/0907) into Y0045. Selection on Ura

6.1.8 Equipment

Device	Manufacturer
2100 Bioanalyzer	Agilent
BD FACSCanto	BD Bioscience
Bioruptor UCD-200	Diagenode
Centrifuge 5424	Eppendorf
Centrifuge 5810 R	Eppendorf
ChemiDoc Touch	Bio-Rad
Design Kaffemühle Basic	Gastroback
E220 evolution	Covaris
Heratherm	Thermo Fisher Scientific
Hybaid Mini 10	Hybaid Limited
HX-2 Block heater	Peqlab
Kern EMB precision balance	Kern
Lab 850 pH meter	SI Analytics
LightCycler 480 II	Roche
Mastercycler nexus	Eppendorf
Mastercycler nexus gradient	Eppendorf
Multiskan Sky	Thermo Fisher Scientific
Multitron Standard	Infors HT
NanoDrop 2000c	Thermo Fisher Scientific
PTR-60	Grant Instruments
Qubit 4 Fluorometer	Invitrogen
Reax Top	Heidolph Instruments
Typhoon FLA 7000	GE Healthcare

Unitwist 3D	Unitwist
U:GENIUS[3]	Syngene
VWR 250V	VWR
VXR basic Vibrax	Ika

6.1.9 Consumables

Consumable	Identifier	Manufacturer
384-qPCR-Plate skirted	Cat# 781358	Brand
Amersham Hybond™-N nylon membrane	Cat# GE10600023	GE Healthcare
AMPure XP	Cat# A63880	Beckman Coulter
BcMag Epoxy-Activated Magnetic Beads	Cat# FC-102	Bioclone
C18 spin columns Pierce ™	Cat# 89873	Thermo Fisher Scientific
Culture Tubes 14ml	Cat# AEX9.1	Carl Roth
Disposable cuvettes	Cat# 759015	Brand
DNA LoBind Tubes 1.5ml	Cat# 022431021	Eppendorf
DNA LoBind Tubes 2ml	Cat# 022431048	Eppendorf
Dynabeads Protein A	Cat# 10001D	Invitrogen
Falcon Tubes 15ml	Cat# 352196	Corning
Falcon Tubes 50ml	Cat# 352070	Corning
Filter Tips 10µl	Cat# 70.3010.355	Sarstedt
Filter Tips 200µl	Cat# 70.3031.355	Sarstedt
Filter Tips 1000µl	Cat# 70.3050.355	Sarstedt
Glass beads 1mm	Cat# 11079110	Biospec products
High Sensitivity DNA Chips	Cat# 5067-4626	Agilent
Immobilon®-P PVDF Membrane	Cat# IPVH00010	Sigma-Aldrich
Henke-Ject syringes 24ml	Cat# 4200-000V0	HenkeSassWolf
microTUBE AFA Fiber Pre-Slit Snap-Cap 6x16mm	Cat# 520045	Covaris
milliTUBE 1ml AFA Fiber	Cat# 520130	Covaris
Novex WedgeWell 4-20% Tris-Glycine Mini Gel	Cat# XP04205BOX	Invitrogen
Nunc Cryotube Vials	Cat# 347627	Thermo Fisher Scientific
NuPAGE 4-12%, Bis-Tris	Cat# NP0322PK2	Invitrogen
Parafilm	Cat# PM-996	Bemis Company
Petri Dishes	Cat# 633180	Greiner Bio-One
Pipettes 5ml	Cat# 606180	Greiner Bio-One
Pipettes 10ml	Cat# 607180	Greiner Bio-One
Pipettes 25ml	Cat# 760180	Greiner Bio-One
Pipette Tips 10µl	Cat# 70.3010.100	Sarstedt
Pipette Tips 200µl	Cat# 70.3030.100	Sarstedt
Pipette Tips 1000µl	Cat# 70.3050.100	Sarstedt
Polystyrene Round-Bottom Tubes 5ml	Cat# 352052	Corning
Protein LoBind Tubes 1.5ml	Cat# 0030108442	Eppendorf
Qubit Assay Tubes	Cat# Q32856	Invitrogen
Safe-Lock Tubes 1.5ml	Cat# 0030120.086	Eppendorf
Safe-Lock Tubes 2ml	Cat# 0030120.094	Eppendorf

Syringe filters Minisart® NY Sterile (EtO-sterilised), 0,45 µm	Cat# 1CL3.1	Carl Roth
Tubes and Domed Caps, strips of 8	Cat# AB0266	Thermo Fisher Scientific

6.1.10 Software and algorithms

Software and algorithms	Source
Adobe Illustrator	Adobe
Bowtie2 v2.4.5	Open source
FlowJo v10	BD Bioscience
GenomicAlignments v1.30.3	Open source
GenomicRanges v1.46.1	Open source
ImageJ	NIH
Microsoft Office	Microsoft
Proteome Discoverer v2.5	Thermo Fisher Scientific
R v4.1.2	Open source
Samtool v1.14	Open source
Skyline 22.2	Open source
Snakemake.minimal v5.2.4	Open source
Zoo package v1.8-10	Open source

6.2 Methods

6.2.1 Creation of plasmids and yeast strains

Unless noted otherwise, standard techniques were used for cloning of plasmids and transformation of yeast cells (Boeke et al., 1987; Gietz and Schiestl, 2007). Complete lists of oligonucleotides, plasmids and yeast strains can be found in the material section of this work. The respective cloning strategies can be found there as well.

6.2.1.1 Creation of chemical competent yeast cells

Yeast strains of interest were grown for at least two days on YPD plates at 30°C. One colony got inoculated into 25ml YPD medium. Cells were grown over night at 30°C with shaking speed around 200rpm. The 25ml culture was transferred into 75ml YPD medium. Cells were grown at 30°C until they reached an OD600 of ~0.5 - 0.8. Afterwards, cells were harvested by centrifugation at 3000g for 5min. Cells were washed with 50ml sterile H_2O before centrifuging again at 3000g for 5min. Cells were resuspended in 1ml of sterile H_2O, transferred to a suitable tube and pelleted at 3000g for 5min. The Supernatant was removed and the cell pellet resuspended in 1ml filter sterilized 4°C cold competent cell solution (5% v/v glycerol, 10% v/v DMSO). 50µl cells were dispensed into 1.5ml Eppendorf tubes. The tubes were placed into a box with Styrofoam and store the box in a -80°C freezer.

6.2.1.2 Yeast transformation

Competent cells of interest were thawed at 37°C by holding them in the hand for 15-30sec. Cells were centrifuged at 3000g for 2min to remove supernatant. In the meantime, the

transformation solution was made for the planned number of transformations plus a negative control. The transformation solution for one reaction consisted of: 260µl 50% (w/v) PEG4000, 36µl 1M LiAc, 10µl salmon sperm DNA (10mg/ml), 1-5µg linear DNA fragment for homologous recombination, and H_2O to a final volume of 360µl. The salmon sperm DNA had to be boiled for 5min at 95°C prior to addition. After the centrifugation, the supernatant was removed and the transformation solution including the DNA to be transformed was added to the cell pellet. After carefully pipetting up and down to mix, the mixture was incubated at 42°C for 15min. After centrifuging at 3000g for 30sec, the supernatant was removed and 100µl of sterile H_2O was added to the transformation tube to resuspend the pellet. This cell suspension was plated onto the respective growth plate with the required selection marker. The plates were incubated at 30°C for at least three days. Positive clones were then stored as glycerol stocks. To do so, respective clones were cultured in 3ml liquid YPD medium and grown to stationary phase. Afterwards, 0.5ml of the culture is mixed with 0.5ml 30% (v/v) glycerol in 1.5ml cryovials. Tubes were inverted a couple of times to mix and the stored at -80°C

6.2.1.3 Plasmid cloning

Plasmids in this work were cloned by using either a standard restriction digestion and ligation approach (Cohen et al., 1973) or by Gibson assembly (Gibson et al., 2009).

For the restriction digestion approach, backbone and insert DNA fragments were digested in a 30µl reaction, which included 1µg of the respective DNA fragments, 1µl of the needed respective restriction enzymes (provided by NEB), 3µl of the respective restriction enzyme buffer (provided by NEB) and H_2O to the final volume of 30µl. This reaction was incubated for 1h at the necessary temperature depending on the restriction enzyme. Afterwards, 1.5µl of Antarctic Phosphatase and 3.5 µl of the respective buffer was added to the sample containing the backbone DNA in order to prevent relegation later on. After another 1.5h at 37°C, both samples were purified using a PCR purification kit. To assess correct sizes of the created fragments, the samples are analyzed using an agarose gel. To further reduce background, instead of the PCR purification kit, the whole restriction sample can be loaded onto an 1% agarose gel with subsequent gel purification of the desired fragments. For the ligation reaction, at least 10ng of backbone was mixed with 5x more insert DNA. 1µl T4 DNA ligase was added together with 2µl of the respective T4 DNA ligase buffer. H_2O was added to a final volume of 20µl. After 1h at room temperature, 10µl of the reaction was transformed into chemical competent DH5 alpha *E.coli* cells.

In the Gibson assembly, 50-100ng of backbone DNA is mixed with ~5x more insert DNA. 10µl of the Gibson Assembly Master Mix from the kit is added, as well as H_2O to a final volume of 20µl. The sample is incubated for either 15min at 50°C when 2-3 fragments are being

assembled, or 60min at 50°C when 4-6 fragments are being assembled. Afterwards, 10μl of this reaction was transformed into chemical competent DH5 alpha *E.coli* cells.

6.2.1.4 Creation of chemical competent DH5alpha *E.coli* cells

50ml SOB medium was inoculated with DH5alpha *E.coli* from glycerol stocks. The culture was incubated at 37°C over night on a shaker with 180rpm. The next day, 200ml SOB medium was inoculated to OD_{600}=0.2 using the overnight culture. The culture was then incubated at 37° on a shaker with 180rpm until the OD_{600} reaches 0.5. The culture was then distributed to 4x50ml tubes and centrifuged at 4°C and 4000rpm for 10min. The supernatant was discarded and the pellets were resuspended in 15ml buffer TfbI (30mM Kac, 50mM $MnCl_2$, 100mM KCl, 15% glycerol, pH5.8 adjusted with 0.2M acetic acid, filtrated through a 0.22μm filter). After 20min incubation on ice, the suspension was centrifuged again at 4°C and 4000rpm for 10min. The supernatant was again discarded and the cell pellets were resuspended and combined in a total volume of 4ml buffer TfbII (10mM MOPS, 75mM $CaCl_2$, 10mM KCl, 15% glycerol, pH7adjusted with 10M NaOH, filtrated through a 0.22μm filter). After another 10-20min incubation on ice, 100μl aliquots of the competent cells were prepared.

6.2.1.5 *E.coli* transformation

Chemical competent DH5alpha cells were thawed in the palm of the hand for ~1min. The cells were then transferred to a 1.5ml Eppendorf tube. 10μl of the ligation reactions of the plasmid was added to the cells. To mix the samples, it was carefully pipetted up and down several times. The samples were stored on ice for 30min. Afterwards, the tubes were transferred to a heating block and left at 42°C for 60sec. Immediately, the samples were put back on ice afterwards, allowing them to cool down for 1-2min. 800μl LB medium was added to the samples, before putting them at 37°C for ~30min in a shaking heating block. After spinning cells down at 2000rpm for 1min, the LB medium was removed in a way so that only ~50-100μl was remaining. Cells were resuspended again and the whole sample was plated onto a LB agar plate containing the respective antibiotic.

6.2.2 Yeast cell culture for the site-specific recombination assay

Yeast cells competent for recombination were cultured in YPR medium at 30°C to an OD_{600} of 1.0. Cells were then simultaneously arrested in G1 phase by addition of alpha-factor (50ng/ml) and expression of R recombinase induced by addition of galactose to a final concentration of 2% (w/v). Cells were grown for an additional 2h at 30°C before harvesting by centrifugation for 10min at 7.000g at 4°C, yielding approximately 1.5g of yeast cells wet weight per liter of medium. Cells were resuspended with water, before being pelleted in sealed 25ml syringes by centrifugation for 10min at 7.000g at 4°C. The supernatant was decanted, the syringe unsealed and the cells were extruded into liquid nitrogen. The resulting cell "spaghetti" can be stored at -80°C until further usage.

6.2.3 Coupling of rabbit IgG antibodies to epoxy-activated magnetic beads

The IgG-coupled magnetic beads for the chromatin ring isolation through protein A affinity purification had to be prepared since they were not commercially available To generate this affinity resin a published protocol (Hamperl et al., 2014) was followed. In short, 300mg of BcMag epoxy-activated magnetic beads were suspended in 10ml 50% acetone in a 50ml falcon tube under vigorous shaking on a vortex mixer. The suspension was centrifuged at 820g for 2 min min and the supernatant was removed. The beads were washed three times with 0.1M sodium phosphate buffer pH7.4. The supernatant was removed after each washing by centrifuging at 820g for 2 min. Afterwards, the beads were suspended in 16ml 0.1M sodium phosphate buffer pH7.4 before gently rotating for 5min at room temperature. In the meantime, 100mg rabbit IgGs were dissolved in 7ml H_2O. The IgG suspension was clarified by centrifugation for 10min at 13000g at 4°C. 3.5ml of the supernatant is transferred to a new 50ml falcon tube, while the remaining 3.5ml could be frozen away and stored for future uses. The IgG solution is diluted with 9.85ml of 0.1M sodium phosphate buffer pH7.4, followed by dropwise addition of 6.65ml 3M ammonium sulfate in 0.1M sodium phosphate buffer pH7.4 under gentle mixing. The IgG solution was centrifuged for 3min at 820g and 4°C and the supernatant was added to the magnetic bead suspension. The tube was incubated over night for at least 18h at 30°C with gentle rotation. The supernatant was then removed by centrifuging at 820g for 2 min. The beads were washed with 20ml 100mM glycine-HCl pH2.5. The supernatant had to be removed quickly by centrifuging at 820g for 2 min to avoid denaturation of the IgG polypeptides. Afterwards, the beads were washed with 20ml 10mM Tris-HCl pH8.8. The supernatant was removed by centrifuging at 820g for 2 min. 20ml 0.1M triethylamine was added to the beads with gentle rotation for 5-10min to inactivate residual epoxy groups. The supernatant was removed by centrifuging at 820g for 2 min. The beads were washed four times with 20ml PBS pH7.4 for 5min with gentle rotation. The supernatant was removed after each washing by centrifuging at 820g for 2 min. The beads were washed twice with 20ml PBS pH7.4 with 0.5% Triton X-100 (w/v) for 5min and 15min each with gentle rotation. The supernatant was removed after each washing by centrifuging at 820g for 2 min. The beads were then resuspended in a final volume of 16ml PBS pH7.4 with 0.02% sodium azide (w/v) and stored as 1ml aliquots at 4°C until usage.

6.2.4 Affinity purification of chromatin domains

Both basic and TEV elution followed the same protocol until the washing steps. For that, a commercial coffee grinder was pre-cooled by grinding 30–50g of dry ice twice. The resulting powder of dry ice was discarded. 3g of frozen cells were mixed with ~90g of dry ice in the coffee mill. Grinding was repeated ten times for 30sec with 30sec breaks to prevent overheating of the coffee mill. Shaking of the coffee mill while grinding prevented the dry ice–cell powder from sticking to the inside wall of the grinding chamber. The fine powder of ground

yeast can be stored at −80°C. After evaporation of dry ice, the powder was dissolved in 0.75ml of cold buffer MB200 (20mM Tris–HCl (pH 8), 200mM KCl, 5mM MgAc, 0.5% Triton X-100, 0.1% Tween-20, 1mM DTT) or buffer MB150 (20mM Tris–HCl (pH 8), 150mM KCl, 5mM MgAc, 0.5% Triton X-100, 0.1% Tween-20, 1mM DTT), both supplied with 1× protease and phosphatase inhibitors (Protease and Phosphatase Inhibitor Cocktail 100x) and 1x histone deacetylase inhibitors (0.5µM Trichostatin A, 25µM Sirtinol), per 1g of ground yeast cells. The respective MB200 or MB150 buffer was then used throughout the complete purification. The cell lysate was cleared from cell debris by centrifugation with 16.000g for 30min at 4°C. The IgG coupled magnetic beads (see 6.2.3) were equilibrated with buffer MB with 1× protease and phophatase inhibitors (Protease and Phosphatase inhibitor Cocktail 100x) and 1x histone deacetylase inhibitors (0.5µM Trichostatin A, 25µM Sirtinol) before use. For the purification of the chromatin rings 333µl of magnetic bead slurry with coupled IgGs were added to the cell lysate. The cell lysate-bead suspension was incubated on a rotating wheel for 2h at 4°C.

6.2.4.1 Basic elution

After the 2h incubation, the beads were washed three times with 750µl of cold buffer MB with 1× Protease and Phophatase inhibitors (Protease and Phosphatase Inhibitor Cocktail 100x) and 1x histone deacetylase inhibitors (0.5µM Trichostatin A, 25µM Sirtinol). Between each washing step, the beads were gently rotated for 5min. Finally, the beads were washed twice with 750µl of cold buffer AC (100mM NH_4Ac pH 7.4 titrated with 2M NH_3, 0.1mM $MgCl_2$). Chromatin rings were eluted by adding 500µl 0.5M NH_4OH, thorough mixing and incubating at room temperature for 30min. This process was repeated once and both eluates were combined to a final volume of 1ml and frozen at -80 °C before submission to mass spectrometry.

6.2.4.2 TEV elution

After the 2h incubation, the beads were washed five times with 750µl of cold buffer MB with 1× Protease and Phophatase inhibitors (Protease and Phosphatase Inhibitor Cocktail 100x) and 1x histone deacetylase inhibitors (0.5µM Trichostatin A, 25µM Sirtinol). Between each washing step, the beads were gently rotated for 5min. An additional washing step with 750µl buffer MB was added last, for a total of six washing steps. After the washing, the beads were resuspended in 100µl buffer MB containing 10µg TEV-protease. This mixture was then incubated over night at 4°C under gentle rotation. Afterwards, the supernatant was transferred to a new Eppendorf tube and residual chromatin rings are washed from the beads once with another 100µl buffer MB. The two elution samples were then combined to a total volume of 200µl. At this point, samples could either be submitted to mass spectrometry, or a second affinity purification step using the CBP moiety of the LexA protein could be performed.

6.2.4.3 Calmodulin affinity purification

For a consecutive calmodulin affinity purification, the samples after the TEV elution were adjusted to a total volume of 400µl with buffer MB and supplemented with 0.1M $CaCl_2$ to a final concentration of 2mM. This sample was then applied to 100µl calmodulin sepharose beads that had been equilibrated by washing two times with 1ml buffer MB containing 2mM $CaCl_2$ and a subsequent incubation step with this buffer for 2h at 4°C under gentle rotation. The sample bead suspension was then incubated for 1h on a rotating wheel to allow binding of the LexA protein to the affinity matrix. The sample is centrifuged for 2min and 2000rpm and the supernatant was collected as flowthrough sample. The beads were then washed four times with buffer CWB (20mM Tris-HCl pH8, 300mM KCl, 5mM MgAc, 2mM $CaCl_2$, 1mM DTT, 0.5% Triton X-100, 0.1% Tween-20). Removal of supernatant was always performed with a centrifugation step at 2000rpm for 2min. After the washing, the chromatin rings were then eluted by the addition of 200µl buffer CEB (20mM Tris-HCl, 200mM KCl, 1mM EDTA, 10mM EGTA, 1mM DTT, 0.5% Triton X-100, 0.1% Tween-20). After incubation for 20min at 4°C on a rotating wheel, the supernatant is collected and the elution step was repeated another time with 200µl buffer CEB. The two elution samples were then combined to a final volume of 400µl.

6.2.5 DNA analysis of the purification fractions

H_2O was added to the DNA samples taken during the purification process to a final volume of 100µl. 1ng of plasmid K71 was also added to every sample as a spike-in to normalize for different DNA extraction efficiencies. 100µl of IRN buffer (50mM Tris-HCl pH8, 20mM EDTA, 0.5M NaCl) was added together with 1µl of RNAse A (10mg/ml), followed by a 1h incubation step at 37°C. Subsequently, 200µl of a Phenol:Chloroform:Isoamyl Alcohol (25:24:1, v/v) was added, followed by 2 x 10sec thorough vortexing. The solution was centrifuged for 5min at 16.000g. The supernatant was transferred to a fresh 1.5ml tube containing 600µl of ethanol and 1.5µl glycogen (10mg/ml). The tube was left at -20°C overnight. Next, the solution was centrifuged with 16.000g at 4°C for 30min. The supernatant was discarded and 150µl of 70% ethanol was added to the pellet. After another centrifugation step with 16.000g at 4°C for 10min, the supernatant was discarded and the DNA pellet dried at room temperature for 10min. The dried pellet was then resuspended in 50µl H_2O. For further analysis, a restriction digestion was performed to analyze the DNA samples in subsequent qPCR reactions. The restriction enzymes used for linearizing the circular DNA were HpaI (ARS305+/-3), BbsI (ARS313+/-3), NcoI (ARS315+/-3) and HpaI (ARS316+/-3). qPCR analysis was performed using the following primer pairs: ARS305: 0463/0466; ARS313: 0552/0553; ARS315: 0970/0971; ARS316: 0837/0838. Primers 0137 and 0138 are used to detect the K71 spike-in and primers 0301 and 0302 were used to detect the unrelated genomic PDC1 locus.

6.2.6 Filter aided sample preparation (FASP) digest of protein samples for mass spectrometry

The eluates from the purified samples were dried using a speed vac vacuum concentrator and resolved in 300µl 50mM ammonium bicarbonate (ABC) and digested using a modified FASP procedure (Grosche et al., 2016; Wiśniewski et al., 2009). After protein reduction and alkylation using DTT and IAA according to these protocols, the proteins were centrifuged on a 30kDa cutoff filter device, washed thrice with UA buffer (8M urea in 0.1M Tris/HCl pH 8.5) and twice with 50mM ABC. The proteins were digested for 2h at room temperature using 0.5µg Lys-C and for 16h at 37°C using 1µg trypsin. After centrifugation for 10min at 14.000 g the eluted peptides were acidified with 0.5% TFA and stored at -20°C.

6.2.7 LC-MS/MS measurements and quantitative data analysis using Progenesis QI for proteomics

LC-MS/MS analysis was performed on a Q-Exactive HF and HF-X mass spectrometer online coupled to an Ultimate 3000 nano-RSLC. Tryptic peptides were automatically loaded on a C18 trap column (300 µm inner diameter (ID) × 5 mm, Acclaim PepMap100 C18, 5 µm, 100 Å, LC Packings) at 30µl/min flow rate prior to C18 reversed phase chromatography on the analytical column (nanoEase MZ HSS T3 Column, 100Å, 1.8µm, 75µm x 250mm, Waters) at 250nl/min flow rate in a 95 minutes non-linear acetonitrile gradient from 3 to 40% in 0.1% formic acid. Profile precursor spectra from 300 to 1500 m/z were recorded at 60000 resolution with an automatic gain control (AGC) target of 3e6 and a maximum injection time of 30ms and 50ms. TOP10 and TOP15 fragment spectra of charges 2 to 7 were recorded at 15000 resolution with an AGC target of 1e5, a maximum injection time of 50ms, an isolation window of 1.6 m/z, a normalized collision energy of 28 and a dynamic exclusion of 30 seconds.

6.2.8 Protein Identification and label-free quantification

Proteome Discoverer 2.5 software (version 2.5.0.400) was used for peptide and protein identification via a database search (Sequest HT search engine) against Swissprot yeast data base (Release 2017_04, 6721 sequences), considering full tryptic specificity, allowing for up to two missed tryptic cleavage sites, precursor mass tolerance 10 ppm, fragment mass tolerance 0.02Da. Carbamidomethylation of Cys was set as a static modification. Dynamic modifications included deamidation of Asn, Gln and Arg, oxidation of Pro and Met; and a combination of Met loss with acetylation on protein N-terminus. Percolator was used for validating peptide spectrum matches and peptides, accepting only the top-scoring hit for each spectrum, and satisfying the cutoff values for FDR <5%, and posterior error probability <0.01. The final list of proteins complied with the strict parsimony principle. The quantification of proteins was based on abundance values for unique peptides. Abundance values were normalized on total peptide amount to account for sample loading errors. The protein abundances were calculated summing up the abundance values for admissible peptides. The

final protein ratio was calculated using median abundance values of three replicate analyses each. The statistical significance of the ratio change was ascertained employing the T-test approach described in (Navarro et al., 2014) which is based on the presumption that we look for expression changes for proteins that are just a few in comparison to the number of total proteins being quantified. The quantification variability of the non-changing "background" proteins can be used to infer which proteins change their expression in a statistically significant manner.

6.2.9 Histone PTM analysis

Bulk histones from asynchronous and G1-arrested cells were extracted from a 50ml yeast culture in YPR at OD_{600} of 0.8. Cells were harvested by centrifugation for 5min at 4°C at 3000g. The pellets were washed twice with water, followed by two washing steps with buffer 1 (1M sorbitol, 50mM Tris-HCl pH7.5, 5mM $MgCl_2$). The supernatant was then discarded and the pellets snapfrozen in liquid nitrogen. Cells were washed three times in 0.9mL cold buffer A (15mM Tris-HCl pH 7.4, 80mM KCl, 2mM EDTA pH 8, 2mM EGTA pH 8, 0.5mM spermidine, 0.2mM spermine, 0.5µM Trichostatin A, 25µM Sirtinol, 1× Protease and Phophatase inhibitors (Protease and Phosphatase Inhibitor Cocktail 100x). After each wash, cells were pelleted for 2min with 16.000g at 4°C, and the supernatant was discarded. Cells were resuspended in 350µl buffer A before addition of 500µl glass beads (1mm) until the cell suspension was completely immersed in the beads. Cell lysis was then performed using a VXR basic IKA Vibrax orbital shaker at 2200rpm for 10min at 4°C. To remove the glass beads and collect the cell lysate, the microtubes were inverted and the tube tips pierced with a hot syringe needle. The tubes were placed with the tip to the bottom in a 15 mL falcon tube which was then centrifuged for 2min at 4°C with 130g to recover the cell lysate. Subsequently, the lysate was transferred to a new 1.5ml tube where crude nuclei are pelleted for 1min at 4°C with 16.000g. The supernatant was removed and the pellet was washed once with 900µl cold buffer A before pelleting again for 1min at 4°C with 16.000g. After removing the supernatant, the crude nuclei were snapfrozen in liquid nitrogen and stored at -80°C until further use. For bulk histone extraction, nuclei were resuspended in 5x nuclei pellet volumes of ice-cold 0.2M sulfuric acid and mixed on a rotation wheel overnight at 4°C. Insolubilized nuclear debris was pelleted by centrifugation for 10min at 4°C at 16000g. The supernatant was transferred to a fresh low-protein binding Eppendorf tube and histone proteins were precipitated by adding ice-cold trichloroacetic acid (TCA) to the final concentration of 20% (v/v) followed by 120 min incubation on ice. Precipitated histone proteins were pelleted by centrifugation for 10min at 4°C at 16000g, washed 3 times with ice cold acetone (-20°C) and resuspended in MS grade water. Extracted histones were prepared for LC-MS/MS analysis using hybrid chemical derivatization method as described previously (Maile et al., 2015). In brief, 4µg aliquots of purified histones were diluted with MS grade water to a total volume of 18µl and buffered to pH 8.5 by addition

of 2µl of 1M triethylammonium bicarbonate buffer (TEAB). Propionic anhydride was mixed with MS grade water in a ratio of 1:100 and 2µl of the anhydride-mixture was added immediately to the histone sample while vortexing and the resulting mixture was incubated for 5min at room temperature. The reaction was quenched by adding 2µl of 80 mm hydroxylamine followed by 20min incubation at room temperature. Tryptic digestion was performed overnight with 0.5µg trypsin per sample at 37°C. A 1% v/v solution of phenyl isocyanate (PIC) in acetonitrile was freshly prepared and 6µl added to each sample and incubated for 60min at 37°C. Samples were acidified by adding trifluoroacetic acid (TFA) to the final concentration of 1%. Peptides were de-salted with C18 spin columns following the manufacture protocol. Peptides were eluted from C18 spin columns with 70% acetonitrile, partially dried in a speedvac, resuspended in 30µl 0.1% TFA and subsequently used for LC-MS analysis.

For the histone PTM analysis of the origin chromatin domains, the affinity purification was performed as described above with minor modifications. Instead of 3g wet weight of yeast cells, 6g of cells were used and the IP was performed with 400µl of magnetic bead slurry with coupled IgGs. After the washing step with buffer AC, the supernatant was discarded and the beads were directly snapfrozen in liquid nitrogen. Histones were then directly extracted from the beads by boiling them at 95°C for 5 min in 40µl 1X Laemmli buffer. Eluted proteins were then resolved on 4-20% polyacrylamide gels (WedgeWell™ Tris-Glycin-Minigel) followed by Coomassie staining. Histone protein bands were excised from the gel, destained in a destaining buffer (100mM triethylammonium bicarbonate in 50% acetonitrile), and prepared for LC-MS analysis using the hybrid derivatization method (Maile et al., 2015) adopted for in-gel digestion. Specifically, after destaining, the gel pieces were dehydrated with 200µL of 100% acetonitrile for 10min at RT after which acetonitrile was discarded. A propionylation solution was prepared by mixing 50mM triethylammonium bicarbonate buffer pH8.5 (TEAB) and freshly prepared 1% (v/v) propionic anhydride solution in water at a 100:1 ratio. Immediately after preparation, 100µl of propionylation solution was added to the dehydrated gel pieces followed by 10min incubation at RT. The propionylation reaction was quenched by the addition of 10µl of 80mM hydroxylamine and subsequent incubation for 20 min. at RT. The propionylation solution was discarded and gel pieces were dehydrated with 200µL of 100% acetonitrile for 10min at RT. Afterwards, the acetonitrile solution was discarded and 20µl of 50ng/µl trypsin solution in 100mM TEAB was added. Trypsin digestion was performed overnight at 37°C. The next day, 50µL of 100mM TEAB solution was added to each sample followed by 30min incubation in a thermo shaker at 37°C and 1500rpm rotation. A 1% (v/v) solution of phenyl isocyanate (PIC) in acetonitrile was freshly prepared and 15µl added to each sample and incubated for 60min at 37°C. Samples were acidified by the addition of 24µl 1% trifluoroacetic acid. Peptides were desalted with C18 spin columns following the manufacturer's instructions,

dried in a speed-vac, resuspended in 50µl 0.1% trifluoroacetic acid and subsequently used for LC-MS analysis.

The resulting peptide mixtures were analyzed using nano-flow liquid chromatography tandem mass spectrometry (LC-MS/MS) on a Q-Exactive HF mass spectrometer coupled to an Ultimate 3000 nano- UPLC (Ultimate 3000, Dionex, Sunnyvale, CA) in data-dependent acquisition (DDA) mode. ~300ng peptide aliquot was used per one sample per one injection. Peptides were loaded automatically on a trap column (300µm inner diameter ×5 mm, Acclaim PepMap100 C18, 5µm, 100Å; LC Packings, Sunnyvale, USA) prior to C18 reversed phase chromatography on the analytical column (nanoEase MZ HSS T3 Column, 100 Å, 1.8µm, 75µm × 250mm; Waters, Milford, USA). Peptides were separated at flowrate of 0.250µl per minute by a linear gradient from 1% buffer B (0.1% (v/v) formic acid, 98% (v/v) acetonitrile) to 25% buffer B over 40min followed by a linear gradient to 40% B in 20min, then to 85% B in 5min. After 5 min at 85% buffer B, the gradient was reduced to 1% buffer B over 2min and then allowed to equilibrate for 8min. Full mass range spectra were at 60,000 resolution (at m/z 400), and product ions spectra were collected in a "top 15" data dependent scan cycle at 15.000 resolution. RAW MS data were analyzed using an open-source Skyline software. The mass spectrometry proteomics data have been deposited to the ProteomeXchange Consortium via the PRIDE (Perez-Riverol et al., 2022) partner repository with the dataset identifier PXD031984.

6.2.10 Replication timing measurement by qPCR

A 50ml yeast culture in YPD was grown to OD_{600} of 0.6 and then arrested in G1 phase by addition of alpha-factor (50ng/ml) for 2h. As indicated, cells were treated with auxin at a concentration of 1mM for 30min at 30°C to degrade AID-tagged ASK1 or with nocodazole at a concentration of 15µg/ml together with 1%DMSO for 2h at 30°C to destabilize microtubules. To release the cells from the arrest, 125U of Pronase and potassium phosphate buffer pH7 to a final concentration of 20mM was added. If necessary, 200mM HU was added in the release to induce S phase checkpoint activation. Samples for genomic DNA extraction were taken before the release and every 8min after releasing the cells from the arrest by adding 4.5ml of the culture to 500µl of 1% sodium azide solution (w/v) in 0.2M EDTA. The cells were washed once with water (4.000g, 3min at 4°C) and the resulting yeast pellets were snapfrozen in liquid nitrogen.

For DNA extraction, the cell pellets were resuspended in 500µl buffer RINB (50mM Tris-HCl pH8, 0.1M EDTA, 0.1% (v/v) β-Mercaptoethanol). Zymolyase was added to a final concentration of 2% (w/v). After incubating for 1h at 37°C, the solution was supplemented with 1% SDS (w/v), 0.2M NaCl, 0.1mg/ml RNAse A, and 0.2 mg/ml proteinase K. After incubation for 1h at 55°C, DNA was isolated by a phenol extraction. For that an equal amount of

Phenol:Chloroform:Isoamyl Alcohol (25:24:1, v/v) was added. After vortexing thoroughly, the mixture was centrifuged for 5min at full speed. The supernatant was taken and supplemented with potassium acetate to a final concentration of 0.1M, as well as 0.6 volumes of isopropanol. After vortexing thoroughly, the mixture was left at -20°C over night. After centrifuging for 20min at 4°C and full speed, the supernatant was removed and the pellet was washed once with 70% ethanol. After drying for 5-10 min at room temperature, the DNA pellets were suspended in 50µl of H_2O. 5 – 10µg of DNA was then digested with EcoRI. The reactions were diluted 1:10 in H_2O and analyzed by quantitative PCR using primers 0463/0466 (ARS305), 0552/0553 (ARS313), 0970/0971 (ARS315), 0837/0838 (ARS316), and 0834/0835 (ChrVI).

6.2.11 DNA copy number sequencing

The DNA samples from the replication timing experiments were treated an additional time with 0.2 mg/ml RNAse A for 1h at 37°C. A DNA cleanup step was performed using the GeneJET PCR purification Kit. The DNA was eluted in 130µl H_2O. The whole DNA was added to Covaris sonication tubes (microTUBE AFA Fiber Pre-Slit Snap-Cap 6x16mm) for 3min with the following settings: Cycles/burst: 200, intensity: 4, Duty cycle: 10%. The integrity of the DNA was determined by running the sample on the Bioanalyzer according the manufacturer's protocol. Afterwards 50µl of the solution was used for the library prep using the NEBNext ultra II DNA library prep kit following the manufacturer's protocol. Again, after the preparation, the sample was run on a Bioanalyzer to check for the integrity and concentration of the sample. To remove remaining adapter primers, two subsequent cleanup steps were performed using AMPure SPRI beads. Since for the sequencing in this case all the samples had to be pooled to a 5nM concentration in 25µl, the cleanup was performed for all equimolar pooled samples in a concentration of 15nM to account for losses during the cleanup. Beads were added in a 1:1 ratio to the pooled libraries. After a 5min incubation step, the supernatant was removed using a magnetic rack. After two washing steps with 80% EtOH for 30sec, the beads were dried at room temperature for approximately 2min. The DNA was then eluted from the beads using 60µl H_2O after the first washing step and 29µl H_2O after the second washing step. To make sure that there were no adapters left, the sample was a final time run on a Bioanalyzer.

6.2.12 Bioinformatic analysis of the DNA copy number sequencing

Paired-end sequencing reads were mapped to the reference genome (Saccharomyces cerevisiae R64-1-1.dna.toplevel.fa) using bowtie2 (version 2.4.5) with the parameters --end-to-end --very-sensitive --no-unal --no-mixed -- no-discordant -I 10 -X 1000. Aligned reads were filtered for mapping quality using samtools (version 1.14) with the parameter -q 12. Read pairs were counted in 500 bp or 1000 bp consecutive genomic windows using R/Bioconductor packages (R version 4.1.2, GenomicAlignments version 1.30.0 and GenomicRanges version 1.46.1). Reads mapped to the mitochondrial genome were excluded from the analysis. Read counts were normalized by the total number of mapped reads and were converted to bedgraph

files upon smoothing by the rollmean function (zoo package, version 1.8-10). The log2 ratio between 60 min or 24 min and G1 samples was calculated for each replicate in each condition (i.e. genotype or treatment), respectively. The lowest 5th percentile of the data was filtered out prior log2 transformation. Replicate datapoints were visualized as dot plots, whereas the average of the replicates is shown as a further smoothed curve along the chromosome with a bin size of 500 or 1000bp as indicated. The replicate 'Y19_24_1' was removed as outlier. Differential regions were obtained using Welch two sample t-test (unequal variances) in each genomic bin with a p-value cutoff of 0.05 and a mean difference of at least 0.1. Plots were generated using R base graphics. All analysis steps were carried out in a reproducible pipeline using snakemake (version snakemake-minimal 5.2.4) and are available upon request.

6.2.13 Data availability

DNA copy number sequencing data are available on GEO with the accession number GSE212974. Reviewers token: mxunkwauljcbnwv. The mass spectrometry proteomics data have been deposited to the ProteomeXchange Consortium (http://proteomecentral.proteomexchange.org) via the PRIDE partner repository with the dataset identifier PXD031984.

6.2.14 Chromatin Immunoprecipitation (ChIP)

100ml yeast culture was grown to OD_{600} of 0.6 and then arrested at G1 phase by addition of alpha-factor (50ng/ml) for 2h. 45ml of the culture were transferred to a 50ml falcon tube. For crosslinking, formaldehyde was added to a final concentration of 1%. After 15min shaking at 30°C, the reaction was quenched by the addition of glycine to a final concentration of 128mM. After 5min more shaking at 30°C, cells were pelleted by centrifugation at 3.000g for 2min at 4°C. The cells were washed once with 45ml cold PBS. After pelleting again, cells were resuspended in 1ml cold PBS and then transferred into a 1.5ml cup. After another centrifugation step at 16.000g for 1min at 4°C, the supernatant was discarded and the remaining yeast pellet was frozen in liquid nitrogen for storage at -20°C.

The pellets were washed with 500µl Lysis buffer (50mM Hepes pH 7.5, 140mM NaCl, 5mM EDTA pH8, 5mM EGTA pH8, 1% Triton-X100 (w/v), 0.1% DOC (w/v), 1× protease and phosphatase inhibitors (Protease and Phosphatase Inhibitor Cocktail 100x) and then resuspended with 500µl Lysis buffer. Precooled glass beads (1mm) were added to cover the whole suspension. Cells were disrupted on a VXR basic IKA Vibrax orbital shaker at 2200rpm for three times 15min at 4°C with 10min breaks on ice in between. To remove the beads from the lysate, the bottom of the 1.5ml tube was pierced using a hot needle and placed into a 15ml falcon tube. After centrifugation (130g, 2min at 4°C), the beads remained in the 1.5ml tube and the lysate could be collected in the 15ml tube. The volume of the suspension was increased to 1ml with Lysis buffer and transferred to a 1ml Covaris sonication glass tube. Sonification was

performed on a Covaris instrument (25min, Peak Incident Power: 140W, Duty Factor: 5%, Cycles/Burst: 200). Afterwards, the sheared chromatin was cleared by centrifugation (20min, 16.000g at 4°C). The supernatant was then transferred to a low-binding 1.5ml tube. The resulting chromatin extract was split into two aliquots. A total of 140µl served as an input control, and 700µl was diluted with 290µl Lysis buffer and incubated for 120min at 4°C with 40µl of Lysis buffer pre-equilibrated Protein A bead slurry and 10µg of the indicated antibodies.

After immunoprecipitation, the beads were washed three times with lysis buffer, twice with washing buffer I (50mM HEPES pH7.5, 500mM NaCl, 2mM EDTA, 1% [vol/vol] Triton X-100, 0.1% [wt/vol] DOC), and twice with washing buffer II (10mM Tris-HCl pH8.0, 250mM LiCl, 2mM EDTA, 0.5% [vol/vol] Nonidet P-40, 0.5% [w/v] DOC), followed by a final washing step with TE buffer (10mM Tri-HCl pH 8.0, 1mM EDTA). A total of 390µl of buffer IRN (50mM Tris-

After immunoprecipitation, the beads were washed three times with lysis buffer, twice with washing buffer I (50mM HEPES pH7.5, 500mM NaCl, 2mM EDTA, 1% [vol/vol] Triton X-100, 0.1% [wt/vol] DOC), and twice with washing buffer II (10mM Tris-HCl pH8.0, 250mM LiCl, Tris-HCl pH8.0, 20mM EDTA, 500mM NaCl) or 250µl was added to the immunoprecipitation (IP) beads and to the input samples, respectively. DNA was isolated by incubation with 10µl RNAse A (10µg/µl) at 37°C. SDS was added to a final concentration of 0.5% together with 10µl Proteinase K (10µg/µl). After incubation for 1h at 56°C, Input and IP samples were decrosslinked at 65°C overnight. DNA was then isolated by phenol-chloroform extraction followed by ethanol precipitation. Both input and IP DNA pellets were suspended in 50µl H_2O and analyzed by quantitative PCR using indicated primers.

6.2.15 Western blot analysis

For western blot detection of specific proteins from yeast strains, 2.5 OD_{600} units (1 OD_{600} unit = 1ml of a yeast culture with OD_{600} = 1) of yeast cells were harvested by centrifugation for 5min at 3000g at room temperature. Cells were resuspended in 200µl 0.1M NaOH followed by incubation at room temperature for 5min. Whole cell extracts were pelleted for 5min with 3000g at room temperature and the pellet was resuspended in 50µl sample buffer (1x NuPAGE LDS sample buffer, 5% $β$-Mercaptoethanol). After boiling the samples for 3min at 95°C, samples were either stored at -20°C or directly used for SDS-PAGE.

If samples from the chromatin ring affinity purifications were analyzed, H_2O was added to the samples to a volume of 10µl. Afterwards 10µl 2x sample buffer (2x NuPAGE LDS sample buffer, 10% $β$-Mercaptoethanol) was added. After boiling the samples for 3min at 95°C, samples were either stored at -20°C or directly used for SDS-PAGE.

A precast gel (NuPAGE 4-12%, Bis-Tris) was used for the run in 1x NuPAGE MES running buffer. 10µl of the samples were applied on the gel which was then run at 120V for ~90min

until the front reached the end of the gel. In the meantime, 2 Whatman paper and a polyvinylidene difluoride membrane (Immobilon®-P PVDF Membrane) were cut to the size of the gel. The whatman papers were soaked in 1x western transfer buffer and the membrane for 1min in methanol. Afterwards, the "transfer-sandwich" was assembled in a cassette within a tray containing 1x western transfer buffer in the following order: Sponge - Whatman paper – SDS gel – Membrane – Whatman paper – Sponge. The cassette was closed and then placed into the transfer tank filled with 1x western transfer buffer considering the right orientation. The transfer was the performed at 300mA for 3h in the cold room. After the transfer, the membrane is transferred to a suitable container and then blocked with 5% milk powder, 0.05% Tween-20 in PBS-T for 30min at room temperature under gentle shaking. Afterwards, the membrane is washed twice with PBS-T at room temperature. The first antibody was then applied for either 2h at room temperature or over night at 4°C, always under gentle shaking. All antibodies were diluted in 3%BSA in PBS-T. The respective dilutions can be found in 6.1.6. After the first antibody step, the membrane was washed three times in PBS-T for each 5min at room temperature under gentle shaking. Then the second antibody was applied, followed by an 45min incubation steep at room temperature under gentle shaking. After another three washes in PBS-T for each 5min at room temperature under gentle shaking, the chemoluminescent detection of the proteins was performed with the SuperSignal West Pico Plus Kit.

6.2.16 Southern blot analysis

2-15µg digested genomic DNA was resolved on an 1% agarose gel. TBE was used as running buffer. The blotting was performed by a capillary transfer. First the gel was transferred to a suitable tray and soaked in depurination solution (0.2M HCl) for 20min at room temperature. Afterwards, the gel was rinsed once with H_2O, before adding denaturing solution (0.5M NaOH, 1.5M NaCl) to cover the gel. The gel was washed twice with this solution for each 15min on a shaker. Then the gel was again rinsed with H_2O. Another two washing steps were performed with transfer buffer (1M NH_4OAc) for each 15min. In the meantime, a strip of nylon membrane (Amersham Hybond™-N) was cut to the size of the gel, as well as two Whatman paper longer as the gel. The nylon membrane was soaked in H_2O and the Whatman papers in transfer buffer (1M NH_4OAc). Another two Whatman paper as well as paper towels were cut the same size of the gel. A stable platform was placed onto a tray containing ~1.5l of transfer buffer (1M NH_4OAc). The long Whatman papers soaked with transfer buffer (1M NH_4OAc) were placed on the platform, ensuring no air bubbles are trapped. It was made sure that the edge of the Whatman papers is in contact with the buffer in the tray. The gel was placed face down onto the Whatman papers. Again, it was ensured that no air bubbles are trapped. The two gel-sized Whatman papers were placed on top of the gel. The stack of paper towels was then placed on top of the Whatman papers. A light weight of ~0.5kg was placed on top of the paper towels. This assembly was left over night (at least 12h). After the transfer was completed, the

membrane was placed in a UV crosslinker on automatic setting. Radioactive probes were created using the RadPrime DNA labeling system with incorporation of [α−32P]dATP according to the instructions of the manufacturer. For the hybridization, the blot was transferred into a hybridization tube. The membranes were rinsed with 10-15ml 2x SSC buffer and the prehybridized for 1h at 65°C in hybridization buffer (0.5M sodium phosphate pH 7.2, 7% SDS). Afterwards, the buffer for prehybridization was discarded and new 15ml of prewarmed hybridization buffer was added. Salmon sperm DNA was boiled at 95°C for 5min and then added to the radioactive labelled probe to a final concentration of 100µg/ml. This mixture is then added to the blot. Hybridization took place over night at 65°C with gentle rotation in a hybridization oven. After the hybridization, the probe was transferred to a 50ml falcon for storage. The blot was then rinsed with 30ml 3x SSC, 0.1% SDS at 65°C. Afterwards, the blot was washed with different washing buffers, Wash1 (0.3x SSC, 0.1% SDS), Wash2 (0.1xSSC, 0.1%SDS), and Wash3 (0.1xSSC, 1.5% SDS). Each wash step was repeated twice for 15min at 65°C. Afterwards, the blot was dried and stored at room temperature. The blot was then put in an appropriate cassette and exposed to a screen. After several days of exposure, images were aquired using the FLA 7000 imaging system.

6.2.17 Flow cytometry

500µl samples were taken from yeast cultures (~OD600 of 0.6). The cells were centrifuged at 3.000g for 2min at RT. The supernatant was discarded and 1ml 70% Ethanol was added to the pellet. After thorough vortexing, the fixed cell suspensions can be stored at 4°C until further use. 500µl of the suspensions were transferred to a fresh tube and then centrifuged (3.000g, 2min RT). The supernatant was discarded and the pellet dissolved in 300µl 50mM sodium citrate and 0.1mg/ml RNAse A. After 2h incubation at 50°C, proteinase K was added to a final concentration of 0.1mg/ml, followed by another 2h incubation at 50°C. 30µl of this sample was then mixed with 170µl 50mM sodium citrate and 0.5µM Sytox Green (S7020, Thermo Fisher Scientific). Prior to the FACS analysis, the samples were briefly sonicated (Bioruptor, 5x15sec) to detach cell clumps before proceeding with the analysis.

6.2.18 Spot tests

Sensitivity of temperature-sensitive yeast strains to hydroxyurea (HU) was determined by spotting serial dilutions of exponentially growing yeast cultures on YPD plates with or without 10mM hydroxyurea and incubation at the indicated temperatures.

7   References

Anderson, J.D., Widom, J., 2001. Poly(dA-dT) promoter elements increase the equilibrium accessibility of nucleosomal DNA target sites. Mol. Cell. Biol. 21, 3830–3839. https://doi.org/10.1128/MCB.21.11.3830-3839.2001

Aparicio, J.G., Viggiani, C.J., Gibson, D.G., Aparicio, O.M., 2004. The Rpd3-Sin3 histone deacetylase regulates replication timing and enables intra-S origin control in Saccharomyces cerevisiae. Mol. Cell. Biol. 24, 4769–4780. https://doi.org/10.1128/MCB.24.11.4769-4780.2004

Aparicio, O.M., Billington, B.L., Gottschling, D.E., 1991. Modifiers of position effect are shared between telomeric and silent mating-type loci in S. cerevisiae. Cell 66, 1279–1287. https://doi.org/10.1016/0092-8674(91)90049-5

Azmi, I.F., Watanabe, S., Maloney, M.F., Kang, S., Belsky, J.A., MacAlpine, D.M., Peterson, C.L., Bell, S.P., 2017. Nucleosomes influence multiple steps during replication initiation. eLife 6, e22512. https://doi.org/10.7554/eLife.22512

Batrakou, D., Heron, E., Nieduszynski, C., 2018. Rapid high-resolution measurement of DNA replication timing by droplet digital PCR. Nucleic Acids Res. 46. https://doi.org/10.1093/nar/gky590

Beinoravičiūtė-Kellner, R., Lipps, G., Krauss, G., 2005. In vitro selection of DNA binding sites for ABF1 protein from Saccharomyces cerevisiae. FEBS Lett. 579, 4535–4540. https://doi.org/10.1016/j.febslet.2005.07.009

Belsky, J.A., MacAlpine, H.K., Lubelsky, Y., Hartemink, A.J., MacAlpine, D.M., 2015. Genome-wide chromatin footprinting reveals changes in replication origin architecture induced by pre-RC assembly. Genes Dev. 29, 212. https://doi.org/10.1101/gad.247924.114

Berbenetz, N.M., Nislow, C., Brown, G.W., 2010. Diversity of eukaryotic DNA replication origins revealed by genome-wide analysis of chromatin structure. PLoS Genet. 6, e1001092. https://doi.org/10.1371/journal.pgen.1001092

Bernstein, B.E., Liu, C.L., Humphrey, E.L., Perlstein, E.O., Schreiber, S.L., 2004. Global nucleosome occupancy in yeast. Genome Biol. 5, R62. https://doi.org/10.1186/gb-2004-5-9-r62

Boeke, J.D., Trueheart, J., Natsoulis, G., Fink, G.R., 1987. 5-Fluoroorotic acid as a selective agent in yeast molecular genetics. Methods Enzymol. 154, 164–175. https://doi.org/10.1016/0076-6879(87)54076-9

Breier, A.M., Chatterji, S., Cozzarelli, N.R., 2004. Prediction of Saccharomyces cerevisiae replication origins. Genome Biol. 5, R22. https://doi.org/10.1186/gb-2004-5-4-r22

Brewer, B.J., Fangman, W.L., 1988. A replication fork barrier at the 3' end of yeast ribosomal RNA genes. Cell 55, 637–643. https://doi.org/10.1016/0092-8674(88)90222-x

Broach, J.R., Li, Y.-Y., Feldman, J., Jayaram, M., Abraham, J., Nasmyth, K.A., Hicks, J.B., 1983. Localization and Sequence Analysis of Yeast Origins of DNA Replication. Cold Spring Harb. Symp. Quant. Biol. 47, 1165–1173. https://doi.org/10.1101/SQB.1983.047.01.132

Byrum, S.D., Raman, A., Taverna, S.D., Tackett, A.J., 2012. ChAP-MS: a method for identification of proteins and histone posttranslational modifications at a single genomic locus. Cell Rep. 2, 198–205. https://doi.org/10.1016/j.celrep.2012.06.019

Byrum, S.D., Taverna, S.D., Tackett, A.J., 2013. Purification of a specific native genomic locus for proteomic analysis. Nucleic Acids Res. 41, e195. https://doi.org/10.1093/nar/gkt822

Cayrou, C., Ballester, B., Peiffer, I., Fenouil, R., Coulombe, P., Andrau, J.-C., Helden, J. van, Méchali, M., 2015. The chromatin environment shapes DNA replication origin organization and defines origin classes. Genome Res. 25, 1873–1885. https://doi.org/10.1101/gr.192799.115

Celniker, S.E., Sweder, K., Srienc, F., Bailey, J.E., Campbell, J.L., 1984. Deletion mutations affecting autonomously replicating sequence ARS1 of Saccharomyces cerevisiae. Mol. Cell. Biol. 4, 2455–2466. https://doi.org/10.1128/mcb.4.11.2455-2466.1984

Chacin, E., Reusswig, K.-U., Furtmeier, J., Bansal, P., Karl, L.A., Pfander, B., Straub, T., Korber, P., Kurat, C.F., 2023. Establishment and function of chromatin organization at replication origins. Nature 616, 836–842. https://doi.org/10.1038/s41586-023-05926-8

Chang, F., May, C.D., Hoggard, T., Miller, J., Fox, C.A., Weinreich, M., 2011. High-resolution analysis of four efficient yeast replication origins reveals new insights into the ORC and putative MCM binding elements. Nucleic Acids Res. 39, 6523–6535. https://doi.org/10.1093/nar/gkr301

Chang, F., Theis, J.F., Miller, J., Nieduszynski, C.A., Newlon, C.S., Weinreich, M., 2008. Analysis of Chromosome III Replicators Reveals an Unusual Structure for the ARS318 Silencer Origin and a Conserved WTW Sequence within the Origin Recognition Complex Binding Site. Mol. Cell. Biol. 28, 5071–5081. https://doi.org/10.1128/MCB.00206-08

Chang, V.K., Donato, J.J., Chan, C.S., Tye, B.K., 2004. Mcm1 Promotes Replication Initiation by Binding Specific Elements at Replication Origins. Mol. Cell. Biol. 24, 6514–6524. https://doi.org/10.1128/MCB.24.14.6514-6524.2004

Cohen, S.N., Chang, A.C., Boyer, H.W., Helling, R.B., 1973. Construction of biologically functional bacterial plasmids in vitro. Proc. Natl. Acad. Sci. U. S. A. 70, 3240–3244. https://doi.org/10.1073/pnas.70.11.3240

Costanzo, M., VanderSluis, B., Koch, E.N., Baryshnikova, A., Pons, C., Tan, G., Wang, W., Usaj, M., Hanchard, J., Lee, S.D., Pelechano, V., Styles, E.B., Billmann, M., van Leeuwen, J., van Dyk, N., Lin, Z.-Y., Kuzmin, E., Nelson, J., Piotrowski, J.S., Srikumar, T., Bahr, S., Chen, Y., Deshpande, R., Kurat, C.F., Li, S.C., Li, Z., Usaj, M.M., Okada, H., Pascoe, N., San Luis, B.-J., Sharifpoor, S., Shuteriqi, E., Simpkins, S.W., Snider, J., Suresh, H.G., Tan, Y., Zhu, H., Malod-Dognin, N., Janjic, V., Przulj, N., Troyanskaya, O.G., Stagljar, I., Xia, T., Ohya, Y., Gingras, A.-C., Raught, B., Boutros, M., Steinmetz, L.M., Moore, C.L., Rosebrock, A.P., Caudy, A.A., Myers, C.L., Andrews, B., Boone, C., 2016. A global genetic interaction network maps a wiring diagram of cellular function. Science 353, aaf1420. https://doi.org/10.1126/science.aaf1420

Cseresnyes, Z., Schwarz, U., Green, C.M., 2009. Analysis of replication factories in human cells by super-resolution light microscopy. BMC Cell Biol. 10, 88. https://doi.org/10.1186/1471-2121-10-88

Cutler, S., Lee, L.J., Tsukiyama, T., 2018. Chromatin Remodeling Factors Isw2 and Ino80 Regulate Chromatin, Replication, and Copy Number of the Saccharomyces cerevisiae Ribosomal DNA Locus. Genetics 210, 1543–1556. https://doi.org/10.1534/genetics.118.301579

Czajkowsky, D.M., Liu, J., Hamlin, J.L., Shao, Z., 2008. DNA combing reveals intrinsic temporal disorder in the replication of yeast chromosome VI. J. Mol. Biol. 375, 12–19. https://doi.org/10.1016/j.jmb.2007.10.046

Dao, F.-Y., Lv, H., Wang, F., Feng, C.-Q., Ding, H., Chen, W., Lin, H., 2019. Identify origin of replication in Saccharomyces cerevisiae using two-step feature selection technique. Bioinformatics 35, 2075–2083. https://doi.org/10.1093/bioinformatics/bty943

Das, S.P., Borrman, T., Liu, V.W.T., Yang, S.C.-H., Bechhoefer, J., Rhind, N., 2015. Replication timing is regulated by the number of MCMs loaded at origins. Genome Res. 25, 1886–1892. https://doi.org/10.1101/gr.195305.115

Davé, A., Cooley, C., Garg, M., Bianchi, A., 2014. Protein Phosphatase 1 Recruitment by Rif1 Regulates DNA Replication Origin Firing by Counteracting DDK Activity. Cell Rep. 7, 53–61. https://doi.org/10.1016/j.celrep.2014.02.019

Deegan, T.D., Yeeles, J.T., Diffley, J.F., 2016. Phosphopeptide binding by Sld3 links Dbf4-dependent kinase to MCM replicative helicase activation. EMBO J. 35, 961–973. https://doi.org/10.15252/embj.201593552

Dietzen, M., Zhai, H., Lucas, O., Ward, S., Guo, Y., Ting-Lu, W., Pich, O., Zaccaria, S., Swanton, C., McGranahan, N., Kanu, N., 2022. Abstract 3620: Investigating the role of altered replication timing during tumor evolution in lung and breast cancer. Cancer Res. 82, 3620. https://doi.org/10.1158/1538-7445.AM2022-3620

Diffley, J.F., Stillman, B., 1988. Purification of a yeast protein that binds to origins of DNA replication and a transcriptional silencer. Proc. Natl. Acad. Sci. U. S. A. 85, 2120–2124. https://doi.org/10.1073/pnas.85.7.2120

Dimitrova, D.S., Gilbert, D.M., 1999. The Spatial Position and Replication Timing of Chromosomal Domains Are Both Established in Early G1 Phase. Mol. Cell 4, 983–993. https://doi.org/10.1016/S1097-2765(00)80227-0

Donovan, S., Harwood, J., Drury, L.S., Diffley, J.F., 1997. Cdc6p-dependent loading of Mcm proteins onto pre-replicative chromatin in budding yeast. Proc. Natl. Acad. Sci. U. S. A. 94, 5611–5616. https://doi.org/10.1073/pnas.94.11.5611

Du, Q., Bert, S.A., Armstrong, N.J., Caldon, C.E., Song, J.Z., Nair, S.S., Gould, C.M., Luu, P.-L., Peters, T., Khoury, A., Qu, W., Zotenko, E., Stirzaker, C., Clark, S.J., 2019. Replication timing and epigenome remodelling are associated with the nature of chromosomal rearrangements in cancer. Nat. Commun. 10, 416. https://doi.org/10.1038/s41467-019-08302-1

Duan, Z., Andronescu, M., Schutz, K., McIlwain, S., Kim, Y.J., Lee, C., Shendure, J., Fields, S., Blau, C.A., Noble, W.S., 2010. A three-dimensional model of the yeast genome. Nature 465, 363–367. https://doi.org/10.1038/nature08973

Dukaj, L., Rhind, N., 2021. The capacity of origins to load MCM establishes replication timing patterns. PLoS Genet. 17, e1009467. https://doi.org/10.1371/journal.pgen.1009467

Eaton, M.L., Galani, K., Kang, S., Bell, S.P., MacAlpine, D.M., 2010a. Conserved nucleosome positioning defines replication origins. Genes Dev. 24, 748–753. https://doi.org/10.1101/gad.1913210

Eaton, M.L., Galani, K., Kang, S., Bell, S.P., MacAlpine, D.M., 2010b. Conserved nucleosome positioning defines replication origins. Genes Dev. 24, 748–753. https://doi.org/10.1101/gad.1913210

Ebrahimi, H., Robertson, E.D., Taddei, A., Gasser, S.M., Donaldson, A.D., Hiraga, S., 2010. Early initiation of a replication origin tethered at the nuclear periphery. J. Cell Sci. 123, 1015–1019. https://doi.org/10.1242/jcs.060392

Eriksson, P.R., Clark, D.J., 2021. The yeast ISW1b ATP-dependent chromatin remodeler is critical for nucleosome spacing and dinucleosome resolution. Sci. Rep. 11, 4195. https://doi.org/10.1038/s41598-021-82842-9

Evrin, C., Clarke, P., Zech, J., Lurz, R., Sun, J., Uhle, S., Li, H., Stillman, B., Speck, C., 2009. A double-hexameric MCM2-7 complex is loaded onto origin DNA during licensing of eukaryotic DNA replication. Proc. Natl. Acad. Sci. 106, 20240–20245. https://doi.org/10.1073/pnas.0911500106

Fang, D., Lengronne, A., Shi, D., Forey, R., Skrzypczak, M., Ginalski, K., Yan, C., Wang, X., Cao, Q., Pasero, P., Lou, H., 2017. Dbf4 recruitment by forkhead transcription factors defines an upstream rate-limiting step in determining origin firing timing. Genes Dev. 31, 2405–2415. https://doi.org/10.1101/gad.306571.117

Ferguson, B.M., Brewer, B.J., Reynolds, A.E., Fangman, W.L., 1991. A yeast origin of replication is activated late in S phase. Cell 65, 507–515. https://doi.org/10.1016/0092-8674(91)90468-E

Fernández-Cid, A., Riera, A., Tognetti, S., Herrera, M.C., Samel, S., Evrin, C., Winkler, C.,

Gardenal, E., Uhle, S., Speck, C., 2013. An ORC/Cdc6/MCM2-7 Complex Is Formed in a Multistep Reaction to Serve as a Platform for MCM Double-Hexamer Assembly. Mol. Cell 50, 577–588. https://doi.org/10.1016/j.molcel.2013.03.026

Foss, E.J., Lao, U., Dalrymple, E., Adrianse, R.L., Loe, T., Bedalov, A., 2017. SIR2 suppresses replication gaps and genome instability by balancing replication between repetitive and unique sequences. Proc. Natl. Acad. Sci. U. S. A. 114, 552–557. https://doi.org/10.1073/pnas.1614781114

Foss, E.J., Sripathy, S., Gatbonton-Schwager, T., Kwak, H., Thiesen, A.H., Lao, U., Bedalov, A., 2021. Chromosomal Mcm2-7 distribution and the genome replication program in species from yeast to humans. PLoS Genet. 17, e1009714. https://doi.org/10.1371/journal.pgen.1009714

Francis, L.I., Randell, J.C.W., Takara, T.J., Uchima, L., Bell, S.P., 2009. Incorporation into the prereplicative complex activates the Mcm2–7 helicase for Cdc7–Dbf4 phosphorylation. Genes Dev. 23, 643–654. https://doi.org/10.1101/gad.1759609

Fujita, T., Asano, Y., Ohtsuka, J., Takada, Y., Saito, K., Ohki, R., Fujii, H., 2013. Identification of telomere-associated molecules by engineered DNA-binding molecule-mediated chromatin immunoprecipitation (enChIP). Sci. Rep. 3, 3171. https://doi.org/10.1038/srep03171

Ganapathi, M., Palumbo, M.J., Ansari, S.A., He, Q., Tsui, K., Nislow, C., Morse, R.H., 2011. Extensive role of the general regulatory factors, Abf1 and Rap1, in determining genome-wide chromatin structure in budding yeast. Nucleic Acids Res. 39, 2032–2044. https://doi.org/10.1093/nar/gkq1161

Gauchier, M., van Mierlo, G., Vermeulen, M., Déjardin, J., 2020. Purification and enrichment of specific chromatin loci. Nat. Methods 17, 380–389. https://doi.org/10.1038/s41592-020-0765-4

Gershon, L., Kupiec, M., 2021. The Amazing Acrobat: Yeast's Histone H3K56 Juggles Several Important Roles While Maintaining Perfect Balance. Genes 12, 342. https://doi.org/10.3390/genes12030342

Gibson, D.G., Young, L., Chuang, R.-Y., Venter, J.C., Hutchison, C.A., Smith, H.O., 2009. Enzymatic assembly of DNA molecules up to several hundred kilobases. Nat. Methods 6, 343–345. https://doi.org/10.1038/nmeth.1318

Gietz, R.D., Schiestl, R.H., 2007. High-efficiency yeast transformation using the LiAc/SS carrier DNA/PEG method. Nat. Protoc. 2, 31–34. https://doi.org/10.1038/nprot.2007.13

Gietz, R.D., Sugino, A., 1988. New yeast-Escherichia coli shuttle vectors constructed with in vitro mutagenized yeast genes lacking six-base pair restriction sites. Gene 74, 527–534. https://doi.org/10.1016/0378-1119(88)90185-0

Griesenbeck, J., Boeger, H., Strattan, J.S., Kornberg, R.D., 2004a. Purification of defined chromosomal domains. Methods Enzymol. 375, 170–178. https://doi.org/10.1016/s0076-6879(03)75011-3

Griesenbeck, J., Boeger, H., Strattan, J.S., Kornberg, R.D., 2004b. Purification of defined chromosomal domains. Methods Enzymol. 375, 170–178. https://doi.org/10.1016/s0076-6879(03)75011-3

Griesenbeck, J., Boeger, H., Strattan, J.S., Kornberg, R.D., 2003. Affinity Purification of Specific Chromatin Segments from Chromosomal Loci in Yeast. Mol. Cell. Biol. 23, 9275–9282. https://doi.org/10.1128/MCB.23.24.9275-9282.2003

Grosche, A., Hauser, A., Lepper, M.F., Mayo, R., von Toerne, C., Merl-Pham, J., Hauck, S.M., 2016. The Proteome of Native Adult Müller Glial Cells From Murine Retina. Mol. Cell. Proteomics MCP 15, 462–480. https://doi.org/10.1074/mcp.M115.052183

Hafner, L., Lezaja, A., Zhang, X., Lemmens, L., Shyian, M., Albert, B., Follonier, C., Nunes, J.M., Lopes, M., Shore, D., Mattarocci, S., 2018. Rif1 Binding and Control of

Chromosome-Internal DNA Replication Origins Is Limited by Telomere Sequestration. Cell Rep. 23, 983–992. https://doi.org/10.1016/j.celrep.2018.03.113

Hamperl, S., Bocek, M.J., Saldivar, J.C., Swigut, T., Cimprich, K.A., 2017. Transcription-Replication Conflict Orientation Modulates R-Loop Levels and Activates Distinct DNA Damage Responses. Cell 170, 774-786.e19. https://doi.org/10.1016/j.cell.2017.07.043

Hamperl, S., Brown, C.R., Garea, A.V., Perez-Fernandez, J., Bruckmann, A., Huber, K., Wittner, M., Babl, V., Stoeckl, U., Deutzmann, R., Boeger, H., Tschochner, H., Milkereit, P., Griesenbeck, J., 2014. Compositional and structural analysis of selected chromosomal domains from Saccharomyces cerevisiae. Nucleic Acids Res. 42, e2. https://doi.org/10.1093/nar/gkt891

Hawkins, M., Retkute, R., Müller, C.A., Saner, N., Tanaka, T.U., de Moura, A.P.S., Nieduszynski, C.A., 2013. High-Resolution Replication Profiles Define the Stochastic Nature of Genome Replication Initiation and Termination. Cell Rep. 5, 1132–1141. https://doi.org/10.1016/j.celrep.2013.10.014

He, Y., Petrie, M.V., Zhang, H., Peace, J.M., Aparicio, O.M., 2022. Rpd3 regulates single-copy origins independently of the rDNA array by opposing Fkh1-mediated origin stimulation. Proc. Natl. Acad. Sci. 119, e2212134119. https://doi.org/10.1073/pnas.2212134119

Hiraga, S., Alvino, G.M., Chang, F., Lian, H., Sridhar, A., Kubota, T., Brewer, B.J., Weinreich, M., Raghuraman, M.K., Donaldson, A.D., 2014. Rif1 controls DNA replication by directing Protein Phosphatase 1 to reverse Cdc7-mediated phosphorylation of the MCM complex. Genes Dev. 28, 372–383. https://doi.org/10.1101/gad.231258.113

Hiraga, S., Robertson, E.D., Donaldson, A.D., 2006. The Ctf18 RFC-like complex positions yeast telomeres but does not specify their replication time. EMBO J. 25, 1505–1514. https://doi.org/10.1038/sj.emboj.7601038

Hoggard, T., Müller, C.A., Nieduszynski, C.A., Weinreich, M., Fox, C.A., 2020. Sir2 mitigates an intrinsic imbalance in origin licensing efficiency between early- and late-replicating euchromatin. Proc. Natl. Acad. Sci. U. S. A. 117, 14314–14321. https://doi.org/10.1073/pnas.2004664117

Hoggard, T.A., Chang, F., Perry, K.R., Subramanian, S., Kenworthy, J., Chueng, J., Shor, E., Hyland, E.M., Boeke, J.D., Weinreich, M., Fox, C.A., 2018. Yeast heterochromatin regulators Sir2 and Sir3 act directly at euchromatic DNA replication origins. PLOS Genet. 14, e1007418. https://doi.org/10.1371/journal.pgen.1007418

Hoshina, S., Yura, K., Teranishi, H., Kiyasu, N., Tominaga, A., Kadoma, H., Nakatsuka, A., Kunichika, T., Obuse, C., Waga, S., 2013. Human origin recognition complex binds preferentially to G-quadruplex-preferable RNA and single-stranded DNA. J. Biol. Chem. 288, 30161–30171. https://doi.org/10.1074/jbc.M113.492504

Hozák, P., Hassan, A.B., Jackson, D.A., Cook, P.R., 1993. Visualization of replication factories attached to a nucleoskeleton. Cell 73, 361–373. https://doi.org/10.1016/0092-8674(93)90235-I

Hozak, P., Jackson, D.A., Cook, P.R., 1994. Replication factories and nuclear bodies: the ultrastructural characterization of replication sites during the cell cycle. J. Cell Sci. 107, 2191–2202. https://doi.org/10.1242/jcs.107.8.2191

Huang, Y., Kowalski, D., 2003. WEB-THERMODYN: Sequence analysis software for profiling DNA helical stability. Nucleic Acids Res. 31, 3819–3821. https://doi.org/10.1093/nar/gkg562

Huo, L., Wu, R., Yu, Z., Zhai, Y., Yang, X., Chan, T., Yeung, J.T.F., Kan, J., Liang, C., 2012. The Rix1 (Ipi1p-2p-3p) complex is a critical determinant of DNA replication licensing independent of their roles in ribosome biogenesis. Cell Cycle Georget. Tex 11, 1325–

1339. https://doi.org/10.4161/cc.19709

Irlbacher, H., Franke, J., Manke, T., Vingron, M., Ehrenhofer-Murray, A.E., 2005. Control of replication initiation and heterochromatin formation in Saccharomyces cerevisiae by a regulator of meiotic gene expression. Genes Dev. 19, 1811–1822. https://doi.org/10.1101/gad.334805

Jenni, S., Harrison, S.C., 2018. Structure of the DASH/Dam1 Complex Shows its Role at the Yeast Kinetochore-Microtubule Interface. Science 360, 552–558. https://doi.org/10.1126/science.aar6436

Johnson, D.S., Mortazavi, A., Myers, R.M., Wold, B., 2007. Genome-wide mapping of in vivo protein-DNA interactions. Science 316, 1497–1502. https://doi.org/10.1126/science.1141319

Johnson, M.A., Sharma, M., Mok, M.T.S., Henderson, B.R., 2013. Stimulation of in vivo nuclear transport dynamics of actin and its co-factors IQGAP1 and Rac1 in response to DNA replication stress. Biochim. Biophys. Acta 1833, 2334–2347. https://doi.org/10.1016/j.bbamcr.2013.06.002

Joung, J.K., Sander, J.D., 2013. TALENs: a widely applicable technology for targeted genome editing. Nat. Rev. Mol. Cell Biol. 14, 49–55. https://doi.org/10.1038/nrm3486

Kajino, H., Nagatani, T., Oi, M., Kujirai, T., Kurumizaka, H., Nishiyama, A., Nakanishi, M., Yamatsugu, K., Kawashima, S.A., Kanai, M., 2020. Synthetic hyperacetylation of nucleosomal histones. RSC Chem. Biol. 1, 56–59. https://doi.org/10.1039/D0CB00029A

Kamimura, Y., Masumoto, H., Sugino, A., Araki, H., 1998. Sld2, Which Interacts with Dpb11 in Saccharomyces cerevisiae, Is Required for Chromosomal DNA Replication. Mol. Cell. Biol. 18, 6102–6109.

Kelpsch, D.J., Tootle, T.L., 2018. Nuclear actin: from discovery to function. Anat. Rec. Hoboken NJ 2007 301, 1999–2013. https://doi.org/10.1002/ar.23959

Kennedy-Darling, J., Guillen-Ahlers, H., Shortreed, M.R., Scalf, M., Frey, B.L., Kendziorski, C., Olivier, M., Gasch, A.P., Smith, L.M., 2014. Discovery of Chromatin-Associated Proteins via Sequence-Specific Capture and Mass Spectrometric Protein Identification in Saccharomyces cerevisiae. J. Proteome Res. 13, 3810–3825. https://doi.org/10.1021/pr5004938

Kim, T., Buratowski, S., 2009. Dimethylation of H3K4 by Set1 recruits the Set3 histone deacetylase complex to 5′ transcribed regions. Cell 137, 259–272. https://doi.org/10.1016/j.cell.2009.02.045

Kitamura, E., Blow, J.J., Tanaka, T.U., 2006. Live-cell imaging reveals replication of individual replicons in eukaryotic replication factories. Cell 125, 1297–1308. https://doi.org/10.1016/j.cell.2006.04.041

Knott, S.R.V., Peace, J.M., Ostrow, A.Z., Gan, Y., Rex, A.E., Viggiani, C.J., Tavaré, S., Aparicio, O.M., 2012. Forkhead transcription factors establish origin timing and long-range clustering in S. cerevisiae. Cell 148, 99–111. https://doi.org/10.1016/j.cell.2011.12.012

Knott, S.R.V., Viggiani, C.J., Tavaré, S., Aparicio, O.M., 2009. Genome-wide replication profiles indicate an expansive role for Rpd3L in regulating replication initiation timing or efficiency, and reveal genomic loci of Rpd3 function in Saccharomyces cerevisiae. Genes Dev. 23, 1077–1090. https://doi.org/10.1101/gad.1784309

Kuo, L.J., Yang, L.-X., 2008. Gamma-H2AX - a novel biomarker for DNA double-strand breaks. Vivo Athens Greece 22, 305–309.

Kurat, C.F., Yeeles, J.T.P., Patel, H., Early, A., Diffley, J.F.X., 2017. Chromatin Controls DNA Replication Origin Selection, Lagging-Strand Synthesis, and Replication Fork Rates. Mol. Cell 65, 117–130. https://doi.org/10.1016/j.molcel.2016.11.016

Lacefield, S., Lau, D.T.C., Murray, A.W., 2009. Recruiting a microtubule-binding complex to

DNA directs chromosome segregation in budding yeast. Nat. Cell Biol. 11, 1116–1120. https://doi.org/10.1038/ncb1925

Lee, C.S.K., Cheung, M.F., Li, J., Zhao, Y., Lam, W.H., Ho, V., Rohs, R., Zhai, Y., Leung, D., Tye, B.-K., 2021. Humanizing the yeast origin recognition complex. Nat. Commun. 12, 33. https://doi.org/10.1038/s41467-020-20277-y

Leonhardt, H., Rahn, H.P., Weinzierl, P., Sporbert, A., Cremer, T., Zink, D., Cardoso, M.C., 2000. Dynamics of DNA replication factories in living cells. J. Cell Biol. 149, 271–280. https://doi.org/10.1083/jcb.149.2.271

Li, N., Lam, W.H., Zhai, Y., Cheng, J., Cheng, E., Zhao, Y., Gao, N., Tye, B.-K., 2018. Structure of the origin recognition complex bound to DNA replication origin. Nature 559, 217–222. https://doi.org/10.1038/s41586-018-0293-x

Li, S., Wasserman, M.R., Yurieva, O., Bai, L., O'Donnell, M.E., Liu, S., 2022. Nucleosome-directed replication origin licensing independent of a consensus DNA sequence. Nat. Commun. 13, 4947. https://doi.org/10.1038/s41467-022-32657-7

Li, Y., Bachant, J., Alcasabas, A.A., Wang, Y., Qin, J., Elledge, S.J., 2002. The mitotic spindle is required for loading of the DASH complex onto the kinetochore. Genes Dev. 16, 183–197. https://doi.org/10.1101/gad.959402

Lian, H.-Y., Robertson, E.D., Hiraga, S., Alvino, G.M., Collingwood, D., McCune, H.J., Sridhar, A., Brewer, B.J., Raghuraman, M.K., Donaldson, A.D., 2011. The effect of Ku on telomere replication time is mediated by telomere length but is independent of histone tail acetylation. Mol. Biol. Cell 22, 1753–1765. https://doi.org/10.1091/mbc.E10-06-0549

Lin, S., Kowalski, D., 1997. Functional equivalency and diversity of cis-acting elements among yeast replication origins. Mol. Cell. Biol. 17, 5473–5484. https://doi.org/10.1128/MCB.17.9.5473

Lipford, J.R., Bell, S.P., 2001. Nucleosomes positioned by ORC facilitate the initiation of DNA replication. Mol. Cell 7, 21–30. https://doi.org/10.1016/s1097-2765(01)00151-4

Long, H., Zhang, L., Lv, M., Wen, Z., Zhang, W., Chen, X., Zhang, P., Li, T., Chang, L., Jin, C., Wu, G., Wang, X., Yang, F., Pei, J., Chen, P., Margueron, R., Deng, H., Zhu, M., Li, G., 2020. H2A.Z facilitates licensing and activation of early replication origins. Nature 577, 576–581. https://doi.org/10.1038/s41586-019-1877-9

Lõoke, M., Kristjuhan, K., Värv, S., Kristjuhan, A., 2013. Chromatin-dependent and -independent regulation of DNA replication origin activation in budding yeast. EMBO Rep. 14, 191–198. https://doi.org/10.1038/embor.2012.196

Maile, T.M., Izrael-Tomasevic, A., Cheung, T., Guler, G.D., Tindell, C., Masselot, A., Liang, J., Zhao, F., Trojer, P., Classon, M., Arnott, D., 2015. Mass spectrometric quantification of histone post-translational modifications by a hybrid chemical labeling method. Mol. Cell. Proteomics MCP 14, 1148–1158. https://doi.org/10.1074/mcp.O114.046573

Mantiero, D., Mackenzie, A., Donaldson, A., Zegerman, P., 2011. Limiting replication initiation factors execute the temporal programme of origin firing in budding yeast. EMBO J. 30, 4805–4814. https://doi.org/10.1038/emboj.2011.404

Marahrens, Y., Stillman, B., 1992. A yeast chromosomal origin of DNA replication defined by multiple functional elements. Science 255, 817–823. https://doi.org/10.1126/science.1536007

Masumoto, H., Hawke, D., Kobayashi, R., Verreault, A., 2005. A role for cell-cycle-regulated histone H3 lysine 56 acetylation in the DNA damage response. Nature 436, 294–298. https://doi.org/10.1038/nature03714

Masumoto, H., Muramatsu, S., Kamimura, Y., Araki, H., 2002. S-Cdk-dependent phosphorylation of Sld2 essential for chromosomal DNA replication in budding yeast. Nature 415, 651–655. https://doi.org/10.1038/nature713

Mattarocci, S., Shyian, M., Lemmens, L., Damay, P., Altintas, D.M., Shi, T., Bartholomew, C.R., Thomä, N.H., Hardy, C.F.J., Shore, D., 2014. Rif1 controls DNA replication timing in yeast through the PP1 phosphatase Glc7. Cell Rep. 7, 62–69. https://doi.org/10.1016/j.celrep.2014.03.010

McGuffee, S.R., Smith, D.J., Whitehouse, I., 2013a. Quantitative, genome-wide analysis of eukaryotic replication initiation and termination. Mol. Cell 50, 123–135. https://doi.org/10.1016/j.molcel.2013.03.004

McGuffee, S.R., Smith, D.J., Whitehouse, I., 2013b. Quantitative, genome-wide analysis of eukaryotic replication initiation and termination. Mol. Cell 50, 123–135. https://doi.org/10.1016/j.molcel.2013.03.004

Miranda, J.L., King, D.S., Harrison, S.C., 2007. Protein Arms in the Kinetochore-Microtubule Interface of the Yeast DASH Complex. Mol. Biol. Cell 18, 2503–2510. https://doi.org/10.1091/mbc.e07-02-0135

Morawska, M., Ulrich, H.D., 2013. An expanded tool kit for the auxin-inducible degron system in budding yeast. Yeast Chichester Engl. 30, 341–351. https://doi.org/10.1002/yea.2967

Müller, C.A., Boemo, M.A., Spingardi, P., Kessler, B.M., Kriaucionis, S., Simpson, J.T., Nieduszynski, C.A., 2019. Capturing the dynamics of genome replication on individual ultra-long nanopore sequence reads. Nat. Methods 16, 429–436. https://doi.org/10.1038/s41592-019-0394-y

Muramatsu, S., Hirai, K., Tak, Y.-S., Kamimura, Y., Araki, H., 2010. CDK-dependent complex formation between replication proteins Dpb11, Sld2, Pol (epsilon}, and GINS in budding yeast. Genes Dev. 24, 602–612. https://doi.org/10.1101/gad.1883410

Nakamura, H., Morita, T., Sato, C., 1986. Structural organizations of replicon domains during DNA synthetic phase in the mammalian nucleus. Exp. Cell Res. 165, 291–297. https://doi.org/10.1016/0014-4827(86)90583-5

Natale, D.A., Umek, R.M., Kowalski, D., 1993. Ease of DNA unwinding is a conserved property of yeast replication origins. Nucleic Acids Res. 21, 555–560.

Natsume, T., Müller, C.A., Katou, Y., Retkute, R., Gierliński, M., Araki, H., Blow, J.J., Shirahige, K., Nieduszynski, C.A., Tanaka, T.U., 2013. Kinetochores coordinate pericentromeric cohesion and early DNA replication by Cdc7-Dbf4 kinase recruitment. Mol. Cell 50, 661–674. https://doi.org/10.1016/j.molcel.2013.05.011

Natsume, T., Tanaka, T.U., 2010. Spatial regulation and organization of DNA replication within the nucleus. Chromosome Res. Int. J. Mol. Supramol. Evol. Asp. Chromosome Biol. 18, 7–17. https://doi.org/10.1007/s10577-009-9088-0

Navarro, P., Trevisan-Herraz, M., Bonzon-Kulichenko, E., Núñez, E., Martínez-Acedo, P., Pérez-Hernández, D., Jorge, I., Mesa, R., Calvo, E., Carrascal, M., Hernáez, M.L., García, F., Bárcena, J.A., Ashman, K., Abian, J., Gil, C., Redondo, J.M., Vázquez, J., 2014. General Statistical Framework for Quantitative Proteomics by Stable Isotope Labeling. J. Proteome Res. 13, 1234–1247. https://doi.org/10.1021/pr4006958

Nguyen, A.T., Zhang, Y., 2011. The diverse functions of Dot1 and H3K79 methylation. Genes Dev. 25, 1345–1358. https://doi.org/10.1101/gad.2057811

Ostrow, A.Z., Kalhor, R., Gan, Y., Villwock, S.K., Linke, C., Barberis, M., Chen, L., Aparicio, O.M., 2017. Conserved forkhead dimerization motif controls DNA replication timing and spatial organization of chromosomes in S. cerevisiae. Proc. Natl. Acad. Sci. 114, E2411–E2419. https://doi.org/10.1073/pnas.1612422114

Ostrow, A.Z., Nellimoottil, T., Knott, S.R.V., Fox, C.A., Tavaré, S., Aparicio, O.M., 2014. Fkh1 and Fkh2 Bind Multiple Chromosomal Elements in the S. cerevisiae Genome with Distinct Specificities and Cell Cycle Dynamics. PLoS ONE 9, e87647. https://doi.org/10.1371/journal.pone.0087647

Parisis, N., Krasinska, L., Harker, B., Urbach, S., Rossignol, M., Camasses, A., Dewar, J.,

Morin, N., Fisher, D., 2017. Initiation of DNA replication requires actin dynamics and formin activity. EMBO J. 36, 3212–3231. https://doi.org/10.15252/embj.201796585

Parker, M.W., Botchan, M.R., Berger, J.M., 2017. Mechanisms and regulation of DNA replication initiation in eukaryotes. Crit. Rev. Biochem. Mol. Biol. 52, 107–144. https://doi.org/10.1080/10409238.2016.1274717

Pasero, P., Bensimon, A., Schwob, E., 2002. Single-molecule analysis reveals clustering and epigenetic regulation of replication origins at the yeast rDNA locus. Genes Dev. 16, 2479–2484. https://doi.org/10.1101/gad.232902

Pasero, P., Braguglia, D., Gasser, S.M., 1997. ORC-dependent and origin-specific initiation of DNA replication at defined foci in isolated yeast nuclei. Genes Dev. 11, 1504–1518. https://doi.org/10.1101/gad.11.12.1504

Peace, J.M., Ter-Zakarian, A., Aparicio, O.M., 2014. Rif1 Regulates Initiation Timing of Late Replication Origins throughout the S. cerevisiae Genome. PLOS ONE 9, e98501. https://doi.org/10.1371/journal.pone.0098501

Peace, J.M., Villwock, S.K., Zeytounian, J.L., Gan, Y., Aparicio, O.M., 2016. Quantitative BrdU immunoprecipitation method demonstrates that Fkh1 and Fkh2 are rate-limiting activators of replication origins that reprogram replication timing in G1 phase. Genome Res. 26, 365–375. https://doi.org/10.1101/gr.196857.115

Perez-Riverol, Y., Bai, J., Bandla, C., García-Seisdedos, D., Hewapathirana, S., Kamatchinathan, S., Kundu, D.J., Prakash, A., Frericks-Zipper, A., Eisenacher, M., Walzer, M., Wang, S., Brazma, A., Vizcaíno, J.A., 2022. The PRIDE database resources in 2022: a hub for mass spectrometry-based proteomics evidences. Nucleic Acids Res. 50, D543–D552. https://doi.org/10.1093/nar/gkab1038

Pijnappel, W.W.M.P., Schaft, D., Roguev, A., Shevchenko, A., Tekotte, H., Wilm, M., Rigaut, G., Séraphin, B., Aasland, R., Stewart, A.F., 2001. The S. cerevisiae SET3 complex includes two histone deacetylases, Hos2 and Hst1, and is a meiotic-specific repressor of the sporulation gene program. Genes Dev. 15, 2991–3004. https://doi.org/10.1101/gad.207401

Poli, J., Gerhold, C.-B., Tosi, A., Hustedt, N., Seeber, A., Sack, R., Herzog, F., Pasero, P., Shimada, K., Hopfner, K.-P., Gasser, S.M., 2016. Mec1, INO80, and the PAF1 complex cooperate to limit transcription replication conflicts through RNAPII removal during replication stress. Genes Dev. 30, 337–354. https://doi.org/10.1101/gad.273813.115

Pryde, F., Jain, D., Kerr, A., Curley, R., Mariotti, F.R., Vogelauer, M., 2009. H3 K36 Methylation Helps Determine the Timing of Cdc45 Association with Replication Origins. PLOS ONE 4, e5882. https://doi.org/10.1371/journal.pone.0005882

Raghuraman, M.K., Winzeler, E.A., Collingwood, D., Hunt, S., Wodicka, L., Conway, A., Lockhart, D.J., Davis, R.W., Brewer, B.J., Fangman, W.L., 2001. Replication dynamics of the yeast genome. Science 294, 115–121. https://doi.org/10.1126/science.294.5540.115

Rao, H., Marahrens, Y., Stillman, B., 1994. Functional conservation of multiple elements in yeast chromosomal replicators. Mol. Cell. Biol. 14, 7643–7651. https://doi.org/10.1128/mcb.14.11.7643-7651.1994

Rao, H., Stillman, B., 1995. The origin recognition complex interacts with a bipartite DNA binding site within yeast replicators. Proc. Natl. Acad. Sci. U. S. A. 92, 2224–2228. https://doi.org/10.1073/pnas.92.6.2224

Recht, J., Tsubota, T., Tanny, J.C., Diaz, R.L., Berger, J.M., Zhang, X., Garcia, B.A., Shabanowitz, J., Burlingame, A.L., Hunt, D.F., Kaufman, P.D., Allis, C.D., 2006. Histone chaperone Asf1 is required for histone H3 lysine 56 acetylation, a modification associated with S phase in mitosis and meiosis. Proc. Natl. Acad. Sci. 103, 6988–6993. https://doi.org/10.1073/pnas.0601676103

Reinapae, A., Jalakas, K., Avvakumov, N., Lõoke, M., Kristjuhan, K., Kristjuhan, A., 2017. Recruitment of Fkh1 to replication origins requires precisely positioned Fkh1/2 binding sites and concurrent assembly of the pre-replicative complex. PLOS Genet. 13, e1006588. https://doi.org/10.1371/journal.pgen.1006588

Remus, D., Beall, E.L., Botchan, M.R., 2004. DNA topology, not DNA sequence, is a critical determinant for Drosophila ORC–DNA binding. EMBO J. 23, 897–907. https://doi.org/10.1038/sj.emboj.7600077

Remus, D., Beuron, F., Tolun, G., Griffith, J.D., Morris, E.P., Diffley, J.F.X., 2009. Concerted loading of Mcm2-7 double hexamers around DNA during DNA replication origin licensing. Cell 139, 719–730. https://doi.org/10.1016/j.cell.2009.10.015

Reusswig, K.-U., Bittmann, J., Peritore, M., Courtes, M., Pardo, B., Wierer, M., Mann, M., Pfander, B., 2022. Unscheduled DNA replication in G1 causes genome instability and damage signatures indicative of replication collisions. Nat. Commun. 13, 7014. https://doi.org/10.1038/s41467-022-34379-2

Rhind, N., Gilbert, D.M., 2013. DNA replication timing. Cold Spring Harb. Perspect. Biol. 5, a010132. https://doi.org/10.1101/cshperspect.a010132

Rine, J., Herskowitz, I., 1987. Four genes responsible for a position effect on expression from HML and HMR in Saccharomyces cerevisiae. Genetics 116, 9–22. https://doi.org/10.1093/genetics/116.1.9

Rizzardi, L.F., Dorn, E.S., Strahl, B.D., Cook, J.G., 2012. DNA replication origin function is promoted by H3K4 di-methylation in Saccharomyces cerevisiae. Genetics 192, 371–384. https://doi.org/10.1534/genetics.112.142349

Rodriguez, J., Lee, L., Lynch, B., Tsukiyama, T., 2017. Nucleosome occupancy as a novel chromatin parameter for replication origin functions. Genome Res. 27, 269–277. https://doi.org/10.1101/gr.209940.116

Rowley, A., Cocker, J.H., Harwood, J., Diffley, J.F., 1995. Initiation complex assembly at budding yeast replication origins begins with the recognition of a bipartite sequence by limiting amounts of the initiator, ORC. EMBO J. 14, 2631–2641. https://doi.org/10.1002/j.1460-2075.1995.tb07261.x

Saner, N., Karschau, J., Natsume, T., Gierliński, M., Retkute, R., Hawkins, M., Nieduszynski, C.A., Blow, J.J., de Moura, A.P.S., Tanaka, T.U., 2013. Stochastic association of neighboring replicons creates replication factories in budding yeast. J. Cell Biol. 202, 1001–1012. https://doi.org/10.1083/jcb.201306143

Santos, M.M., Johnson, M.C., Fiedler, L., Zegerman, P., 2022. Global early replication disrupts gene expression and chromatin conformation in a single cell cycle. Genome Biol. 23, 217. https://doi.org/10.1186/s13059-022-02788-7

Santos-Rosa, H., Millan-Zambrano, G., Han, N., Leonardi, T., Klimontova, M., Nasiscionyte, S., Pandolfini, L., Tzelepis, K., Bartke, T., Kouzarides, T., 2021. Methylation of histone H3 at lysine-37 by Set1 and Set2 prevents spurious DNA replication. Mol. Cell 81, 2793-2807.e8. https://doi.org/10.1016/j.molcel.2021.04.021

Sharma, K., Weinberger, M., Huberman, J.A., 2001. Roles for internal and flanking sequences in regulating the activity of mating-type-silencer-associated replication origins in Saccharomyces cerevisiae. Genetics 159, 35–45. https://doi.org/10.1093/genetics/159.1.35

Shyian, M., Mattarocci, S., Albert, B., Hafner, L., Lezaja, A., Costanzo, M., Boone, C., Shore, D., 2016. Budding Yeast Rif1 Controls Genome Integrity by Inhibiting rDNA Replication. PLOS Genet. 12, e1006414. https://doi.org/10.1371/journal.pgen.1006414

Simpson, R.T., 1990. Nucleosome positioning can affect the function of a cis-acting DMA elementin vivo. Nature 343, 387–389. https://doi.org/10.1038/343387a0

Singh, V.K., Kumar, V., Krishnamachari, A., 2018. Prediction of replication sites in

Saccharomyces cerevisiae genome using DNA segment properties: Multi-view ensemble learning (MEL) approach. Biosystems 163, 59–69. https://doi.org/10.1016/j.biosystems.2017.12.005

Skene, P.J., Henikoff, S., 2017. An efficient targeted nuclease strategy for high-resolution mapping of DNA binding sites. eLife 6, e21856. https://doi.org/10.7554/eLife.21856

Stevenson, J.B., Gottschling, D.E., 1999. Telomeric chromatin modulates replication timing near chromosome ends. Genes Dev. 13, 146–151. https://doi.org/10.1101/gad.13.2.146

Stinchcomb, D.T., Struhl, K., Davis, R.W., 1979. Isolation and characterisation of a yeast chromosomal replicator. Nature 282, 39–43. https://doi.org/10.1038/282039a0

Taddei, A., Hediger, F., Neumann, F.R., Bauer, C., Gasser, S.M., 2004. Separation of silencing from perinuclear anchoring functions in yeast Ku80, Sir4 and Esc1 proteins. EMBO J. 23, 1301–1312. https://doi.org/10.1038/sj.emboj.7600144

Tanaka, S., Nakato, R., Katou, Y., Shirahige, K., Araki, H., 2011. Origin association of Sld3, Sld7, and Cdc45 proteins is a key step for determination of origin-firing timing. Curr. Biol. CB 21, 2055–2063. https://doi.org/10.1016/j.cub.2011.11.038

Theis, J.F., Newlon, C.S., 1997. The ARS309 chromosomal replicator of Saccharomyces cerevisiae depends on an exceptional ARS consensus sequence. Proc. Natl. Acad. Sci. U. S. A. 94, 10786–10791. https://doi.org/10.1073/pnas.94.20.10786

Umek, R.M., Kowalski, D., 1990. The DNA unwinding element in a yeast replication origin functions independently of easily unwound sequences present elsewhere on a plasmid. Nucleic Acids Res. 18, 6601–6605. https://doi.org/10.1093/nar/18.22.6601

Unnikrishnan, A., Gafken, P.R., Tsukiyama, T., 2010a. Dynamic changes in histone acetylation regulate origins of DNA replication. Nat. Struct. Mol. Biol. 17, 430–437. https://doi.org/10.1038/nsmb.1780

Unnikrishnan, A., Gafken, P.R., Tsukiyama, T., 2010b. Dynamic changes in histone acetylation regulate origins of DNA replication. Nat. Struct. Mol. Biol. 17, 430–437. https://doi.org/10.1038/nsmb.1780

Van Houten, J.V., Newlon, C.S., 1990. Mutational analysis of the consensus sequence of a replication origin from yeast chromosome III. Mol. Cell. Biol. 10, 3917–3925. https://doi.org/10.1128/mcb.10.8.3917-3925.1990

Vashee, S., Cvetic, C., Lu, W., Simancek, P., Kelly, T.J., Walter, J.C., 2003. Sequence-independent DNA binding and replication initiation by the human origin recognition complex. Genes Dev. 17, 1894–1908. https://doi.org/10.1101/gad.1084203

Venditti, P., Costanzo, G., Negri, R., Camilloni, G., 1994. ABFI contributes to the chromatin organization of Saccharomyces cerevisiae ARS1 B-domain. Biochim. Biophys. Acta 1219, 677–689. https://doi.org/10.1016/0167-4781(94)90227-5

Vermeulen, M., Déjardin, J., 2020. Locus-specific chromatin isolation. Nat. Rev. Mol. Cell Biol. 21, 249–250. https://doi.org/10.1038/s41580-020-0217-0

Vogelauer, M., Rubbi, L., Lucas, I., Brewer, B.J., Grunstein, M., 2002. Histone acetylation regulates the time of replication origin firing. Mol. Cell 10, 1223–1233. https://doi.org/10.1016/s1097-2765(02)00702-5

Walker, S.S., Francesconi, S.C., Eisenberg, S., 1990. A DNA Replication Enhancer in Saccharomyces Cerevisiae. Proc. Natl. Acad. Sci. U. S. A. 87, 4665–4669.

Wang, A., Kurdistani, S.K., Grunstein, M., 2002. Requirement of Hos2 Histone Deacetylase for Gene Activity in Yeast. Science 298, 1412–1414. https://doi.org/10.1126/science.1077790

Wang, W., Klein, K.N., Proesmans, K., Yang, H., Marchal, C., Zhu, X., Borrman, T., Hastie, A., Weng, Z., Bechhoefer, J., Chen, C.-L., Gilbert, D.M., Rhind, N., 2021. Genome-wide mapping of human DNA replication by optical replication mapping supports a stochastic model of eukaryotic replication. Mol. Cell 81, 2975-2988.e6. https://doi.org/10.1016/j.molcel.2021.05.024

Weber, J., Irlbacher, H., Ehrenhofer-Murray, A., 2008. Control of replication initiation by the Sum1/Rfm1/Hst1 histone deacetylase. BMC Mol. Biol. 9, 100. https://doi.org/10.1186/1471-2199-9-100

Weiβ, M., Chanou, A., Schauer, T., Tvardovskiy, A., Meiser, S., König, A.-C., Schmidt, T., Kruse, E., Ummethum, H., Trauner, M., Werner, M., Lalonde, M., Hauck, S.M., Scialdone, A., Hamperl, S., 2023. Single-copy locus proteomics of early- and late-firing DNA replication origins identifies a role of Ask1/DASH complex in replication timing control. Cell Rep. 42, 112045. https://doi.org/10.1016/j.celrep.2023.112045

Westermann, S., Avila-Sakar, A., Wang, H.-W., Niederstrasser, H., Wong, J., Drubin, D.G., Nogales, E., Barnes, G., 2005. Formation of a Dynamic Kinetochore- Microtubule Interface through Assembly of the Dam1 Ring Complex. Mol. Cell 17, 277–290. https://doi.org/10.1016/j.molcel.2004.12.019

Wilmes, G.M., Bell, S.P., 2002. The B2 element of the Saccharomyces cerevisiae ARS1 origin of replication requires specific sequences to facilitate pre-RC formation. Proc. Natl. Acad. Sci. U. S. A. 99, 101–106. https://doi.org/10.1073/pnas.012578499

Wiśniewski, J.R., Zougman, A., Nagaraj, N., Mann, M., 2009. Universal sample preparation method for proteome analysis. Nat. Methods 6, 359–362. https://doi.org/10.1038/nmeth.1322

Wyrick, J.J., Aparicio, J.G., Chen, T., Barnett, J.D., Jennings, E.G., Young, R.A., Bell, S.P., Aparicio, O.M., 2001. Genome-wide distribution of ORC and MCM proteins in S. cerevisiae: high-resolution mapping of replication origins. Science 294, 2357–2360. https://doi.org/10.1126/science.1066101

Xu, W., Aparicio, J.G., Aparicio, O.M., Tavaré, S., 2006. Genome-wide mapping of ORC and Mcm2p binding sites on tiling arrays and identification of essential ARS consensus sequences in S. cerevisiae. BMC Genomics 7, 276. https://doi.org/10.1186/1471-2164-7-276

Yeeles, J.T.P., Deegan, T.D., Janska, A., Early, A., Diffley, J.F.X., 2015. Regulated eukaryotic DNA replication origin firing with purified proteins. Nature 519, 431–435. https://doi.org/10.1038/nature14285

Yoshida, K., Bacal, J., Desmarais, D., Padioleau, I., Tsaponina, O., Chabes, A., Pantesco, V., Dubois, E., Parrinello, H., Skrzypczak, M., Ginalski, K., Lengronne, A., Pasero, P., 2014. The histone deacetylases sir2 and rpd3 act on ribosomal DNA to control the replication program in budding yeast. Mol. Cell 54, 691–697. https://doi.org/10.1016/j.molcel.2014.04.032

Yuan, Z., Riera, A., Bai, L., Sun, J., Nandi, S., Spanos, C., Chen, Z.A., Barbon, M., Rappsilber, J., Stillman, B., Speck, C., Li, H., 2017. Structural basis of Mcm2-7 replicative helicase loading by ORC-Cdc6 and Cdt1. Nat. Struct. Mol. Biol. 24, 316–324. https://doi.org/10.1038/nsmb.3372

Zappulla, D.C., Sternglanz, R., Leatherwood, J., 2002. Control of replication timing by a transcriptional silencer. Curr. Biol. CB 12, 869–875. https://doi.org/10.1016/s0960-9822(02)00871-0

Zegerman, P., Diffley, J.F.X., 2007. Phosphorylation of Sld2 and Sld3 by cyclin-dependent kinases promotes DNA replication in budding yeast. Nature 445, 281–285. https://doi.org/10.1038/nature05432

Zhang, H., Petrie, M.V., He, Y., Peace, J.M., Chiolo, I.E., Aparicio, O.M., 2019. Dynamic relocalization of replication origins by Fkh1 requires execution of DDK function and Cdc45 loading at origins. eLife 8, e45512. https://doi.org/10.7554/eLife.45512

Zhao, P.A., Sasaki, T., Gilbert, D.M., 2020. High-resolution Repli-Seq defines the temporal choreography of initiation, elongation and termination of replication in mammalian cells. Genome Biol. 21, 76. https://doi.org/10.1186/s13059-020-01983-8

8 Abbreviations

5-FOA	5-Fluoroorotic acid
ABC	ammonium bicarbonate
Abf1	ARS binding factor 1
ac	acetylation
ACS	ARS consensus sequence
AID	auxin-inducible degron
amp	ampicillin
ARS	autonomously replicating sequence
B	beads
bp	basepair(s)
BSA	bovine serum albumin
CBP	calmodulin binding protein
CEN	centromere
CDK	cyclin dependent kinase
ChAP-MS	chromatin affinity purification with mass spectrometry
ChIP-Seq	chromatin immunoprecipitation-sequencing
chr4	chromosome 4
ChrIII	chromosome 3
CIA	cytosolic iron-sulfur protein assembly
CMG helicase	Cdc45/Mcm2-7/GINS-helicase
CX	cell extract
DDK	Dbf4-dependent kinase
DMSO	dimethylsulfoxide
DNA	desoxyribonucleic acid
DOC	doxycycline
DTT	dithiothreitol
DUE	DNA unwinding element
E	elution
EACS	extended ACS
E.coli	*Escherichia coli*
EDTA	ethylenediaminetetraacetic acid
EE	early-replicating and efficient
EGTA	ethyleneglycol-bis(β-aminoethyl)-N,N,N',N'-tetraacetic acid
FACT complex	facilitates chromatin transcription-complex
FASP	filter aided sample preparation
FT	flowthrough
g	gram(s)
h	hour(s)
HDAC	histone deacetylase
HEPES	4-(2-hydroxyethyl)-1-piperazineethanesulfonic acid
HU	hydroxyurea
HyCCAP	hybridization capture of chromatin-associated proteins for proteomics
IgG	immunglobulin G

|	
IAA	iodoacetamide
IN	input
kb	kilobasepairs
kDa	kilodalton
KO	knockout
L	liter(s)
LC-MS/MS	liquid chromatography tandem mass spectrometry
LI	late-replicating and inefficient
Lys-C	lysyl endopeptidase
M	molar
Mcm complex	mini-chromosome maintenance complex
me	methylation
mg	milligram(s)
min	minute(s)
ml	milliliter(s)
mM	millimolar
MOPS	3-(N-morpholino)propanesulfonic acid
NDR	nucleosome-depleted region
OD	optical density
ORC	origin recognition complex
p	p value
P	pellet
PAGE	polyacrylamide gel electrophoresis
PBS	phosphate buffered saline
pCYC1	CYC1 promoter
PIC	phenyl isocyanate
Pre-RC	pre-replicative complex
Prot A	protein A
pTEF2	TEF2 promoter
PTM	post-translational modification
qPCR	quantitative real-time PCR
r	Spearman's Correlation Coefficient
Rap1	repressor-activator protein1
rDNA	ribosomal DNA
RNA	ribonucleic acid
Rpm	rotations per minute
RS site	recombination site for the site-specific R-recombinase
RT	replication timing
S.cerevisiae	*Saccharomyces cerevisiae*
SCF complex	Skp, Cullin, F-box containing complex
SDS	Sodium dodecyl sulfate
sec	second(s)
SGD	Saccharomyces Genome Database
SPB	spindle pole body
TALE protein	transcription-activator-like effector protein
TAP	tandem affinity purification
TEV	tobacco etch virus

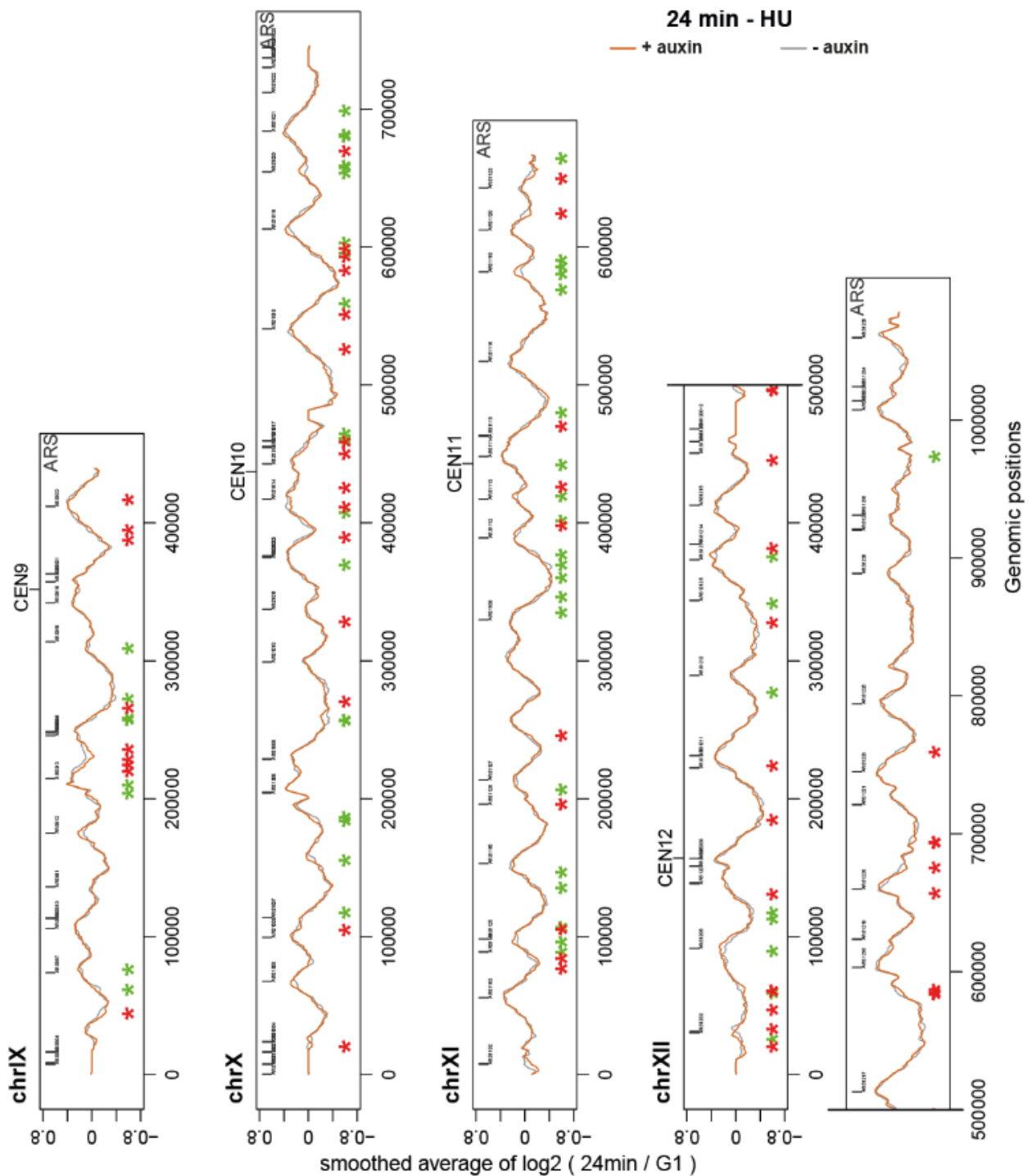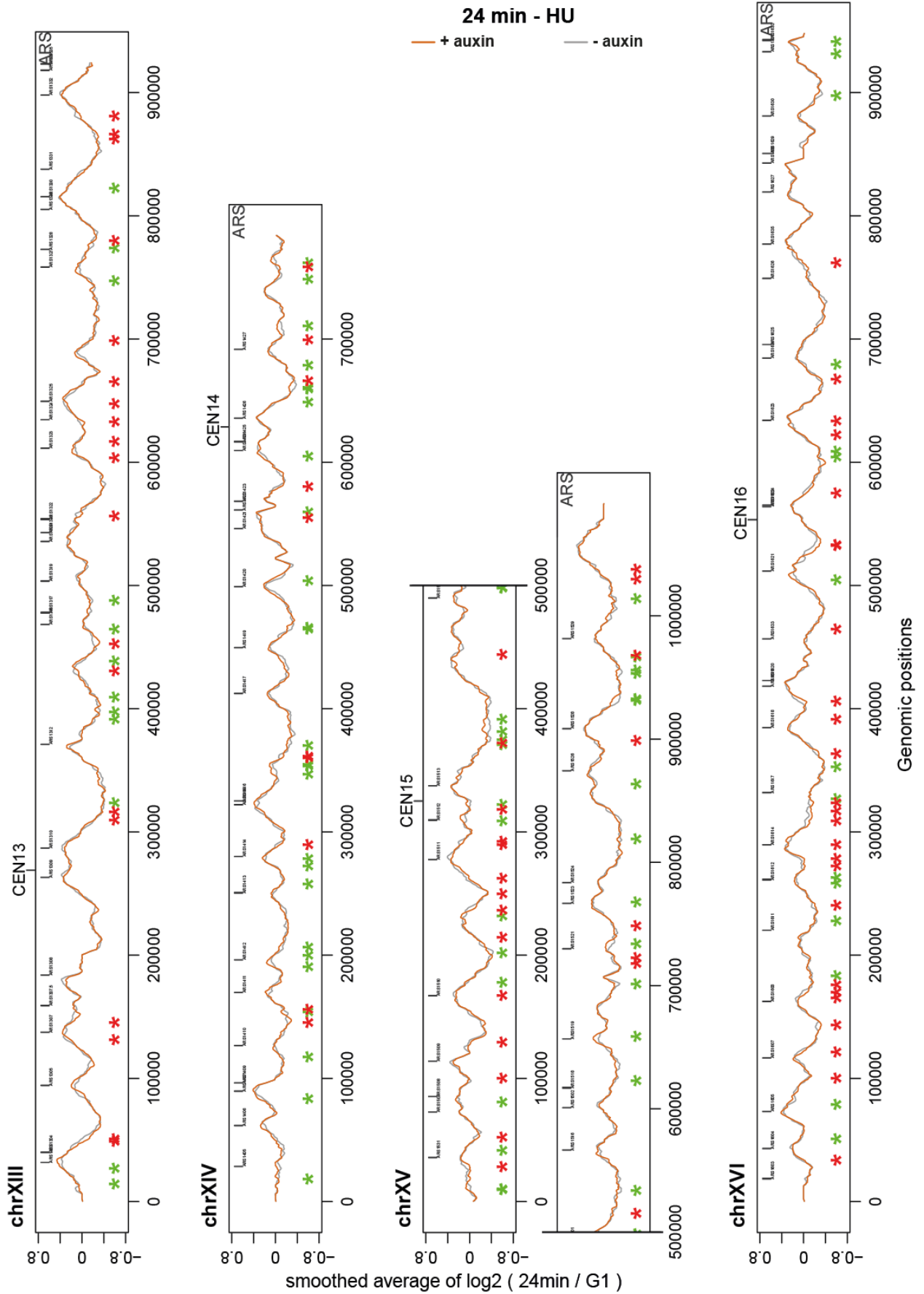|	
Tris	tris (hydroxymethyl) aminomethane
U	unit(s)
WT	wild type

9   Appendix
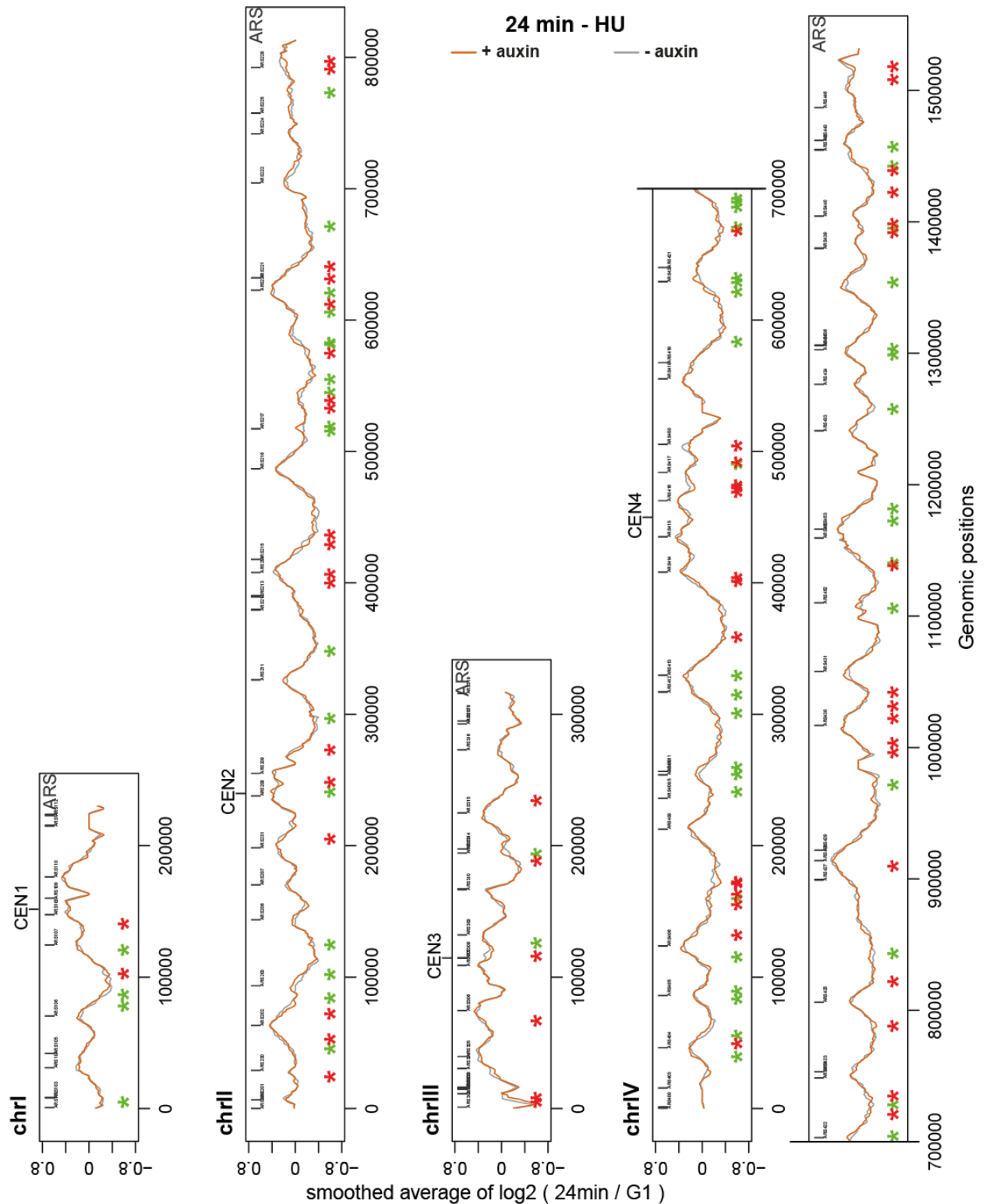
Appendix 1 DNA copy number sequencing to determine the effect of Ask1 degradation
Replication profiles of chromosome I-IV at 24min after release into S phase with and without degrading Ask1 by addition of auxin in the strain Y0123. Regions that significantly increased or decreased replication timing were obtained using Welch two sample t-test (unequal variances) in each genomic bin with a p-value cutoff of 0.05 and a mean difference of at least 0.1 and indicated with green or red asterisks, respectively.
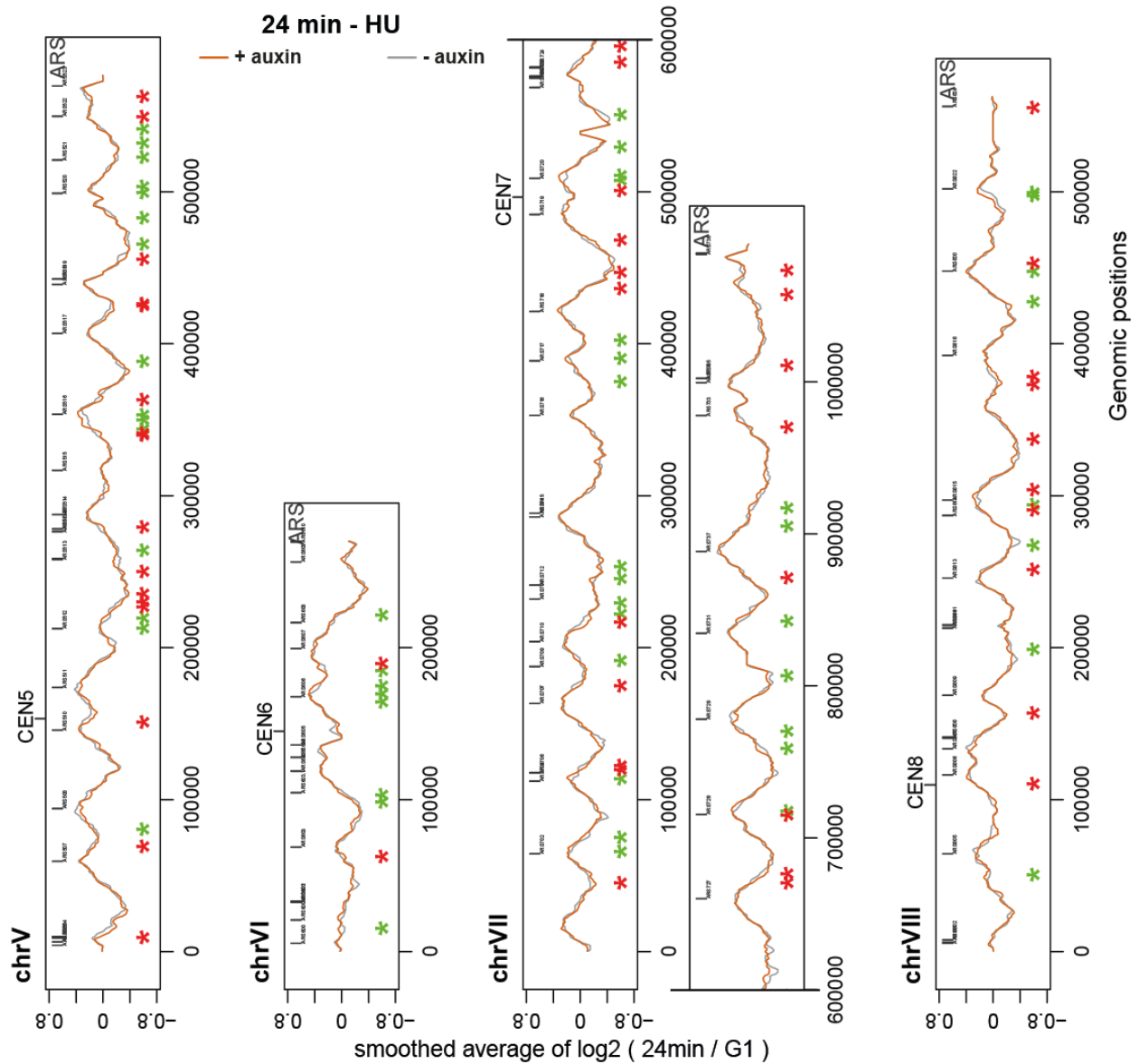
Appendix 2 DNA copy number sequencing to determine the effect of Ask1 degradation
Replication profiles of chromosome V-VIII at 24min after release into S phase with and without degrading Ask1 by addition of auxin in the strain Y0123. Regions that significantly increased or decreased replication timing were obtained using Welch two sample t-test (unequal variances) in each genomic bin with a p-value cutoff of 0.05 and a mean difference of at least 0.1 and indicated with green or red asterisks, respectively.

Appendix 3 DNA copy number sequencing to determine the effect of Ask1 degradation
Replication profiles of chromosome IX-XII at 24min after release into S phase with and without degrading Ask1 by addition of auxin in the strain Y0123. Regions that significantly increased or decreased replication timing were obtained using Welch two sample t-test (unequal variances) in each genomic bin with a p-value cutoff of 0.05 and a mean difference of at least 0.1 and indicated with green or red asterisks, respectively.

Appendix 4 DNA copy number sequencing to determine the effect of Ask1 degradation
Replication profiles of chromosome XIII-XVI at 24min after release into S phase with and without

degrading Ask1 by addition of auxin in the strain Y0123. Regions that significantly increased or decreased replication timing were obtained using Welch two sample t-test (unequal variances) in each genomic bin with a p-value cutoff of 0.05 and a mean difference of at least 0.1 and indicated with green or red asterisks, respectively.

10   Acknowledgements

Five years ago, I started this PhD journey not really knowing what will be ahead of me. It was a journey that created great and enjoyable moments, but also could be tough and frustrating with times where nothing seemed to work. However, despite these occasional hardships, I never had any doubt in finishing this journey with great success. The reason for that were all the people that accompanied me during this time, people who I knew for a long time that were there from the start, but also people that I was incredibly lucky to meet on the way. Without them, this whole project would certainly not have been as successful and, therefore, I want to use this last section to thank everybody that has been a part of it, regardless of whether scientifically or in any other way.

Most importantly, thank you Stephan for giving me the opportunity to be part of your lab. It was an enormous pleasure for me to have such an amazing boss as you are. You created a wonderful lab with great people where I enjoyed every single minute. Not only did you teach me a lot of things and drastically improve my scientific thinking through the many conversations we had, but you also always showed a kind and positive attitude, no matter what, which is something I really admire. You were a great inspiration for me and a big reason why I could push this project until the end. I am eternally grateful for everything you did and I hope we will be able to still frequently meet in the future.

Also thank you Maria Elena. Your scientific advice was always immensely helpful, whether it was during our TAC meetings, or any other kind of presentation I gave, or simply when I stumbled through your door and had any kind of questions. You always had an open ear which I really appreciated. Also, without you this whole institute wouldn't exist as it does right now. Being part and experiencing such a nice international environment with this great atmosphere is something I grew to love and hopefully will also experience in my future career. Apart from science, the occasional tennis matches were something I obviously enjoyed as well.

I also want to thank the other group leaders, Eva, Antonio, and Nico. All of you, as well, had great comments and suggestions to my project during the IES seminars or my lab meetings which was super helpful to me. The sometimes really challenging questions also helped me a lot to improve my way of thinking.

I am thankful to all my collaborators who also helped a lot to make this project a success, especially Andrey and Anne. Without you, the whole mass spectrometry part of the project would not have been possible.

I am really grateful to all Hamperl lab member. Each one of you is an amazing person and I am really happy that I met all of you. Elisabeth as the first member of the lab and my desk neighbor, you were the best lab manager possible. Thank you for all the work in general that

you did for the whole institute, but also especially for my project. Also, the desk-to-desk conversations with you were amazing and you became a really close friend during this time. Also thank you to all the other PhD students and postdocs, also all of you became really good friends over time. Henning, it was always fun being around you, I really enjoyed your humor and the parties that happened when you were around were always a blast. Anna, you always had a smile on your face and stayed positive which I really enjoyed and obviously you also helped a lot in my project, thank you for that. To the other PhD students who joined the lab later on, Manuel, Marcel, and Atiqa, all of you also always helped me when I needed some help in the lab or needed feedback for my project, thank you all for that. Maxime, the first postdoc of the lab, you have a great personality and an even greater sense of humor. I appreciated every conversation I had with you, being it scientific about my project, or just some random topics that often turned to hilarious nonsense. I loved that and it often brightened up my day. Thank you for all of that and I really hope that we will still frequently meet in the future. Last but not least also thank you Clare for being the super nice person you are, it was always nice being around you. And of course, big thanks to you for finishing the review.

I am also thankful to all the members of the other labs of the IES. All of you were always supportive and helpful whenever I needed help, all of you gave great feedback to my project in the countless seminars, and all of you were generally nice people to be around which made the workplace such a nice place to be. Especially to Camille and Ane, I enjoyed the lunch breaks with you so much, having this time of the day with you where my mind could reset was something I needed to keep going. To Clara, you became a very close friend of mine. I appreciated all the talks about our projects, but also all the little afternoon breaks and the time we spent outside the lab. To Yung-Li, thank you for all scientific help and the nice anime and manga conversations. To Mrinmoy, for helping me with the sequencing and for being such a positive person. To Manuel, for always trying to make everybody smile even when times were tough. To Marion, for all the little enjoyable conversations about the lab and our future. To Tsune, for giving me all these nice suggestions on what to read.

Apart from the lab, also my other friends were really important to me in order to get my mind away from the project, which was often needed to refuel my energy. Especially thank you to Mike, Mev, Dani, Thi, and Klaus. All of you are amazing. The times on discord just playing some games with you were always fun, really helping me to relax after tough days. Or all the other times we met when I was visiting home, having some beers and just having a relaxed time. All of that really helped me a lot in that project, even if you were not aware of that. Also big thanks to Cortexe, Brack, Bokeh, and Zi, I really appreciate you guys always being there and joining me. This always made feel great, which, again, was something that allowed me to get through tough days in anticipation of having such great people around.